Polyoxometalate Cluster-Based Functional Materials: Syntheses, Characterizations and Application Studies

A Thesis
Submitted for the Degree of
DOCTOR OF PHILOSOPHY

By

T. ARUMUGANATHAN

School of Chemistry
University of Hyderabad
Hyderabad 500 046
INDIA

October 2008

Dedicated

To my

Family & friends

“Nothing originates by chance, but everything is due to specific reason and the force of necessity.”

- Democritus

STATEMENT

I hereby declare that the mater embodied in this thesis is the result of investigation carried out by me in the School of Chemistry, University of Hyderabad, Hyderabad, India, under the supervision of **Dr. Samar K. Das**.

In keeping with the general practice of reporting scientific observations, due acknowledgements have been made wherever the work described is based on the findings of other investigators. Any omission, which might have occurred by oversight or error, is regretted.

T. ARUMUGANATHAN

CERTIFICATE

Certified that the work contained in the thesis entitled **"Polyoxometalate Cluster-Based Functional Materials: Syntheses, Characterizations and Application Studies"** has been carried out by Mr. T. Arumuganathan under my supervision and the same has not been submitted elsewhere for a degree.

Dr. Samar K. Das

(Thesis Supervisor)

Dean

School of Chemistry

ACKNOWLEDGEMENTS

I convey my profound gratitude and sincere thanks to my thesis supervisor Dr. Samar K. Das for his invaluable guidance, constant encouragement and for the liberty he gave me in carrying my research work. His positive approach in every aspect was admirable and inspiring. He has always been approachable, helpful, completely supportive and cooperative. I consider my association with him as a pleasant experience in my life.

I thank Prof. D. Basavaiah, Dean, School of Chemistry and former Deans for providing us the facilities needed for our research work.

I extend my heartfelt thanks to all faculty members of the School of Chemistry for their co-operation on various occasions. Special thanks to Prof. S. Pal for his valuable suggestions and allowing me to perform electrochemical studies in his laboratory during my research work. I express my sincere thanks to Prof. M. V. Rajasekaran for his valuable suggestions and discussions related to magnetism study. I would like to thank Prof. K. P. N. Murthy, Dr. Senthilkumar and Dr. Rajashree for their wonderful suggestions.

It is my great pleasure to acknowledge Dr. Tapas Kumar Maji (JNCASR, Bangalore) and Prof. A. R. Chakravarty (IISc. Bangalore) for helping me to collect the variable temperature magnetic data.

I take this opportunity to thank Mr. Franklin for his valuable ideas associated with TGA / Mass studies and Mr. Shafy for his in time help for ICP measurement, finally for their friendship.

I love to thank my seniors Dr. Shivaiah, Dr. Supriya, Dr. Madhu, Dr. Raghavaiah, Dr. Prabhakar, and Dr. Pradeep for their help, pleasant company, valuable suggestions and their ideas, starting from my initial research period to till now.

It is certainly great pleasure to thank my colleagues Mr. Tanmay, Mr. Rambabu, Mr. Srinivasa Rao, Mr. Durga Prasad, Mr. Bharat, Mr. Kishore, Ms. Monima, Mrs.

Sridevi, Mrs. Jhansi, Mr. Sunil and Mr. Shiva, Mr. Narayana for their cooperation, assistance, and creating pleasant working atmosphere.

I thank all non-teaching staff of the School of Chemistry for their assistance on various occasions. I specifically thank Mr. Shetty, Mr. Vara Prasad, Mr. Durgesh, Mr. Sambasiva Rao, Mr. Santhosh for their in time help during my course and Mr. Satyanarayana, Mr. Bhaskar Rao, Ms. Asia Parwez for providing relevant spectral data. A special note of thanks goes to Dr. Raghavaiah for his help and suggestions regarding single crystal XRD data measurement, finally also for his friendship.

I also thank Mr. Murthy and Dr. Manjunath for their assistance in various circumstances. Particularly I thank Mr. Suresh for providing EPR and CD measurements and Mr. Nageswara Rao for providing me Powder XRD data.

I thank all my teachers who taught me at various levels of my academic career. Prof. Azhagappan, Dr. P. Sivasamy, Dr. Sevagapandian, Dr. Kannan, Dr. Velusamy, Dr. Anantharam Dr. Vanangamudi, Dr. Bhoopathi and Dr. Meenakshi Sundaram are specially acknowledged.

Specifically, I thank Dr. Vairaprakash, my immediate senior in my graduation and post graduation studies, who introduced me to this campus. The diverse discussions and reside with him in hostel are remarkable. His in depth observation in every aspect is my first inspiration.

I would like to thank Drs. V. S. Senthil Kumar, S. Sivakumar, Jayakumar, Ashok, Perumal, Philip, Anbazahan, Padmanabhan, Mariappan, Shiva, Sundaram, Venkatesh, Natamai Senthil, Bharathi, Dhamodharan for their enormous helpful comments, criticisms and suggestions.

I am extremely thankful to my friends Balaraman, Selva, Prakash, Senthil Boss, Francis and Hemu. The stay with them in *I-110*, NRS Hostel was glorious days and still etched in my mind. I feel pleasure to thank them for their constant help, encouragement, and their friendship.

I feel very fortunate to have friends Vijayan, Arun, Sakthivel, Kannan, Ganavel, Kabali Vijayan, Muralisankar, Uma, Murali, Viji, Santhanam, Vignesh, Ganesh, Suresh, Deva, Navin, Meeran, Muthu, Senthil, Sathish, Saravanan, Robin, Sundars, Prabhu, Jeeva, Prem, Antony, Sankars, Bhuvana, Devi, Anitha, Nishas, Pavithra, Manasa, Poorani, Deepthi, Soumya and Parameswari who shared my cheerfulness and made the present here more enjoyable.

I like to thank my colleagues Biju, Jagadesh, Bipul, Ranjith, Naba, Prasanth, Shiva, Anwar, Prasad, Kishore, Jayaprakash, Rameshs, Abhijit, Rajeshs, Narahari, Arvind, Sekhar, Shiva, Bhuvan, Phani, Anji, Venu, Arindam, Sandeep, Sathish, DK Srinu, Chaitanya, Ramu, Raji, Bhargavi, Manasi, Anindita, Tulika, Hema, Saritha for their pleasant company and cooperation during my research.

I take this occasion to thank my all B. Sc, M. Sc. Classmates and colleagues, specifically I acknowledge Ranjith, Mayil, Sundaravel, Senthil, Chairmanand, Srinivas, Ragu, Muthumani, Karpagavel, Jeeva, Subbu, Meenakshi, Pon, Selvaraj, Kesavan, Chandru for their support. I extend thanks to my company mates Ravi, Senthil and Mani.

I would like to thank my home town friends Ravi, Jaichandran, Sundaravel, Sankar and Senthil for their help in various occasions and their companionship.

Most of all, I would like to thank my parents, sister, and relatives for their selfless helps, caring, love, affection and above all, for their confidence on me. All my efforts are the outcome of my family member’s encouragements and blessings.

Finally, I thank DST funded National Single Crystal X-ray diffraction Facility, UGC / UPE for providing the research infrastructure available in HCU and CSIR for the financial support.

T. Arumuganathan

CONTENTS

Chapter 1

==========

INTRODUCTION

==========

1.1. Preface

The development of the useful technologies often hinge on the availability of solid state materials with appropriate physical and chemical properties. Oxygen is not only the most abundant terrestrial element but it is also highly reactive; consequently, oxides exist for all of the elements with the exceptions of radon and the lighter noble gases. The significant contemporary interest in solid state oxides reflects a structural and compositional diversity that endows these materials with a range of physical properties that yield applications to magnetism, conducting polymers, microporous inorganic crystalline zeolite materials, opto-electronics, sorption, catalysis, bio-mineralization, and solar energy conversion etc.. For example, approximately six decades ago, pure semiconductors were prepared as single crystals that have enormous effect on the development of today's electronics industry. However, despite the practical and fundamental importance of inorganic oxides, the design and synthesis of such materials remain an elusive goal. This thesis work deals with the synthesis, characterization and application studies of early-transition metal oxo clusters which are termed as Polyoxometalates (POMs) clusters. In this chapter, we have discussed briefly about the properties and applications of POMs based solid state materials, starting from history of POMs to present progress.

1.2. General Concepts of Polyoxometalate Chemistry

1.2.1. What is Polyoxometalate (POM)

Polyoxometalate is a large family of metal-oxygen clusters, which are generally formed by the inner transition metals Mo, W, V, Nb and Ta ("addenda atoms") and have been viewed as ideal inorganic building blocks for the design and construction of multi-functional material.[1a] A large number of potential coordination sites (both terminal and bridging oxygen atoms) from the POM cluster-surfaces are the main source for the multifunctional activity. In general, POM clusters are known in anionic form, hence appropriate cations are needed for their successful isolation.

The formation of POMs depends on (i) the appropriate relationship of coulombic factors of ionic radius and charge (cationic radius should be within the range of 0.65 0.80 Å; for addenda atoms V^{5+} (0.68 Å), Mo^{6+} (0.77 Å), W^{6+} (0.74 Å) whereas for Cr^{6+} (0.58 Å)). (ii) On the accessibility of empty d orbital for metal oxygen bonding. Inner-transition metals Mo, W, V, Nb and Ta satisfy the above mentioned conditions, that is the reason why the formation of POMs clusters are limited to only those metals and not by other metals.

1.2.2. Classifications and Types

In a general point of view, POM clusters are classified as (i) Isopolyanions ("IPA"; generic formula: $H_nM_mO_y^p$) (ii) Heteropolyanions[2] ("HPA"; generic formula: $X_xM_mO_y^q$, x m) where M are the addenda atoms and X is hetero element namely P, S, Si, As, etc. At present, more than 70 different element including most non-metals and transition metals can function as hetero atom. POM anions can also be classified into three types, based on the presence of number of oxygen attached to the addenda atom. The "mono-oxo" (C_{4v}) class (or) type I, which has one terminal oxo group in which Lowest Unoccupied Molecular Orbital (LUMO) is approximately non-bonding and metal

centered and hence type I class POM clusters may be reduced reversibly to mixed valence species. Whereas in type II or "cis-dioxo" (C_{2v}) class exhibit two terminal oxo groups[1b], LUMO for the octahedral is strongly anti-bonding with respect to the M = O bonds. Type III anions (which is observed very rarely) have both kinds of M atom sites. The above entire discussion is offered in the Scheme 1

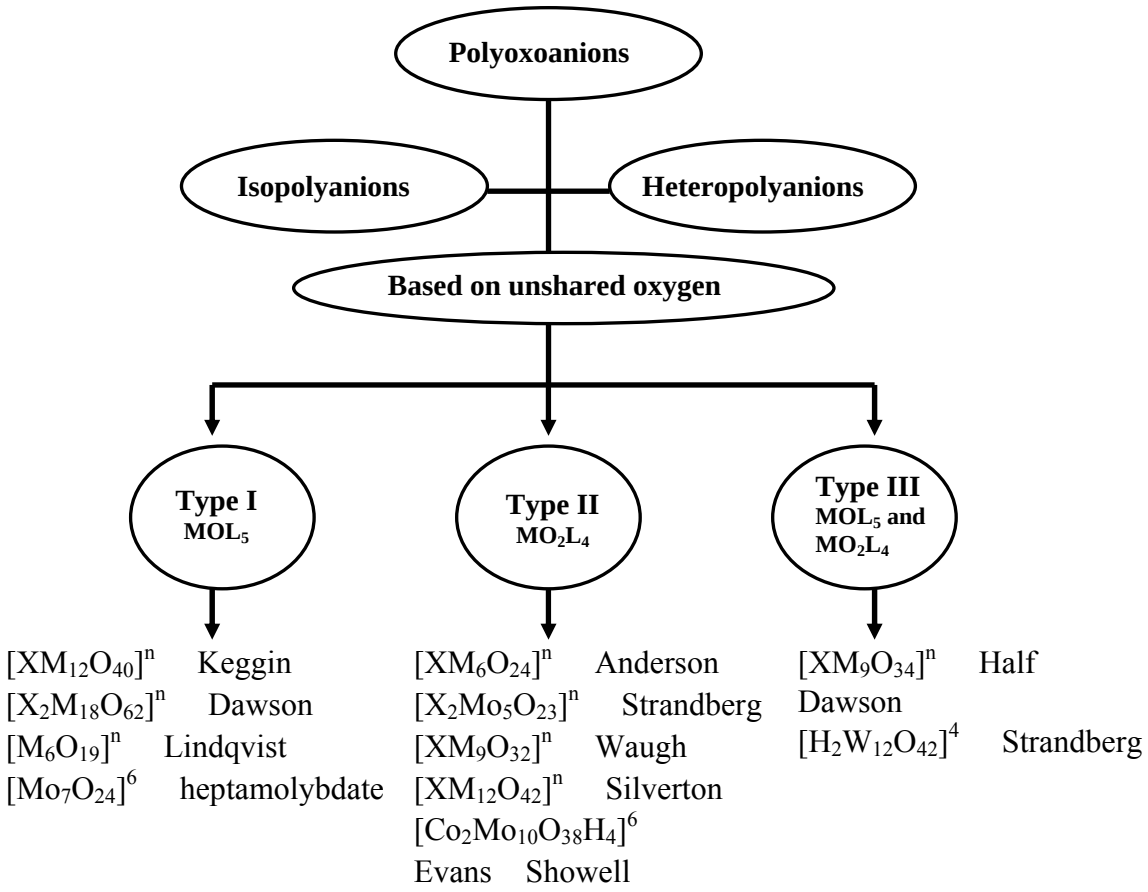

Scheme 1. Classification of POM anions based on composition and unshared oxygen attached to M atom.

The polyanion structures, that contain three or more terminal oxo groups, are not observed. A restriction which has been explained in terms of strong trans influence of the terminal M O bonds facilitating dissociation of the cluster. This restriction is named as "Lipscomb principle".[1b]

1.2.3. Historical Background of POMs Anion Chemistry

The first polyoxoanion was reported almost two centuries ago, but that could be characterized structurally more than 100 years later. Ammonium phosphomolybdate $[NH_4]_3[PMo_{12}O_{40}]$. xH_2O can be prepared by adding Ammonium molybdate and Phosphoric acid in aqueous medium, which is one of the earliest metal oxide clusters synthesized by Berzelius in 1826.[3]

1.3. Basic Principles in POMs Cluster Structure, Synthesis and Properties

1.3.1 Structure

POM cluster anions comprised of aggregates of metal oxygen units, where the metal adopted in the center of a polyhedron and the oxygen ligands defining the vertices of the polyhedron. The formation of a POM cluster can be considered via a self-assembly process, in which either linking or aggregation of the polyhedra are involved.[4] Consequently, the overall structure of a polyanion cluster can be represented by a group of polyhedra that have corner or edge sharing modes, (Figure 1.1.), face sharing is also possible but very rarely seen.

(**a**)

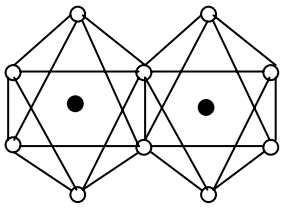

(**b**)

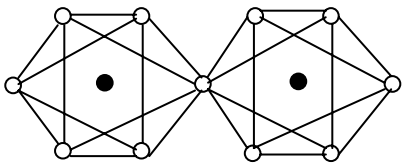

Figure 1.1. The linking modes of two adjacent polyhedra (a) via edge sharing (b) via corner sharing. Black circles represent the inner transition metals Mo, W, and V etc., and white circles represent oxygen atoms.

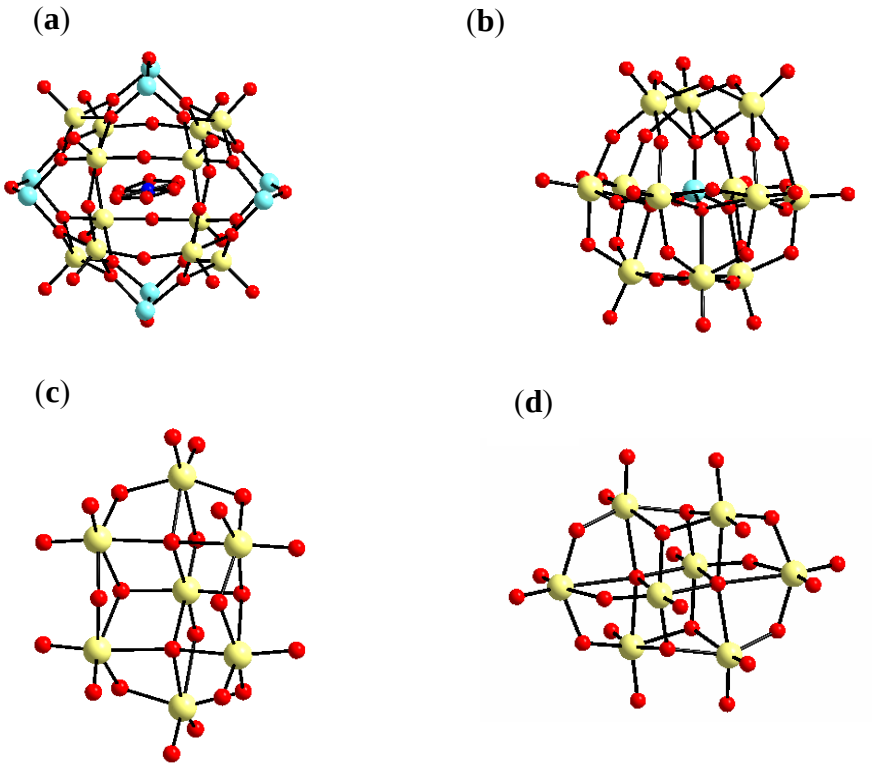

Figure 1.2. Some of the POMs structures which are common in literature: (a) $[V_{12}As_8O_{40}(NO_3)]^n$ (b) $[SiW_{12}O_{40}]^4$ (c) $[Mo_7O_{24}]^6$ (d) $[Mo_8O_{24}]^6$. Color code: O, red; N, blue; V (a), W (b) and Mo (c,d), yellow; As (a) and Si (b), cyan.

In 1933, Keggin described the X-ray crystallographic structure of "$H_3[PW_{12}O_{40}]\cdot 5H_2O$".[5a] The structure of keggin anion can be illustrated as the arrangement of twelve MoO_6 or WO_6 octahedral surrounding a central XO_4 (where X = Si or P) tetrahedron by edge and corner sharing. Later, other POMs clusters like Lindqvist[5b], Anderson[5c], and Strandberg[5d] etc. were well characterized by X-ray crystallographic technique. Some of the POMs structures which are common in the literature are shown in Figure 1.2.

1.3.2. Synthesis and Properties

In practice, POMs are most frequently prepared in one-pot synthesis, by proton induced condensation followed by dehydration in aqueous medium. The mechanism of the formation of polyoxometalate is still not clear and usually described as self assembly. Therefore it is not possible to design a multi-step sequence for the synthesis of novel POMs cluster anions. The successful isolation of POMs cluster anions mainly depends on (i) concentration of the reactants (ii) pH of the medium (iii) temperature (iv) solvent (v) sequence of reagents addition (vi) presence of reducing agents / additional ligands etc.,

(a) Synthesis of plenary POMs from aqueous and non-aqueous medium:

The acidification of aqueous solution contains simple oxoanions such as MoO_4^{2} or WO_4^{2} resulting in the formation of Isopolyanion (IPA) and Heteropolyanion (HPA). The formation of isopolyanion and heteropolyanion can be described as

$$7MoO_4^{2} + 8H^{+} \longrightarrow [Mo_7O_{24}]^{6} + 4H_2O$$

$$6MoO_4^{2} + [Cr(H_2O)_6]^{3+} + 6H^{+} \longrightarrow [Cr(OH)_6Mo_6O_{18}]^{3} + 6H_2O$$

In non-aqueous solutions, the hexa and decatungstate anions are well characterized. The syntheses of isopolyanions from organic solutions were performed by Jahr and Fuchs.[6] The synthesis was performed by the hydrolysis of metal esters in presence of organic bases. The formation of hexatungstate in non-aqueous medium can be described as

$WO(OEt)_4 + NR_4OH + H_2O \longrightarrow [NR_4]_2[W_6O_{19}]$ (where R = alkyl groups)

(b) Derivative of POMs anions:

Functionalization of POMs anion can be achieved in three possible different ways.

(i) By substitution of transition metasl:

By the treatment of base to the heteropoly species can produce defect POMs structure so-called “lacunary” heteropoly species wherein one or more addenda atoms

have been eliminated from the structure along with the oxygen those addenda were not sharing with other atoms. Lacunary species are more readily react with a wide variety of octahedral coordinating metal ions to refill the vacant sites. The unshared coordination position of a substituted metal ion is available for coordination of other ligands, so that produces transition metal ion substituted POMs. For example,

$$[A\ \alpha\ SiW_9O_{34}]^{10} + 3Cu^{2+} + 3H_2O \longrightarrow [Cu_3(H_2O)_3(A\ \alpha\ SiW_9O_{34}]^4$$

(ii) **By the support of Transition Metal Complexes (TMCs) or organic moieties:**

Attachment of a transition metal complex (TMC) on the surface of a POM anion using covalent bonds can produce discrete POMs supported transition metal complex. The covalent attachment of organic groups to POM extends their applications in pharmaceutical industries.[7]

(iii) **Multidimensional inorganic organic hybrid materials:**

The POMs anions (discrete clusters) are suitable building block to obtain extended framework type materials. Two adjacent POMs clusters are connected by one or more number of transition metal complexes, in which transition metal complex acts as a linker. Added organic ligand may acts as either coordinating ligand / template or both. A 'template' can be defined as structure directing ligand during the course of reaction time or acts as space filling agents.

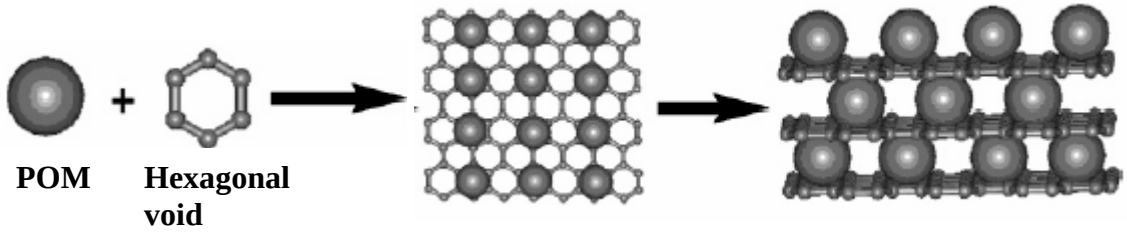

Figure 1.3. The incorporation of POMs cluster in the hexagonal voids present in porous multidimensional structure.

The organic ligands, especially, amine templates including RNH_2, R_2NH, R_3N, R_4N^+ and diamines either may coordinate to the transition metal or merely acts as counter cation by protonation. Coordination dimension mainly depends on the number of possible coordination sites available in POMs cluster and transition metal complexes. By taking the advantage of the ability of POMs to act as ligands, variety of multidimensional structures including 1D, 2D, and 3D have been synthesized by hydro thermal technique and a significant contribution was made by Jon Zubieta *et al*.[8] In this particular field of research work, some of the structures are known with open framework containing well defined cavity.[8b] The following Figure 1.3 illustrates the incorporation of POMs in voids present in the multidimensional structure.

1.4 Higher Nuclear POM Clusters and Applications

1.4.1. Polyoxovanadate

Polyoxovanadate anions are structurally very flexible and the central vanadium atom exists in tetrahedral, trigonal-bipyramidal, square pyramidal and octahedral geometries.

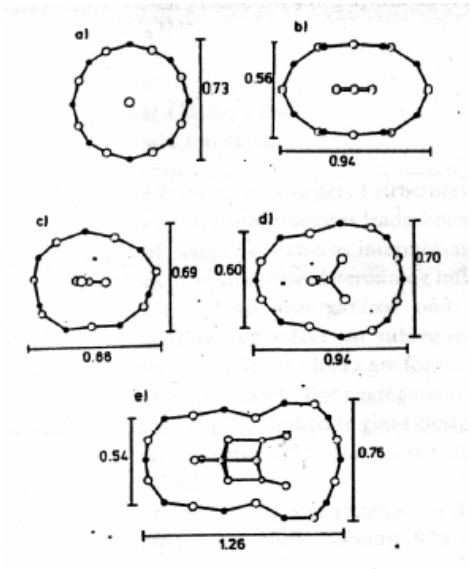

Figure 1.4. Simplified representation of the shape and size (measurements in nm) of the several polyoxovanadate cluster anions: (a) $[H_4V_{18}O_{42}(X)]^9$ (X = Cl, Br, I), (b) $[H_2V_{18}O_{44}(N_3)]^5$, (c) $[HV_{18}O_{44}(NO_3)]^{10}$, (d) $[HV_{22}O_{54}(ClO_4)]^6$, (e) $[V_{30}O_{74}(\{V_4O_4(O_{term})_4)]^{10}$.

In tetrahedral / trigonal-bipyramidal case, vanadium always found in +5 oxidation state whereas in square pyramidal and octahedral the central metal atom either in +4 (or) +5 oxidation state. The square pyramidal geometry is the responsible for the formation of cluster shells / cages in which templates (generally anion occasionally neutral molecules) are accommodated as guest molecules. Higher Nuclear cluster shells / cages are known from $\{V_{12}\}$ to $\{V_{34}\}$ with various topologies,[9] among those, many exist in mixed valence (V^{4+}/V^{5+}). Cluster (Host) templates (Guest) molecules are stabilized by weak forces (in the case of anionic guest weak repulsive force). Figure 1.4 describes the growth of cluster shells/cages by the effect of the templates. Many polyoxovanadate cluster shells / cages acts as cryptands / clatharate host for neutral, cation or anionic molecules.

1.4.1.1. Molecular Magnetism

It is well known that, only two isopolyanions $[V_{10}O_{28}]^6$ and $[V_{12}O_{32}]^4$ are known in which all the vanadium centers are in +5 oxidation state.[9c,10] Several polyoxovanadates are known in mixed valence (nearly all ratios of V^{4+} to V^{5+} are known) and some of them are known in which all the vanadium centers are in $V^{4+}(d^1)$[9d] oxidation stgate. Especially, the mixed valence (V^{5+}/V^{4+}) and reduced (only V^{4+}) vanadium clusters show an interesting magnetic behavior. In such a way, fully reduced vanadium clusters (containing only V^{4+}) can be viewed as fully magnetic cluster in which V^{4+} centers are anti-ferromagnetically coupled with spin S = ½ for each V^{4+}. Consequently, the intermolecular magnetic interactions are expected to be a maximum which open up a new gateway in molecular magnetism.

(i) Single Molecule Magnets (SMMs)

In the context of above discussion the best known single molecule magnets (SMMs) are Mn_4[11a], Mn_{12}[11b], Mn_{16}[11c], Mn_{18}[11d], Mn_{26}[11e], Mn_{30}[11f], Fe_4[11g], Fe_8[11h], Fe_{10}[11i], Fe_{19}[11j], V_4[11k], Co_4[11L], Ni_4[11m], Ni_{12}[11n] and Ni_{21}[11o]. A single molecule magnet can be defined as “a class of molecules exhibiting magnetic properties similar to those observed in

conventional bulk magnets, but of molecular origin". A molecule should have two basic requirements to behave as a single molecule magnet. They are (a) high spin ground state (b) high zero field splitting (due to high magnetic anisotropy). The combination of these two properties can lead to an energy barrier and hence the molecular system can be trapped in one of the high spin energy wells at low temperatures. SMMs have potential applications on high data storage and quantum computation as quantum bits.[12] Recently heteropolyvanadate clusters $K_6[V_{15}As_6O_{42}(H_2O)]\cdot 8H_2O$ and $[NH_4]_6[V_{14}As_8O_{42}(SO_3)]$ also known as (V15) and (V14) respectively have been shown to exhibit some of the properties of SMM.[9d,9e] A cartoon representation of the spin orientation of V15 molecule is presented in Scheme 2. These types of molecules contain a finite number of paramagnetic spin centers and provide an opportunity to study about the magnetic interactions.

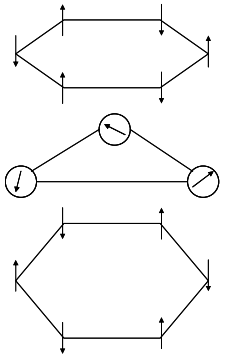

Scheme 2. Spin frustration in magnetic layers of $K_6[V_{15}As_6O_{42}(H_2O)]\cdot 8H_2O$.

1.4.2. Heteropoly Blue and Brown

As we discussed earlier, type I POMs such as Keggin, Well-Dawson, and Lindqvist can be reduced to mixed valence heteropoly blue and brown. The reduction of heteropolyanion to heteropoly blue or brown involves the reversible addition of one or more electrons. The added electron must be entered into the non-bonding orbital. The availability of non-bonding orbital is possible only in type I POMs, whereas in the type II (two terminal oxygen atoms) metal d orbitals are involved in σ and π bonding. Consequently type II POMs does not undergo reversible reduction to heteropoly blue or

brown. The extinction coefficient of reduced "molybdenum blue" or "tungsten blue" is significantly comparable to those of organic dyes. Molybdenum blue solution is instantaneously formed by the reduction of Mo^{6+} to Mo^{5+} in aqueous acidic solution (pH 3). Reducing agents such as B_2H_6, $NaBH_4$, N_2H_4, NH_2OH, H_2S, SO_2, SO_3^{2} , $S_2O_4^{2}$, $S_2O_3^{2}$, $SnCl_2$, $MoCl_5$, $MoOCl_5^{2}$, HCOOH, C_2H_5OH, ascorbic acid and metals like Cu, Zn, Al etc., can be used successfully to generate "molybdenum blue".[1,13] Strong reducing conditions are needed to generate brown species. Regarding "molybdenum blue" pioneer contribution has been done by Müller *et. al.* and published variety of articles in which molybdenum higher nuclear clusters are decorated by diverse architectures.[1] The molecular growth of high nuclear molybdenum cluster evolution can be described as follows,

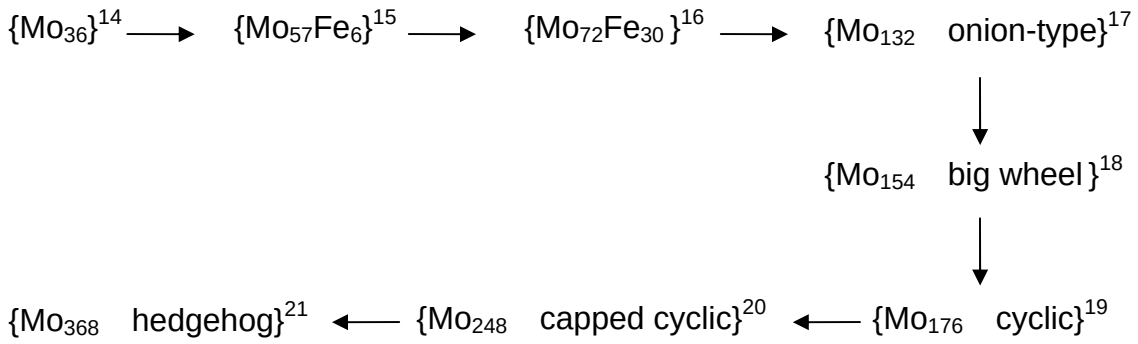

1.4.3. POM in Catalysis

The mainstream of POMs applications is found in the area of catalysis. The redox properties of these POMs make them important to act as catalyst for a number of oxidation and dehydrogenation reactions of organic substrates. The main role of POMs cluster anion in catalysis is in the activation of hydrogen peroxide, alkylhydroperoxide etc. As a result of the activation of peroxides, an inorganic peroxo, hydro peroxo, alkyl peroxo, or acyl peroxo intermediates are formed and those are very reactive species and

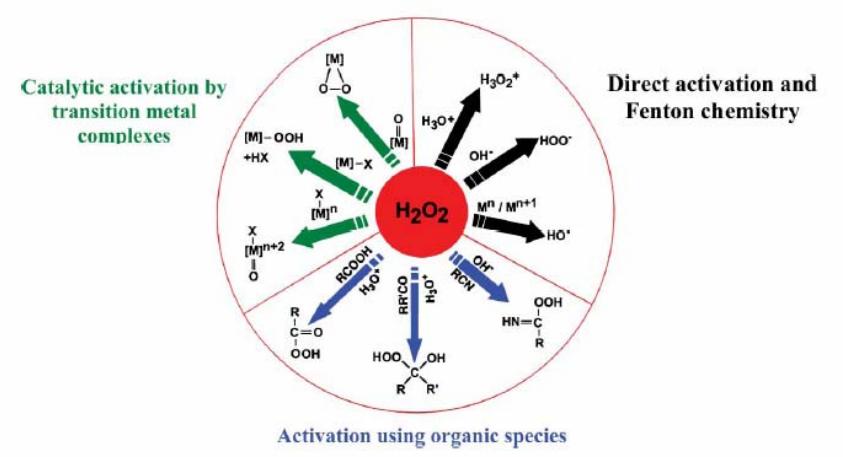

Figure 1.5. Activation of hydrogen peroxide by a catalytst.

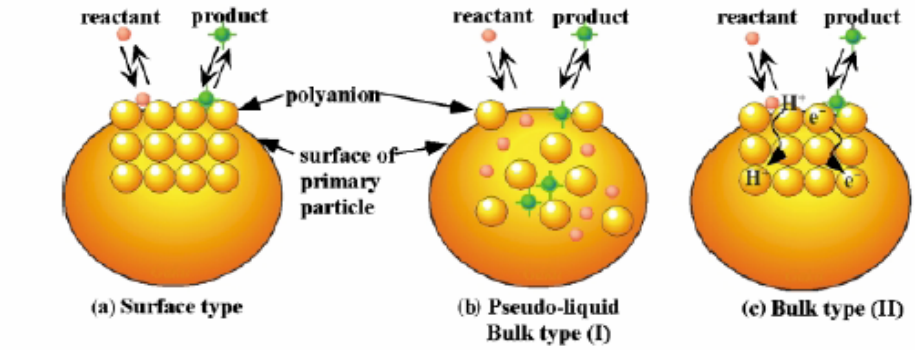

Figure 1.6. Depicts the catalytic approach of a solid heteropoly anion: (a) surface type (b) Pseudo-liquid Bulk type (I) (c) Bulk type (II).

hence lead to oxygenation of the organic substrate. Overall literature[22] survey of the activation of hydrogenperoxide by a catalyst is represented in Figure 1.5. The stability of POM towards molecular oxygen and hydrogen peroxide makes them efficient catalyst when compared to others. Mostly transition metal substituted POMs clusters or POMs supported transition metal complexes have shown applications in catalysis. The literature shows about 85% of the patents and applications of POMs are related with catalysis.[23]

There are three different approaches are available for POM catalysis related literature[24] in which solid heteropolyoxometalates are act as catalyst. (Figure 1.6).

(a) Surface type: In this approach, heterogeneous catalyst used and reaction takes place on the solid surface. (Figure 1.6(a))

(b) Pseudo liquid Bulk type (I): When the diffusion rate of reactant molecules are faster than the reaction (diffusion considered in the solid lattice rather than in the solid pores) the solid bulk forms a pseudo liquid phase in which catalytic reactions can be performed. (Figure 1.6(b))

(c) Bulk type (II): When the gaseous / liquid phase reactant molecules penetrate in between the solid POM molecules the distance between the polyanions increased and reaction takes place inside the bulk solid. The products are released as gas / liquid phase to the surface of the bulk solid. (Figure 1.6(c))

1.4.4. POM in medicine

Research work on the application of POMs in medicinal field is mainly focused on antitumor and antiviral (including anti HIV) properties. The mechanism of the antitumor activity of POMs is first proposed by Yamase and his co-workers.[25] They were found that revolving around single electron reduction / oxidation cycle is a key point for antitumoral activity. The reduced form of heptamolybdate, $[Mo_7O_{23}(OH)]^6$ is highly toxic, whereas the oxidized form $[Mo_7O_{24}]^6$ is not toxic. This group also proposed that some domains in tumour cells reduce $[Mo_7O_{24}]^6$ to $[Mo_7O_{23}(OH)]^6$ while other domains re-oxidize $[Mo_7O_{23}(OH)]^6$ to $[Mo_7O_{24}]^6$. On the basis of the toxicity of the two forms, POMs-oxidation and tumour cell reduction process that kills the cells. The first antiviral activity of POMs was reported in 1971. The inhibition of viral adsorption / fusion as a function of POM structure in a cell-based assay was first studied by Hill *et al*.[26] This

study pointed out the POMs anions $[SiW_{12}O_{40}]^4$, $[BW_{12}O_{40}]^5$ and $[NaSb_9W_{21}O_{86}]^{18}$ were able to completely inhibit cell fusion in HIV-infected lymphocytes.

The current attention of POMs has been focused on the applications in medicinal chemistry. Particularly this area of interest would be requiring chiral POM. Since much biological activity is expected to depend on the chiral configuration. Chiral POMs structures are classified in three different classes in the literature. (i) The structure which undergoes rapid racemization via water exchange, partial hydrolysis, or fluxinol behaviour. Some of the examples like $[X_2MO_{21}]^n$ (X = OP, RP, S, Se; M = Mo, W)[27] $[(MeAsO_3)Mo_6O_{18}(H_2O)_6]^2$, $[X^vMo_9O_{31}(H_2O)_3]^3$, $[X_2{}^vMo_{18}O_{62}]^6$, and $[M^{iv}Mo_9O_{32}]^6$ [M = Mn, Ni] [28 31] (ii) The structure which are non labile but with enantiomer so similar that separation has not been achieved. (e.g., $[\beta_2\ SiW_{11}O_{39}]^6$, $[\alpha\ P_2W_{17}O_{61}]^{10}$ and their metal substituents and $[WM_3(H_2O)_2(XW_9O_{34})_2]^{12}$ [M = X = Zn, Co][32 33] (iii) The structure which are non-labile but enantiomer can be separate[34 35] (e.g., $[Co_2Mo_{10}O_{38}H_4]^6$ and $[P_2W_{18}O_{79}]^{20}$.

1.4.5. Research in Nuclear Waste

Much research work was carried out on the safe disposal of the long lived radioisotopes such as Np 237 etc. The f block elements are highly oxophilic and always prefer higher coordination number. Besides this, POMs (generally in anionic nature) are nucleophilic consists vast number of oxygen on the surface for coordination and most of the time acts as multi-dentate ligand. Combination of these two preferably shows applications on nuclear waste treatment process. POMs readily form complexes with tri and tetravalent lanthanides and actinides.[36] A large amount of research have been carried out on AsW_9[37] and $P_2W_{17}O_{61}$[38] to use the POMs clusters as coordinating ligand in radioactive waste treatment via sequestration of trans-uranium elements. The outstanding

similarity of coordination chemistry in POMs may have great significance in the development of new waste treatment technologies.

1.4.6. Supramolecular Interactions in POMs

Supramolecular chemistry can be defined as the interaction between two or more number of molecules which leads to the supramolecular assembly. Supramolecular chemistry deals with non-covalent interactions which are broadly differ from the traditional organic chemistry (where making and breaking of covalent bonds to construct desired molecules). When a metal center is a part of the structure, a supramolecular framework can be constructed in two different ways.

(i) Through coordinate covalent bonds by linking metal and organic ligands.[8]

(ii) Through weak non-covalent intermolecular forces such as hydrogen bonding, Van der waals forces, π π interactions, hydrophobic / hydrophilic interactions, ionic forces, etc. Structures are held together by above mentioned weak intermolecular forces consequently that offers extra stability to the framework. Supramolecular chemistry often used as a tool to develop new functions like high-tech sensors, pharmaceutical therapies etc. that cannot appear from a single molecule. Since POMs are basically oxo-clusters, which contains many number of oxygen atoms on the cluster surface and also crystallized with significant number of lattice water molecules; the crystal structure often stabilized by O H···O hydrogen bonding interactions (in case of hybrid compounds C H···O, N H···O, C H···N etc. also included).

1.4.7. Other Applications

Apart from the aforementioned discussions, an intense research work on the applications of POMs are known in the literature such as conductivity,[39] photochromism,[40] corrosion,[41] analytical,[42] gas sensors,[43] fuel cells,[44] wood pulp bleaching,[45] protein precipitating agents,[46] etc.

1.5. Motivation of this Thesis

Above mentioned discussion presents general over-view of POMs and their related topics. Since that time, first POMs cluster discovered, till now the application of POMs as a material is grown step by step. Currently we are in the position to seek out such category of materials with some unique properties. Further work on developing reliable and versatile functional materials with useful properties is essential. The studies on solid state properties of POMs based crystalline materials in new perspectives open up unexplored solid state aspects on their possible applications in the interdisciplinary areas. In general, POMs are in anionic form which can be isolated crystalline material with appropriate cation and the properties of the same also can be tuned to a large extent. The present work describes POMs based materials synthesis, crystal structures, and their possible studies in application point of view. We have chosen V/As/O polyoxovanadate system (which is not explored as much as V/P/O system) as ligand and interaction of those with f-block elements results the formation of inorganic coordination polymer in which the thermal stability is increased significantly when compare to the corresponding discrete clusters. The relevant crystal and TGA/Mass studies have been described in chapter 2. By using aminopyridine derivatives as templates, a series of isopolyoxometalate were isolated and catalytic activity also studied towards the oxidation of primary and secondary alcohols to their corresponding aldehyde and ketone respectively and results are described in chapter 3. In chapter 4, intake and releasing of water molecules from ionic crystal lattice in a crystal to crystal transformation has been discussed. The ionic crystal is made by trinuculear macrocation and keggin POMs as anion. The interaction of Schiff base coordinated Mn^{3+} complexes and keggin POMs have been described in chapter 5. Mainly, chapter 6 deals the supramolecular interactions such as O H···O, C H···O and N H···O of organc ligands with POMs. Non-covalent weak O···O interactions among isopolyanion using a cis-$\{MoO_2\}$ moiety is surveyed and the displacement of racemate equilibrium in Strandberg type POM, in favor of one

enantiomer by the presence of enantiopure optically active compound also discussed in the same chapter.

1.6. References

1. a) M. T. Pope, *Heteropoly and Isopoly Oxometalates;* Springer-Verlag: Berlin, 1983; b) M. T. Pope, *Heteropoly and Isopoly Oxometalates;* Springer-Verlag: New York, 1983.
2. a) G. B. Kouffman, P. F. Vartanian, *J. Chem. Edu.,* **1970**, *47*, 212; b) M. T. Pope, *Inorg. Chem.* **1972**, *11*, 1973.
3. J. Berzelius, *Pogg. Ann.,* **1826**, *6*, 369.
4. a) A. Müller, P. Kögerler, C. Kuhlmann, *Chem. Commun*. **1999**, 1347; b) A. Müller, P. Kögerler, H. Bögge, *Mol. Self-assembly* **2000**, *96*, 203.
5. a) J. F. Keggin, *Proc. Roy. Soc., A.* **1934**, *144*, 75; b) I. Lindqvist, *Arkiv Kemi*., **1950**, *2*, 325; c) J. S. Anderson, *Nature*, **1937**, *140*, 850; d) R. Strandberg, *Acta Chem. Scand*., **1973**, *27*, 1004.
6. a) K. F. Jahr, J. Fuchs, *Chem. Ber*., **1963**, *96*, 2457; b) J. Fuchs, K. F. Jahr, *Chem. Ber*., **1963**, *96*, 2460; c) J. Fuchs, K. F. Jahr, *Chem. Ber*., **1963**, *96*, 2472.
7. J. T. Rhule, C. L. Hill, D. A. Judd, R. F. Schinazi, *Chem. Rev.* **1998**, *98*, 327.
8. a) E. Burkholder, V. Golub, C. J. P'Connor, J. Zubieta, *Inorg. Chem. Commun*. **2004**, *7*, 363; b) V. Soghomonian, Q. Chen, R. C. Haushalter, J. Zubieta, C. J. O'Connor, *Science*, **1993**, *259*, 1596.
9. a) A. L. Barra, D. Gatteschi, B. S. Tsukerblatt, J. Doring, A. Müller, L. C. Brunel, *Inorg. Chem.* **1992**, *31*, 5132; b) W. G. Klemperer, T. A. Marquart, O. M. Yaghi, *Angew. Chem., Int. Ed.* **1992**, *31*, 49; c) V. W. Day, W. G. Klemperer, O. M. Yaghi, *J. Am. Chem. Soc.* **1989**, *111*, 5959; d) A. L. Barra, D. Gatteschi, L. Pardi, A. Müller, J. Doring, *J. Am. Chem. Soc.* **1992**, *114*, 8509; e) Gatteschi, L. Pardi,

A. L. Barra, A. Müller, J. Doring, *Nature*, **1991**, *354*, 463; f) A. Müller, J. Doring, *Angew. Chem., Int. Ed. Engl.* **1988**, *27*, 1721; g) A. Müller, E. Krickemeyer, M. Penk, R. Rohlfing, A. Armatage, H. Bögge, *Angew. Chem., Int. Ed.* **1991**, *30*, 1674; h) A. Müller, R. Rohlfing, J. Doring, M. Penk, *Angew. Chem., Int. Ed. Engl.* **1991**, *30*, 588.

10. H. T. Evans, Jr., *Inorg. Chem.* **1966**, *5*, 967.

11. a) S. M. J. Aubin, M. W. Wemple, D. M. Adams, H. L. Tsai, G. Christou, D. N. Hendrickson, *J. Am. Chem. Soc.* **1996**, *118*, 7746; b) R. Sessoli, H. L. Tsai, A. R. Schake, S. Wang, J. B. Vincent, K. Folting, D. Gatteschi, G. Christou, D. N. Hendrickson, *J. Am. Chem. Soc.* **1993**, *115*, 1804; c) J. P. Price, S. R. Batten, B. Moubaraki, K. S. Murray, *Chem. Commun.* **2002**, 762; d) E. K. Brechin, C, Boskovic, W. Wernsdorfer, J. Yoo, A. Yamaguchi, E. C. Sañudo, T. R. Concolino, A. L. Rheingold, H. Ishimoto, D. N. Hendrickson, G. Christou, *J. Am. Chem. Soc.* **2002**, *124*, 9710; e) L. F. Jones, E. K. Brechin, D. Collison, A. Harrison, S. J. Teat, W. Wernsdorfer, *Chem. Commun.* **2002**, 2974; f) M. Soler, W. Wernsdorfer, K. Folting, M. Pink, G. Christou, *J. Am. Chem. Soc.* **2004**, *126*, 2156; g) D. Gatteschi, R. Sessoli, A. Cornia, *Chem. Commun.* **2000**, 725; h) C. Delfs, D. Gatteschi, L. Pardi, R. Sessoli, K. Wieghardt, D. Hanke, *Inorg. Chem.* **1993**, *32*, 3099; i) C. Benelli, J. Cano, Y. Journaux, R. Sessoli, G. A. Solan, R. E. P. Winpenny, *Inorg. Chem.* **2001**, *40*, 188; j) J. C. Goodwin, R. Sessoli, D. Gatteschi, W. Wernsdorfer, A. K. Powell, S. L. Heath, *J. Chem. Soc., Dalton Trans.* **2000**, 1835; k) Z. Sun, C. M. Grant, S. L. Castro, D. N. Hendrickson, G. Christou, *Chem. Commun.* **1998**, 721; l) E. –Ch. Yang, D. N. Hendrickson. W. Wernsdorfer, M. Nakano, L. N. Zakharo, R. D. Sommer, A. L. Rheingold, M. Ledezma–Gairaud, G. Christou, *J. Appl. Phys.* **2002**, *91*, 7382; m) C. Boskovic, E. Rusanov, H. Stoeckli–Evans, H. U. Gudel, *Inorg. Chem. Commun.* **2002**, *5*, 881; n) C. Cadiou, M. Murrie, C. Paulsen, V. Villar, W. Wernsdorfer, R. E. P. Winpenny, *Chem. Commun.* **2001**, 2666; o) S. T. Ochsenbein, M. Murrie, E.

Rusanov, H. Stoeckli–Evans, C. Sekine, H. U. Gudel, *Inorg.Chem.* **2002**, *41*, 5133.

12. a) M. N. Leuenberger, D. Loss, *Nature*, **2001**, *410*, 789; b) S. Hill, R. S. Edwards, N. Aliaga-Alcalde, G. Christou, *Science*, **2003**, *302*, 1015; c) R. Sessoli, H. –L. Tsai, Ann. R. Schake, S. Wang, J. B. Vincent, K. Folting, D. Gatteschi, G. Christou, D. N. Hendrickson, *J. Am. Chem. Soc.* **1993**, *115*, 1804.
13. a) A. Müller, J. Meyer, E. Krickemeyer, E. Diemann, *Angew. Chem., Int. Ed.* **1996**, *35*, 1206.
14. A. Müller, E. Krickemeyer, S. Dillinger, H. Bögge, W. Plass, A. Proust, L. Dloczik, C. Menke, J. Meyer, R. Rohlfing, *Z. Anorg. Allg. Chem.* **1994**, *620*, 599.
15. a) S. -W. Zhang, G. -Q. Huang, M. –C. Shao, Y. –Q. Tang, *J. Chem. Soc., Chem. Commun*, **1993**, 37; b) A. Müller, E. Krickemeyer, S. Dillinger, H. Bögge, A. Proust, W. Plass, R. Rohlfing, *Naturwissenschaften* **1993**, *80*, 560; c) A. Müller, H. Bögge, E. Krickemeyer, S. Dillinger, *Bull. Pol. Acad. Sci., Chem.* **1994**, *42*, 291.
16. A. Müller, E. Krickemeyer, H. Bögge, M. Schmidtmann, F. Peters, *Angew. Chem., Int. Ed.* **1998**, *37*, 3360.
17. A. Müller, E. Krickmeyer, S. K. Das, P. Kögerler, D. –Chem., S. Sarkar, H. Bögge, M. Schmidtmann, S. Sarkar, *Angew. Chem. Int. Ed.* **2000**, *39*, 1612.
18. a) A. Müller, E. Krickemeyer, J. Meyer, H. Bögge, F. Peters, W. Plass, E. Diemann, S. Dillinger, F. Nonnenbruch, M. Randerath, C. Menke, *Angew. Chem. Int. Ed. **1995***, *34*, 2122.
19. a) A. Müller, E. Krickemeyer, H. Bögge, M. Schmidtmann, C. Beugholt, P. Kögerler, C. Lu, *Angew. Chem., Int. Ed.* **1998**, *37*, 1220; b) C. C. Jiang, Y. G. Wei, Q. Liu, S. W. Zhang, M. C. Shao, Y. Q. Tang, *Chem. Commun.* **1998**, 1937.
20. A. Müller, S. Q. N. Shah, H. Bögge, M. Schmidtmann, *Nature*, **1999**, *397*, 48.
21. A. Müller, E. Beckmann, H. Bögge, M. Schmidtmann, A. Dress, *Angew. Chem., Int. Ed.* **2002**, *41*, 1162.

22. J. M. Brégeault, *J. Chem. Soc., Dalton Trans.,* **2003**, 3289.

23. D. E. Katsoulis, *Chem. Rev.* **1998**, *98*, 359.

24. M. Misono, *Chem. Commun.,* **2001**, 1141.

25. T. Yamase, *Mole. Eng*. **1993**, *3*, 241.

26. C. L. Hill, M. Hartnup, M. Faraj, M. Weeks, C. M. Prosser-Mccartha, R. B. Brown Jr., M. Kadkhodayan, J, -P, Sommadossi, R. F. Schinazi, *In Advances in Chemotherapy of AIDS*; R. B. Diasio, J. –P. Sommadossi, Eds.; Pergamon Press, Inc.: New York, 1990.

27. a) R. Strandberg, *Acta Chem. Scand.* **1973**, *27*, 1004; b) K. Y. Matsumoto, M. Kato, Y. Sasaki, *Bull. Chem. Soc. Jpn.* **1976**, *49*, 106; c) V. W. Day, M. F. Fredrich, W. G. Klemperer, W. Shum, *J. Am. Chem. Soc.* **1977**, *99*, 952; d) B. Hedman, *Acta Chem. Scand.* **1977**, *27*, 3335; e) W. H. Knoth, R. L. Harlow, *J. Am. Chem. Soc.* **1981**, *103*, 1865.

28. K. Y. Matsumoto, *Bull. Chem. Soc. Jpn,* **1979**, *52*, 3284.

29. M. T. Pope, *Inorg. Chem.* **1976**, *15*, 2008.

30. a) R. Strandberg, *Acta Chem. Scand., Ser. A.* **1975**, *29*, 350; b) H. D'Amour, *Acta Crystallogr., Sect. B.* **1976**, *32*, 729; c) J. F. Garvey, M. T. Pope, *Inorg. Chem.* **1978**, *17*, 1115.

31. a) A. Tézé, G. J. Hervé, *Inorg. Nucl. Chem.* **1977**, *39*, 999; b) A. Tézé, G. J. Hervé, *Inorg. Nucl. Chem.* **1977**, *39,* 2151.

32. a) R. Contant, J. P. Ciabrini, *J. Chem. Res.* **1977**, *M*, 2601; b) R. Contant, J. P. Ciabrni, *J. Chem. Res.* **1977**, *S*, 222; c) R. Contant, J. P. Ciabrini, *J. Chem. Nucl. Chem.* **1981**, *43*, 1525; d) S. P. Harmalker, Ph. D Thesis, Georgetown University, 1982; e) M. Kozik, L. C. W. Baker, *Polyoxometalates: From Platonic Solids to Antiretro Viral Activity*, M. T. Pope, A. Müller, Eds.; Kluwer Academic Publisher: The Netherlands, 1994; f) C. M. Tourné, G. F. Tourné, F. Zonnevijlle, *J. Chem. Soc., Dalton Trans.* **1991**, 143.

33. a) H. T. Evans Jr., J. S. Showell, *J. Am. Chem. Soc.* **1969**, *91*, 6881; b) T. Ada, J. Hidaka, R. Shimura, *Bull. Chem. Soc. Jpn,* **1970**, *43*, 2654.

34. a) J. C. T. Waugh, D. P. Schoemaker, L. Pauling, *Acta Crystallogr.* **1954**, *7*, 438; b) L. C. W. Baker, T. J. R. Weakley, *J. Inorg. Nucl. Chem.* **1966**, *28*, 447; c) K. Nomiya, R. Kobayashi, M. Miwa, *Bull. Chem. Soc. Jpn,* **1983**, *56*, 3505.

35. a) J. Fuchs, R. Z. Z. Palm, *Naturforsch., B: Chem. Sci.* **1988**, *43*, 1529; b) R. Acerete, J. Server-Carrió, *J. Am. Chem. Soc.* **1990**, *112*, 9386.

36. A. B. Yosov, V. P. Shilov, *Radiochemistry*, **1999**, *41*, 3.

37. a) K. Wassermann, M. T. Pope, M. Salmen, J. N. Dann, H. –J. Lunk, *J. Solid State Chem.* **2000**, *149*, 378; b) M. T. Pope, X. Wei, K. Wassermann, M. H. C. R. Dickman, *Acad. Sci., Ser. IIc* **1998**, *I*, 297; c) K. Wassermann, M. H. Dickman, M. T. Pope, *Angew. Chem. Int. Ed.* **1997**, *36*, 1445.

38. a) N. Y. Kremlyakova, A. P. Novikov, B. F. Myasoedov, N. V. Katargin, *J. Radioanal. Nucl. Chem.,* **1990**, *145*, 183; b) N. P. Molochnikova, V. Y. Frenkel, B. F. Myasoedov, *Radiokhimiya*, **1989**, *31*, 65.

39. J. Peng, E. Wang, Y. Zhou, Y. Xing, H. Jia, Y. Lin, Y. Shen, *J. Chem. Soc., Dalton Trans.,* **1998**, 3865.

40. Coué, R. Dessapt, M. Bujoli-Doeuff, M. Evain, S. Jobic, *Inorg. Chem.* **2007**, *46*, 2824.

41. a) S. V. Lomakina, T. S. Shatova, L. P. Kazansky, *Corros. Sci*., **1994**, *36*, 1645; b) N. Wu, S. Wang, H. Xu, J. Fang, *Yingyong Huaxu*., **1993**, *10*, 5.

42. V. Svec, V. Mikulaj, R. Hazel, *J. Radioanal. Nucl. Chem*., **1996**, *208*, 487.

43. a) A. Polak, P. Young, U. S. Patent 4714482, 1987; *Chem. Abstr.* **1988**, *108*, 95874; b) S. Petty-Weeks, U.S. Patent 4661211, 1987; *Chem. Abstr.* **1987**, *107*, 69923.

44. a) O. Nakamura, T. Kodama, I. Ogino, Y. Miyake, Japanese Patent JP 51106694, 1976; *Chem Abstr.* **1976**, *86*, 19085; b) O. Nakamura, T. Kodama, I. Ogino, Y. Miyake, U. S. Patent 4024036, 1977.

45. T. Kaneda, K. Jinnai, T. Koshizuka, A. Kimura, Japanese Patent JP07082243 A2, 1995, *Chem Abstr.* **1995**, *123*, 82854.

46. a) D. T. Vallance, D. J. Byrne, A. F. Winder, *Clin. Chim. Chim. Acta*., **1994**, *229*, 77; b) H. Y. Yeang, E. Sunderasan, A. R. S. Bahri, *J. Nat. Rubber. Res*., **1994**, *9*, 70.

****

Chapter 2

==========

Functionalization of Polyoxovanadate Clusters by Rare Earth Metal Ions: Syntheses, Characterization, Magnetic and Thermal Properties

==========

2.1. Introduction

The synthesis of novel materials with interesting physical and chemical properties, especially towards magnetic, electronic and conductive applications is a challenging task in modern inorganic chemistry.[1] These materials may be constructed either by supramolecular or covalent interactions using a well-defined building block. A minimum criterion / requirement for a molecule to become a material is its stability towards external stimulus factors, e.g., light, heat etc. Thermal stability for a material is of prime importance, because practical applications (e.g., host guest properties, catalysis, sensing) require elevated temperatures in most cases. To achieve a considerable thermal stability, meaningful contacts / connections are essential in this approach of "molecule to material". Polyoxometalate (POMs) clusters have been proved to be potential building units to obtain a range of materials of numerous applications in the field of material chemistry.[2] This is because POMs are generally metal-oxide based clusters that can be generated simply from an aqueous solution and have well-defined topologies.[3] Indeed, how a POM cluster / molecule goes to a material is a major subject of research in modern materials chemistry and numerous publications appeared in this regard in recent time.[4] Polyoxovanadates (henceforth will be called as POVs) comprise of an important class of POMs that have received considerable attention because of their diverse topologies, structural, electronic properties, and versatile industrial applications, e.g., in catalysis and materials science (e.g., as cathodes in lithium batteries).[5] The catalysis, driven by the POVs, is accelerated by the facile change of oxidation states of vanadium center (V^V can

be converted to V^{IV} and vice versa). Among POVs, a major subclass is V/As/O heteropoly system that is not as explored as V O (or) V P O system.[6] In general, V/As/O heteropoly system can be divided into five different groups based on the number of As and V atoms present in these clusters.[7] (i) $[As_6V_{15}O_{42}]^n$, (ii) $[As_8V_{14}O_{42}]^n$, (iii) $[As_8V_{12}O_{40}]^n$, (iv) $[As_2V_{10}O_{26}]^n$, and (v) $[As_8V_6O_{26}]^n$. Compounds of (i) and (ii) types are extremely popular as far as magnetic materials are concerned. It was discussed that these compounds should mimic the properties of bulk magnet. In the single molecular magnets series, the oxovanadate systems have attracted considerable interest.[8] The investigations of magnetic properties of compounds V15 and V14 have demonstrated how magnetic susceptibility and EPR spectra can allow a reasonably detailed understanding of the preferred spin arrangement in high nuclearity spin clusters using variable temperature parameter.[9]

The current chapter deals with the linking propensity of well studied water encapsulated POV cluster $[As_6V_{15}O_{42}(H_2O)]^6$ and sulfite anion encapsulated POV cluster $[As_8V_{14}O_{42}(SO_3)]^6$ towards lanthanide cation. Since our intention is to achieve a stable material from this POV cluster, we intended to avoid "metal-coordination complexes with organic ligands" as linkers / connectors. The literature on polymeric POMs / POVs (one-dimensional, two-dimensional or three-dimensional networks), that are connected through rare earth metal ions, d-block transition metal ion / coordination complex cations are numerous.[10,11] Even though, V15 and V14 heteropoly system based coordination polymer that is free of organic moieties are not studied earlier to the best of our knowledge.

2.2. Experimental Section

2.2.1. Materials

The lanthanides were purchased from Across / Loba and used as such. The distilled water was used throughout the experiments. All other chemicals were of laboratory grade available commercially and were used as received. The POV precursor compound $[H_6As_6V_{15}O_{42}(H_2O)]\cdot 9H_2O$ (**1**) was synthesized by slightly modifying the reported procedure.[12a] and $[NH_4]_6[As_8V_{14}O_{42}(SO_3)]$ was prepared by exactly following the reported procedure without any further modifications.[12b]

2.2.2. Physical Measurements

All the synthesized compounds were characterized by usual spectroscopic methods. Infrared spectra were recorded by using KBr pellets on a JASCO-5300 FT-IR spectrophotometer. The UV-visible spectra were measured using a 3101 Philips spectrophotometer. The solid powders of compounds were spreaded over a black background disk and the diffuse reflectance spectra obtained were the Kubelka-Munk corrected with black disk background. Micro-analytical (C, H, N and S) data were obtained with Perkin-Elmer Model 240C elemental analyzer and FLASH EA 1112 Series CHNS analyzer. The Powder X-ray diffraction spectra were recorded using Cu-Kα (λ = 1.54 Å) radiation on a Phillips PW 3710 diffractometer at a scanning speed of 3^o min^{-1}. The TGA / Mass analyses were performed on a NETZSCH – STA 409PC with NETZSCH-QMS 403C (Aëolos) mass setup at a scan rate of 5^oC min^{-1}. ESR spectra were recorded on a Bruker ECS 106 spectrometer. Inductively Coupled Plasma (ICP) analyses were carried out on JY ULTIMA spectrometer.

2.2.3. Synthesis and Characterization

The majority of the POM / POV – supported metal complexes with multi dimensional structures, reported earlier, have been synthesized by hydrothermal

techniques.[10h v] We have isolated the following compounds at room temperature and characterized crystallographically.

$[H_6As_6V_{15}O_{42}(H_2O)] \cdot 9H_2O$ (**1**)

$[\{La(H_2O)_7\}_2(As_6V_{15}O_{42}(H_2O)] \cdot 12H_2O$ (**2**)

$[\{Sm(H_2O)_7\}_2(As_6V_{15}O_{42}(H_2O)] \cdot 13HO$ (**3**)

$[\{Ce(H_2O)_7\}_2(As_6V_{15}O_{42}(H_2O)] \cdot 11H_2O$ (**4**)

$[\{\{Ce(H_2O)_5\}_6As^{v}V_{12}{}^{v}O_{38}\}(V_6{}^{iv}V_6{}^{v}As_8O_{40}(NO_3))(V_7{}^{iv}V_5{}^{v}As_8O_{40}(NO_3))] \cdot 52H_2O$ (**5**)

$[\{La(H_2O)_6\}_2(As_8V_{14}O_{42}(SO_3)] \cdot 8H_2O$ (**6**)

$[\{Sm(H_2O)_6\}_2(As_8V_{14}O_{42}(SO_3)] \cdot 8H_2O$ (**7**)

$[\{Ce(H_2O)_6\}_2(As_8V_{14}O_{42}(SO_3)] \cdot 8H_2O$ (**8**)

We introduced a new technique (a controlled synthesis), called "U-tube-synthesis" to isolate the crystalline products of compounds **2** **8**. Even though the reaction (equation 1 and 2) to obtain these compounds looks simple, the mixing of both reactants in an aqueous medium invariably results in the immediate formation of brown precipitate,

$$[H_6As_6V_{15}O_{42}(H_2O)] + 2Ln(NO_3)_3 \xrightarrow{H_2O} [\{Ln(H_2O)_7\}_2As_6V_{15}O_{42}(H_2O)] + 6HNO_3 \quad (1)$$

Where Ln = La^{3+} (**2**), Sm^{3+} (**3**) and Ce^{3+} (**4**)

$$[NH_4]_6[As_8V_{14}O_{42}(SO_3)] + 2Ln(NO_3)_3 \xrightarrow{H_2O} [\{Ln(H_2O)_6\}_2As_8V_{14}O_{42}(SO_3)] + 6NH_4NO_3 \quad (2)$$

Where Ln = La^{3+} (**6**), Sm^{3+} (**7**) and Ce^{3+} (**8**)

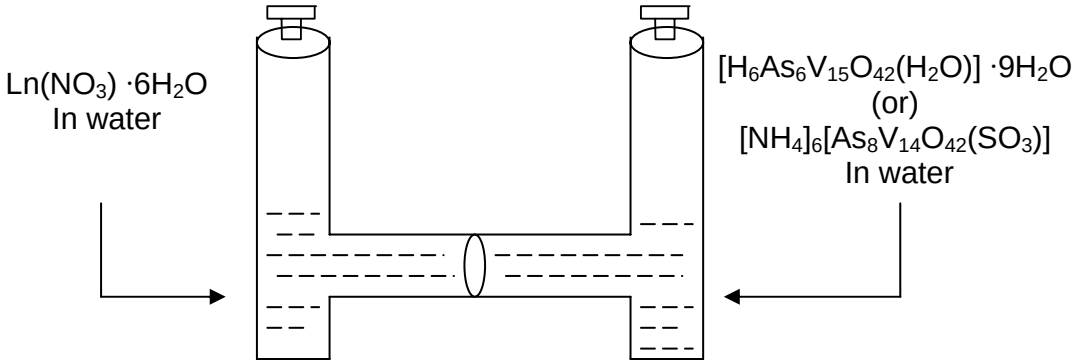

Scheme 1. U-tube-synthesis apparatus setup

which could not be characterized by single crystal X-ray structure determination technique. We, thus, performed the synthesis using slow mixing technique called "U-tube-synthesis". The schematic representation of this technique is shown in Scheme 1. Two branches of U–shaped tube were separated by G4 crucible bead. The dissolved reactant components in water were taken in two branches of the U-tube (as shown in above) to mix slowly and single crystals, suitable for X-ray structure determination, were formed on the side wall of the U – tube. These crystals were collected and washed with cold water.

$[H_6As_6V_{15}O_{42}(H_2O)] \cdot 9H_2O$ (1)

Compound **1** was synthesized by following the reported procedure with slight modifications.[12a] To a 100 mL of aqueous solution at 85^{o}C, 3.62 g of $NaVO_3$ (29.71 mmol) and 1.42 g of As_2O_3 (7.18 mmol) were added. After 5 10 minutes, 0.71 g (17.75 mmol) of NaOH pellets were added, then the flask was covered by a watch glass. The resulting reaction mixture was stirred for half an hour. Afterwards 2.50 g (19.21 mmol) of $N_2H_4.H_2SO_4$ was added stepwise and stirring was continued another 15 minutes. The resulting reaction mixture was filtered and kept open for crystallization.

After 10 days settled brown block colored crystals were filtered and washed with very little amount of cold water. The crystals were dried and used as starting precursor for the preparation of compounds **2** **5**.

Selected data for **1**: IR (KBr pellet) (υ/cm^{-1}) 3327(s), 1589(m), 1520(m), 1089(s), 972(s), 709(m), 630(s).

[{La(H_2O)$_7$}$_2$($As_6V_{15}O_{42}$(H_2O)] 12H_2O (2)

0.2 g of (0.10 mmol) compound **1** was dissolved in 10 mL of H_2O and the resulting solution taken in one branch of U-shape tube (see Scheme 1). The other branch was filled by 10 mL of H_2O in which 0.405 g of $La(NO_3)_3 \cdot 6H_2O$ (0.94 mmol) was dissolved. The two branches of U- shape tube were separated by a G4 crucible bead. After one week, crystals thus obtained, were separated out and washed thoroughly with water and one of the single crystals suitable for X-ray diffraction study was selected and characterized structurally.

Selected data for **2**: IR (KBr pellet) (υ/cm^{-1}) 3368(br), 1622(s), 987(s), 727(m), 634(m), 462(m).

[{Sm(H_2O)$_7$}$_2$($As_6V_{15}O_{42}$(H_2O)] ·13H_2O (3)

0.2 g of (0.10 mmol) compound **1** was dissolved in 10 mL of H_2O and the resulting solution taken in one branch of U-shape tube. The other branch was filled by 10 mL of H_2O in which 0.463 g of $Sm(NO_3)_3 \cdot 6H_2O$ (1.04 mmol) was dissolved. The two branches of U shape tube were separated by a G4 crucible bead. After one week formed crystals were separated out and washed thoroughly with water and one of the single crystals suitable for X-ray diffraction study was selected and characterized structurally.

Selected data **3**: IR (KBr pellet) (υ/cm^{-1}) 3400(br), 1612(s), 1388(s), 1346(s), 978(s), 831(m), 671(m), 597(m).

$[\{Ce(H_2O)_7\}_2(As_6V_{15}O_{42}(H_2O)] \cdot 11H_2O$ (4)

0.2 g of (0.10 mmol) compound **1** was dissolved in 10 mL of H_2O and the resulting solution taken in one branch of U-shape tube. The other branch was filled by 10 mL of H_2O in which 0.35 g of $Ce(NO_3)_3$. $6H_2O$ (0.81 mmol) was dissolved. The two branches of U- shape tube were separated by a G4 crucible bead. After one week, crystals, thus formed, were separated out and washed thoroughly with water and one of the single crystals suitable for X-ray diffraction study was selected and characterized structurally.

Selected data for **4**: IR (KBr pellet) (υ/cm^{-1}) 3368(br), 1618(m), 1458(m), 991(m), 721(m), 613(m), 430(m).

$[\{\{Ce(H_2O)_5\}_6As^{v}V_{12}{}^{V}O_{38}\}(V_6{}^{iv}V_6{}^{v}As_8O_{40}(NO_3))(V_7{}^{iv}V_5{}^{v}As_8O_{40}(NO_3))] \cdot 52H_2O$ (5)

0.2 g of (0.10 mmol) compound **1** was dissolved in 10 mL of H_2O and the resulting solution taken in one branch of U-shape tube. The other branch was filled by 10 mL of H_2O in which 0.4 g of $(NH_4)_2Ce(NO_3)_6$ (0.73 mmol) was dissolved. The two branches of U- shape tubes were separated by a G4 crucible bead. After two weeks formed green colored crystals were separated out and washed thoroughly with water and one of the single crystals suitable for X-ray diffraction study was selected and characterized structurally.

Selected data for **5**: IR (KBr pellet) (υ/cm^{-1}) 3371(br), 1610(s), 1392(s), 1344(s), 989(s), 931(s), 831(s), 677(s), 596(s), 420(s)

[{La(H$_2$O)$_6$}$_2$As$_8$V$_{14}$O$_{42}$(SO$_3$)] ·8H$_2$O (6)

The starting precursor [NH$_4$]$_6$[As$_8$V$_{14}$O$_{42}$(SO$_3$)] (0.30 g, 0.14 mmol) was dissolved in 5 mL of H$_2$O taken in one branch of U-shape tube. The other branch of the U tube was filled by 5 mL of H$_2$O in which of 0.4 g of La(NO$_3$)$_3$·6H$_2$O (0.92 mmol) was dissolved. The two branches of U- shape tube were separated by G4 crucible bead. After one week, single crystals were separated out and washed thoroughly with water and one of the single crystals from each, suitable for X-ray diffraction study, was selected and characterized structurally. The purity of the bulk crystals was checked by X-ray powder diffraction methods. Yield: 0.12 g (32% based on ammonium salt of vanadium cluster, the starting precursor) Anal. calcd for As$_8$V$_{14}$SLa$_2$H$_{40}$O$_{65}$: H, 1.49; S, 1.18; V, 26.39; As, 22.18; La, 10.28. Found: H, 1.47; S, 1.19; V, 26.32 (ICP); As, 22.07 (ICP); La, 9.98 (ICP). Selected data for **6**: FT-IR (KBr pellet) (υ/cm^{-1}): υ(O-H) 3395 (w); (H-O-H bending) 1620; (V=O) 984, 941; (SO_3^2) 902 (m); (As-O) 687 (m).

[{Sm(H$_2$O)$_6$}$_2$As$_8$V$_{14}$O$_{42}$(SO$_3$)] 8H$_2$O (7)

The starting precursor [NH$_4$]$_6$[As$_8$V$_{14}$O$_{42}$(SO$_3$)] (0.30 g, 0.14 mmol) was dissolved in 5 mL of H$_2$O taken in one branch of U-shape tube. The other branch of the U tube was filled by 5 mL of H$_2$O in which of 0.41 g of Sm(NO$_3$)$_3$·6H$_2$O (0.92 mmol) was dissolved. The two branches of U- shape tube were separated by G4 crucible bead. After one week, single crystals were separated out and washed thoroughly with water and one of the single crystals from each, suitable for X-ray diffraction study, was selected and characterized structurally. The purity of the bulk crystals was checked by X-ray powder diffraction methods. Yield: 0.10 g (27% based on ammonium salt of vanadium cluster, the starting precursor). Anal. calcd for As$_8$V$_{14}$SSm$_2$H$_{40}$O$_{65}$: H, 1.48; S, 1.17; V, 26.16; As, 21.99; Sm, 11.03. Found: H, 1.42; S, 1.29; V, 25.89 (ICP); As, 22.17 (ICP); Sm, 10.88 (ICP) Selected data for **7**: FT-IR (KBr pellet) (υ/cm^{-1}): (O-H) 3383 (w); (H-O-H bending) 1618; (V=O) 978, 945; (SO_3^{2-}) 904(m); (As-O) 686 (m).

[{Ce(H$_2$O)$_6$}$_2$As$_8$V$_{14}$O$_{42}$(SO$_3$)] 8H$_2$O (8)

The starting precursor [NH$_4$]$_6$[As$_8$V$_{14}$O$_{42}$(SO$_3$)] (0.30 g, 0.14 mmol) was dissolved in 5 mL of H$_2$O taken in one branch of U-shape tube. The other branch of the U tube was filled by 5 mL of H$_2$O in which 0.40 g of Ce(NO$_3$)$_3$ 6H$_2$O (0.92 mmol) was dissolved. The two branches of U- shape tube were separated by G4 crucible bead. After one week, single crystals were separated out and washed thoroughly with water and one of the single crystals from each, suitable for X-ray diffraction study, was selected and characterized structurally. The purity of the bulk crystals was checked by X-ray powder diffraction methods. Yield 0.12 g (32% based on ammonium salt of vanadium cluster, the starting precursor). Anal. calcd for As$_8$V$_{14}$SCe$_2$H$_{40}$O$_{65}$: H, 1.49; S, 1.19; V, 26.36; As, 22.16; Ce, 10.36. Found: H, 1.45; S, 1.18; V, 26.55 (ICP); As, 22.38 (ICP); Ce, 10.02 (ICP). Selected data for **8**: FT-IR (KBr pellet) (υ/cm^{-1}): (O-H) 3400 (w); (H-O-H bending) 1618; (V=O) 979, 941; (SO_3^{2-}) 904 (m); (As-O) 688 (m).

2.2.4. Single Crystal Structure Determination

Single crystal X-ray data for all compounds were measured on a Bruker SMART APEX CCD area detector system [λ(Mo Kα) = 0.71073 Å], graphite monochromator, 2400 frames were recorded with an ω scan width of 0.3°, each for 5 second, a crystal detector distance of 60 mm, and a collimator of 0.5 mm. The data were reduced using SAINTPLUS,[13a] the structures were solved using SHELXS-97,[13b] and refined using SHELXL-97.[13c] DIAMOND[14] software was used for molecular graphics. All non hydrogen atoms were refined anisotropically. We tried to locate the hydrogen atoms of solvent water molecules through differential Fourier maps, but couldn't succeed. Hydrogen bonding interactions were discussed based on respective D···A contacts. A summary of the crystallographic data and structure determination parameters for **1–8** is provided in Tables 2.1, 2.2 and 2.3.

2.3. Results and Discussion

2.3.1. Infrared Spectroscopy

All compounds **1** **8** are characterized by IR bands appeared around 941 991 cm^{-1} due to the V=O stretching vibration and stretching in the range of 613 686 cm^{-1} is most likely due to As O stretching. The IR stretching in the region of 3327 3400 cm^{-1} is due to the O H stretching. The bands at 1612 1622 cm^{-1} are due to the H O H bending. The peak around 902 904 is corresponding to the encapsulated SO_3^{2} for compounds **6** **8**.

2.3.2. Electronic Spectroscopy

The diffuse reflectance spectra of compounds **1** **4** are recorded at room temperature, are presented in Figure 2.1(a). All Compounds show broad feature in the region of 650 700 nm, that can be assigned to d d transitions for $V^{4+}(d^1)$ ion. The sharp band around 350 nm is due to the LMCT (O→V) transition. The strong transitions in the region of 200 360 nm are due to the O→V, ligand to metal charge transfer (LMCT).

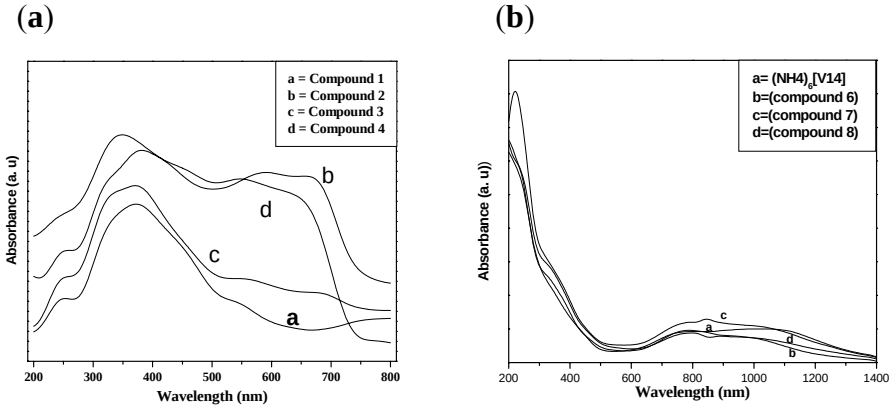

Figure 2.1. Solid state diffuse reflectance spectra: (a) for compounds **1** **4**; (b) for compounds **6** **8**.

The diffuse reflectance spectra of compounds **6 8** are recorded at room temperature, are presented in Figure 2.1(b). All Compounds show a broad feature in the region of 700 – 1100 nm, and two more additional peaks in the region of 200 360 nm. The broad peak around 1100 nm, are assigned to d d transitions for $V^{4+}(d^1)$ ion. The sharp band around 350 nm is due to the LMCT (O→V) transition. Similar transitions are observed in the electronic spectra for other related compounds.[15] A weak feature is clearly observed around 800 nm in the electronic spectrum of compound $[\{Sm(H_2O)_6\}_2As_8V_{14}O_{42}(SO_3)]$ $8H_2O$ (**7**) (inset picture of Figure 2.1(b)), which can be assigned to f f transition of Sm^{3+} ion.

2.3.3. EPR Spectroscopy

The EPR spectra of compounds **2 4**, and **6 8** in the solid state were recorded at -150°C, are shown in Figure 2.2

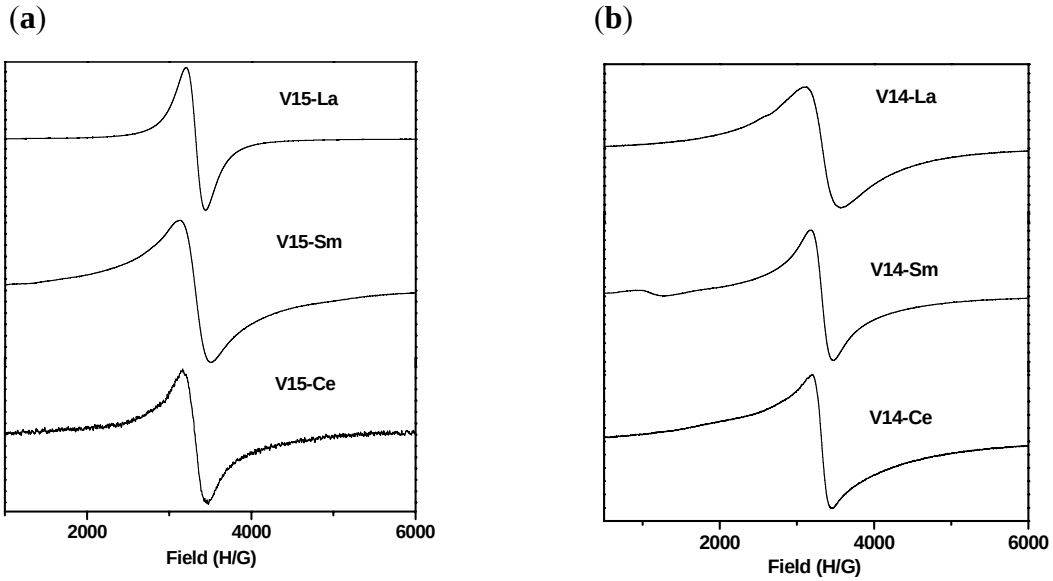

Figure 2.2. EPR spectra of powdered samples at 150°C in the solid state:
(a) compounds **2 4**; (b) compounds **6 8**.

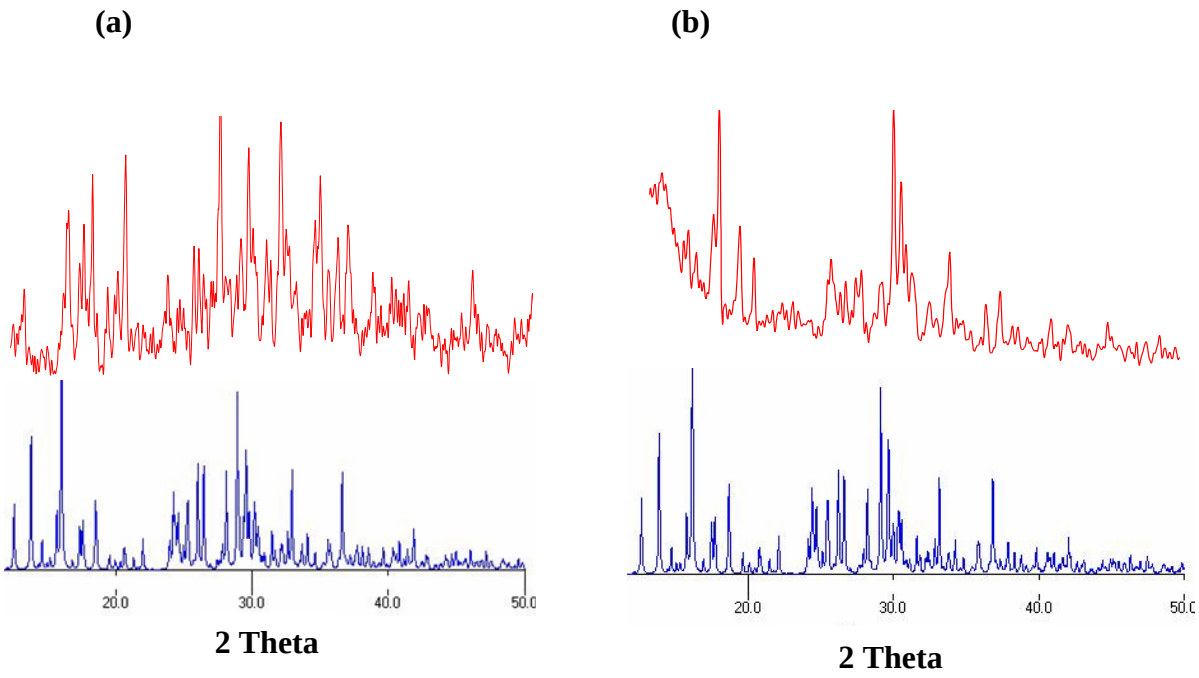

Figure 2.3. Experimentally obtained X-ray powder diffraction patterns (top) and computer-generated simulated patterns using the single crystal X-ray data (down) of compounds **6** **8**: (a) compound **6**; (b) compound **7**; (c) compound **8**.

The single line ESR signals (except the spectrum of compound **7**) at g = 1.952 for **2**, g = 1.955 for **3**, g = 1.960 for **4**, g = 1.967 for **6**, g = 1.967 for **7**, and g = 1.970 for **8** confirm that the vanadium atoms, present in the compounds **2** **4**, and **6** **8** are in +4 oxidation states. In the case of compound **7**, an additional feature is observed at g = 5.924, due to the presence of Sm^{3+} ion.

2.3.4. Powder X-ray Diffraction (PXRD)

The powder X-ray diffraction spectra of compounds **6** **8** have been recorded, and their diagrams are presented in Figures 2.3. The computer simulated patterns were obtained by using the single crystal X-ray data for the compounds **6** **8** and these match very well with respective experimentally observed patterns. This confirms the homogeneity and the phase purity of the bulk samples of **6** **8**.

2.3.5. Thermogravimetric / Mass Analyses (TGA / Mass)

The thermogravimetric analyses of all compounds were performed in flowing N_2 with a heating rate of $5^oC\ min^{-1}$ in the temperature range of 30 1100^{o}C. The compounds **2** **4** are isostructural and consequently compound **4** is selected as representative sample for TGA studies. The typical TG curve shows two sharp weight losses (Figure 2.4(a)). The first weight loss of 14.33% in the range of 30 200^{o}C is due to the loss of 21 water molecules (eleven lattice water molecules, one cluster encapsulated water molecule and nine cerium coordinated water molecules) per formula unit. The second weight loss 19.81% in the temperature region of 300 500^{o}C is assigned for the decomposition of structure.

Compound **5** is highly hydrated (contains fifty three lattice water molecules per formula unit) and hence there is a possibility of loosing few number of lattice water molecules in room temperature itself. The TG plot of compound **5** (Figure 2.4(b)) shows

first weight loss 15.41% is due to the loss of 64 water molecules (calculated mass loss for 64 water molecules is 15.42%). The second weight loss of 17.10% is due to the evolution of H_2O, N_2O and NO molecules. The evolutions of gaseous molecules are evidenced by corresponding mass loss curves (Figure 2.4(b)) as shown in different colors.

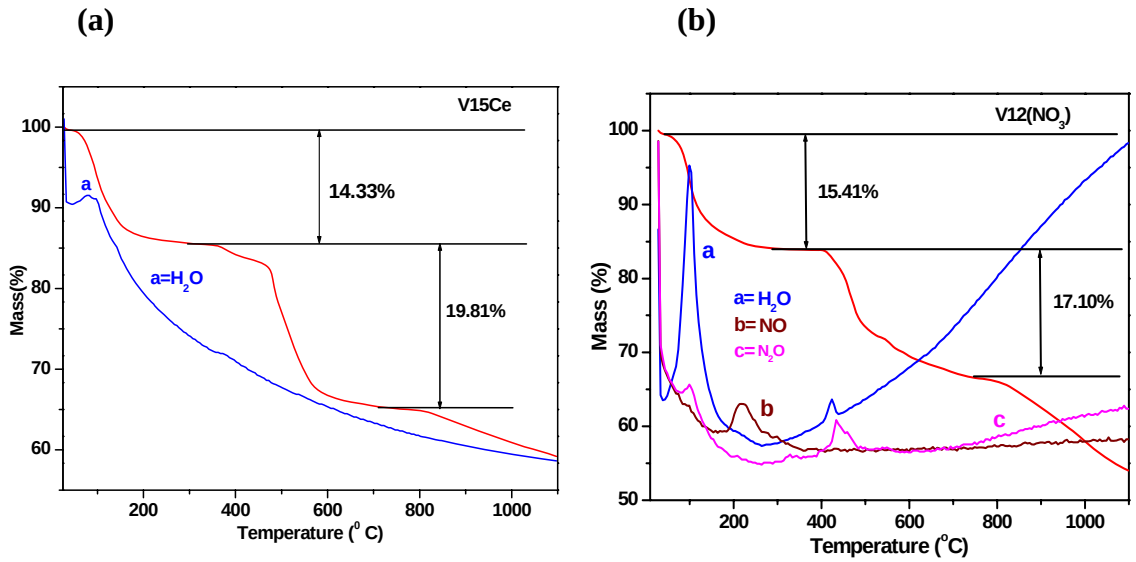

Figure 2.4. TGA / Mass plots: (a) compound **4**; (b) compound **5**. Color code: TGA curve, red line; water mass loss curve, blue line; nitric oxide loss curve, brown; nitrogen dioxide, purple.

Thermal Studies: How linking of the POV Cluster Anion with Lanthanide-aqua Complex Cations Offer Extra-stability

The discrete cluster $[NH_4]_6[As_8V_{14}O_{42}(SO_3)]$ (starting precursor) was synthesized from the reported procedure[12b] and the TG curve of this shows the first weight loss of 5.18%, which corresponds to the loss of 6 ammonium cations per formula unit in the temperature range 35 – 134°C (calculated mass loss for six ammonium ion is 4.97%). The major loss observed in the temperature range of 480 – 520°C is due to the removal of encapsulated SO_3 molecule as SO_2 gas, followed by the cluster decomposition. The evolution of SO_2 gas at this temperature is evidenced by the TGA / Mass curve as shown

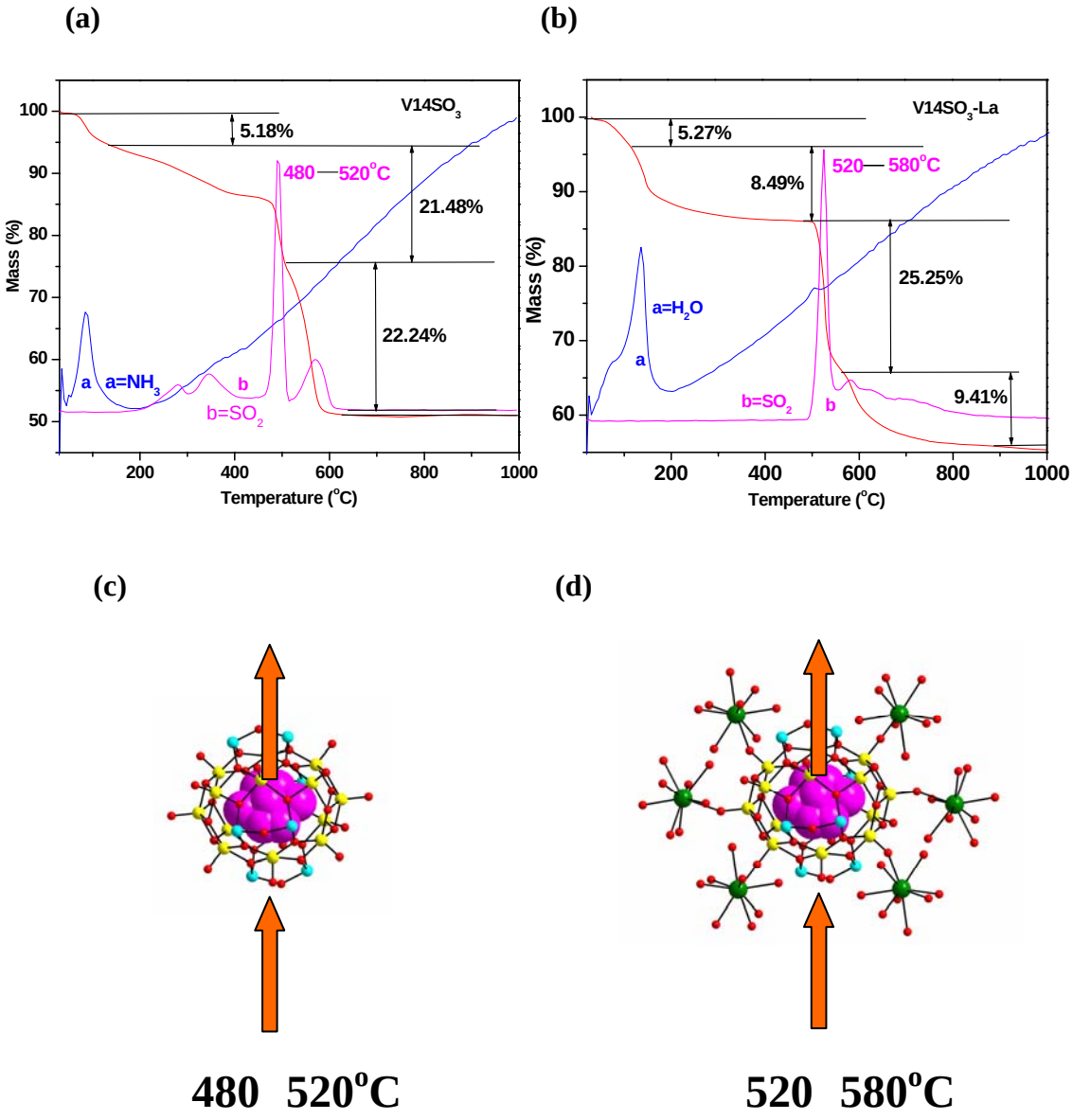

Figure 2.5. (a) TGA / Mass plot of the starting precursor $[NH_4]_6[As_8V_{14}O_{42}(SO_3)]$; (b) TGA / Mass plot of the compound $[\{La(H_2O)_6\}_2As_8V_{14}O_{42}(SO_3)]\ 8H_2O$ (**6**); (c) The pictureoral representation of the evolution of sulfur trioxide (as exclusion of SO_2 gas) which is encapsulated in the cavity of the cluster anion, $[As_8V_{14}O_{42}]^4$ in the starting precursor $[NH_4]_6[As_8V_{14}O_{42}(SO_3)]$; (d) The schematic representation of the evolution of sulfur trioxide (as exclusion of SO_2 gas) which is encapsulated in the cavity of the cluster anion, $[As_8V_{14}O_{42}]^4$ in compound $[\{La(H_2O)_6\}_2As_8V_{14}O_{42}(SO_3)]\cdot 8H_2O$ (**6**).

in Figure 2.5(a). The TGA / Mass curve for compound $[\{La(H_2O)_6\}_2As_8V_{14}O_{42}(SO_3)]$ $8H_2O$ (**1**) is shown in Figure 2.5(b). This can be divided into four stages. The first weight loss of 5.27% is assigned due to the loss of eight lattice water molecules (see formula of compound **6)** in the temperature range 35 – 128°C (calculated mass loss is 5.33% for eight water molecules). The observed second weight loss of 8.49% should be due to the loss of twelve lanthanum coordinated water molecules that occur in the temperature range of 128 500°C (calculated mass loss is 7.99% for twelve water molecules). The third and fourth mass losses of 22.25% and 9.41% respectively in the temperature range of 500 – 1050°C are due to the decomposition of encapsulated sulfur trioxide (as exclusion of SO_2 gas) and $\{V_{14}\}$ cluster decomposition respectively. The identification of sulfur dioxide was elucidated by the mass of SO_2 gas in the TGA / Mass curve (Figure 2.5(b)) that particularly occurs in the temperature range of 520 – 580°C. Thus, in compound **6**, the structure decomposition is observed in the temperature range of 520 – 580°C, but the same decomposition of the discrete ammonium cluster occurs in the temperature range of 480 – 520°C. We believe that this elevation in the decomposition temperature of compound **6** (in comparison with discrete cluster compound) has been achieved because of the following reasons: (i) the compounds **6 8** are organic free framework material; (ii) in the framework, each cluster anion exhibits hexa-coordination with its surrounding six different lanthanum cations leading to a two-dimensional coordination polymer that offer extra-stability to the $\{V_{14}\}$ cluster anion; (iii) the cluster anion is involved in forming a supramolecular hydrogen bonded three-dimensional network that also provides extra-thermal stability; and (iv) encapsulated sulfur trioxide anion, that is found to interact with inner wall of the cluster anion, may offer more rigidity to the cluster anion. In order to check, whether the first two weight losses in the TG curve (Figure 2.5(b)) are due the loss of water molecules, we performed TG experiments with preheated samples of compound **6**. The sample, obtained by heating at 200°C for 3 hours, shows first loss 6.12% in the temperature range 35 – 176°C, that correspond to the loss of nine water molecules per

formula unit. (calculated mass loss is 5.99% for nine water molecules).We believe that these water molecules are lanthanum-coordinated water molecules. There are total twelve lanthanum coordinated water molecules per formula unit; probably three of these got lost

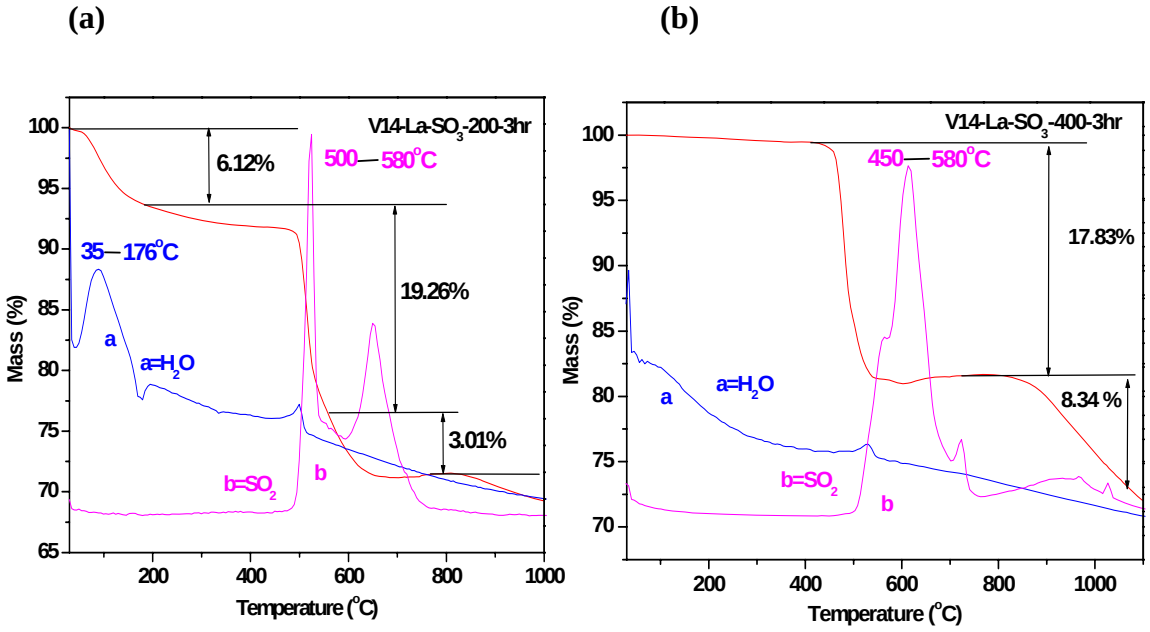

Figure 2.6. TGA / Mass plot of preheated compound **6** (a) at 200°C 3hr (b) at 400°C 3hr. Color code: TGA curve, red line; water mass loss curve, blue line; sulfur dioxide mass loss curve, purple line.

with solvent water molecules from the crystal lattice during pre-heating at 200°C. The second and third losses of 19.26% and 3.01% are due to the loss of encapsulated sulfur trioxide molecule (as SO_2 gas) followed by the structural decomposition. The corresponding TGA graph has been shown in the Figure 2.6(a). The preheated sample at 400°C for 3 hours shows the weight loss in two steps. The first loss of 17.83% in the temperature range 450 580°C is due to the loss of encapsulated SO_3^{2} (confirmed by the mass of released SO_2 gas) and second loss of 8.34% is due to the cluster decomposition. The relevant TGA graph is shown in the Figure 2.6(b).

The compounds **6-8** are isostructural, and hence show the identical TGA / Mass spectra and exhibit similar type of weight losses. The TGA / Mass curve for compound **7** can be divided in four stages. The experimentally observed first weight loss of 5.58% is assigned due to the loss of eight lattice water molecules in the temperature range 35 – 139^{o}C (calculated mass loss is 5.28% for eight water molecules). The observed second weight loss of 7.90% should be due to the loss of twelve samarium-coordinated water molecules per formula unit that occur in the temperature range of 139 – 500^{o}C. (calculated mass loss is 7.92% for twelve water molecules per formula unit of **7**). The third and fourth mass losses of 23.24% and 6.90% respectively in the temperature range of 500 – 1075^{o}C are due to the decomposition of encapsulated sulfur trioxide (as exclusion of SO_2 gas) and $\{V_{14}\}$ cluster decomposition respectively. The identification of sulfur dioxide was elucidated by the mass of SO_2 gas in the TGA / Mass curve (Figure 2.7(a)) that particularly occurs in the temperature range of 515 580^{o}C. The TGA / Mass curve for compound **8** can also be divided in four stages. The first mass loss 5.22% corresponds to the loss of eight water molecules (the calculated mass loss for eight water molecules is 5.32%). The second weight loss of 7.48% should be due to the loss of twelve, cerium coordinated water molecules per formula unit that occur in the temperature range of 141 500^{o}C (calculated mass loss is 7.98% for twelve water molecules). The third and fourth mass losses of 23.12% and 8.36% respectively in the temperature range of 500 – 1000^{o}C are due to the decomposition of encapsulated sulfur trioxide (as exclusion of SO_2 gas) and $\{V_{14}\}$ cluster decomposition respectively. The identification of sulfur dioxide was again elucidated by the mass of SO_2 gas in the TGA / Mass curve (Figure 2.7b) that occurs in the temperature range of 520 – 580^{o}C. Thus thermogravimetric analyses indicate that this series of compounds has a significant amount of thermal stability in the solid state.

(a) **(b)**

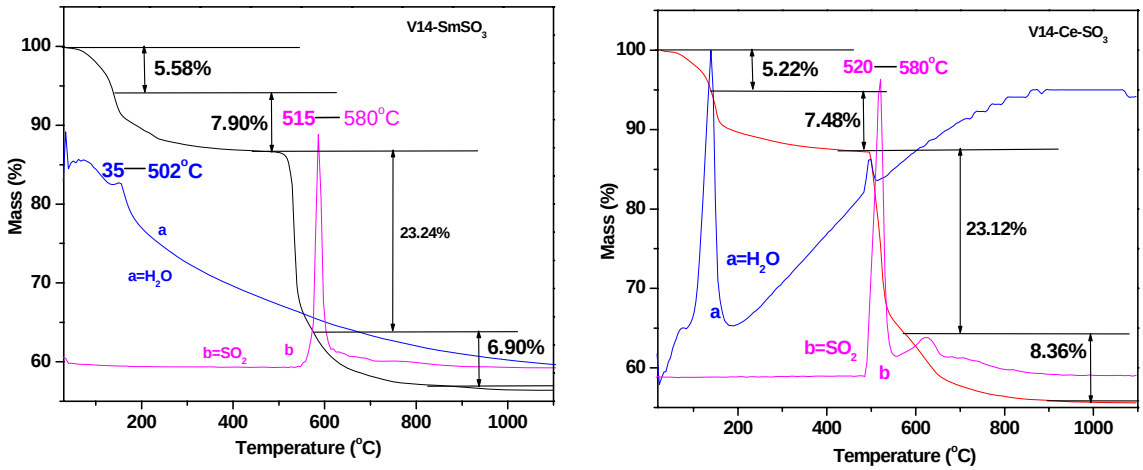

Figure 2.7. (a) TGA / Mass plot of compound **7**; (b) TGA / Mass plot of the compound **8**. Color code: TGA curve, red line; water mass loss curve, blue line; sulfur dioxide mass loss curve, purple line.

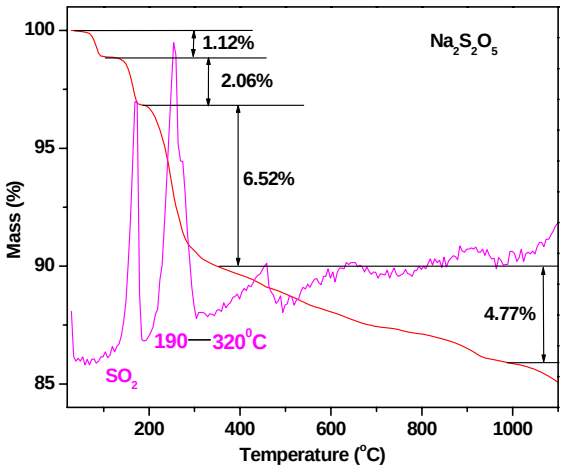

Figure 2.8. TGA / Mass curve for Sodium bisulfite. Color code: TGA curve, red line; sulfur dioxide mass loss curve, purple line.

Sulfite Anion: Inclusion versus Exclusion

In the present series of compounds **6** **8**, the sulfite anion is found to be completely encapsulated in the cavity of the cluster anion $[As_8V_{14}O_{42}]^4$ giving rise to a sulfite encapsulated cluster anion $[As_8V_{14}O_{42}(SO_3)]^6$. It would be interesting to see, how a metal-oxide based rigid cluster cage protects the encapsulated guest against an external force, for example thermal energy. Albeit, an anion inclusion in the cavity of a POV cluster anion is long known, so far, no attempts have been taken to explore the stability of an anion in terms of its inclusion versus exclusion. As shown in Figure 2.5 the decomposition of encapsulated sulfur trioxide is found to occur in the temperature range of 480 – 520°C for the discrete cluster anion and 520 – 580°C for linked system (vide supra). In order to understand the role of cluster cage to protect its incorporated sulfite anion against high temperature, we performed the TGA / Mass studies of bare $NaHSO_3$. As shown in the TGA / Mass plot of bare $NaHSO_3$ (Figure 2.8), complete loss of sulfite as SO_2 gas is found to occur in the temperature range to 190 – 320°C. This clearly indicates that POV cluster anion $[As_8V_{14}O_{42}]^4$ offers substantial protection towards its encapsulated sulfite anion.

2.3.6. Magnetism

The variable temperature magnetic susceptibility of compounds $[\{Sm(H_2O)_6\}_2As_8V_{14}O_{42}(SO_3)]$ $8H_2O$ (**7**) and $[\{Ce(H_2O)_6\}_2As_8V_{14}O_{42}(SO_3)]$ $8H_2O$ (**8**) was measured between 2 to 300 K. Figures 2.9(a) and 2.9(b) show the magnetic behaviors of compounds **7** and **8** in the form of $_M$ versus T and the product $_M$T versus T plots. The $_M$T values of compounds **7** and **8** at 300 K are 3.76 cm^3 K mol^{-1} (5.49 $_B$) and 4.35 cm^3 K mol^{-1} (5.90 $_B$) respectively, which are considerably smaller than those expected for the total spin-only value 5.25 cm^3 K mol^{-1} (6.48 $_B$), that corresponds to the presence of 14 non-interacting V^{4+} ions with S = 1/2. However, these room temperature

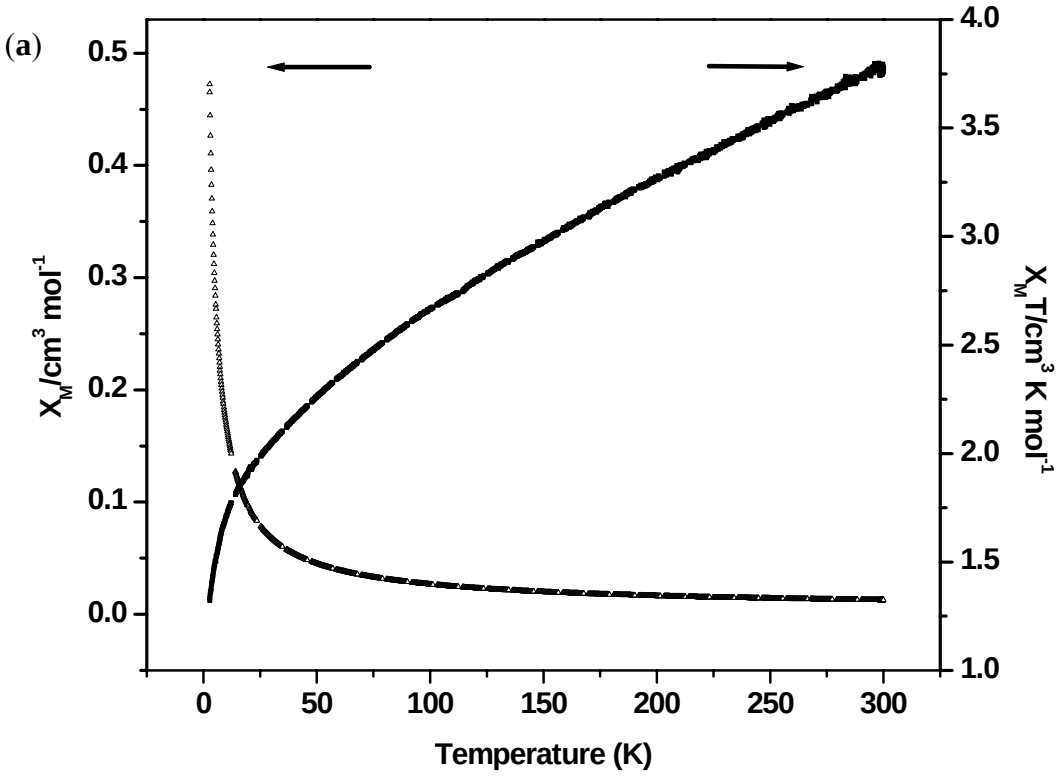

Figure 2.9(a) Temperature dependences of $_M$ (Δ) and $_M$T ( ) of [{Sm(H$_2$O)$_6$}$_2$As$_8$V$_{14}$O$_{42}$(SO$_3$)] 8H$_2$O (**7**).

values (3.76 cm^3 K mol^{-1} for compound **7** and 4.35 cm^3 K mol^{-1} for compound **8**) are relatively higher significantly higher than the room temperature $_M$T value (2.48 cm^3 K mol^{-1}; 4.45 $_B$) of the discrete compound [NH$_4$]$_6$[As$_8$V$_{14}$O$_{42}$(SO$_3$)].[9a] This obviously indicates that the linkers Sm^{3+} ion (4f^5, S = 5/2) and Ce^{3+} ion (4f^1, S = 1/2) contribute to the overall magnetic susceptibilities of compounds **7** and **8** respectively at room temperature. There are two lanthanide ions per POV cluster anion [As$_8$V$_{14}$O$_{42}$(SO$_3$)]^6 in these compounds.

Sm^{3+} has larger experimental value of $_{obsd}$ (1.5-1.6 $_B$) compared to its expected / theoretical value of $_J$ (0.85 $_B$; 0.09cm^3 K mol^{-1}) at 298 K.[16] For compound **7**, if we add the room temperature (experimental) contribution from Sm^{3+} ion (e.g., 1.6 $_B$; 0.32 cm^3 K mol^{-1} per Sm^{3+}) to the experimentally obtained room temperature $_MT$ value of discrete compound $[NH_4]_6[As_8V_{14}O_{42}(SO_3)]$ (2.48 cm^3 K mol^{-1}; 4.45 $_B$),[9a] the resulting calculated $_MT$ value of 3.12 (2.48+ 0.32 + 0.32) cm^3 K mol^{-1} is somewhat smaller than the experimentally obtained $_MT$ value (3.76 cm^3 K mol^{-1}) of samarium compound **7** at room temperature indicating a weak interaction between the linkers (Sm^{3+} ions) and V(IV) centers of $\{V_{14}\}$cluster anion at room temperature.

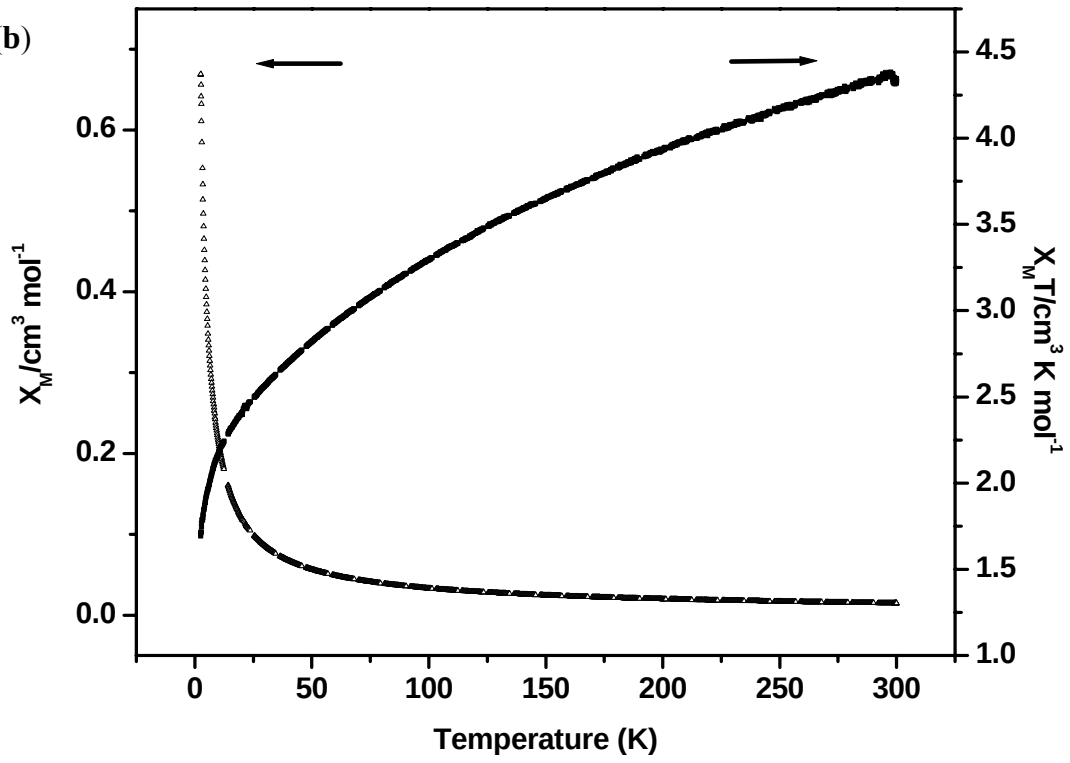

Figure 2.9(b) Temperature dependences of $_M$ (Δ) and $_MT$ ( ) $[\{Ce(H_2O)_6\}_2As_8V_{14}O_{42}(SO_3)]$ $8H_2O$ (**8**)

In the case of Ce^{3+} ion, the theoretical value of $_J$ (2.54 $_B$; 0.806 cm^3 K mol^{-1}) agrees nicely with experimental value of $_{obsd}$ (2.3-2.5 $_B$) at room temperature.[16] For compound **8**, if we add twice of this corresponding $_MT$ value 1.61 (0.806 + 0.806) cm^3 K mol^{-1} to the experimentally obtained room temperature $_MT$ value of discrete compound $[NH_4]_6[As_8V_{14}O_{42}(SO_3)]$, the resulting $_MT$ value of 4.09 (1.61 + 2.48) cm^3 K mol^{-1} is again somewhat smaller than the experimentally obtained $_MT$ value (4.345 cm^3 K mol^{-1}) of cerium compound **8** at room temperature suggesting again a week interaction between Ce^{3+} ion ($4f^1$) and V^{4+} ion ($3d^1$) ions at room temperature.

As temperature decreases, both compound **7** and **8** exhibit identical trend in magnetic behavior as shown by Figures 2.9(a) and 2.9(b) respectively. For both compounds, as temperature decreases the $_MT$ value continuously decreases (in contrast to the temperature dependent magnetic behavior of discrete compound $[NH_4]_6[As_8V_{14}O_{42}(SO_3)]$ as discussed below) reaching a value of 1.99 cm^3 K mol^{-1} (compound **7**) and 2.50 cm^3 K mol^{-1} (compound **8**) at 25 K; below this temperature, the $_MT$ value decreases very rapidly, reaching 1.33 cm^3 K mol^{-1} (for compound **7**) and 1.71 cm^3 K mol^{-1} (for compound **8**) at 2.8 K. This magnetic behavior indicates overall antiferromagnetic coupling interactions (Figures 2.9(a) and 2.9(b)). Since the trends in magnetic behavior for both compounds **7** and **8** are alike, the coupling interactions between Sm^{3+} / Ce^{3+} and V^{4+} ions of $\{V_{14}\}$ cluster anion can be ignored during lowering temperature. If there would exist significant interaction between lanthanide ions (Sm^{3+} / Ce^{3+}) and V^{4+} ions of $\{V_{14}\}$ cluster anions, we would not have observed identical trends in temperature dependent magnetic behavior, because Ce^{3+} ion is a f^1 system (one unpaired electron) and Sm^{3+} ion is a f^5 system (five unpaired electrons). The insignificant coupling interactions between lanthanide ions (Sm^{3+} / Ce^{3+}) and V^{4+} ions of $\{V_{14}\}$ cluster anions with decreasing temperature can also be supported by the fact that the $_MT$ value for the discrete compound $[NH_4]_6[As_8V_{14}O_{42}(SO_3)]$ is 1.78 cm^3 K mol^{-1} at 2 K[9a] and the

$_M$T values for compounds **7** and **8** are 1.33 cm^3 K mol^{-1} and 1.71 cm^3 K mol^{-1} respectively at 2 K. The theoretical values of $_M$T for compounds **7** and **8** are 1.96 (1.78 + 0.09 + 0.09) cm^3 K mol^{-1} and 3.39 (1.78 + 0.806 + 0.806) cm^3 K mol^{-1} respectively at 2 K. This clearly indicates that the sources of antiferromagnetic coupling interactions that are revealed from Figures 2.9(a) and 2.9(b) with decreasing temperature for both compounds **7** and **8**, are solely the $\{V_{14}\}$ cluster with 14 non-interacting V^{4+} ions with S = 1/2 and inter-$\{V_{14}\}$ clusters interactions that are possible due to lanthanide linking (isostructural analogue compound **6** is shown in Figure 2.13(b)). The magnetic behavior of compounds **7** / **8** is in contrast to the temperature dependent magnetic behavior of the discrete compound $[NH_4]_6[As_8V_{14}O_{42}(SO_3)]$, for which the room temperature $_M$T value is 2.48 cm^3 K mol^{-1} (4.45 $_B$). As the temperature decreases, the $_M$T decreases slightly stabilizing at 2.1 cm^3 K mol^{-1} at around 100 K. Subsequently the $_M$T value increases with decreasing temperature reaching a maximum of 2.3 cm^3 K mol^{-1} at 15 K. Finally, below 10K, $_M$T value of $[NH_4]_6[As_8V_{14}O_{42}(SO_3)]$ decreased rapidly and reaching 1.78 cm^3 K mol^{-1} at 2K.[9a] Comparing the temperature dependent magnetic behavior of this discrete cluster with those of compounds **7** and **8**, suggests that linking the $\{V_{14}\}$ clusters has tremendous influence on the magnetism of the discrete cluster irrespective of the type of linker.

For compound $[\{La(H_2O)_6\}_2As_8V_{14}O_{42}(SO_3)]$ $8H_2O$ (**6**), there is no contribution to the magnetic susceptibility from La^{3+} ion (f^0 system) and thus, the room temperature $_M$T value (2.35 cm^3 K mol^{-1}) of **6** is comparable to that (2.48 cm^3 K mol^{-1}) discrete compound $[NH_4]_6[As_8V_{14}O_{42}(SO_3)]$. However, temperature dependent magnetic behavior of compound $[\{La(H_2O)_6\}_2As_8V_{14}O_{42}(SO_3)]$ $8H_2O$ (**6**), that shows continuous fall of $_M$T values with decreasing temperature indicating overall antiferromagnetic coupling interactions, is not comparable to the reported magnetic behavior of the discrete starting precursor $[NH_4]_6[As_8V_{14}O_{42}(SO_3)]$[9a] as described below.

The variable temperature magnetic susceptibility of compounds **6** was measured between 24 to 294 K. Figure 2.9(c) show the magnetic behavior of $[\{La(H_2O)_6\}_2As_8V_{14}O_{42}(SO_3)]\ 8H_2O$ (**6**) in the form of $_M$ versus T and the product $_M$T versus T plots, $_M$ is the molar magnetic susceptibility. The $_M$T value of compound **6** at 294 K is 2.35 cm^3 K mol^{-1} (4.34 $_B$), which is significantly smaller than that expected for the total spin-only value 5.25 cm^3 K mol^{-1} (6.48 $_B$), that corresponds to the presence of 14 non-interacting V^{4+} ions with S = 1/2. As the temperature decreases, the $_M$T value decreases continuously starting from 294 (2.35 cm^3 K mol^{-1}) to 24K (0.44 cm^3 K mol^{-1}). This temperature dependant magnetic behavior of compound **6** clearly indicates the antiferromagnetic coupling between V^{4+} ions.

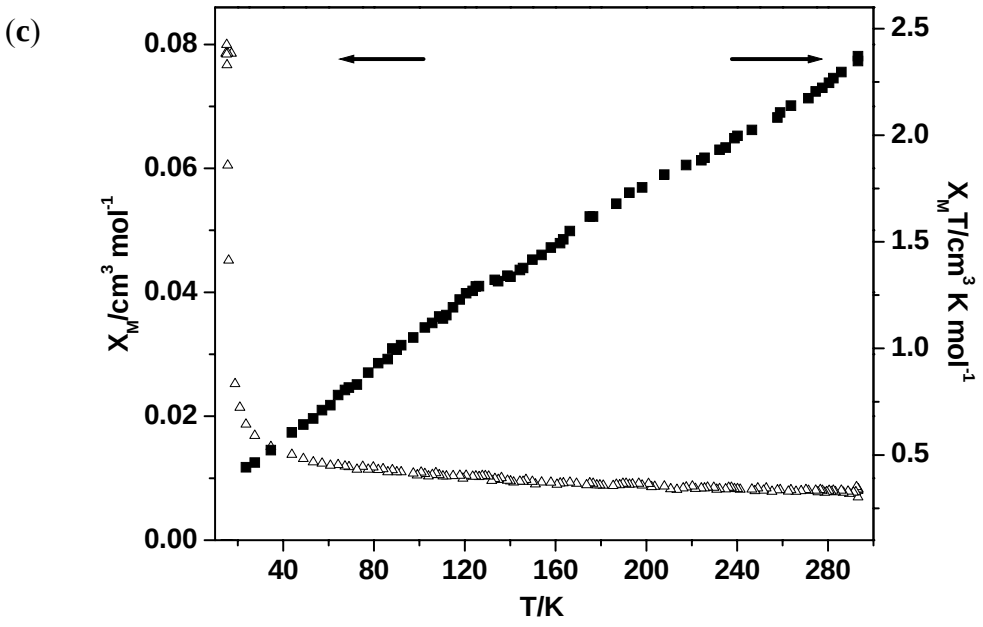

Figure 2.9(c). Temperature dependences of $_M$ (Δ) and $_M$T ( ): (a) for $[\{La(H_2O)_6\}_2As_8V_{14}O_{42}(SO_3)]\ 8H_2O$ (**6**)

In compound **6**, there is no contribution to the magnetic susceptibility from La^{3+} ion (f^0 system) and thus, magnetism of this compound is attributed solely to the presence of V^{4+} ions ($3d^1$, S = ½). The magnetic behavior of compound $[\{La(H_2O)_6\}_2As_8V_{14}O_{42}(SO_3)]\ 8H_2O$ (**6**) (Figure 2.9(c)) should be comparable to the reported magnetic behavior of $[NH_4]_6[As_8V_{14}O_{42}(SO_3)]$.[9a] In order to explain its magnetism, Müller, Gatteschi and co-workers offered an attractive model that can qualitatively be described by scheme 2(b), which can be applied to our present system (compound **6**). According to this scheme, V5 V11, V7 V12, V3 V14 and V1 V9 pairs are in the ground S = 0 state at relatively higher temperature assuming that the di- -oxo bridges correspond to very strong antiferromagnetic coupling[9a] (each of these V5 V11, V7 V12, V3 V14 and V1 V9 pairs are bridged by di- -oxo bridges). This leaves V2, V4, V6, V8, V10 and V13 ions that are largely uncoupled, which is in agreement with the $_M$T value (2.35 cm^3 K mol^{-1} 4.34 $_B$) at room temperature (Figure 2.9(c)) corresponding to six unpaired electrons (expected spin only value = 4.24 $_B$). At lower temperature, these six vanadium ions (V2, V4, V6, V8, V10 and V13) will start to feel coupling interactions through V9 V10, V10 V11, V12 V13, V13 V14, V1 V2, V2 V3, V3 V4, V4 V5, V5 V6, V6 V7, V7 V8, V8 V1, V4 V11, V2 V9, V6 V12, V8 V14 pairs (Scheme 2(b)) through three different coupling constants J_1, J_2 and J_3 as shown in Scheme 3. It was assumed that J_1, J_2 and J_3 are antiferromagnetic coupling constants. The experimental $_M$T value for the present lanthanum-linked compound $[\{La(H_2O)_6\}_2As_8V_{14}O_{42}(SO_3)]\ 8H_2O$ (**6**) is 0.44 cm^3 K mol^{-1} at 24 K (Figure 2.9(c)), which is much smaller in magnitude compared to $_M$T value (1.78 cm^3 K mol^{-1}) for discrete compound $(NH_4)_6[As_8V_{14}O_{42}(SO_3)]$ even at 1.9 K.[9a] This result clearly shows that linking / connecting the $[As_8V_{14}O_{42}(SO_3)]^6$ clusters by La^{3+} ions (f^0 system) has tremendous effect on its magnetism. When a polyoxovanadate (POV) molecule becomes

a material, its $_{M}T$ value decreases considerably at lower temperature compared to its $_{M}T$ value of its discrete state.

Scheme 3

V9 V10, V10 V11, V12 V13, V13 V14 J_1 (each of these pairs is bridged by two AsO groups)

V1 V2, V2 V3, V3 V4, V4 V5, V5 V6, V6 V7, V7 V8, V8 V1 J_2 (each of these pairs is bridged by one AsO and one oxo groups)

V4 V11, V2 V9, V6 V12, V8 V14 J_3 (each of these pairs is bridged by one oxo group)

Interestingly, when we compare the $_{M}T$ versus T plot (Figure 2.9(c)) of polymeric compound $[\{La(H_2O)_6\}_2As_8V_{14}O_{42}(SO_3)]$ $8H_2O$ (**6**) with that of discrete compound $[NH_4]_6[As_8V_{14}O_{42}(SO_3)]$,[9a] we found the plot (Figure 2.9(c)) for linked compound **6** is much more steeper than that of discrete compound $[NH_4]_6[As_8V_{14}O_{42}(SO_3)]$. This clearly indicates more antiferromagnetic coupling in case of linked system compared to a discrete system. This increase in antiferromagnetic coupling from discrete to linked system could be due inter-clusters (V^{4+} V^{4+}) interactions, that are not possible in the case of discrete compound $(NH_4)_6[As_8V_{14}O_{42}(SO_3)]$.[9a] This, again, tells that linking (not the type of linker) that plays key role on affecting the magnetism of discrete cluster, when it is linked to an extended structure. We believe that the linking of the $\{V_{14}\}$ clusters by lanthanide ions probably provides a pathway for exchange interactions among $\{V_{14}\}$ clusters resulting in a strong antiferromagnetic interactions as is evidenced by continuous falling of $_{M}T$ values with decreasing temperature (Figure 2.9). This also explains why the room temperature $_{M}T$ value for the linked system **6** is slightly smaller that that of discrete system $[NH_4]_6[As_8V_{14}O_{42}(SO_3)]$.[9a] Recent literatures also support this inter-cluster antiferromagnetic interactions. [10,11]

For both compounds **7** and **8**, the appearance of the rapid decrease of $_{M}T$ value (Figures 2.9(a) and 2.9(b)) between 25 K and 2 K is an indication of a different exchange path way between linker Sm^{3+} / Ce^{3+} ions and V^{4+} of cluster anions, which is difficult to explain at this stage without fitting the data with a suitable model. Unfortunately, it is not easy to fit the experimental magnetic data for compounds **6**, **7** and **8** using a suitable theoretical model.[17] For this isolated discrete cluster containing compound $[NH_4]_6[As_8V_{14}O_{42}(SO_3)]$, the experimental value of $_{M}T$ at lower temperature agreed with a ground state of S = 1.[9a] The present experimental data for compounds **7** and **8** also agrees with a S = 1 ground state that gets populated at lowest temperature.

2.3.7. Bond Valence Calculation (BVS)

The bond valence sum calculations in **1** **4** confirm, the oxidation states of all **V** atoms are +4 (s = 3.92 4.11, **1;** s = 3.93 4.08, **2;** s = 3.94 4.10, **3;** s = 3.91 4.10, **4;),** and the As atoms are +3 (s = 3.20 3.60, **1;** s = 3.36 3.43, **2;** s = 3.33 3.41, **3;** s = 3.35 3.46, **4;)**

The bond valence sum calculations in compound $[\{\{Ce(H_2O)_5\}_6As^{v}V_{12}{}^{V}O_{38}\}(V_6{}^{iv}V_6{}^{v}As_8O_{40}(NO_3))(V_7{}^{iv}V_5{}^{v}As_8O_{40}(NO_3))\cdot 52H_2O$ (**5**) confirm, V atoms are exists in mixed valence (V^{v} / V^{iv}).

BVS result of $[\{Ce(H_2O)_5\}_6As^{v}V_{12}{}^{V}O_{38}]^{7+}$ cation: s = 3.22 3.36 for Ce; 5.0 for As; s = 4.69 4.74 for V; It confirm, the oxidation state of all Ce atoms are in +3, As atom in +5 and V atom in +5.

$[\{(V_6{}^{iv}V_6{}^{v}As_8O_{40}(NO_3)\}\{(V_7{}^{iv}V_5{}^{v}As_8O_{40}(NO_3)\}]^{7}$ anion: s = 3.97 4.48 for thirteen V^{4+}; s = 4.48 4.63 for eleven V^{5+}; 3.0 for As; It confirm thirteen V^{4+} and eleven V^{5+} are present in the POV anionic cluster.

The bond valence sum calculations in **6 8** confirm, the oxidation states of all **V** atoms are +4 (s = 3.91 4.39, **6;** s = 3.93 4.31, **7;** s = 3.93 4.37, **8;),** and the **As** atoms are +3 (s = 3.42 3.44, **6;** s = 3.38 3.48, **7;** s = 3.40 3.45, **8;)**

2.3.8. X ray Crystallographic Studies

Crystal Structure Description of Compound $[H_6As_6V_{15}O_{40}(H_2O)] \cdot 9H_2O$ (1)

Compound **1** is prepared by following the reported procedure with slight modifications.[12a] One of the brown color crystals of $[H_6As_6V_{15}O_{40}(H_2O)] \cdot 9H_2O$ (**1**), suitable for X-ray structure analysis, has been selected for X-ray data collection. The X-ray analysis shows the pertinent crystals belong to the rhombohedral system with space group *R3C* and single crystal X-ray data obtained at 293 K are summarized in Table 2.1. The asymmetric unit contains one-third numbers of atoms per formula unit. It comprises three lattice water molecules which are labeled as (O16, O17 and O18). Thermal ellipsoidal representation of the molecular structure of compound **1** is presented in Figure 2.10.

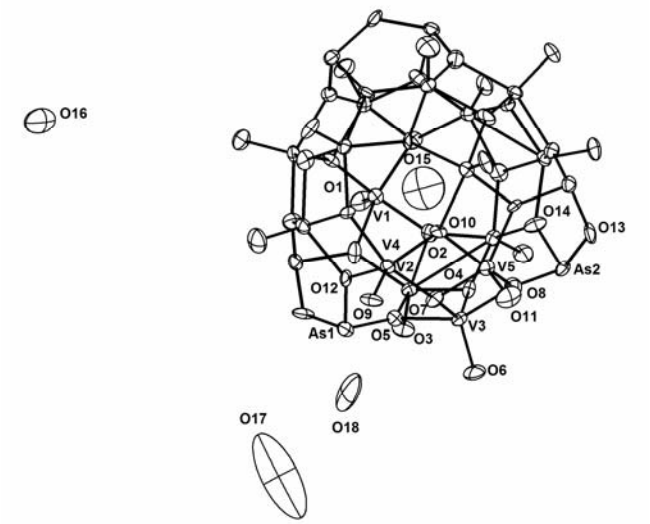

Figure 2.10. Thermal ellipsoidal plot (50 % probability level) of the molecular unit (asymmetric unit is labeled) of compound $[H_6As_6V_{15}O_{40}(H_2O)] \cdot 9H_2O$ (**1**)

Table 2.1. Crystal Data and Structural Refinement for Compounds **1** **3**

	1	**2**	**3**
Empirical formula	$H_{26}As_6V_{15}O_{52}$	$H_{56}As_6La_2V_{15}O_{69}$	$H_{56}As_6Sm_2V_{15}O_{70}$
Formula weight	2071.83	2649.87	2690.77
T [K]	293(2)	293(2)	293(2)
λ (Å)	0.71073	0.71073	0.71073
Crystal system	Rhombohedral	Orthorhombic	Orthorhombic
Space group	*R3C*	*Pna2(1)*	*Pna2(1)*
a [Å]	17.9648(5)	25.9120(12)	25.5591(16)
b [Å]	17.9648(5)	21.1349(9)	20.9615(13)
c [Å]	26.9567(15)	11.9346(5)	11.8495(7)
deg]	90	90	90
β [deg]	90	90	90
deg)	120	90	90
V (Å^3]	7534.3(5)	6536.0(5)	6348.5(7)
Z	6	4	4
D_{calc} [Mg m^{-3}]	2.740	2.693	2.815
μ [mm^{-1}]	6.692	6.450	7.147
F[000]	5910	5052	5132
Crystal size [mm^3]	0.42 x 0.40 x 0.40	0.16 x 0.08 x 0.06	0.18 x 0.07 x 0.06
θ range for data collection [deg]	2.00 to 28.25	1.24 to 25.00	1.59 to 25.00
Reflections Collected/unique	27663 / 4039	23936 / 11201	54390 / 11071
R [int]	0.0771	0.0308	0.0297
Refinement method	Full-matrix least-squares on F^2		
Data/restraints/parameters	4039 / 1 / 221	11201 / 1 / 850	11071 / 1 / 849
Goodness-of-fit on F^2	1.119	1.046	1.087
R_1/wR_2 [$I > 2\sigma(I)$]	0.0353/0.1031	0.0335/0.0819	0.0424/0.1067
R_1/wR_2 [all data]	0.0381/0.1049	0.0373/0.0840	0.0435/0.1077
Largest diff. Peak/hole [e· Å ^{3}]	2.143/-0.864	2.226/-0.692	2.471/-1.004

(a) **(b)**

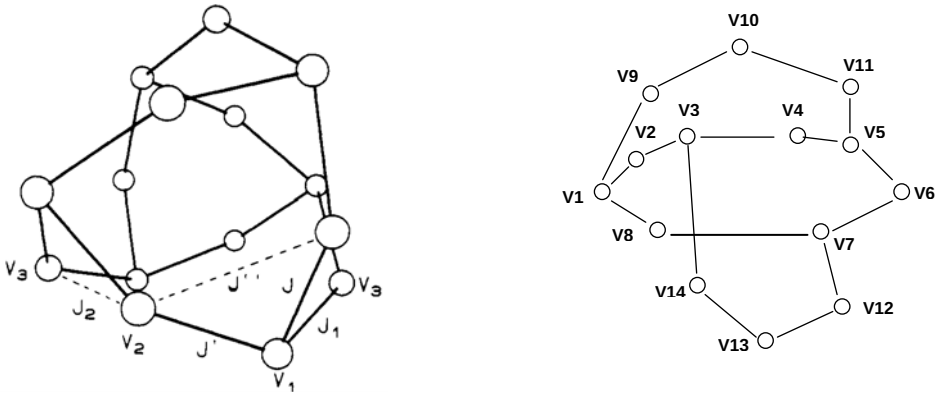

Scheme 2. The outline skeleton for cluster anions: (a) $[As_6V_{15}O_{42}(H_2O)]^6$ (b) $[As_8V_{14}O_{42}(SO_3)]^6$

The cluster anion $[As_6V_{15}O_{40}(H_2O)]^6$ contains 15 paramagnetic V^{IV} ions on a sphere formed by a triangle, sandwiched by two hexagons. It includes at its center a statistically disordered H_2O molecule (O15). The 15 distorted tetragonal pyramids are linked with one another through vertices and edges and with AsO_3 groups only through vertices. The outline skeleton for the formation of V15 structure is depicted in scheme 2(a). The structure of V15 can be explained as follows: Fifteen VO_5 pyramids can be divided into three differently linked groups. The first group contains six VO_5 pyramids joined each other through two edges and three vertices with its neighboring pyramids and through one vertex with an AsO_3 group. The second group contains six VO_5 pyramids, which are joined through three edges with neighboring VO_5 pyramids and through two vertices with two AsO_3 groups. The third group consists of three VO_5 pyramids, joined through two vertices and two edges with four VO_5 pyramids and through two vertices with two As_2O_5 moieties. Two AsO_3 groups are joined to each other via an oxygen bridge forming a handle like As_2O_5 moiety. The oxygen bonding mode in compound **1** can be grouped in three sets: (i) V=Ot (Ot = terminal oxygen) with the bond lengths in the range of 1.565 1.647 Å; (ii) μ_3 –bridgng oxygen lengths in the range of 1.889 2.025 Å; (iii)

μ_2 –bridging oxygen lengths from As O group are in the range of 1.756 1.832 Å. Vanadium and arsenic atoms in the crystal structure of compound **1**, is in +4 and +3 oxidation state respectively. (BVS result, section 2.3.7)

Crystal Structure Description of $[\{Ln(H_2O)_7\}_2(As_6V_{15}O_{42}(H_2O))]\cdot nH_2O$ (n = 12 and Ln = La^{3+} (2), n = 13 and Ln = Sm^{3+} (3), n = 11 and Ln = Ce^{3+} (4)

The basic building block for the compounds **2–4** is $[As_6V_{15}O_{42}(H_2O)]^{6-}$. The crystal structure shows that compounds **2–4** are isostructural and crystallized in orthorhombic space group *Pna2 (1)*. The crystallographic details are summarized in Table 2.1. A thermal ellipsoidal plot of the compound **2** is depicted in Figure 2.11.

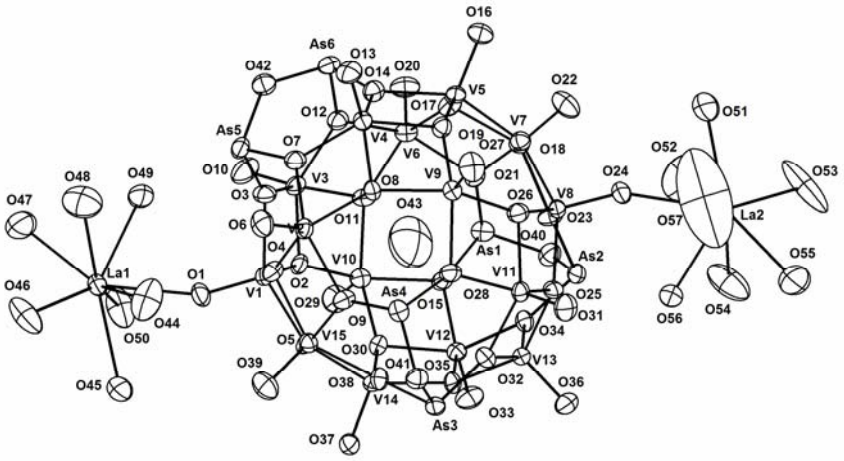

Figure 2.11. Thermal ellipsoidal plot (50 % probability level) of $[\{La(H_2O)_7\}_2(As_6V_{15}O_{42}(H_2O)]\cdot 12H_2O$ (**2**) excluding lattice water molecules and hydrogen atoms.

In the relevant asymmetric unit, polyoxovanadate cluster anion $[As_6V_{15}O_{42}(H_2O)]^{6-}$ is linked by two $[Ln(H_2O)_7]^{3+}$ complexes (where Ln = La^{3+} (**2**), Sm^{3+} (**3**) and Ce^{3+} (**4**)). In crystal structures of each of **2–4,** each $\{V_{15}\}$ cluster is coordinated to its four surrounding lanthanide ions (Ln^{3+}) through terminal oxygen atoms of the $\{V_{15}\}$ cluster as shown in Figure 2.12.

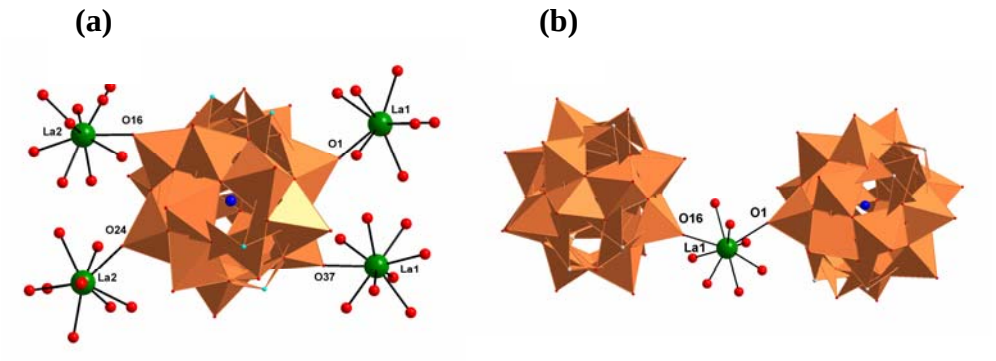

Figure 2.12. The coordination environment around each $[As_6V_{15}O_{42}(H_2O)]^{6-}$ (left) and coordination environment of each $[La(H_2O)_7]^{3+}$ cation (right) in compound **2**. Color code: O, red; La, green; oxygen from encapsulated water molecule, blue; polyhedra are shown in golden yellow color.

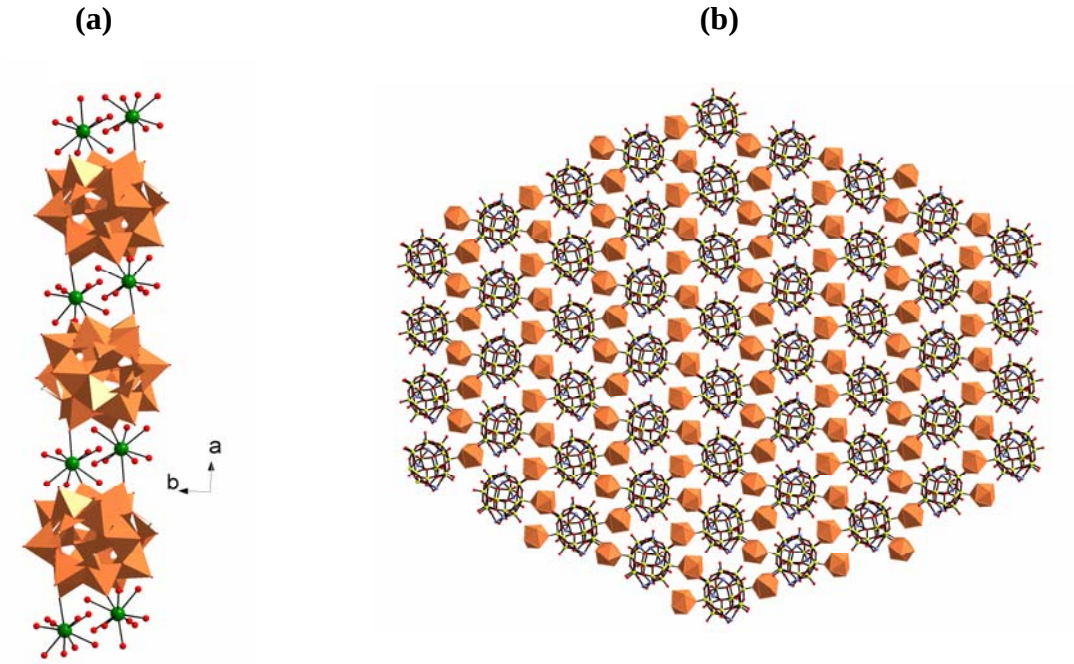

Figure 2.13. (a) The formation of one dimensional (1D) chain along '*c*' axis in $[\{La(H_2O)_7\}_2As_8V_{15}O_{42}(H_2O)] \cdot 12H_2O$ (**2**); Color code same as in Figure 2.12. (b) Two-dimensional (2D) layered structure of in compound **2**. Cluster anions are shown in ball-and-stick model and the lanthanum-aqua complexes are shown in polyhedral representation. Color code: O, red; V, yellow; As, violet;

Similarly, each Ln^{3+} (where Ln^{3+} = La^{3+}, Sm^{3+}, and Ce^{3+}) ion is coordinated to two $\{V_{15}\}$ cluster anions (Figure 2.12). The remaining seven coordination sites of each lanthanide ions are filled by seven water molecules. Thus in the crystal structure, each Ln^{3+} ion attains monocapped square-antiprism geometry. The coordination of lanthanum ions to $\{V_{15}\}$ cluster propagates throughout the crystal lattice resulting in the formation of a one dimensional chain as shown in Figure 2.13(a). Further adjacent chains are laterally interlinked by $[Ln(H_2O)_7]^{3+}$ complexes resulting in the formation of 2D framework as depicted in Figure 2.13(b). In compounds **2 4**, the overall oxygen bonding modes can be divided into four categories, e.g., for lanthanum analogue $[\{La(H_2O)_7\}_2As_6V_{15}O_{42}(H_2O)]\cdot 12H_2O$ (**2**), (i) $V{=}O_t$ (O_t = terminal oxygen) bond lengths observed in the range of 1.578(6) – 1.628(5) Å; (ii) μ_3 –bridging oxygen length in the range of 1.763(5) – 2.004(5) Å; (iii) μ_2–bridging oxygen bond lengths in the range of 1.770(5) – 1.791(5) Å; (iv) La – O bond lengths in the range of 2.435(16) – 2.689(9) Å. Thus the 2D framework in compounds **2 4** is formed by $[As_6V_{15}O_{42}(H_2O)]^{6-}$ and $[La(H_2O)_7]^{3+}$ inorganic moieties, without the presence of any organic ligands. A similar organic free framework compound $[\{Zn(H_2O)_4\}_2][H_2As_6V_{15}O_{42}(H_2O)]\cdot 2H_2O$ is known in the literature;[19] however, in this compound, the formation of framework occurs through O H···O hydrogen bonding interactions (not by coordination covalent bond). Here we report, for the first time, organic free 2D materials in which $\{V_{15}\}$ cluster covalently bonded with lanthanide ions synthesized at room temperature.

Identification of Water Clusters in compound 2

Recent studies focused on small water clusters, formed by water molecules in the crystal host, have attracted considerable research interests. Non-coordinated lattice water molecules, lanthanum-coordinated water molecules and $V{=}O_t$ oxygen atoms (O_t = terminal oxygen) are involved in O H···O hydrogen bonding interactions in compounds **2–4.** The hydrogen bonding distances are measured based on O···O distances.

In the crystal structure of compound **2,** a water dimer (O58 and O68), a water trimer (O60, O61 and O62) and a water pentamer (O62, O65, O67, O68 and O69), which are exclusively formed by the lattice water molecules, are crystallographically characterized. The O···O hydrogen bonding distances are varied in the range of 2.640 – 3.000 Å. The relevant hydrogen bonding parameters are given in Table 2.2. The above mentioned small water clusters, further interact with its surroundings through O H···O hydrogen bonding resulting in a complicated 3D structure.

Table 2.2. Geometrical parameters of the O H···O hydrogen bonds (Å, °) involved in supramolecular network of compound **2**

O(58) O(68)#1	2.640(3)	O(68) O(58)#2	2.640(3)
O(60) O(61)	2.881(17)	O(60) O(62)#3	3.000(14)
O(62) O(60)#4	3.000(14)	O(65) O(67)#5	2.860(2)
O(67) O(65)#6	2.860(2)	O(67) O(66)	2.652(14)
O(66) O(64)#7	2.783(16)	O(64) O(59)#8	2.640(2)
O(64) O(66)#9	2.783(16)	O(59) O(64)#10	2.640(2)

Symmetry transformations used to generate equivalent atoms: #1 -1+x, y, z; #2 1+x, y, z; #3 0.5-x, 0.5+y, 0.5+z; #4 0.5-x, -0.5+y, -0.5-z; #5 1.5-x, -0.5+y, -0.5+z; #6 1.5-x, 0.5+y, 0.5+z; #7 1.5-x, 0.5+y, -0.5+z; #8 1-x, -0.5+y, 0.5+z; #9 1.5-x, -0.5+y, 0.5+z; #10 1-x, 1-y, -0.5+z.

Crystal Structure Description of
$[\{\{Ce(H_2O)_5\}_6As^{v}V_{12}{}^{V}O_{38}\}(V_6{}^{iv}V_6{}^{v}As_8O_{40}(NO_3))(V_7{}^{iv}V_5{}^{v}As_8O_{40}(NO_3))\cdot 52H_2O$ (5)

The cluster degradation reaction of $[H_6As_6V_{15}O_{42}(H_2O)]\cdot 9H_2O$ (**1**) with $(NH_4)_2Ce(NO_3)_6$ in aqueous medium, results in the formation of a novel compound $[\{\{Ce(H_2O)_5\}_6As^{v}V_{12}{}^{V}O_{38}\}(V_6{}^{iv}V_6{}^{v}As_8O_{40}(NO_3))(V_7{}^{iv}V_5{}^{v}As_8O_{40}(NO_3))\cdot 52H_2O$ (**5**) in which cluster expansion and contraction observed together in the crystal structure. The compound **5** crystallizes in triclinic space group *P 1*. Since the compound **5** is highly hydrated, it may loose some of its lattice water molecules in room temperature itself and

hence X-ray data has been collected in 100 K. The relevant crystallographic data is given in Table 2.3.

Table 2.3. Crystal Data and Structural Refinement for Compounds **4** **5**

	4	**5**
Empirical formula	$H_{52}As_6Ce_2V_{15}O_{69}$	$H_{104}N_2As_{17}Ce_6V_{36}O_{212}$
Formula weight	2650.28	7473.05
T [K]	293(2)	100(2)
λ (Å)	0.71073	0.71073
Crystal system	Orthorhombic	Triclinic
Space group	*Pna2(1)*	*P 1*
a [Å]	25.8505(12)	18.979(4)
b [Å]	21.1115(9)	23.097(5)
c [Å]	11.9217(5)	23.952(5)
deg]	90	73.83(3)
β [deg]	90	74.34(3)
deg)	90	89.88(3)
V (Å^3]	6506.2(5)	9680(3)
Z	4	2
D_{calc} [Mg m^{-3}]	2.706	2.564
μ [mm^{-1}]	6.566	6.044
F[000]	5052	7102
Crystal size [mm^3]	0.20 x 0.08 x 0.06	0.28 x 0.20 x 0.08
θ range for data collection [deg]	1.25 to 28.25	1.12 to 25.00
Reflections collected/unique	40350 / 14385	93438 / 34029
R [int]	0.0726	0.0498
Refinement method	Full-matrix least-squares on F^2	
Data/restraints/parameters	14385 / 1 / 829	34029 / 0 / 2461
Goodness-of-fit on F^2	0.948	1.060
R_1/wR_2 [$I > 2\sigma(I)$]	0.0472/0.0997	0.0512/0.1442
R_1/wR_2 [all data]	0.0624/0.1047	0.0732/0.1564
Largest diff. Peak/hole [e· Å ^{3}]	1.770/-1.480	2.426/-5.173

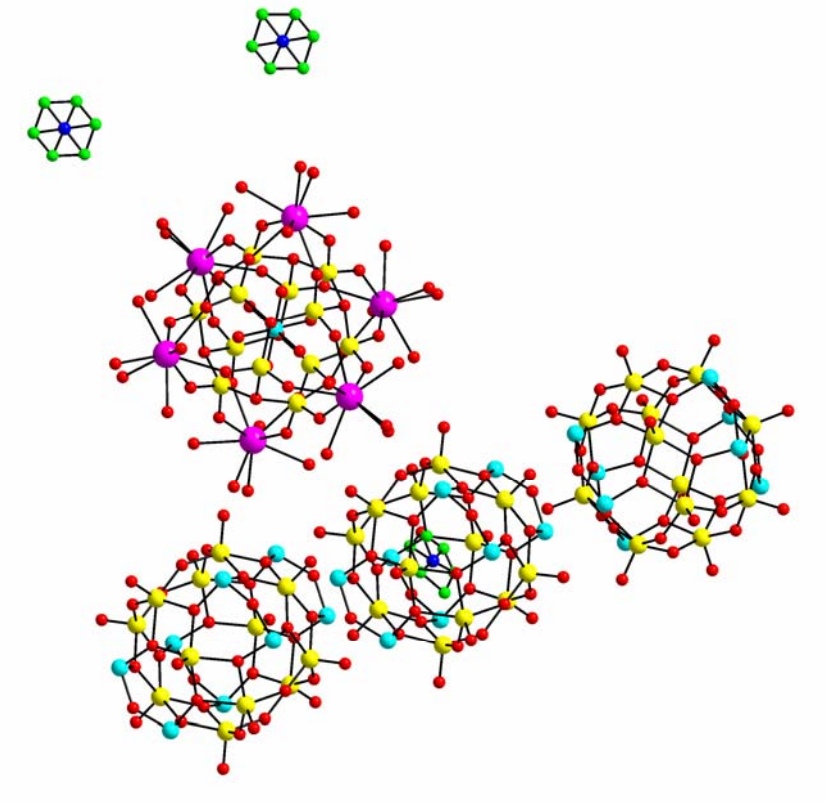

Figure 2.14. Ball – Stick model of the molecular structure of compound $[\{\{Ce(H_2O)_5\}_6As^{v}V_{12}{}^{V}O_{38}\}(V_6{}^{iv}V_6{}^{v}As_8O_{40}(NO_3))(V_7{}^{iv}V_5{}^{v}As_8O_{40}(NO_3))\cdot 52H_2O$ (**5**). Color code: V, yellow; As, cyan; Ce, purple; O, red; N, blue; oxygen atoms from nitrate anion, green.

Crystal structure of the title compound contains $[\{Ce(H_2O)_5\}_6As^{v}V_{12}{}^{V}O_{38}]^{7+}$ as cation, one molecular cluster anion $[V_6{}^{iv}V_6{}^{v}As_8O_{40}(NO_3)]^{3}$, two half units of $[V_4{}^{iv}V_2{}^{v}As_4O_{20}(NO_3)]^{2}$ cluster anions, and fifty-two lattice water molecules. The molecular structure of compound **5** is depicted in the Figure 2.14. Crystal structure of compound **5** shows that the negative charge of a POV cluster anion is counterbalanced by

another POV cation. In general, POM clusters exist in anionic form and can be isolated as crystalline salt by adding appropriate cations such as NH_4^+, metal salts etc. Very rarely POM cationic cluster exists along with a POM anion in the crystal structure.[20] In this particular reaction condition, transformation of cluster to cluster is observed. The contraction of $\{As_6V_{15}\}$ cluster in to $\{As_8V_{12}\}$ cluster is an unusual phenomenon in polyoxometalate chemistry. A graphical representation of $[H_6As_6V_{15}O_{42}(H_2O)] \cdot 9H_2O$ (**1**) cluster contraction in to $[As_8V_{12}O_{40}(NO_3)]^{3-/4}$ cluster along with the encapsulation of nitrate anion is shown in scheme 4.

Structural Description of $[\{Ce(H_2O)_5\}_6As^{V}V_{12}^{V}O_{38}]^{7+}$ Cationic Cluster

The $[Ce_6AsV_{12}O_{38}]^{7+}$ cationic cluster (Figure 2.15(a)) is formed by twelve VO_6 octahedra through edge sharing which also faces with a central AsO_6 octahedron, in which six Ce^{3+} ions are capped. Each Ce^{3+} ion is covalently coordinated to $[AsV_{12}O_{38}]^{11-}$ moiety by four $_2$ bridging oxygen atoms. Five water molecules are coordinated to each Ce^{3+} ion resulting in the coordination number of nine around each Ce^{3+} ion. The geometry around each Ce^{3+} ion is monocapped square-antiprism. The oxidation state of cerium, arsenic and vanadium atoms in $[Ce_6AsV_{12}O_{38}]^{7+}$ cationic cluster is +3, +5 and +5 respectively. This result is in consistent with BVS calculations. (BVS results are described in section 2.3.7.)

Structural Description of $[As_8V_{12}O_{40}O_{40}(NO3)]^{n-}$ Anionic Cluster

The formation of $[As_8V_{12}O_{40}(NO3)]^{3-/4}$ shell is described by twelve tetragonal VO_5 pyramids and four handle-like As_2O_5 groups connected through oxo-bridges resulting in the formation of hollow sphere in the central part. The central cavity size is approximately measured as 4.854 x 4.833 Å whereby a disordered nitrate anion is encapsulated (Figure 2.15(b)).

The geometry around encapsulated nitrate anion is nearly planar. In the crystal structure, anionic shell $[V_{12}As_8O_{40}]^{3/4}$ acts as host and nitrate anion as guest. The stabilization of anion within an anionic host can be explained as follows: The repulsive (O_{pov}··· $O_{nitrate}$) and attractive forces (V^n ··· nitrate anion) are approximately balance each other. This leads to relatively very weak interactions in between host and guest resulting in the pseudo mechanical fixation of the guest by the host.

Scheme 4.

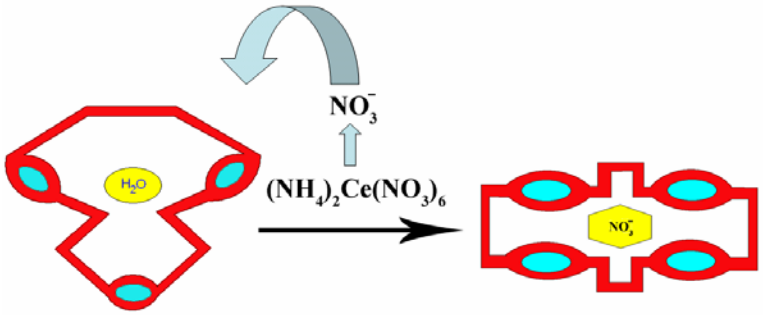

(a) **(b)**

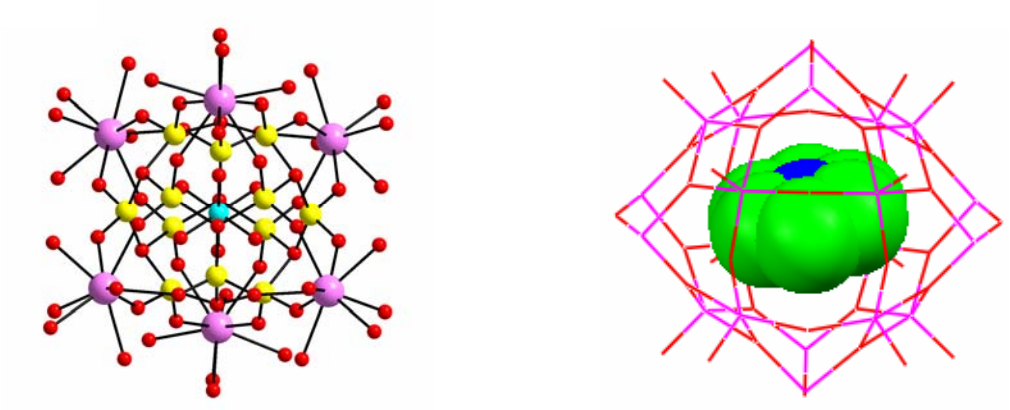

Figure 2.15 (a) Ball – Stick representation of cationic part $[\{Ce(H_2O)_5\}_6\{As^{V}V_{12}{}^{V}O_{38}\}]^{7+}$ in compound **5.** (b) The nitrate ion encapsulation in $[(As_8V_{12}O_{40}(NO3)]^{3/4}$ cluster anion (nitrate ion is shown in space filling model)

Crystal Structure Description of $[\{Ln(H_2O)_6\}_2(As_8V_{14}O_{42}(SO_3))]\cdot 8H_2O$ (Ln = La^{3+} (6), Sm^{3+} (7) and Ce^{3+} (8)

The basic building block for the compounds **6–8** is $[As_8V_{14}O_{42}(SO_3)]^{6-}$. The asymmetrical unit contains seven vanadium atoms, four arsenic atoms, a half of the disordered SO_3^{2-} molecule (with half occupancy of both sulfur and oxygen atoms), a $[Ln(H_2O)_6]^{3+}$ ion attached to the cluster anion by coordinate covalent bond and four crystal water molecules. Thus the general formula of these compounds is described as $[\{Ln(H_2O)_6\}_2As_8V_{14}O_{42}(SO_3)]\cdot 8H_2O$. The thermal ellipsoidal plot of the asymmetric unit of lanthanum analogue is shown in Figure 2.16.

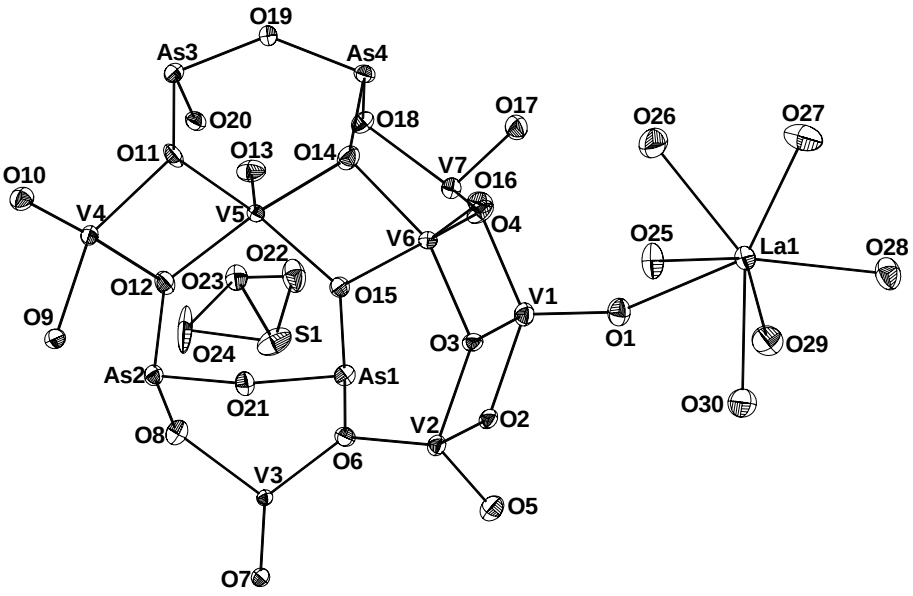

Figure 2.16. The thermal ellipsoidal plot (50% probability) of the asymmetric unit of compound $[\{La(H_2O)_6\}_2As_8V_{14}O_{42}(SO_3)]\cdot 8H_2O$ (**6**) excluding lattice water molecules.

The molecular structure of compound **6** is shown in Figure 2.17. The cluster anion $[As_8V_{14}O_{42}(SO_3)]^{6-}$ consists of 14 distorted $\{VO_5\}$ square pyramids and eight $\{AsO_3\}$ triangular groups, with a disordered SO_3^{2-} anion at the center of the cluster anion

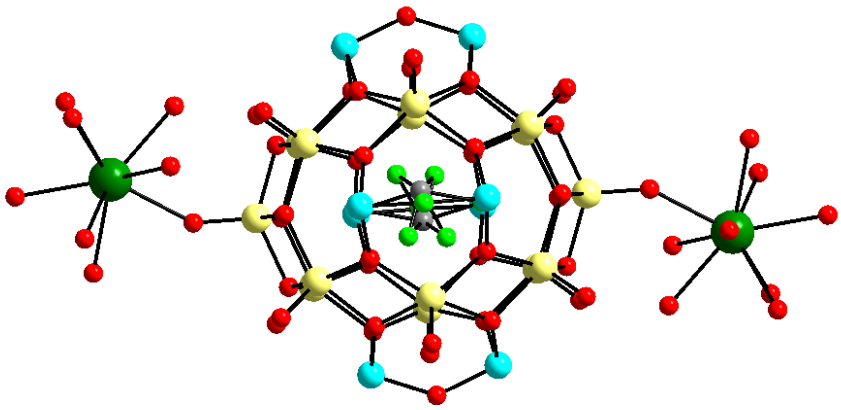

Figure 2.17. The molecular structure of $[\{La(H_2O)_6\}_2As_8V_{14}O_{42}(SO_3)] \cdot 8H_2O$ in compound **6** excluding lattice water molecules. Color code: La, dark green; V, yellow; As, cyan; O, red; S, medium gray; O coordinated sulfur, light green.

(a) **(b)**

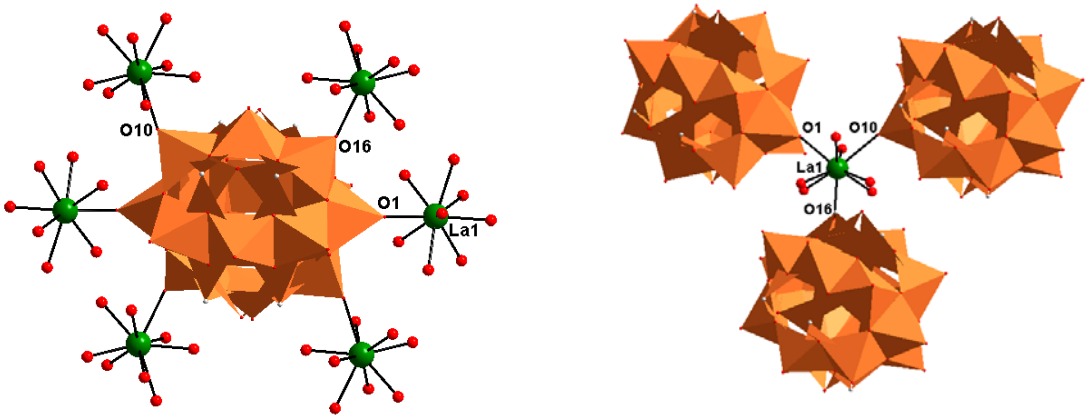

Figure 2.18. (a) The coordination environment of a POV cluster anion, $[As_8V_{14}O_{42}(SO_3)]^6$ with its surrounding lanthanum-aqua complex cations in compound **6** (b) The coordination environment of a lanthanum cation with its surrounding POM clusters in compound **6**. Color code: O, red, La, dark green. polyhedra are shown in golden yellow color.

resulting in the overall charge of the sulfite encapsulated cluster –6. A handle like $\{As_2O_5\}$ moiety is formed from two $\{AsO_3\}$ triangular groups that are linked together by an oxygen bridge. The fourteen $\{VO_5\}$ square pyramids, that are connected by edge sharing, are further linked to $\{As_2O_5\}$ units by sharing oxygen atoms resulting in a sphere-like structure with an approximate D_{2d} symmetry. This cluster anion can also be described by the formation of an octagon-like eight membered ring, formed by edge-shared fusion of eight $\{VO_5\}$ square pyramids and two sets of three vanadium ions which attach diametrically opposed centers on the octagons as shown in Scheme 2(b). In compounds **6 8**, all of the $\{VO_5\}$ square pyramids on respective $\{V_{14}\}$ clusters have typical geometries with apical V=O terminal bond distances and basal V O (in which oxygen is bridging type) bond distances 1.598(5) – 1.641(5) Å and 1.918(4) – 1.998(4) Å respectively. In the $\{As_2O_5\}$ fragments, the As–O distances are in the range of 1.753(4) – 1.797(5) Å with As O As angles in the range of 135.3(2) 136.6(2)°. In the structures of **6–8**, each $\{V_{14}\}$ cluster is coordinated to its six surrounding lanthanide ions (Ln^{3+}) through terminal oxygen atoms of the $\{V_{14}\}$ cluster as shown in Figure 2.18(a). Similarly, each Ln^{3+} (where $Ln^{3+} = La^{3+}$, Sm^{3+} and Ce^{3+}) ion coordinated to three $\{V_{14}\}$ cluster anions (Figure 2.18(b)); the remaining coordination sites of the lanthanide ions are filled by six water molecules with the bond lengths (for La^{3+} analogue) in the range of 2.500(4) – 2.683(4) Å. Thus in the crystal structure, each La^{3+} ion (that has coordination number of nine) attains monocapped square-antiprism geometry. The coordination of lanthanum ions to the $\{V_{14}\}$ cluster anions extends through out the crystal and result in a new type of two-dimensional (2D) network as shown in Figure 2.19(a). The construction of this 2D network can also be described as the formation of a chainlike arrangement (Figure 2.19(b)), in which adjacent $\{V_{14}\}$ clusters are linked by two aqua-lanthanum complexes and then these chains are laterally interlinked by La O V bonds (each of these bonds use V=O terminal bonds) leading to 2D polymeric layered structure of $[\{La(H_2O)_6\}_2As_8V_{14}O_{42}(SO_3)]_n$ (Figure 2.19(a)). As shown in the network (Figures

2.19(a) and 2.19(b)), each $\{V_{14}\}$ cluster anion $[As_8V_{14}O_{42}(SO_3)]^6$ acts as hexa dentate ligand and hence coordinating six surrounding lanthanum complex ions.

Table 2.4. Crystal Data and Structural Refinement for Compounds **6 8**

	6	**7**	**8**
Empirical formula	$As_8V_{14}La_2O_{65}SH_{40}$	$As_8V_{14}Sm_2O_{65}SH_{40}$	$As_8V_{14}Ce_2O_{65}SH_{40}$
Formula weight	2702.71	2725.61	2705.13
T [K]	100	100	293(2)
λ (Å)	0.71073	0.71073	0.71073
Crystal system	Monoclinic	Monoclinic	Monoclinic
Space group	*P2(1)/n*	*P2(1)/n*	*P2(1)/n*
a [Å]	13.4839(7)	13.4156(3)	13.4934(3)
b [Å]	12.3388(6)	12.2588(3)	12.3983(3)
c [Å]	18.3572(10)	18.2501(4)	18.3992(4)
deg]	90.0000	90.000	90.000
β [deg]	108.2570(10)	108.049(3)	108.025(3)
deg)	90.0000	90.000	90.000
V (Å^3]	2900.4(3)	2853.8(10)	2927.0(10))
Z	2	2	2
D_{calc} [Mg m^{-3}]	3.049	3.125	3.024
μ [mm^{-1}]	8.275	8.971	8.295
F[000]	2472	2692	2476
Crystal size [mm^3]	0.22 x 0.18 x 0.10	0.18 x 0.08 x 0.06	0.33 x 0.10 x 0.05
θ range for data collection [deg]	1.65 to 25.00	1.66 to 25.00	1.65 to 25.00
Reflections Collected/unique	27141 / 5106	26836 / 5031	27323 /5147
R [int]	0.0274	0.0293	0.0344
Refinement method	Full-matrix least-squares on F^2		
Data/restraints/parameters	5106 / 0 / 428	5031 / 0 / 424	5147 / 0 / 424
Goodness-of-fit on F^2	1.074	1.065	1.106
R_1/wR_2 [I > 2σ(I)]	0.0340/0.0914	0.0317/0.0832	0.0439/0.1107
R_1/wR_2 [all data]	0.0386/0.0943	0.0364/0.0867	0.0468/0.1128
Largest diff. Peak/hole [e· Å ^{3}]	2.549/-1.011	2.355/-1.067	2.728/-0.701

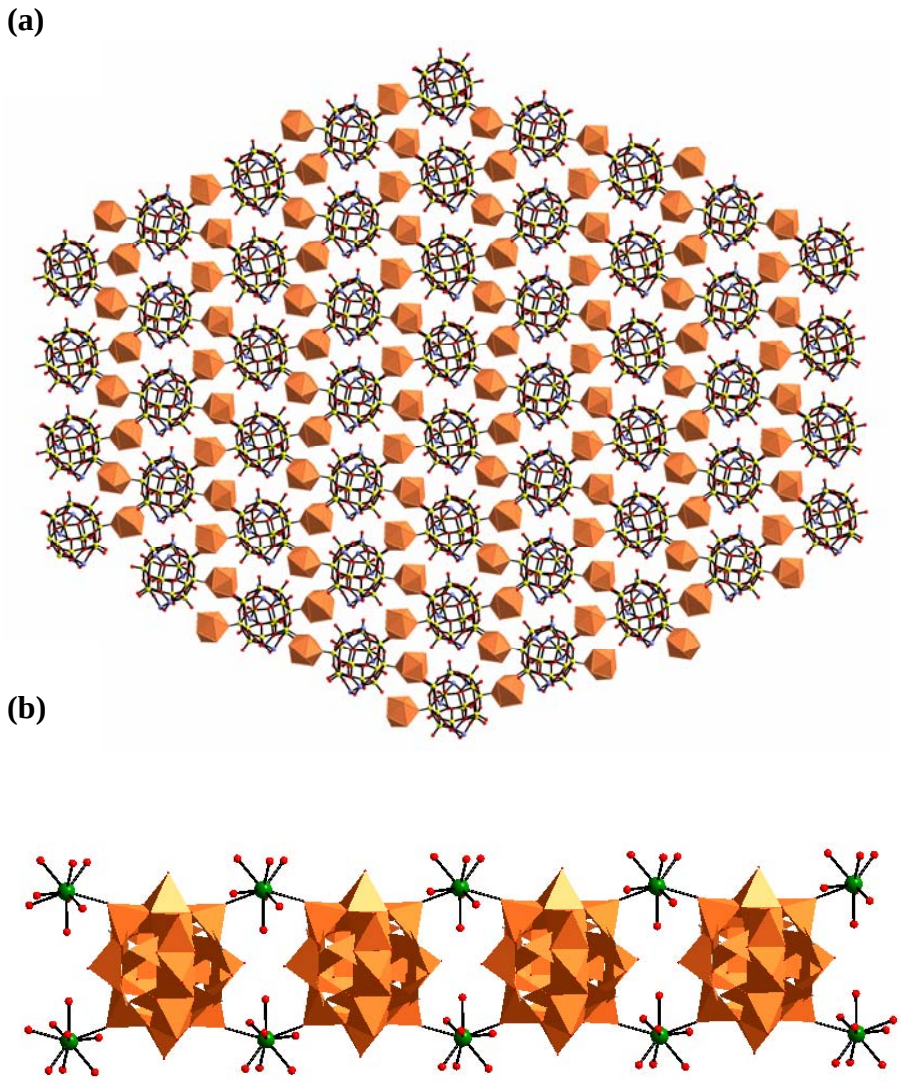

Figure 2.19. (a) The two-dimensional (2D) layered structure of $[\{La(H_2O)_6\}_2As_8V_{14}O_{42}(SO_3)]\cdot 8H_2O$in compound **6**. Cluster anions are shown in ball-and-stick model and the lanthanum-aqua complexes are shown in polyhedral representation; (b) Two adjacent $\{V_{14}\}$ clusters linked by two lanthanum-aqua complexes leading to a one-dimensional (1D) chain. Cluster anions are shown in polyhedral representation and lanthanum-aqua complexes are represented in ball-and-stick model. Color code: O, red; V, yellow; As, cyan; S, medium gray; O from SO_3 molecule, light green. Polyhedra are shown in golden yellow color.

Generally, higher coordination number for a POM anion, coordinating a metal complex ion, is very rarely known. A Silverton type POM cluster anion has been shown to have coordination number of nine in three-dimensional network (which was synthesized hydrothermally) consisting of $[GdMo_{12}O_{42}]^{9}$ and $[Gd(H_2O)_3]^{3+}$ anions and cations respectively.[21] In all the compounds **6 8**, the encapsulated sulfite anion SO_3^{2} is disordered over two positions and these positions are related by symmetry operation.

In compounds **6 8**, the overall oxygen bonding modes can be divided into five categories, e.g., for lanthanum analogue $[\{La(H_2O)_6\}_2As_8V_{14}O_{42}(SO_3)] \cdot 8H_2O$ (**6**), (i) $V{=}O_t$ (O_t = terminal oxygen) bond lengths are observed in the range of 1.602(4) – 1.637(4) Å; (ii) μ_3 –bridging oxygen lengths are in the range of 1.756(4) – 1.994(4) Å; (iii) μ_2–bridging oxygen bond lengths are in the range of 1.771(4) – 1.783(4) Å; (iv) in SO_3^{2-} molecule S–O bond lengths are in the range of 1.389(11) – 1.623(10) Å; and (v) La – O bond lengths are in the range of 2.500(4) – 2.683(4) Å. Two-dimensional polymeric structures based on two types of POV units ($[MV_{13}O_{38}]^{7}$ and $[MV_{12}O_{38}]^{12}$, M = Mn, Ni) are described in recent literature.[22]

Identification of Water Clusters

The compounds **6–8** were isolated from an aqueous medium and expectedly they contain lattice water molecules. It is notable that, all the coordinated ligands are water molecules, because we avoided organic ligands to achieve an organic free material. So, it is not surprising that non-covalent hydrogen bonding interactions of the type O–H···O would be observed. We have analyzed these supramolecular interactions in details for compound **6** and we observed a "Z" shaped of water hexamer $(H_2O)_6$, which is formed exclusively from lattice water molecules O31, O32 and O33 and their symmetry equivalent atoms as shown in Figure 2.20(a). This water hexamer, in turn, is hydrogen

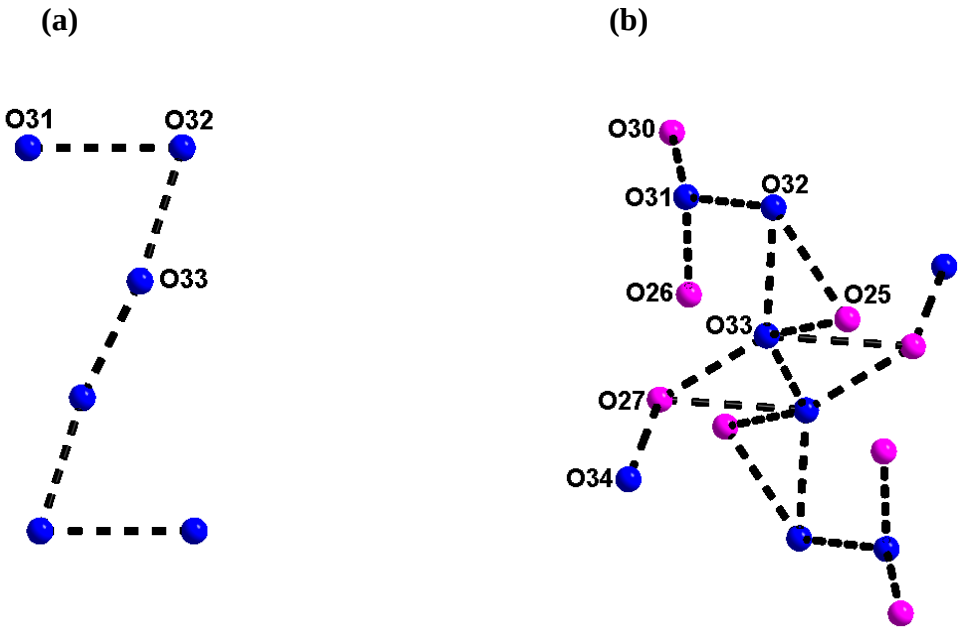

Figure 2.20. (a) A "Z" shaped water hexamer $(H_2O)_6$; (b) The hydrogen bonding interactions of this water hexamer with its surrounding furnishing a $(H_2O)_{16}$ cluster. Color code: lattice water molecules, blue; lanthanum coordinated water molecules, purple; black dotted lines represent the hydrogen bonding interactions.

bonded with eight surrounding lanthanum coordinated water molecules (O25, O26, O27 and O30 and their symmetry equivalent atoms) furnishing a $(H_2O)_{14}$ cluster, which is further hydrogen bonded to two lattice water molecules (O34 and its symmetry equivalent atom) resulting in a $(H_2O)_{16}$ cluster as shown in Figure 2.20(b). The hydrogen atoms of lanthanum coordinated and lattice water molecules could not be located in the crystal structures and thus hydrogen bonding distances of this water structure are taken as O···O distances (Table 2.5). Interestingly, O33 of water hexamer undergoes bifurcating hydrogen bonding interactions with O25 and O27 of lanthanum complex. Similarly, O31 water oxygen is hydrogen bonded to O26 and O30 water molecules in a bifurcating fashion.

Table 2.5. The O···O distances / separations involved in the formation of hydrogen bonds (Å) in compound $[\{La(H_2O)_6\}_2(As_8V_{14}O_{42}(SO_3)]\cdot 8H_2O$ (**6**)

O32	O33 #3	2.758(17)	O32	O3 #1	2.806(6)
O32	O31 #1	2.896(7)	O32	O25 #4	2.891(7)
O32	O5	2.823(7)	O31	O2 #1	2.787(6)
O31	O30 #1	2.755(7)	O31	O26 #2	2.689(7)
O33	O32 #5	2.758(17)	O33	O25 #6	2.911(15)
O33	O27 #6	2.684(13)	O33	O27 #7	2.684(13)
O33	O33 #8	2.54(3)	O34	O27 #9	2.693(8)
O34	O17 #10	2.862(7)	O34	O13 #11	2.873(7)
O25	O1	3.049(6)	O25	O9 #6	2.839(6)
O25	O16 #12	2.890(6)	O27	O16 #12	2.926(7)
O30	O1	3.009(6)	O25	O32 #13	2.891(7)
O27	O33 #14	2.684(13)	O28	O14 #12	2.915(6)
O28	O13 #12	2.722(6)	O28	O13 #11	2.997(6)
O30	O4 #12	3.075(7)	O26	O1	3.047(7)
O26	O17	2.777(6)	O26	O25	2.961(7)
O26	O27	2.837(8)	O26	O31 #15	2.689(7)
O29	O10 #11	2.070(6)	O29	O1	2.897(6)
O21	O19 #2	3.065(6)	O10	O29 #16	3.070(6)
O10	O26 #16	2.905(6)	O17	O34 #17	2.862(7)
O16	O25 #18	2.890(6)	O16	O30 #18	2.775(6)
O16	O27 #18	2.926(7)	O16	O28 #18	2.942(6)
O4	O30 #18	3.075(7)	O13	O28 #16	2.722(6)
O13	O13 #19	2.729(8)	O13	O34 #16	2.873(7)
O13	O28 #18	2.997(6)	O14	O28 #18	2.915(6)
O16	O25 #18	2.890(6)	O5	O29 #1	2.985(6)
O7	O21 #3	3.020(6)	O7	O29 #1	2.901(6)
O18	O21 #15	3.037(6)	O19	O21 #15	3.065(6)
O21	O7 #5	3.020(6)	O21	O18 #2	3.037(6)

Symmetry transformations used to generate equivalent atoms: #1 1-x, 1-y, 1-z; #2 0.5+x, 1.5-y,0.5+z; #3 0.5-x, -0.5+y, 1.5-z; #4 0.5+x, 0.5-y, 0.5+z; #5 0.5-x, 0.5+y, 1.5-z; #6 -x, 1-y, 1-z; #7 x, y, 1+z; #8 -x, 1-y, 2-z; #9 1-x, 1-y, -z; #10 1+x, y, z; #11 0.5+x, 1.5-y, -0.5+z; #12 0.5-x, -0.5+y,0.5-z; #13 -0.5+x, 0.5-y, -0.5-z; #14 x, y, -1+z; #15 -0.5+x, 1.5-y, -0.5+z; #16 -0.5+x, 1.5-y, 0.5+z; #17 -1+x, y, z; #18 0.5-x, 0.5+y, 0.5-z; #19 -x, 2-y, 1-z;

The resulting water cluster $(H_2O)_{16}$ is further hydrogen bonded to its six surrounding $\{V_{14}\}$ clusters that use both terminal and bridging oxygen atoms of the cluster anions resulting in an intricate three-dimensional supramolecular network as shown in Figure 2.21.

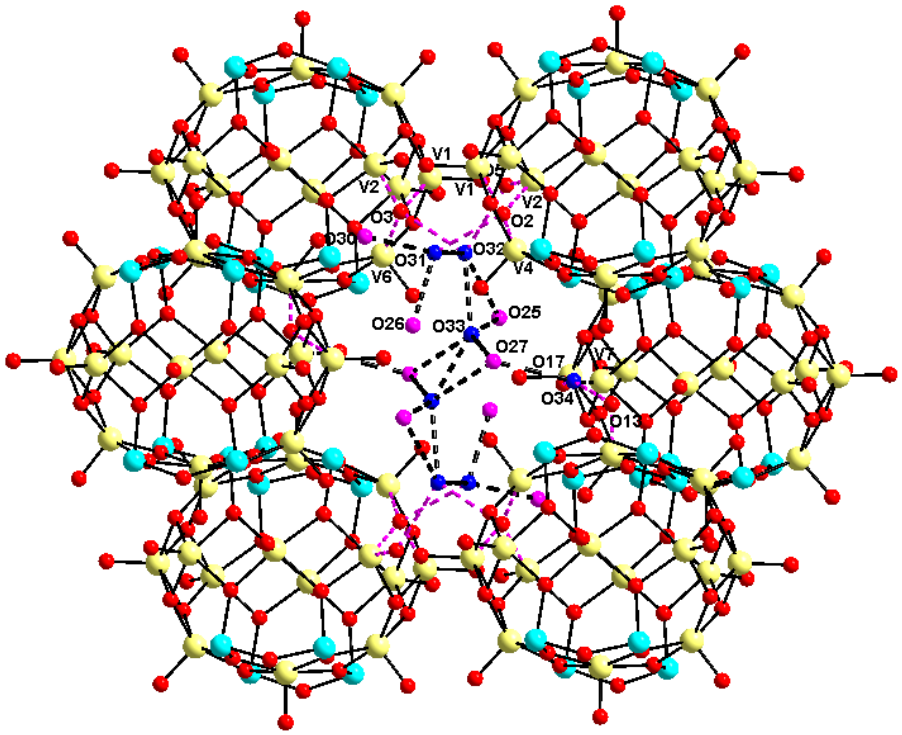

Figure 2.21. The hydrogen bonding situation around a $(H_2O)_{16}$ showing its interactions with six surrounding cluster anions, $[As_8V_{14}O_{42}(SO_3)]^{6}$. Color code, lattice water molecules, blue; lanthanum coordinated water molecules, purple; V, yellow; As, cyan; O, red; black dotted lines represent the hydrogen bonding interactions.

Similarly, in the crystal structure, each $\{V_{14}\}$ cluster is hydrogen bonded with six $(H_2O)_{16}$ water clusters around it (Figure 2.22). Single crystal X-ray diffraction analysis revealed that the compounds 6–**8** are iso-structural and thereby the unit cell dimensions, volumes, other related data for structure determinations are vary only slightly (Table 2.4). Bond

valence sum (BVS) calculations of the compounds **6** **8** suggest that all vanadium and arsenic atoms exist in +4 and +3 oxidation state respectively (BVS details are presented in the section 2.3.7.)

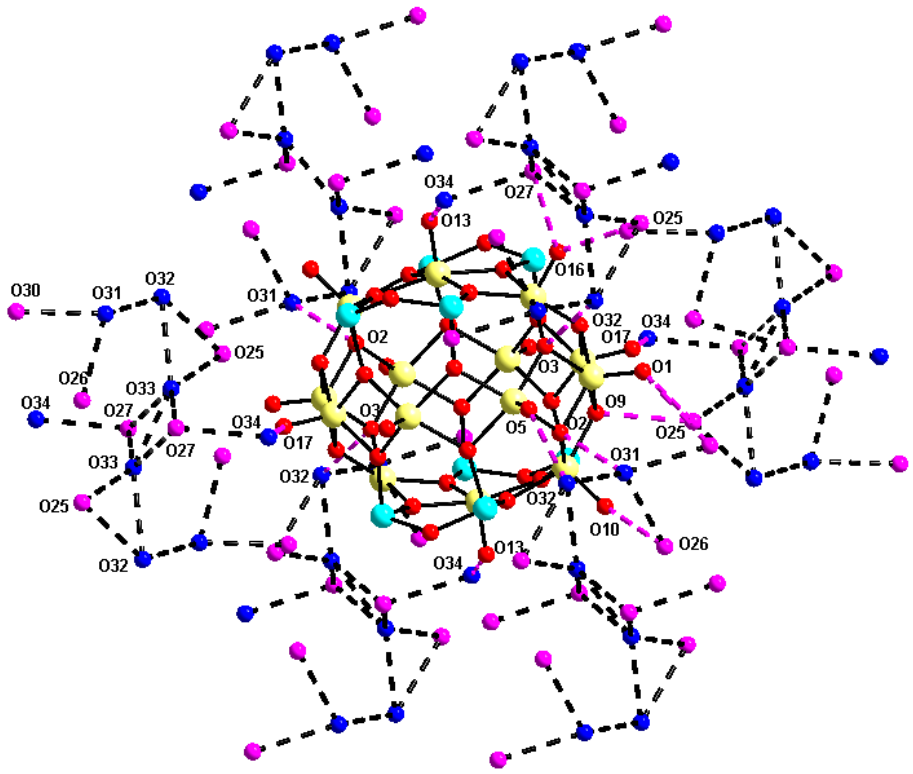

Figure 2.22. Supramolecular hydrogen bonding interactions around the cluster anion, $[As_8V_{14}O_{42}(SO_3)]^6$ that interacts with six surrounding $(H_2O)_{16}$ clusters. Color codes are same as in the caption of Figure 2.21.

2.4. Conclusion

Even though, polyoxovanadate (POV) cluster anions $[As_6V_{15}O_{42}]^4$ and $[As_8V_{14}O_{42}]^4$ have been extensively studied in the context of magnetism, its linking propensity is not explored in that extent. The coordination polymers, reported earlier

based on these POV cluster anions, were synthesized using transition metal coordination complexes (as linkers) with organic fragments as chelating ligands.[10] Organic free extended structures with these POV building unit, that would be more stable system in materials sense, are not yet explored. We have used hepta--aqua-lanthanide complexes, $[Ln(H_2O)_7]^{3+}$ (Ln = La^{3+}, Sm^{3+} and Ce^{3+}) as a linker in constructing two dimensional coordination polymers $[\{Ln(H_2O)_7\}_2(As_6V_{15}O_{42}(H_2O))] \cdot nH_2O$ (n = 12 and Ln = La^{3+} (**2**), n = 14 and Ln = Sm^{3+} (**3**), n = 11 and Ln = Ce^{3+} (**4**). In the crystal structure of compounds **2** **4** each $[As_6V_{15}O_{42}(H_2O)]^6$ cluster anion is coordinated by four $[Ln(H_2O)_7]^{3+}$ and each $[Ln(H_2O)_7]^{3+}$ is bonded by two $[As_6V_{15}O_{42}(H_2O)]^6$ cluster anions. Whereas in compounds **6** **8**, hexa-aqua-lanthanide complexes, $[Ln(H_2O)_6]^{3+}$ (Ln = La^{3+}, (**6**), Sm^{3+}, (**7**), and Ce^{3+}, (**8**)) as a linker in constructing a new class of organic free coordination polymers $[\{Ln(H_2O)_6\}_2As_8V_{14}O_{42}(SO_3)] \cdot 8H_2O$. We have shown that the $[As_8V_{14}O_{42}(SO_3)]^6$ cluster anion is attached to its surrounding six $[Ln(H_2O)_6]^{3+}$ coordination complexes by coordinate covalent bonds, which is very rarely described in polyoxometalate chemistry. This hexa-coordination of a POV cluster anion, demonstrated here, represents the rare example of POV cluster of this kind. All those compounds **2** **4** and **6** **8** can be isolated in a controlled reaction set-up starting from $[H_6V_{15}As_6O_{42}(H_2O)] \cdot 9H_2O$ (**1**) and $[NH_4]_6[As_8V_{14}O_{42}(SO_3)]$ with $Ln(NO_3)_3 \cdot 6H_2O$ respectively. To the best of our knowledge, this is the first example of a V/As/O system based coordination polymers that uses a lanthanide complex as a linker to construct extended structures. This work has an important implication for the conversion of a discrete POV cluster anion into a two-dimensional framework, formed by coordinate covalent bond that further extends to three dimensional networks using supramolecular hydrogen bonding interactions. We observed the co-existence of POV anion and POV cation in the crystal structure of compound **5**. The contraction of $\{As_6V_{15}\}$ cluster in to $\{As_8V_{12}\}$ cluster also noticed in compound **5**, which is an unusual phenomenon in polyoxometalate chemistry. The TGA / Mass analyses of the compounds **6** **8** have been discussed elaborately. We have demonstrated

that the structural decomposition temperature of this new class of coordination polymers have been elevated significantly, compared with that of the discrete cluster compound, $[NH_4]_6[As_8V_{14}O_{42}(SO_3)]$. We have also demonstrated how a metal oxide based cluster cage influences the stability of an inorganic anion, when it is encapsulated in the cavity of that cluster anion. This offers us the possibility to carry an inorganic anion (through its inclusion) to an environment of higher temperature zone where the inorganic anion is otherwise unstable. The magnetic properties of compound **6 8** have been discussed in terms of varying temperature. The f-block elements La^{3+} (**6**), Sm^{3+} (**7**) and Ce^{3+} (**8**) offer significant contribution in anti-ferromagnetic coupling interactions. We have shown, how linking a very well known and well studied magnetic object[9a] $[As_8V_{14}O_{42}(SO_3)]^6$ influences on its magnetism. It has been demonstrated that the anti-ferromagnetic coupling interactions increase in the case polymeric system (compounds **6**, **7** and **8**) compared to its discrete analogue.

2.5. References

1. a) *Molecular Electronics Devices I:* II (ed. Carter. F. L.) (Dekker, New York, 1982; 1987); b) Topical issue on polyoxometalates: Hill, C. L., Guest Ed. *Chem. Rev.* **1998**, *98*, 1 389; c) *Polyoxometalate Chemistry for Nano-Composite Design*; T. Yamase, M. T. Pope, Eds.; *Nanostructure Science and Technology*; Kluwer Academic/Plenum Publishing: New York, 2002; d) *Polyoxometalates: From Platonic Solids to Anti-Retroviral Activity;* M. T. Pope, A. Müller, Eds.; Kluwer: Dordrecht, The Netherlands, 1993; e) M. T. Pope, *Comp. Coord. Chem. II,* **2003,** *4*, 635; f) *Polyoxometalate Molecular Science*; J. J. Borràs-Almenar, E. Coronado, A. Müller, M. T. Pope, Eds.; Kluwer: Dordrecht, The Netherlands, 2003**;** g) L. Chen, F. Jiang, Z. Lin, Y. Zhou, C. Yue, M. Hong, *J. Am. Chem. Soc.* **2005**, *127*, 8588; h) J. Zarembowitch, O. Kahn, *New. J. Chem.* **1991**, *15*, 181.

2. a) A. Müller, F. Peters, M. T. Pope, D. Gatteschi, *Chem. Rev.* **1998**, *98*, 239; b) E. Coronado, C. Giménez-Saiz, C. J. Gómez-García, *Coord. Chem. Rev.* **2005**, *249*, 1776 and references cited therein.

3. a) M. T. Pope, *Heteropoly and Isopoly Oxometalates; Springer-Verlag:* Berlin, **1983**; b) M. I. Khan, S. Ayesh, R. J. Doedens, M. H. Yu, C. J. O'Connor, *Chem. Commun*. **2005**, 4658.

4. a) V. Soghomonian, Q. Chen, R. C. Haushalter, J. Zubieta, C. J. O'Connor, *Science,* **1993**, *25,* 1596; b) D. Hagrman, P. J. Hagrman, J. Zubieta, *Angew. Chem. Int. Ed.* **1999**, *38,* 3165; c) P. J. Hagrman, J. Zubieta, *Inorg. Chem.* **2000**, *39,* 3252; d) D. Hagrman, C. Sangregorio, C. J. O'Connor, J. Zubieta, *J. Chem. Soc., Dalton Trans.* **1998**, 3707; f) P. J. Hagrman, D. Hagrman, J. Zubieta, *Angew. Chem. Int. Ed.* **1999**, *38*, 2638; g) M. I. Khan, *J. Solid State Chem.* **2000**, *152*, 105; h) M. I. Khan, E. Yohannes, D. Powell, *Chem. Commun.* **1999**, 23; i) M. I. Khan, E. Yohannes, D. Dödens, *Angew. Chem. Int. Ed.* **1999**, *38*, 1292; j) M. I. Khan, E. Yohannes, R. J. Dödens, S. Tabussum, S. Cevik, L. Manno, D. Powell, *Cryst. Eng.* **1999**, *2*, 171; k) M. I. Khan, E. Yohannes, D. Powell, *Inorg. Chem.* **1999**, *38*, 212; l) V. Coué, R. Dessapt, M. Bujoli-Doeuff, M. Evain, S. Jobic, *Inorg. Chem.* **2007**, *46*, 2824; m) B. S. Bassil, M. H. Dickman, B. Kammer, U. Kortz, *Inorg. Chem.* **2007**, *46*, 2452; n) X J. Kong, Y P. Ren, P Q. Zheng, Y X. Long, L S. Long, R B. Huang, L S. Zheng, *Inorg. Chem.* **2006**, *45*, 10702.

5. a) V. W. Day, W. G. Klemperer, A. Yagasaki, *Chem. Lett.* **1990**, 1267; b) V. W. Day, W. G. Klemperer, O. M. Yaghi, *J. Am. Chem. Soc.* **1989**, *111*, 4518; c) V. W. Day, W. G. Klemperer, O. M. Yaghi, *J. Am. Chem. Soc.* **1989**, *111*, 5959; d) D. Hou, K. S. Hagen, C. L. Hill, *J. Am. Chem. Soc.* **1992**, *114*, 5864; e) A. Müller, M. Penk, R. Rohlfing, E. Krickemeyer, J. Döring, *Angew. Chem. Int. Ed.* **1990**, *29*, 926; f) D. Hou, K. S. Hagen, C. L. Hill, *J. Chem. Soc., Chem. Commun.* **1993**,

426; g) Y. Chen, X. Gu, J. Peng, Z. Shi, H. Yu, E. Wang, N. Hu, *Inorg. Chem. Commun.* **2004**, *7*, 705; h) Y. Hayashi, K. Fukuyama, T. Takatera, A. Uehara, *Chem. Lett.* **2000**, *29*, 770; i) G. K. Johnson, E. O. Schlemper, *J. Am. Chem. Soc.* **1978**, *100*, 3645; j) A. Müller, M. Penk, E. Krickemeyer, H. Bögge, H. J. Walberg, *Angew. Chem. Int. Ed.* **1988**, *27*, 1719; k) A. Müller, R. Rohlfing, J. Döring, M. Penk, *Angew. Chem. Int. Ed.* **1991**, *30*, 588; l) A. M. Khenkin, L. Weiner, R. Neumann, *J. Am. Chem. Soc.* **2005**, *127*, 9988; m) A. M. Khenkin, R. Neumann, *Angew. Chem. Int. Ed.* **2000**, *39*, 4088; n) A. M. Khenkin, L. Weiner, Y. Wang, R. Neumann, *J. Am. Chem. Soc.* **2001**, *123*, 8531; o) A. Haimov, R. Neumann, *Chem. Commun.* **2002**, 876; p) G. Maayan, B. Ganchegui, W. Leitner, R. Neumann, *Chem. Commun.* **2006**, 2230; q) A. R. Gaspar, D. V. Evtuguin, C. P. Neto, *Ind. Eng. Chem. Res.* **2004**, *43*, 7754; r) A. Bose, P. He, C. Liu, B. D. Ellman, R. J. Twieg, S. D. Huang, *J. Am. Chem. Soc.* **2002**, *124*, 4.

6. a) R. L. LaDuca Jr, R. S. Rarig Jr, J. Zubieta, *Inorg. Chem.* **2001**, *40*, 607; b) P. J. Hagrman, D. Hagrman, J. Zubieta, *Inorg. Chem.* **2001**, *40*, 2800; c) M. Yuan, Y. G. Li, E. B. Wang, Y. Lu, C. W. Hu, N. H. Hu, H. Q. Jia, *J. Chem. Soc., Dalton Trans.* **2002**, 2916; d) Y. Lu, E. B. Wang, M. Yuan, G. Y. Luan, Y. G. Li, *J. Chem. Soc., Dalton Trans.* **2002**, 3029; e) G. Y. Luan, Y. G. Li, S. T. Wang, E. B. Wang, Z. B. Han, C. W. Hu, N. H. Hu, H. Q. Jia, *J. Chem. Soc., Dalton Trans.* **2003**, 233; f) J. Lü, E. H. Shen, M. Yuan, Y. G. Li, E. B. Wang, C. W. Hu, L. Xu, J. Peng, *Inorg. Chem.* **2003**, *42*, 6956; g) Y. M. Chen, E. B. Wang, B. Z. Lin, S. T. Wang, *J. Chem. Soc., Dalton Trans.* **2003**, 519; h) Y. G. Li, E. B. Wang, H. Zhang, G. Y. Luan, C. W. Hu, N. H. Hu, H. Q. Jia, *J. Solid State Chem.* **2002**, *163*, 10; i) B. Z. Lin, S. X. Liu, *Chem. Commun.* **2002**, 2126; j) C. L. Pan, J. Q. Xu, G. H. Li, D. Q. Chu, T. G. Wang, *Eur. J. Inorg. Chem.* **2003**, 1514; k) J. R. D. Debord, R. C. Haushalter, L. M. Meyer, D. J. Rose, P. J. Zapf, J. Zubieta, *Inorg. Chim. Acta* **1997**, *256*, 165.

7. A. Müller, J. Döring, *Z. Anorg, Allg. Chem.* **1991**, *595*, 251; b) G. H. Huan, M. A. Greaney, A. J. Jacobson, *Chem. Commun.* **1991**, 260; c) A. Müller, J. Döring. *Angew. Chem. Int. Ed.* **1988**, *27*, 1721; d) A. Müller, J. Döring, H. Bögge, *Chem. Commun.* **1991**, 273; (e) W. M. Bu, L. Ye, G. Y. Yang, M. C. Shao, Y. G. Pan, J. Q. Xu, *Chem. Commun.* **2000**, 1279; f) E. Dumas, C. Livage, S. Halut, G. Hervé, *Chem. Commun.* **1996**, 2437.

8. a) A. Műller, F. Peters, M. T. Pope, D. Gatteschi, *Chem. Rev.,* **1998**, *98*, 239.

9. a) A. –L. Barra, D. Gatteschi, L. Pardi, A. Müller, J. Döring, *J. Am. Chem. Soc.* **1992**, *114*, 8509; b) D. Gatteschi, L. Pardi, A. –L. Barra, A. Müller, J. Döring, *Nature*, **1991**, *354*, 463.

10. a) G. Zhou, Y. Xu, C. Guo, X. Zheng *Inorg. Chem. Commun.* **2007**, *10*, 849; b) S. T. Zheng, J. Zhang, J-Q. Xu, G. Y. Yang, *J. Solid State Chem.* **2005**, *178*, 3740; c) S. T. Zheng, J. Zhang, G. Y. Yang, *J. Mol. Struct.* **2005**, *752*, 25; d) Y. Qi, Y. Li, E. Wang, H. Jin, Z. Zhang, X. Wang, S. Chang, *Inorg. Chim. Acta* **2007**, *360*, 1841; e) X. B. Cui, Y. Q. Sun, G. Y. Yang, *Inorg. Chem. Commun.* **2003**, *6*, 259; f) S. T. Zheng, J. Zhang, J. Q. Xu, G. Y. Yang, *J. Solid State Chem.* **2005**, *178*, 3695; g) X. Cui, J. Xu, Y. Li, Y. Sun, G. Yang, *Eur. J. Inorg. Chem.* **2004**, 1051; h) H. Jin, C. Qin, Y. G. Li, E. B. Wang, *Inorg. Chem. Commun.* **2006**, *9,* 482; (i) J. P. Wang, X. D. Du, J. Y. Niu, *J. Solid State Chem.* **2006**, *179,* 3260; j) C. D. Wu, C. Z. Lu, H. H. Zhuang, J. S. Huang, *Inorg. Chem.* **2002**, *41*, 5636; k) W. Yang, C. Lu, H. Zhuang, *J. Chem. Soc., Dalton Trans.* **2002**, 2879; l) Y. Xu, L. B. Nie, D. Zhu, Y. Song, G. P. Zhou, W. S. You, *Cryst. Growth Des.* **2007**, *7,* 925; m) V. Soghomonian, Q. Chen, R. C. Haushalter, J. Zubieta, C. J. O'Connor, *Science,* **1993**, *259,* 1596; n) D. Hagrman, P. J. Hagrman, J. Zubieta, *Angew. Chem. Int. Ed.* **1999**, *38,* 3165; o) P. J. Hagrman, J. Zubieta, *Inorg. Chem.* **2000**, *39,* 3252; p) D. Hagrman, C.

Sangregorio, C. J. O'Connor, J. Zubieta, *J. Chem. Soc., Dalton Trans.* **1998**, 3707; q) P. J. Hagrman, D. Hagrman, J. Zubieta, *Angew. Chem., Int. Ed.* **1999**, *38,* 2638; r) M. I. Khan, *J. Solid State Chem.* **2000**, *152*, 105; s) M. I. Khan, E. Yohannes, D. Powell, *Chem. Commun.* **1999**, 23; t) M. I. Khan, E. Yohannes, D. Dödens, *Angew. Chem., Int. Ed.* **1999**, *38,* 1292; u) M. I. Khan, M. I. Yohannes, R. J. Dödens, S. Tabussum, S. Cevik, L. Manno, D. Powell, *Cryst. Eng.* **1999**, *2*, 171; v) M. I. Khan, E. Yohannes, D. Powell, *Inorg. Chem.* **1999**, *38,* 212; w) Y. Cao, H. Zhang, C. Huang, Q. Yang, Y. Chen, R. Sun, F. Zhang, W. Guo, *J. Solid State Chem.* **2005**, *178*, 3563; x) M. X. Li, J. Du, J. P. Wang, J. Y. Niu, *Inorg. Chem. Commun.* **2007**, *10*, 1391; y) Z. H. Yi, X. B. Cui, X. Zhang, Y. Chen, J. Q. Xu, G. D. Yang, Y. B. Liu, X. Y. Yu, H. H. Yu, W. J. Duan, *Inorg. Chem. Commun.* **2007**, *10*, 1448; z) B. Z. Lin, Y. M. Chen, P. D. Liu, *J. Chem. Soc., Dalton Trans.* **2003**, 2474.

11. a) C. M. Liu, D. Q. Zhng, M. Xiong, D. B. Zhu, *Chem. Commun.* **2002**, 1416; b) C. L. Pan, J. Q. Xu, G. H. Li, X. B. Cui, L. Ye, G. D. Yang, *J. Chem. Soc., Dalton Trans.* **2003**, 517; c) A. H. Liu, S. L. Wang, *Inorg. Chem.* **1998**, *37*, 3415; d) J. Sha, J. Peng, Y. Li, P. Zhang, H. Pang, *Inorg. Chem. Commun*. **2008**, *11*, 907; e) R. C. Finn, E. Burkholder, J. Zubieta, *Chem. Commun.* **2001**, 1852; f) J. Chen, J. Q. Sha, J. Peng, Z. Y. Shi, B. X. Dong, A. X. Tian, *J. Mol. Struct.* **2007**, *846*, 128; g) H. An, T. Xu, E. Wang, C. Meng, *Inorg. Chem. Commun.* **2007**, *10*, 1453; h) C. J. Zhang, Y. G. Chen, H. J. Pang, D. M. Shi, M. X. Hu, J. Li, *Inorg. Chem. Commun.* **2008**, *11*, 765; i) M. Sadakane, M. H. Dickman, M. T. Pope, *Angew. Chem. Int. Ed.* **2000**, *39*, 2914; j) Z. Zhang, Y. Li, W. Chen, E. Wang, X. Wang, *Inorg. Chem. Commun*. **2008**, *11*, 879; k) X. Gan, Z. Zhang, S. Yao, W. Chen, E. Wang, H. Zhang, *J. Cluster Sci.* **2008**, *19*, 401; l) J. Y. Niu, Q. Wu, J. P. Wang, *J. Chem. Soc., Dalton Trans.* **2002**, 2512; m) L.

M. Zheng, Y. Wang. Y. X. Wang, J. D. Korp, A. J. Jacobson, *Inorg. Chem.* **2001**, *40*, 1380; n) J. P. Wang, J. W. Zhao, X. Y. Duan, J. Y. Niu, *Cryst. Growth Des.* **2006**, *6*, 507; o) C. J. Zhang, Y. G. Chen, H. J. Pang, D. M. Shi, M. X. Hu, J. Li, *Inorg. Chem. Commun.* **2008**, *11*, 765; p) V. Shivaiah, P. V. Narashimha reddy, L. Cronin, S. K. Das, *J. Chem. Soc., Dalton Trans.* **2002**, 3781; q) V. Shivaiah, M. Nagaraju, S. K. Das, *Inorg. Chem.* **2003**, *42*, 6604; r) G. Liu, Y. G. Wei, Q. Yu, Q. Liu, S. W. Zhang, *Inorg. Chem. Commun.* **1999**, *2*, 434; s) T. Yamase, H. Naruke, *J. Chem. Soc., Dalton Trans.* **1991**, 285; t) C. Gimbnéz Saiz, J. R. Galán Mascarós, S. Triki, E. Coronado, L. Ouahab, *Inorg. Chem.* **1995**, *34*, 524; u) Z. Zhang, Y. Qi, E. Wang, Y. Li, H. Tan, *Inorg. Chim. Acta.* **2008**, *361*, 1797; v) H. An, E. Wang, Y. Li, Z. Zhang, L. Xu, *Inorg. Chem. Commun.* **2007**, *10*, 299.

12. a) A. Müller, J. Döring, *Angew. Chem. Int. Ed.* **1988**, 27, 1721; b) A. Müller, J. Döring, *Z. Anorg, Allg. Chem.* **1991**, *595*, 251.
13. a) *SAINT: Software for the CCD Detector System*; Bruker Analytical X-ray Systems, Inc.: Madison, WI, 1998; b) Sheldrick, G. M. *SHELXS-97*, *Program for Structure Solution*; University of Göttingen: Göttingen, Germany, 1997; c) Sheldrick, G. M. *SHELXL-97*, *Program for Crystal Structure Analysis*; University of Göttingen: Göttingen, Germany, 1997.
14. K. Brandenburg, *DIAMOND Version 2.1e*, Crystal Impact GbR, Bonn, Germany, **2001**.
15. M. Yuan, Y. Li, E. Wang, C. Tian, L. Wang, C. Hu, N. Hu, H. Jia, *Inorg. Chem.* **2003**, *42*, 3670.
16. R. L. Dutta, A. Syamal, *Elements of Magnetochemistry*, 2nd edn.; East-West Press Pvt. Ltd., New Delhi, **1993**.
17. J. Legendziewicz, M. Borzechowska, G. Oczko, G. Meyer, *New J. Chem*. **2000**, *24*, 53.

18. O. Khan, *Molecular Magnetism;* VCH: Weinheim, Germany, **1993**.

19. X. B. Cui, J. –Q. Xu, L. Ding, H. Ding, L. Ye, G. Yu. Yang, *J. Mol. Struct.* **2003**, *660*, 131.

20. a) V. Shivaiah, S. K. Das, *Inorg. Chem.* **2005**, *44*, 8846; b) C. M. Liu, J. L. Luo, D. Q. Zhang, N. L. Wang, Z. J. Chen, D. B. Zhu, *Eur. J. Inorg. Chem.* **2004**, 4774; c) M. Yaun, Y. Li, E. Wang, C. Tian, L. Wang, N. Hu, H. Jia, *Inorg. Chem.* **2003**, *42*, 3670.

21. C. D. Wu, C. Z. Lu, H. H. Zhuang, J. S. Huang, *J. Am. Chem. Soc.* **2002,** *124*, 3836.

22. S. Liu, D. Li, L. Xie, H. Cheng, X. Zhao, Z. Su, *Inorg. Chem.* **2006**, *45*, 8036.

****

Chapter 3

==========

Polyoxometalate Supported Transition Metal Complexes: Synthesis, Supramolecular Structures and Catalysis

==========

3.1. Introduction

Polyoxometalates (henceforth will be called as POM) have become a subject of general interest because of their potential applications in the fields of catalysis, biochemical analysis, medicinal chemistry, and materials science.[1] One of the recent advances in POM chemistry is to synthesize inorganic organic hybrid materials having well defined channels and cavities, that are important in terms of material chemistry.[2] A recent trend in polyoxometalate chemistry is the functionalization of the POM cluster anions, to explore more selective applications. In broad sense, functionalization of a cluster anion can be discussed by three general categories: (i) Multi dimensional inorganic organic hybrid materials that includes porous structures (majority of the materials are synthesized by hydrothermal technique); a significant contribution in this area was made by Zubieta and co-workers[3] and Khan et al.[4] (ii) Replacement of MO_6 octahedra of the pertinent cluster anion with transition metal ions (known as substitution) resulting in a transition metal ion substituted lacunary POM cluster anion with higher negative charges (where M = addenda atoms, such as Mo, W and V etc.). (iii) Attachment of a transition metal complex (TMC) on the surface of a POM anion using covalent bonds (known as addition). Categories (ii) and (iii) have received considerable attention as far as catalysis is concerned. The cluster families, that comes under these two categories, include Keggin type heteropolyanions $[XM_{12}O_{40}]^n$, Dawson type anions $[X_2M_{18}O_{62}]^n$ (where X= Si, P etc.; M = W, Mo etc.), Lindqvist type isopolyanion

$[Mo_6O_{19}]^{2}$, heptamolybdate isopolyanion $[Mo_7O_{24}]^{6}$ and octamolybdate isopolyanion $[Mo_8O_{26}]^{4}$. Kortz and co-workers[5] have described numerous crystal structures of transition metal substituted polyoxometalates including their interesting physical properties. A pioneering work, on catalytic activities of POMs, substituted POMs and POM supported transition metal complexes towards organic transformations of industrial importance has been well-established by Neumann and his group.[6] Cronin group has also made some contribution in this area.[7] One possible route to synthesize POM supported transition metal complexes is to use organic amine cations (e.g., protonated amines) that stabilize the POM cluster anion with the assistance of supramolecular non-covalent interactions.[8] Even though, there are copious reports on the crystal structures of POM supported transition metal complexes,[9] their catalytic applications remain largely unexplored.[10] In this context, it is important to mention that the selective oxidation of alcohols to respective ketone is a central conversion in the organic synthesis.[11] In earlier years, the selective oxidation was carried out by several oxidizing agents such as hypervalent iodines.[12] Since then numerous methods have been developed for this significant reaction, that are, however, associated with several disadvantages. These include severe environmental problems due to the wastage of solvents, reagents and generation of unwanted side products. In recent years, seeking environmentally benign (green chemistry) methods for the same oxidation have been realized and numerous publications have appeared in this direction. The molecular oxygen (O_2) is a green, universal oxidant and several catalytic systems (for example, CuCl.phen,[13a] $H_5PV_2Mo_{10}O_{40,}$[13b-d] PdLn,[13e-g] M-TEMPO,[13h-i] bimetallic systems: Os-Cu and Mo-Cu,[13j-l] ruthenium based catalysts: Ru-biomimetic-coupled systems, Ru-hydroxyapatite, $RuCl_2$(p-cymene)$_2$/Cs_2CO_3, RuO_2 and perruthenate,[13m-q] Pt and Pt/Bi catalyst,[13r-t] Manganese oxide molecular sieves,[13u] and V_2O_5[13v]), that use molecular oxygen as an oxidant for the conversion of alcohols to their corresponding ketones, have successfully been developed. The various aspects of the usage of molecular oxygen (as an oxidant) have been reviewed

by Sheldon et.al in their recent article.[14] Some demerits of the usage of molecular oxygen (O_2) are also to be considered seriously, for example, (i) in many cases only one of the two oxygen atoms from the molecular oxygen (O_2) is used for the oxidation and hence stoichiometric amount of co-reductant also to be needed, (ii) it is difficult to control the reaction and some time it leads to the combustion/blast. By taking into account all these, we found another green oxidant 'hydrogen peroxide' as oxygen source. It contains 47.1% of active oxygen (wt %) which is significantly higher than the other common oxidizing agents such as HNO_3 (25.0%), ^tBuOOH (17.8%), and $NaIO_4$ (29.9%) etc. Furthermore, it is prominently easy to handle and gives only water as the by-product. We report here the synthesis and structural characterization of a new series of polyoxometalate supported transition metal complexes

$[HMTAH]_2[\{Zn(H_2O)_5\}\{Zn(H_2O)_4\{Mo_7O_{24}\}] \cdot 2H_2O$ (**1**)

$[2\text{-ampH}]_4[\{Zn(H_2O)_5\}Mo_7O_{24}] \cdot 9H_2O$ (**2**),

$[3\text{-ampH}]_4[\{Zn(3\text{-ampy})(H_2O)_4\}Mo_7O_{24}] \cdot 4H_2O$ (**3**),

$[3\text{-ampH}]_4[\{Co(3\text{-ampy})(H_2O)_4\}Mo_7O_{24}] \cdot 4H_2O$ (**4**),

$[2,3\text{-diamp}]_4[Co(H_2O)_6][Mo_7O_{24}] \cdot 6H_2O$ (**5**)

$[2,3\text{-diampH}]_2[\{Zn(2,3\text{-diampH})_2(H_2O)_2\}Mo_8O_{27}] \cdot 2H_2O$ (**6**)

(where HMTA = hexamethylenetetramine, amp = aminopyridine and diamp = diaminopyridine)

emphasizing their diversity in supramolecular structures. We have demonstrated compound **1** catalyzes the oxidation of benzyl alcohol to benzaldehyde. We also studied catalytic activity of compound **2** towards the oxidation of a series of secondary alcohols to corresponding ketones using hydrogen peroxide as an oxidant at moderate temperature. All the oxidation reactions were carried out in solvent free, environmentally benign conditions, in which compound **1** and **2** are used as heterogeneous catalyst (in catalytic amount).

3.2. Experimental Section

3.2.1. Materials

All the chemicals and solvents were reagent grade available commercially and were used without any further purification. The distilled water was used throughout the work. Benzyl alcohol is distilled prior to use for catalysis experiment. 30% (w/v) Hydrogen peroxide was used as oxidant.

A general synthetic strategy for secondary alcohols (a) (e) used in catalysis

The secondary alcohols, (a) α methylbenzyl alcohol, (b) 4-methyl α methylbenzyl alcohol, (c) 4 bromo α methylbenzyl alcohol, (d) α ethylbenzyl alcohol, and (e) 4 methyl α ethylbenzyl alcohols were prepared by reducing their corresponding ketones with $NaBH_4$ in methanol as described below: Acetophenone (18 mL, 149 mmol) in 100 mL of methanol in the case of (a), 4-methyl-acetophenone (8 mL, 59.92 mmol) in 50 mL of methanol in the case of (b), 4-bromo-acetophenone (6.14g, 30.8 mmol) in 50 mL of methanol in the case of (c), Propiophenone (13.30 mL, 100 mmol) in 100 mL of methanol in the case of (d) and 4-methyl-propiophenone (8.5 mL, 55.40 mmol) in 200 mL of methanol in the case of (e) was taken in a round bottom flask and cooled to 5^{o}C. To this solution, $NaBH_4$ (11.65g, 308 mmol for (a), 4.6g, 121.6 mmol for (b), 2.34g, 61.9 mmol for (c), 7.6g, 201 mmol for (d) and 4.3g, 114 mmol for (e)) was added slowly by stepwise. The reaction mixture was stirred for one hour at room temperature and then refluxed for 30 hours at 60^{o}C. The evaporation of the methanol results in the formation of colorless semi-solid. To this, water was added and the aqueous layer was extracted with dichloromethane. The alcohols thus obtained were purified by distillation; finally purity has been checked by ^{1}H NMR spectroscopy. Purified alcohols were taken as starting precursors for the catalytic oxidation (vide infra). The product conversion (%) was analyzed by ^{1}H NMR technique. The catalysis scheme

(oxidation of the secondary alcohols to their corresponding ketones) and preparation scheme of the secondary alcohols from their respective ketones are shown in Scheme 1.

Scheme 1.

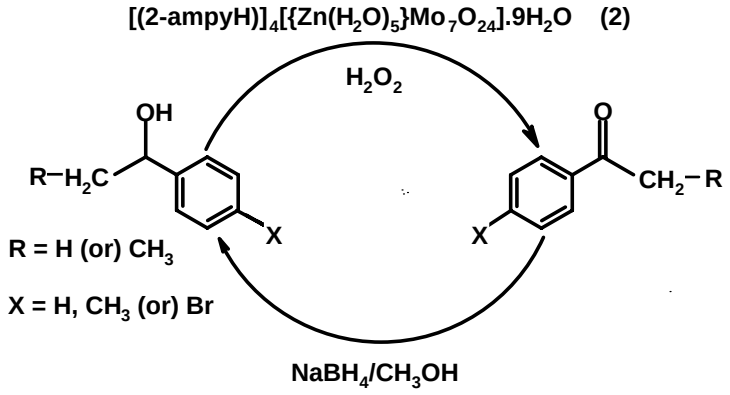

3.2.2. Physical Measurements

Elemental analyses were determined by FLASH EA series 1112 CHNS analyzer. Infra red spectra of solid samples obtained as KBr pellets on a JASCO – 5300 FT – IR spectrophotometer. Thermogravimetric analyses were carried out on a STA 409 PC analyzer and corresponding masses were analyzed by QMS 403 C mass analyzer, under the flow of N_2 gas with a heating rate of $5^oC\ min^{-1}$, in the temperature range of 30-1100^oC. In catalysis experiments, the product analyses were performed by ^1H NMR spectral studies (Bruker DRX 400 spectrometer using $Si(CH_3)_4$ as an internal standard in $CDCl_3$ solvent).

3.2.3. Synthesis and Characterization

$[HMTAH]_2[\{Zn(H_2O)_5\}\{Zn(H_2O)_4\{Mo_7O_{24}\}] \cdot 2H_2O$ (1)

Sodium molybdate (1g, 4.13 mmol) was dissolved in 100 mL of water, and its pH was adjusted to 3.0 by adding conc. HCl. To this solution, a mixture of $Zn(NO_3)_2.6H_2O$ (0.5g, 1.68 mmol) and hexamethylenetetramine (0.2g, 1.42 mmol) dissolved in 20 mL of water was added slowly. The resulting reaction mixture was stirred for 5 hours and then it was filtered. The colorless filtrate was kept in an open beaker at room temperature. After

three days, colorless crystals were filtered and washed thoroughly with water and then dried at room temperature. Yield 0.35 g (36% based on Mo).

Anal calcd. for $C_{12}H_{48}Mo_7N_8O_{35}Zn_2$: C, 8.65; H, 2.90; N, 6.72 %. Found: C, 8.85; H, 3.04; N, 6.58 %. FT-IR (KBr pellet): (ν/cm^{-1}): 3449(br), 1655(m), 1462(s), 1369(s), 1300(s), 1253(s), 1211(s), 1024(s), 979(s), 893(s), 671(s).

A general synthetic strategy for compounds 2 6.

Sodium molybdate (1g, 4.13 mmol in the case of compounds **2 4** and 0.5g, 2.07 mmol in the case of compounds **5 6**) was dissolved in 100 mL of water and its pH was adjusted to 2.0 by conc. HCl acid. In a separate beaker, the metal salt $M(NO_3)_2{\cdot}6H_2O$ (M = Zn^{2+}, 0.5g, 1.68 mmol for compounds **2 3**; 0.25g, 0.86 mmol for compound **6**; Co^{2+}, 0.5g, 1.72 mmol for compound **4** and 0.25g, 0.86 mmol for compound **5**) and aminopyridine derivatives (0.2g, 2.13 mmol of 2-aminopyridine for compound **2** and 3-aminopyridine for compounds **3 4** and 0.12g, 1.10 mmol of 2,3 diaminopyridine for compounds **5 6**) were dissolved in 20 mL of water. This reaction mixture of aminopyridine derivative and divalent metal salt was added drop-wise to the sodium molybdate solution with stirring. The resulting reaction mixture was stirred for 6 hours (during stirring, the formation of precipitate / turbidity was dissolved by heating the reaction mixture at 70–80^{o}C in three to fours slots). The reaction mixture was then filtered and kept in open beaker for crystallization without any disturbance at room temperature. After one week, crystals formed, were filtered, washed with plenty of water and finally dried at room temperature. One of the single crystals from each, suitable for X-ray diffraction study, was selected and characterized structurally.

$[2\text{-ampH}]_4[\{Zn(H_2O)_5\}Mo_7O_{24}]\cdot 9H_2O$ (2)

Yield: 0.42g (41% based on Mo) Anal. calcd for $C_{20}N_8H_{56}ZnMo_7O_{38}$: C, 13.70; H, 3.22; N, 6.39. Found: C, 13.57; H, 3.21; N, 6.33. IR (KBr pellet): (ν/cm^{-1}): 3329, 3171, 1658, 1622, 1541, 1475, 1383, 1327, 1244, 1168, 991, 889, 829, 765, 617.

$[3\text{-ampH}]_4[\{Zn(3\text{-ampy})(H_2O)_4\}Mo_7O_{24}]\cdot 4H_2O$ (3)

Yield: 0.35g (34% based on Mo) Anal. Calcd for $C_{25}N_{10}H_{50}ZnMo_7O_{32}$: C, 17.26; H, 2.90; N, 8.05. Found: C, 17.10 ; H, 2.86; N, 7.95. IR (KBr pellet): (ν/cm^{-1}): 3337, 3229, 3057, 2085, 1614, 1560, 1485, 1398, 1332, 1280, 1072, 922, 885, 829, 679, 584.

$[3\text{-ampH}]_4[\{Co(3\text{-ampy})(H_2O)_4\}Mo_7O_{24}]\cdot 4H_2O$ (4)

Yield: 0.32g (31% based on Mo) Anal. Calcd for $C_{25}N_{10}H_{50}CoMo_7O_{32}$: C, 17.32; H, 2.91; N, 8.08. Found: C, 17.11; H, 2.98; N, 7.97. IR (KBr pellet): (ν/cm^{-1}): 3329, 3202, 3057, 1635, 1556, 1481, 1394, 1338, 1275, 889, 669, 615, 462.

$[2,3\text{-diampH}]_4[Co(H_2O)_6][Mo_7O_{24}]\cdot 6H_2O$ (5)

Yield: 0.17g (33% based on Mo) Anal. Calcd for $C_{20}N_{12}H_{56}CoMo_7O_{36}$: C, 13.56; H, 3.19; N, 9.49. Found: C, 13.65; H, 3.10; N, 9.65. IR (KBr pellet): (ν/cm^{-1}): 3420, 3310, 3190, 3078, 2918, 1647, 1614, 1570, 1464, 1386, 1313, 1230, 1182, 1086, 920, 883, 605.

$[2,3\text{-diampH}]_2[\{Zn(2,3\text{-diampH})_2(H_2O)_2\}Mo_8O_{27}]\cdot 2H_2O$ (6)

Yield: 0.14g (31% based on Mo) Anal.Calcd for $C_{20}N_{12}H_{40}ZnMo_8O_{31}$: C, 13.51; H, 2.27; N, 9.46. Found: C, 13.99; H, 2.22; N, 10.01. IR (KBr pellet): (ν/cm^{-1}): 3368, 3188, 3082, 1655, 1560, 1466, 1093, 922, 881, 690, 580.

3.2.4. Single Crystal Structure Determination

Data were measured on a Bruker SMART APEX CCD area detector system [λ(Mo Kα) = 0.71073 Å], graphite monochromator, 2400 frames were recorded with an ω scan width of 0.3°, each for 5 second, a crystal detector distance of 60 mm, and a collimator of 0.5 mm. The data were reduced using SAINTPLUS,[15a] the structures were solved using SHELXS-97,[15b] and refined using SHELXL-97,[15c] DIAMOND[16] software

was used for molecular graphics. All non hydrogen atoms were refined anisotropically. We tried to locate the hydrogen atom of solvent water molecules through differential Fourier maps, but couldn't succeed. A summary of the crystallographic data and structure determination parameters for **1–3** is provided in Table 3.1, and for **4 6**, it is given in Table 3.4.

3.3. Results and Discussion

3.3.1. Infrared Spectroscopy

The infra red spectrum of compound **1** shows the characteristic strong peaks at 902 and 945cm^{-1}, that are attributed to the vibrations of Mo=O bonds. The sharp peaks at 1300 and 1253cm^{-1} are probably due to the C H stretching aroused from hexamethylenetetramine ligand. The zinc-coordinated water molecules along with lattice water molecules are reflected by a broad feature at around 3450 cm^{-1} and a relatively sharp band at around 1650 cm^{-1}. The IR spectra of compounds **2 6** have some common features as far as molybdenum-oxygen bonds are concerned because compounds **2 5** contain the same $[Mo_7O_{24}]^6$ isopolyanion[17] and compound **6** includes similar cluster anion $[Mo_8O_{27}]^6$. A very similar feature in the range of 880 990 cm^{-1} in the IR spectra of compounds **2 6** is assigned to the characteristic peaks of Mo O_t. (O_t terminal oxygen). The vibrational bands aroused in the region of 1000 1650 cm^{-1} can be assigned to the bending vibrations (either C H or N H) or aromatic ring stretching frequencies of the aminopyridine moieties. Compound [2-ampH]$_4$[{Zn(H_2O)$_5$}Mo_7O_{24}]·9H_2O (**2**) shows a considerable amount of red shift for C N vibration in its IR spectrum when compared to the C N vibration of free 2-aminopyridine molecule, that appears at 1442 cm^{-1}. This red shift is occurred due to the protonation of ring nitrogen atom in 2-aminopyridine. In compounds **3-6**, the similar red shifts are observed for C N vibration.

3.3.2. Thermogravimetric / Mass Analyses (TGA / Mass)

The thermogravimetric analyses for compounds **1** **4** were performed in flowing nitrogen with a heating rate of 5^{o} per minute in the temperature range from 30 to 1100^{o}C. Compound **1** shows four weight losses. The first weight loss includes 7.51% in the temperature range of 35 180^{o}C that corresponds to the loss of seven water molecules (calculated mass loss for seven water molecules is 7.55%). These seven water molecules seem to be two lattice water molecules and five water molecules from the penta-aqua-metal coordination site. The second weight loss of 4.63% in the temperature range of 180 250^{o}C is due to the loss of four water molecules (calculated mass loss for four water molecules is 4.31%). The source of these four water molecules should be the tetra-aqua Zn-complex, supported on the POM anion by two coordinate covalent bonds (as if the heptamolybdate anion is a bidentate ligand towards this $Zn(H_2O)_4$ complex). The removal of these four water molecules at later stage and higher temperature is logical because this tetra-aqua-zinc complex is more strongly held by the POM anion support (two coordinate covalent bonds) compared to the penta-aqua-zinc complex (one coordinate covalent bond). Thus two dissimilar zinc-aqua coordination complexes, supported on a same POM anion, can be realized by the TGA plot. This also helps to understand, how stability of a metal-aqua complex increases with its number of coordination to the support (which is a metal oxide based cluster anion in the present case). The corresponding mass losses are given in the TGA/Mass graph presented in Figure 3.1(a). The evolution of water molecules in these two stages have been evidenced by the mass loss curve. The third and fourth weight losses are 5.23% and 21.14% respectively that are due the structural decomposition including the organic amines, evidenced by the evolution of carbon dioxide gas as shown in purple color curve in the TGA / Mass plot (Figure 3.1(a)). TG curve for compound $[2\text{-ampH}]_4[\{Zn(H_2O)_5\}Mo_7O_{24}]\cdot 9H_2O$ (**2**) shows the first weight loss of 14.01% in the temperature range of 35 130^{o}C. This weight loss corresponds to the loss of fourteen water molecules (calculated mass loss for fourteen water molecules

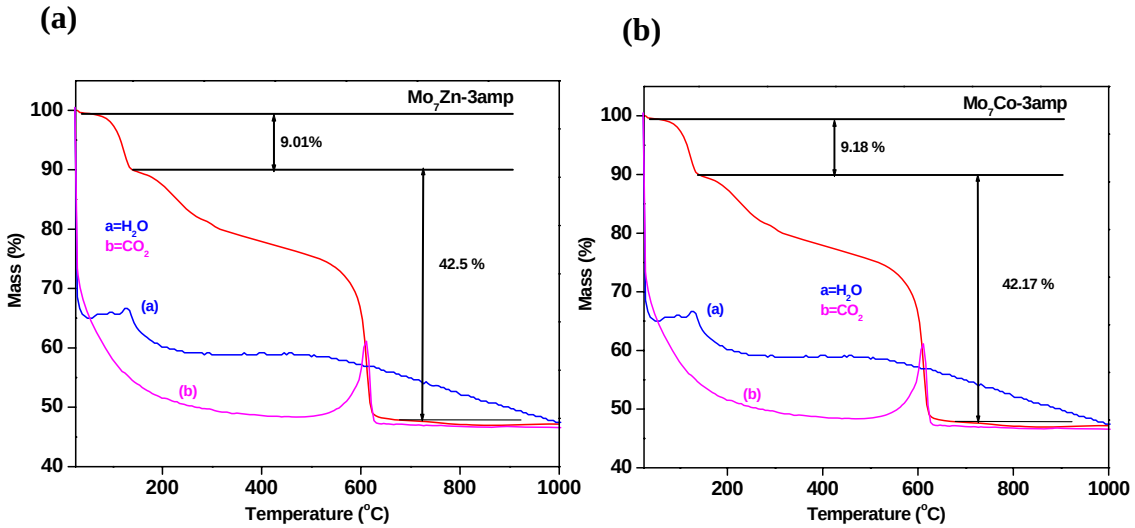

Figure 3.1. (a) TGA/Mass plot of the compound HMTAH]$_2$[{Zn(H_2O)$_5$}{Zn(H_2O)$_4${Mo_7O_{24}}]·2H_2O (**1**) (b) TGA / Mass plot of the compound [2-ampH]$_4$[{Zn(H_2O)$_5$}Mo_7O_{24}]·9H_2O (**2**) Color code: TGA curve, red line; water mass loss curve, blue line; carbon dioxide mass loss curve, purple.

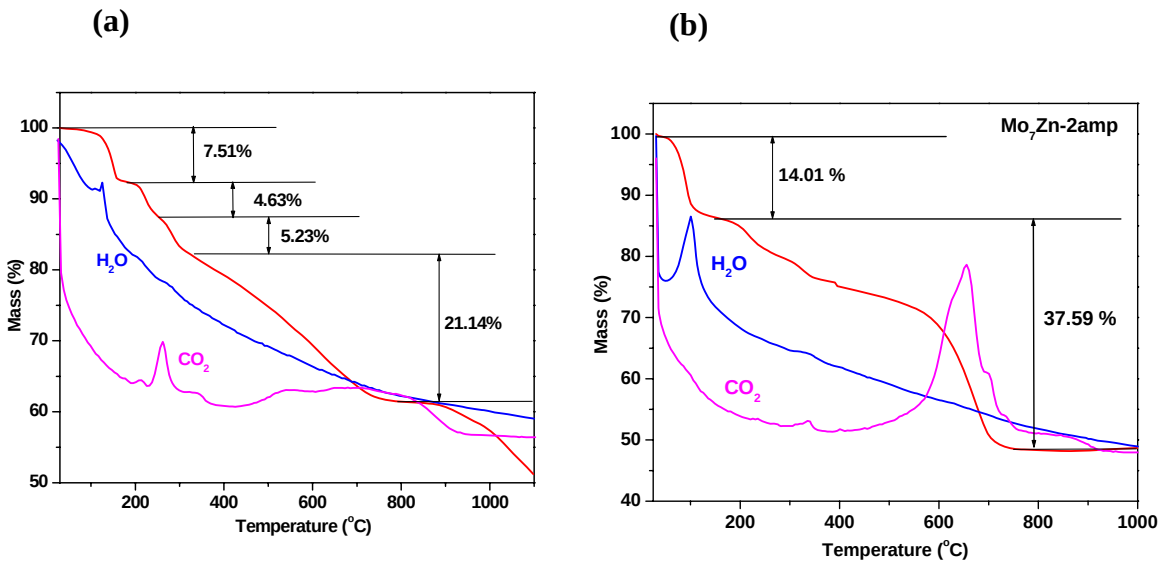

Figure 3.2. (a) TGA/Mass plot of the compound [3-ampH]$_4$[{Zn(3-ampy)(H_2O)$_4$}Mo_7O_{24}]·4H_2O (**3**) (b) TGA/Mass plot of the compound [3-ampH]$_4$[{Co(3-ampy)(H_2O)$_4$}Mo_7O_{24}]·4H_2O (**4**). Color code as shown in Figure 3.1. caption

is 14.37%). This includes nine non-coordinated and five zinc coordinated water molecules per formula unit. We have used compound **2** as a catalyst after its heating at 70-80^{o}C for the oxidation of secondary alcohols and found it is stable in many cycles. This means that we have used partially dehydrated compound **2** (as catalyst) as far TGA results are concerned. The total weight loss in the temperature range of 150 750^{o}C is 38% is due to the oxidation of 2-aminopyridine molecules and the structural decomposition of $\{ZnMo_7O_{24}\}^{4-}$ moiety (Figure 3.1(b)). The water mass loss and carbon dioxide evolution curves have been shown in blue and purple color respectively in the Figure 3.1(b). Compounds **3** and **4** are isostructural and hence show identical TG / Mass curves. Each compound contains eight (four lattice and four metal coordinated water molecules) water molecules which are evolved in the temperature range of 35 150^{o}C with a loss of 9.01% for **3**, and 9.18% for **4** (calculated mass loss for eight water molecules is 8.28% for **3**, and 8.31% for **4**). The total weight loss in the temperature range of 150 750^{o}C is 42.5% for **3** and 42.17% for **4** is due to the oxidation of 3-aminopyridine molecules and the structural decomposition of $\{ZnMo_7O_{24}\}^{4}$ and $\{CoMo_7O_{24}\}^{4}$ moieties respectively. The corresponding loss of water and carbon dioxide mass loss curves are shown in blue and purple color respectively (Figures 3.2(a) and (b)).

3.3.3. X-ray Crystallographic Studies

Majority of the POM cluster-supported transition metal complexes are synthesized hydrothermally and in most cases it results in the formation of multidimensional structures.[18] The compound $[HMTAH]_2[\{Zn(H_2O)_5\}\{Zn(H_2O)_4\{Mo_7O_{24}\}] \cdot 2H_2O$ (**1**) has been synthesized in an one-pot wet synthesis starting from sodium molybdate, zinc nitrate and hexamethylenetetramine from an aqueous medium of pH 3.0. We believe that aqueous molybdate solution results in the formation of heptamolybdate anion, $[Mo_7O_{24}]^{6}$ at pH of

3.0. The formation of this cluster anion, $[Mo_7O_{24}]^6$ can be explained by the protonation of molybdate anion at lower pH (3.0) followed by a series of condensation reactions. The overall reaction for this cluster formation is shown in equation 1. The zinc aqua-complexes $[Zn(H_2O)_5]^{2+}$ and $[Zn(H_2O)_4]^{2+}$, formed in situ from zinc nitrate and water, in this reaction are subsequently coordinated to the POM cluster anion $[Mo_7O_{24}]^6$ resulting the POM supported zinc-aqua complexes, $[\{Zn(H_2O)_5\}\{Zn(H_2O)_4\{Mo_7O_{24}\}]^2$ (equation 2). Finally, the two negative charges of this anionic species is counter-balanced by two mono-protonated hexamethylenetetramine cations ($[HMTAH]^+$) resulting in the isolation of the title compound **1**. It is important to note that, even though the cyclic amine (hexamethylenetetramine) is, in principle, capable of coordinating to Zn^{2+} ion through its nitrogen donors, this did not happen in this synthesis. We argue that low pH (3.0) is not favorable for such metal nitrogen bond, because the metal-nitrogen bond undergoes facile acid-hydrolysis reaction at a lower pH.

$$7[MoO_4]^2 + 8H^+ \quad [Mo_7O_{24}]^6 + 4H_2O \qquad (1)$$

$$[Mo_7O_{24}]^6 + [Zn(H_2O)_5]^{2+} + [Zn(H_2O)_4]^{2+} \quad [\{Zn(H_2O)_5\}\{Zn(H_2O)_4\{Mo_7O_{24}\}]^2 \qquad (2)$$

We have isolated compounds $[2\text{-ampH}]_4[\{Zn(H_2O)_5\}Mo_7O_{24}]\cdot 9H_2O$ (**2**), $[3\text{-ampH}]_4[\{Zn(3\text{-ampy})(H_2O)_4\}Mo_7O_{24}]\cdot 4H_2O$ (**3**), $[3\text{-ampH}]_4[\{Co(3\text{-ampy})(H_2O)_4\}Mo_7O_{24}]\cdot 4H_2O$ (**4**), $[2,3\text{-diamp}]_4[Co(H_2O)_6][Mo_7O_{24}]\cdot 6H_2O$ (**5**) and $[2,3\text{-diampH}]_2[\{Zn(2,3\text{-diampH})_2(H_2O)_2\}Mo_8O_{27}]\cdot 2H_2O$ (**6**) in a conventional wet synthesis at room temperature and we found that, compounds **2–5** are discrete and **6** is a coordination polymer. The crystal structure of cobalt analogue of compound **2** is reported very recently, for which synthesis was performed by hydrothermal technique and in the relevant article it was mentioned that this hydrothermal procedure remained unsuccessful to produce zinc analogue.[19] Our present synthesis offers the successful preparation of both zinc (**2**) and cobalt (**2a**) analogues. The compounds **2** and **2a** are crystallized in orthorhombic space group, *Pna2(1)* (crystal data for **2a**: a = 14.9527(6), b = 17.2509(6), c = 19.4734(7) Å, = = =90°), which is identical to that of published cobalt compound.

The crystal structure of compound **2a** will not be discussed further in this chapter; however its catalytic activity would be described, that was not known earlier. All the compounds **2–6** were isolated in acidic aqueous medium (pH 3 6). For compounds **2 5**, the POM cluster anion is heptamolybdate anion, the formation of which can be explained by the protonation of molybdate anion at lower pH followed by a series of condensation reactions. In the case of compounds **2 3**, the heptamolybdate anion (formed in situ at a low pH, eq 1) undergoes coordination reaction with a $[M^{II}(H_2O)_5]^{2+}$ / $[M^{II}(H_2O)_4L]^{2+}$ complex (L is a N donor ligand) cation resulting in the formation of a POM supported transition metal complex anion $[\{M^{II}(H_2O)_5\}$ / $\{M^{II}(H_2O)_4L\}Mo_7O_{24}]^4$, that is counter balanced by four protonated L (protonation of L is not unlikely at the low pH of this synthesis), with the isolation of compounds $[2\text{-ampH}]_4[\{Zn(H_2O)_5\}Mo_7O_{24}] \cdot 9H_2O$ (**2**), $[3\text{-ampH}]_4[\{Zn(3\text{-ampy})(H_2O)_4\}Mo_7O_{24}] \cdot 4H_2O$ (**3**), $[3\text{-ampH}]_4[\{Co(3\text{-ampy})(H_2O)_4\}Mo_7O_{24}] \cdot 4H_2O$ (**4**).

Scheme 2

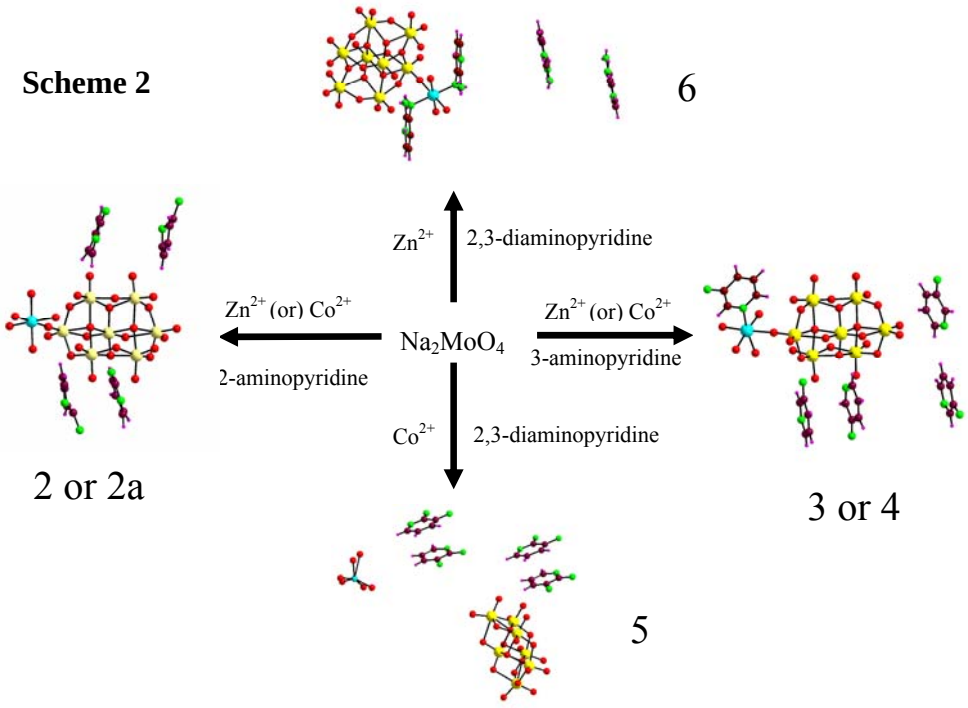

In this series, compound $[2,3\text{-diamp}]_4[Co(H_2O)_6][Mo_7O_{24}]\cdot 6H_2O$ (**5**) is unique in the sense that the hexa-aquo-cobalt complex is not coordinated to the heptamolybdate anion. The various synthetic pathways were briefly represented in scheme 2. In the case of compound $[2,3\text{- diampH}]_2[\{Zn(2,3\text{-diampH})_2(H_2O)_2\}Mo_8O_{27}]\cdot 2H_2O$ (**6**), the POM cluster anion is an unusual octamolybdate anion, $[Mo_8O_{27}]^6$. This unusual POM cluster $[Mo_8O_{27}]^6$ (the usual one is $[Mo_8O_{26}]^4$) can be described by the formation of a linear chain of hypothetical cluster $[H_2Mo_8O_{28}]^6$, arising from a condensation reaction as shown in Scheme 3. This justifies the molecular formula of this condensed corner sharing chain as $[Mo_8O_{27}]_n^{6n}$, because each $[Mo_8O_{26}]^4$ cluster anion shares two bridging oxygen atoms (from the opposite sides) along the axis of the chain.

Scheme 3.

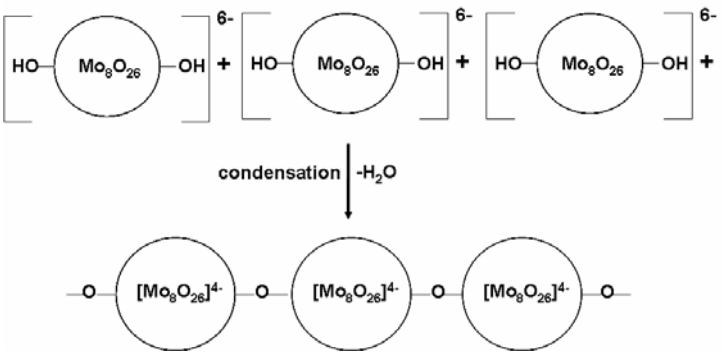

Crystal Structure Description of Compound $[HMTAH]_2[\{Zn(H_2O)_5\}\{Zn(H_2O)_4\{Mo_7O_{24}\}]\cdot 2H_2O$ (1)

The single crystal X-ray structure determination of compound **1** shows that, one heptamolybdate cluster anion, that is functionalized by two dissimilar zinc-aqua complexes $[Zn(H_2O)_5]^{2+}$ and $[Zn(H_2O)_4]^{2+}$, two protonated hexamethylenetetramines as cations ($[HMTAH]^+$) and two lattice water molecules are present in its asymmetric unit and hence compound **1** can be formulated as $[HMTAH]_2[\{Zn(H_2O)_5\}\{Zn(H_2O)_4\{Mo_7O_{24}\}]\cdot 2H_2O$. The relevant crystallographic data and refinement parameters are given in Table 3.1. Thermal ellipsoidal representation of

the anionic part of compound **1** is given in Figure 3.3. The POM cluster anion $[Mo_7O_{24}]^6$ act as a ligand coordinating two different zinc-aqua complexes $[Zn(H_2O)_5]^{2+}$ and $[Zn(H_2O)_4]^{2+}$ in two different modes. In the case of penta-aqua complex $[Zn(H_2O)_5]^{2+}$, the cluster anion is coordinated to Zn^{2+} ion via the terminal oxygen O(14) of heptamolybdate and the remaining coordination sites of zinc ion in the complex are occupied by five water molecules completing a distorted octahedral geometry around zinc ion (Figure 3.3).

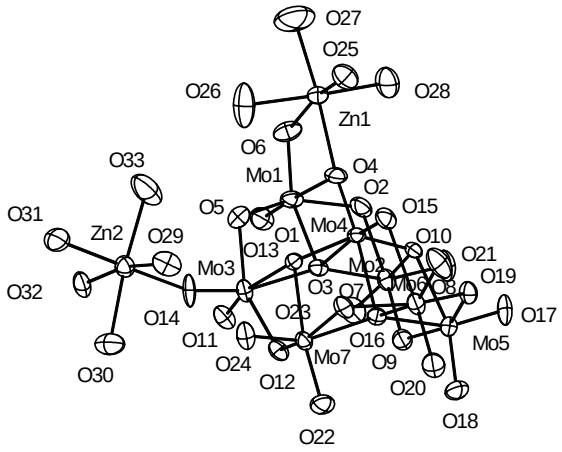

Figure 3.3. Thermal ellipsoidal representation of $[\{Zn(H_2O)_5\}\{Zn(H_2O)_4\}\{Mo_7O_{24}\}]^{2}$ cluster anion with 50% probability.

In tetra-aqua complex $[Zn(H_2O)_4]^{2+}$, the Zn^{2+} ion is chelated to the anionic cluster in bidentate fashion via $O_t(6)$ and $O_b(4)$ (O_t and O_b are terminal and bridging oxygen atoms of the cluster anion respectively). Four water molecules are additionally coordinated to Zn^{2+} ion leading to an octahedral geometry around zinc ion. The bond angles Zn(1) O(6) Mo(1) and Zn(1) O(4) Mo(1) in the tetra-aqua complex are 91.23 and 115.00^o respectively. This is one of the rare examples of a POM supported metal coordination complex, in which a bridging oxygen atom of POM anion has extended its coordination to the metal ion (in the present case Zn^{2+} ion). The cyclic organic amine HMTA can be described as four nitrogen atoms interconnected by six methylene groups forming a bi-cyclic adamantane like structure with twelve C N bonds, in which there are

no C C and N N bonds. It is worth mentioning that HMTA has been used as a versatile ligand in metallo-supramolecular chemistry via its possible coordination modes (one to four nitrogen atoms are involved in coordination) leading to novel topological architectures.[20]

Table 3.1. Crystal Data and Structural Refinement for Compounds **1 3**

	1	**2**	**3**
Empirical formula	$C_{12}H_{48}Mo_7N_8O_{35}Zn_2$	$C_{20}H_{56}Mo_7N_8O_{38}Zn$	$C_{25}H_{50}Mo_7N_{10}O_{32}Zn$
Formula weight	1666.90	1753.68	1739.70
T [K]	293(2)	293(2)	293(2)
λ (Å)	0.71073	0.71073	0.71073
Crystal system	Monoclinic	Orthorhombic	Monoclinic
Space group	*C2/c*	*Pnma*	*Cc*
a [Å]	43.12(3)	14.9216(12)	18.328(4)
b [Å]	12.399(10)	19.4883(15)	13.624(3)
c [Å]	16.285(13)	17.2325(13)	20.406(4)
deg]	90.00	90	90
β [deg]	111.131(11)	90	96.377(3)
deg]	90.00	90	90
V [Å^3]	8122(11)	5011.2(7)	5063.9(19)
Z	8	4	4
D_{calc} [Mg m^{-3}]	2.726	2.324	2.282
μ [mm^{-1}]	3.367	2.276	2.244
F[000]	6480	3440	3400
Crystal size [mm^3]	0.25 x 0.15 x 0.08	0.20 x 0.10 x 0.08	0.42 x 0.40 x 0.32
θ range for data collection [deg]	1.01 to 26.05	1.58 to 26.08	1.87 to 26.08
Reflections collected/unique	31611 / 7363	50413 / 5109	25307 / 9875
R [int]	0.0539	0.0334	0.0192
Refinement method	Full-matrix least-squares on F^2		
Goodness-of-fit on F^2	1.110	1.302	1.086
R_1/wR_2 [$I > 2\sigma(I)$]	0.0636/0.1940	0.0832/0.1811	0.0188/0.0496
R_1/wR_2 [all data]	0.0867/0.2238	0.0841/0.1814	0.0189/0.0497
Largest diff. Peak/hole [e· Å ^{3}]	1.527/-1.357	1.976/-2.014	0.661/-0.618

However, in the present study, we would not expect HMTA to coordinate to the zinc ion at the pH maintained in the synthesis (vide supra). Previously, by using protonated hexamethylenetetramine ($HMTAH^+$) as counter ion, Cronin and co-workers were able to stabilize and isolate a highly charged POM anion, $[H_2Mo^{V}_4Mo^{VI}_{16}O_{52}]^{10-}$ (Mo_{16} cluster) , which represents a new structural type.[21a] They have also shown that this $\{Mo_{16}\}$ cluster anion decomposes in the presence of divalent transition metal cations (Fe^{2+} and Mn^{2+}} in high concentrations, to produce the isostructural $\{Mo_7M_2\}$-type compounds $(HMTAH^+)_2[Fe_2(H_2O)_9Mo_7O_{24}] \cdot 2H_2O$ and $(HMTAH^+)_2[Mn_2(H_2O)_9Mo_7O_{24}] \cdot 2H_2O$ which are based on individual heptamolybdate fragments.[21b] In the crystal structure, four types of hydrogen bonding interactions are expected: N H···O/O H···N, O H···O, C H···O and N H···N hydrogen bonds. Since the hydrogen atoms on nitrogen base and water oxygens could not be located, and only one nitrogen of each organic amine is protonated, it would not be possible to distinguish between N H···O, O H···N hydrogen bonds around organic amine cation. One of the organic amines (can be named as N1N2N3N4) undergoes three N H···O / O H···N hydrogen bonding interactions with two surrounding zinc-aqua complexes and one lattice water (O34) molecule (Figure 3.4(a)). Similarly the other organic amine (namely N5N6N7N8) interacts with three surrounding zinc-aqua complexes and one lattice water (O35) molecule by N H···O / O H···N hydrogen bonds (Figure 3.4(b)). The N H···O / O H···N and O H···O hydrogen bonds are represented as N···O and O···O distances respectively in Table 3.2. There are two lattice water molecules O34 and O35. The O34 water molecule is hydrogen bonded to one organic amine via N4 nitrogen atom (N H···O / O H···N hydrogen bond) and three terminal oxygen atoms (O1, O8 and O17) from two surrounding heptamolybdate anions (O H···O hydrogen bonds). On the other hand, the O35 water molecule is hydrogen bonded to O35 itself (related by a symmetry operation) forming a water dimer (O H···O hydrogen bond), a zinc-coordinated water molecule

O31 (O H···O hydrogen bond) , a terminal oxygen atom O21 of a hetamolybdate anion (O H···O hydrogen bond) and organic amine via N5 nitrogen atom (N H···O / O H···N hydrogen bond). The hydrogen bonding situation of these lattice water molecules are depicted in Figures 3.5 (a) and (b). The hydrogen bonding situation (O H···O hydrogen bonds) around the cluster anion $[Mo_7O_{24}]^{6}$ is shown in Figure 3.6.

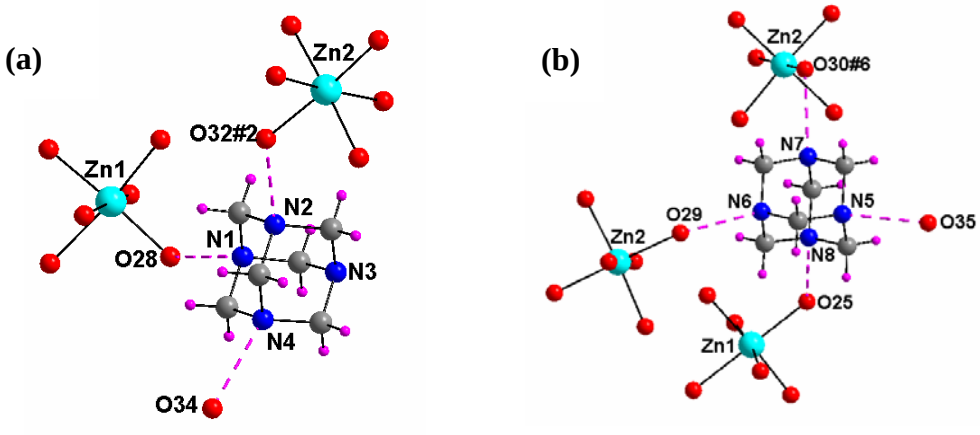

Figure 3.4. (a) The Hydrogen bonding interaction of the amine cations [namely (a) 'N1N2N3N4 and (b) 'N5N6N7N8'] with surrounding zinc complexes and lattice water molecules. Color code: O, red; C, gray; H, purple; Zn, cyan; N, blue; purple dotted lines represent the N H···O / O H···N hydrogen bonding interactions.

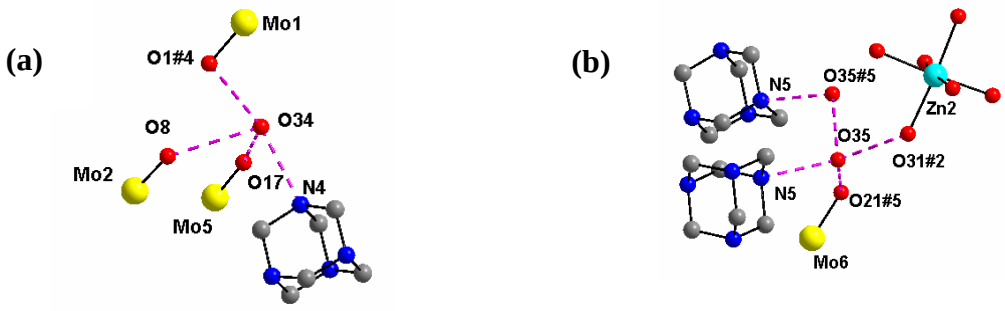

Figure 3.5. (a) The hydrogen bonding situation (only N H···O / O H···N interaction) around the lattice water molecules (O34 and O35); (a) around O34 water molecule (b) around O35 water molecule (hydrogen atoms of organic amines are omitted for clarity). Color code: O, red; Mo, yellow; C, gray; Zn, cyan; N, blue; purple dotted lines represent the hydrogen bonding interactions.

Table 3.2. Geometrical parameters of the N H···O / O H···N and O H···O hydrogen bonds (Å) represented as N···O and O···O distances respectively, involved in supramolecular network in the crystal structure of compound $[HMTAH]_2[\{Zn(H_2O)_5\}\{Zn(H_2O)_4\{Mo_7O_{24}\}] \cdot 2H_2O$ (**1**)

O(34) O(1)#4	2.888(17)	O(34) O(8)	3.013(16)
O(34) O(17)	2.810(16)	O(34) N(4)	2.679(17)
O(35) N(5)	2.740(18)	O(35) O(35)#5	2.890(4)
O(35) O(21)#5	2.842(18)	O(35) O(31)#2	2.942(18)
O(31) O(18)#6	2.735(15)	O(31) O(22)#6	2.642(15)
O(31) O(35)#7	2.942(18)	O(33) O(9)#6	2.914(15)
O(32) N(2)#7	2.730(16)	O(32) O(21)#7	2.718(13)
O(29) N(6)	2.882(14)	O(29) O(24)	2.791(14)
O(14) O(5)	2.709(13)	O(14) O(13)	2.873(11)
O(14) O(11)	2.707(13)	O(30) N(7)#8	2.808(14)
O(14) O(12)	2.778(13)	O(26) O(11)#6	2.797(17)
O(26) O(7)#6	2.836(15)	O(6) O(5)	2.813(13)
O(6) O(1)	2.767(14)	O(4) O(13)	2.779(12)
O(4) O(3)	2.713(11)	O(4) O(2)	2.878(15)
O(4) O(10)	2.807(12)	O(4) O(15)	2.737(13)
O(28) O(2)#3	2.955(14)	O(28) N(1)	2.926(17)
O(25) N(8)	2.806(15)	O(25) O(17)#1	2.867(13)
O(27) O(8)#3	2.841(17)	O(17) O(25)#9	2.867(13)
O(7) O(26)#8	2.836(15)	O(21) O(32)#2	2.718(13)
O(11) O(26)#8	2.797(17)	O(18) O(31)#8	2.735(15)
O(1) O(34)#10	2.888(17)	O(22) O(31)#8	2.642(15)
N(2) O(32)#2	2.730(16)	N(7) O(30)#6	2.808(14)
O(21) O(35)#5	2.842(18)		

Symmetry transformations used to generate equivalent atoms: #1 x, 1-y, 0.5+z; #2 x, -1+y, z; #3 0.5-x, 1.5-y, 1-z; #4 0.5-x, -0.5+y, 0.5-z; #5 -x, y, 0.5-z; #6 x, 2-y, 0.5+z; #7 x, 1+y, z; #8 x, 2-y, -0.5+z; #9 x, 1-y, -0.5+z; #10 0.5-x, 0.5+y, 0.5-z.

This shows that the heptamolybdate anion is hydrogen bonded to five surrounded zinc-aqua complexes besides two zinc-aqua complexes that are supported by the cluster anion through coordinate covalent bonds. Both zinc-aqua complexes undergo both O H···O and N H···O / O H···N hydrogen bonding interactions with surrounding heptamolybdate anion and organic amine cations resulting in a complicated hydrogen

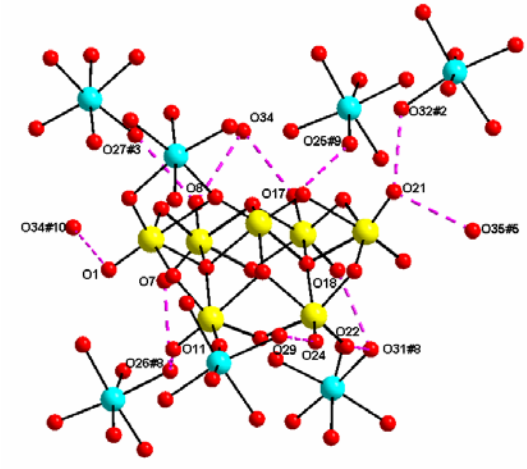

Figure 3.6. The hydrogen bonding situation around the cluster anion $[Mo_7O_{24}]^6$. Color code: O, red; Mo, yellow; C, gray; Zn, cyan; purple dotted lines represent the O H···O hydrogen bonding interaction.

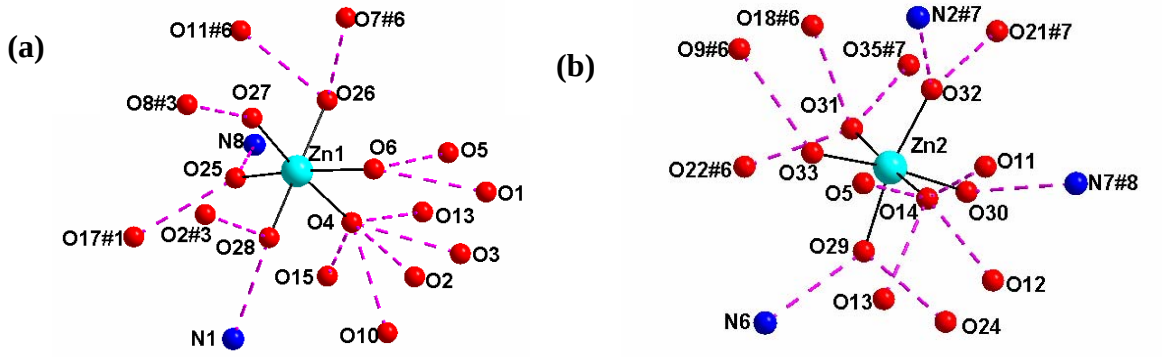

Figure 3.7. The weak supramolecular O H···O and N H···O / O H···N hydrogen bonding interactions of zinc-aqua complexes with surrounding heptamolybdate anion and organic amine cations resulting in a complicated hydrogen bonding situation. Color code: O, red; Zn, cyan; N, blue; purple dotted lines represents the hydrogen bonding interactions.

bonding situation (Figure 3.7). The organic amine cations use their C H bonds to form C H···O hydrogen bonds with surrounding POM anions. As shown in Figure 3.8, organic amines 'N1N2N3N4' and 'N5N6N7N8' are hydrogen bonded with five and four surrounding heptamolybdate anions respectively. Similarly, in the crystal structure, each isopolyanion is attached to six adjacent organic amine cations (Figure 3.9).

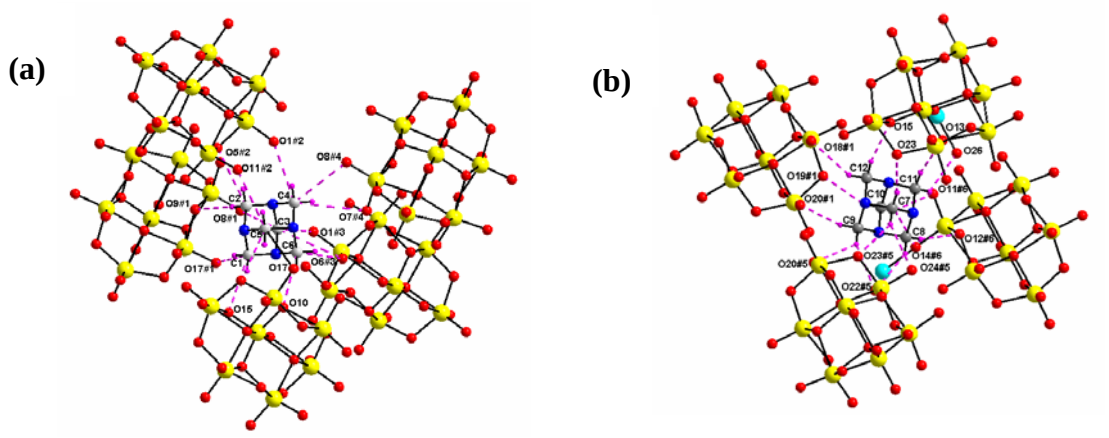

Figure 3.8. The C H···O hydrogen bonding interactions of organic amine cations with surrounding cluster anion: (a) 'N1N2N3N4' and (b) 'N5N6N7N8'. Color code: O, red; Mo, yellow; C, gray; H, purple; Zn, cyan; N, blue; purple dotted lines represents the hydrogen bonding interactions.

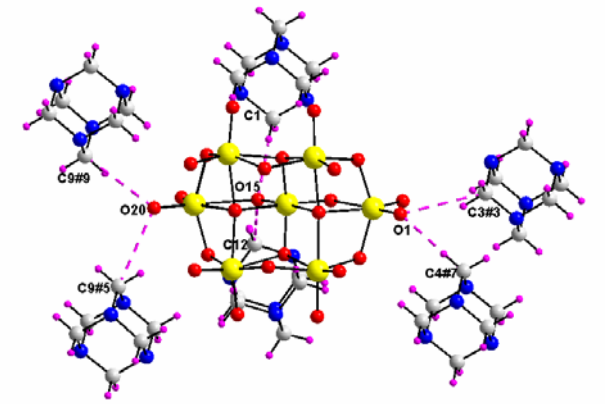

Figure 3.9. The C H···O hydrogen bonding interactions of $[Mo_7O_{24}]^{6}$ anion with surrounding amine cations. Color codes are same as mentioned in Figure 3.5.

This results in an intricate three-dimensional supramolecular network having well-defined channels in a view looking down to the crystallographic *c* axis, as shown in Figure 3.10. The C H···O hydrogen bonding parameters are presented in Table 3.3. In compound **1,** Bond Valence Sum (BVS) calculation confirms that all the Mo and Zn atoms are in +6 and +2 respectively. The BVS results can be described as: Mo atoms are +6 (s = 6.05 6.18) and Zn atoms are +2 (s = 1.88).

Description of the Crystal Structures: Crystal Structure $[2\text{-ampH}]_4[\{Zn(H_2O)_5\}Mo_7O_{24}]\cdot 9H_2O$ (2)

Compound $[2\text{-ampH}]_4[\{Zn(H_2O)_5\}Mo_7O_{24}]\cdot 9H_2O$ (**2**) is crystallizes in orthorhombic space group, *pnma*. The relevant asymmetric unit contains $[Mo_5O_{16}]^3$ (three Mo atoms and eight oxygen atoms are in half occupancies), one zinc-aqua complex $[Zn(H_2O)_4]^{2+}$, that is covalently linked to isopolyanion (zinc atom and three oxygen atoms of three water molecules are in half occupancies), two protonated 2-aminopyridine molecules and five lattice water molecules (one of these water molecules in half occupancy). The asymmetric unit is shown in Figure 3.11(a) excluding organic amine cations. Based on this asymmetric unit, molecular formula of **2** can be formulated as $[2\text{-ampH}]_4[\{Zn(H_2O)_5\}Mo_7O_{24}]\cdot 9H_2O$ (**2**). The molecular structure is shown in Figure 3.11(b). In the crystal structure, the divalent zinc-aqua complex $[Zn(H_2O)_5]^{2+}$ is supported by the heptamolybdate $[Mo_7O_{24}]^6$ cluster anion via Mo-O_t-Zn coordinate covalent bond (where O_t is a terminal oxygen on molybdenum), resulting in the formation of POM supported zinc-aqua complex $[Mo_7O_{24}\{Zn(H_2O)_5\}]^4$, the negative charges of which have been compensated by four mono protonated 2-aminopyridine molecules. The oxygen bonding modes in the POM supported zinc-aqua complex $[Mo_7O_{24}\{Zn(H_2O)_5\}]^4$ can be classified in to four different (O_t, μ_2, μ_3, and μ_4) categories. Those are in the ranges of Mo O$_t$ 1.705(9) 1.743(13) Å, Mo O(μ_2) 1.754(12) 2.543(11) Å, Mo O(μ_3) 1.881(8) 2.252(8) Å, and Mo O(μ_4) 2.149(12) 2.231(8) Å. The zinc cation is linked to the cluster anion via Zn(1) O(1) Mo(1), and the remaining five coordination sites of zinc atom is satisfied by aqua ligands and hence the metal ion possesses distorted octahedral geometry. The bond lengths of Zn O varies in the range of 1.998(16) 2.105(12) Å. The bond angle of Zn(1) O(1) Mo(1) is 177.1(7)^o which clearly indicates the transition metal complex $\{Zn(H_2O)_5\}^{2+}$ linked the $[Mo_7O_{24}]^6$ cluster anion via Mo O$_t$ bond in a nearly linear fashion. The C(6) atom of one of the

2-aminopyridine rings is largely disordered; N(4A) and N(4B) of the same 2-aminopyridine molecule are characterized with half occupancies.

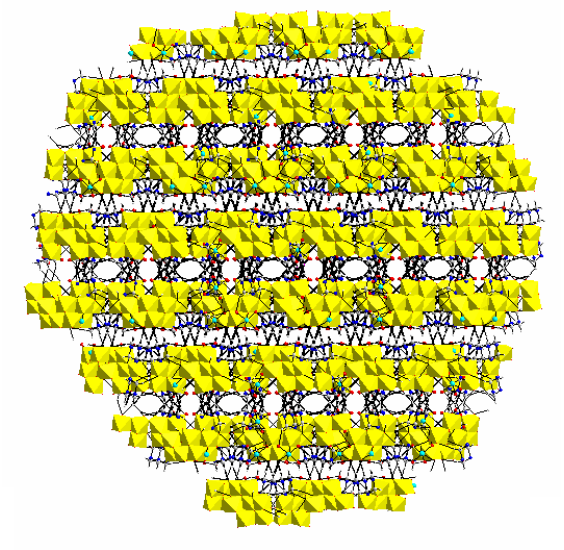

Figure 3.10. Three-dimensional supramolecular network (formed by N H···O/O H···N, O H···O, C H···O and N H···N hydrogen bonding interactions) having well-defined channels in a view looking down to the crystallographic *c* axis in compound **1**.

(**a**)

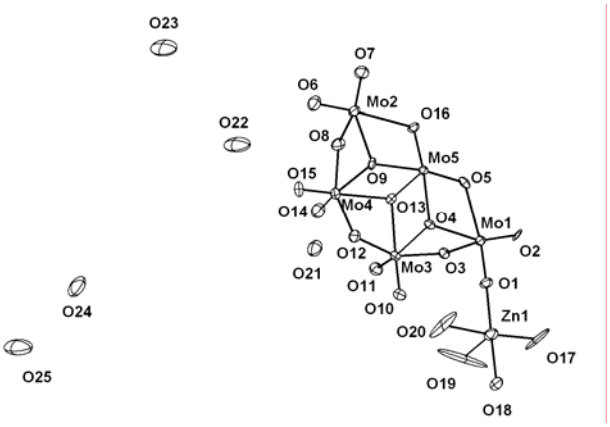

(**b**)

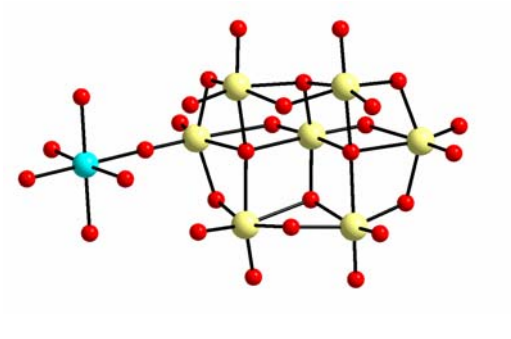

Figure 3.11. (a) The thermal ellipsoidal plot (50% probability) of the asymmetric unit of compound $[2\text{-ampH}]_4[\{Zn(H_2O)_5\}Mo_7O_{24}]\cdot 9H_2O$ (**2**) excluding 2-aminopyridine cations; (b) The molecular structure of $[2\text{-ampH}]_4[\{Zn(H_2O)_5\}Mo_7O_{24}]\cdot 9H_2O$ in compound **2** excluding 2-aminopyridine cations and lattice water molecules. Color code: Mo, yellow; Zn, cyan; O, red.

Table 3.3. Geometrical parameters of the C H···O hydrogen bonds (Å, °) involved in supramolecular network of compound **1**. D = donor; A = acceptor.

D H···A	d(D···H)	d(H···A)	d(D···A)	(DHA
C1 H1A O15	0.97	2.34	3.257(16)	158.2
C1 H1B O17#1	0.97	2.51	3.411(19)	155.2
C2 H2A O9#1	0.97	2.54	3.511(17)	179.3
C2 H2B O5#2	0.97	2.46	3.361(16)	154.9
C3 H3A O1#3	0.97	2.55	3.298(15)	133.5
C3 H3B O8#1	0.97	2.55	3.444(18)	152.6
C4 H4A O1#2	0.97	2.37	3.262(16)	153.0
C4 H4B O7#4	0.97	2.73	3.541(15)	140.9
C5 H5B O11#2	0.97	2.65	3.578(19)	159.8
C5 H5A O17	0.97	2.59	3.379(17)	139.0
C5 H5A O19	0.97	2.42	3.327(18)	155.1
C6 H6A O6#3	0.97	2.65	3.492(18)	144.9
C6 H6B O10	0.97	2.36	3.314(17)	166.9
C7 H7A O23	0.97	2.38	3.328(16)	164.8
C7 H7B O24#5	0.97	2.60	3.470(17)	148.7
C7 H7B O23#5	0.97	2.51	3.354(16)	145.7
C8 H8A O12#6	0.97	2.42	3.372(14)	165.9
C8 H8B O22#5	0.97	2.50	3.349(17)	146.4
C9 H9A O20#5	0.97	2.45	3.140(16)	127.5
C9 H9A O22#5	0.97	2.50	3.355(17)	147.3
C9 H9B O20#1	0.97	2.28	3.217(16)	163.1
C10 H10A O11#6	0.97	2.45	3.331(15)	151.4
C10 H10A O14#6	0.97	2.64	3.471(16)	144.4
C10 H10B O19#1	0.97	2.56	3.473(16)	157.6
C11 H11A O26	0.97	2.63	3.292(19)	125.8
C11 H11B O13	0.97	2.54	3.482(17)	164.5
C12 H12A O18#1	0.97	2.54	3.388(19)	146.6
C12 H12B O15	0.97	2.21	3.153(19)	162.7

Symmetry codes are already specified in the footnote of Table 3.2.

Studies on Supramolecular Interactions in [2-ampH]$_4$[{Zn(H$_2$O)$_5$}Mo$_7$O$_{24}$]·9H$_2$O (2): Identification of a New Type of Water Chain (C10)

Interestingly, an extensive hydrogen bonding interactions (O H O, N H O and C H O) have been observed in the crystal structure of **2**, that involve terminal and bridging oxygen atoms of heptamolybdate anion, zinc coordinated water molecules, protonated 2-aminopyridine moieties. Compound **2** contains nine lattice water molecules per formula unit, and further five water molecules (as aqua ligands) coordinated to zinc cation and hence the existence of O H···O hydrogen bonding interactions leading to the formation of supramolecular water clusters is expected in the crystal lattice of **2**. The four lattice water molecules (namely, O21, O23, O24, O25) and their corresponding symmetry equivalents form a water heptamer $(H_2O)_7$ cluster (water heptamer is taken instead of water octamer because each O24 water oxygen is characterized with half occupancy), that self assembles into a supramolelcular water chain running along crystallographic *b* axis. Infantes and Motherwell published a classic paper on the patterns of water clusters within the Cambridge Structural Database (CSD) that have been classified as discrete rings and chains, infinite chains and tapes, and layer structures.[22] According to them, the second most common pattern of water clusters is the infinite water chain. The nomenclature for these infinite water chains, that do not involve water rings, is Cn for 'n' water molecules that are traversed in order to reach the unit cell repeat atom, for example C3 means that three water molecules form the unit cell repeat unit of the infinite chain irrespective of crystallographic independence of these water molecules. Based on this Infantes-Motherwell classification, the nomenclature of the present water chain is C10 (Figure 3.12(a)). From CSD, chains are found for patterns C2–C8, C10, C12 and C14; among these patterns, C2 and C4 dominate (together 78%) and C10 is only 1.1%.[22] The formation of this water chain (Figure 3.12(b)) is favored by its supramolelcular hydrogen bonding interactions with its surrounding POM supported complex cation as shown in Figure 3.12(b).

Table 3.4. Crystal Data and Structural Refinement for Compounds **4** **6**

	4	**5**	**6**
Empirical formula	$C_{25}H_{50}Mo_7N_{10}O_{32}Co$	$C_{20}H_{56}CoMo_7N_{12}O_{36}$	$C_{20}H_{40}ZnMo_8N_{12}O_{31}$
Formula weight	1733.26	1771.28	1777.53
T [K]	293(2)	293(2)	293(2)
λ [Å]	0.71073	0.71073	0.71073
Crystal system	Monoclinic	Monoclinic	Monoclinic
Space group	*Cc*	*C2/c*	*C2/c*
a [Å]	18.1750(8)	20.8890(10)	20.377(9)
b [Å]	13.5872(8)	17.2244(8)	10.406(5)
c [Å]	20.3409(10)	13.7320(7)	21.189(9)
deg]	90.00	90	90
β [deg]	96.4820(10)	97.7880(10)	98.383(7)
deg)	90.00	90	90
V [Å^3]	4991.0(4)	4895.2(4)	4445(3)
Z	4	4	4
D_{calc} [Mg m^{-3}]	2.307	2.403	2.656
μ [mm^{-1}]	2.129	2.180	2.822
F[000]	3388	3476	3432
Crystal size [mm^3]	0.40 x 0.30 x 0.12	0.32 x 0.10 x 0.08	0.26 x 0.10 x 0.04
θ range for data collection [deg]	1.88 to 28.29	1.54 to 26.02	1.94 to 28.29
Reflections collected/unique	26096 / 11568	25092 / 4823	24570 / 5281
R [int]	0.0180	0.0268	0.0333
Refinement method	Full-matrix least-squares on F^2		
Goodness-of-fit on F^2	1.100	1.054	1.066
R_1/wR_2 [$I > 2\sigma(I)$]	0.0214/0.0578	0.0407/0.1052	0.0473/0.1325
R_1/wR_2 [all data]	0.0215/0.0579	0.0438/0.1074	0.0524/0.1358
Largest diff. Peak/hole [e· Å ^{3}]	2.050/ 0.812	1.929/ 2.479	1.165/ 5.008

.

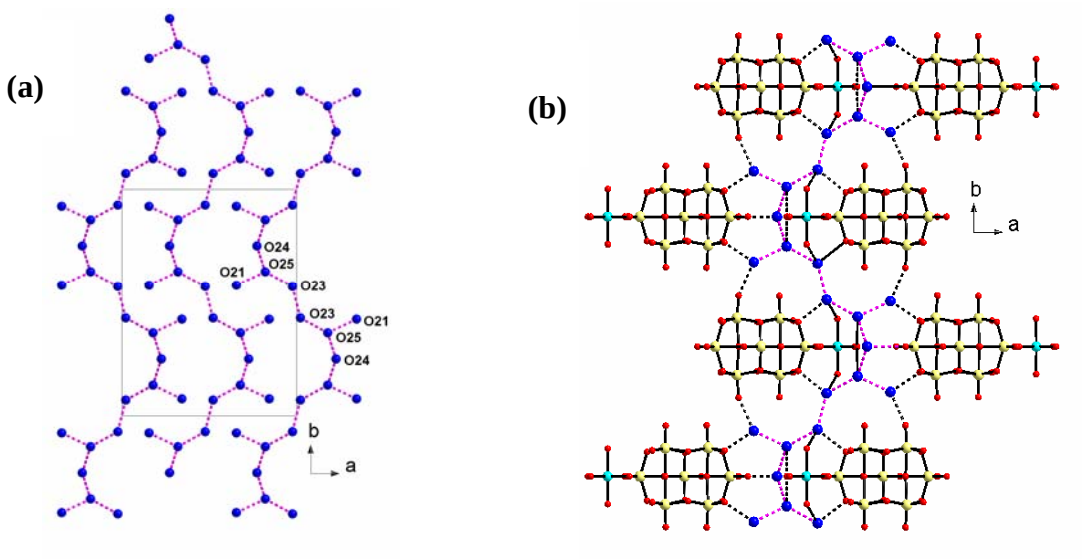

Figure 3.12. (a) The formation of supramolecularly hydrogen bonded water chains, in a view along crystallographic '*c*' axis in compound **2**. (b) Supramolecular O H···O hydrogen bonding interactions of a water chain with its surrounding POM supported complex cation in compound **2**. Color code: Mo, yellow; Zn, cyan; O, red; oxygen atom from water chain, blue; purple and black dotted lines represent O H···O hydrogen bonding interactions within water chain and water chain with its surrounding respectively.

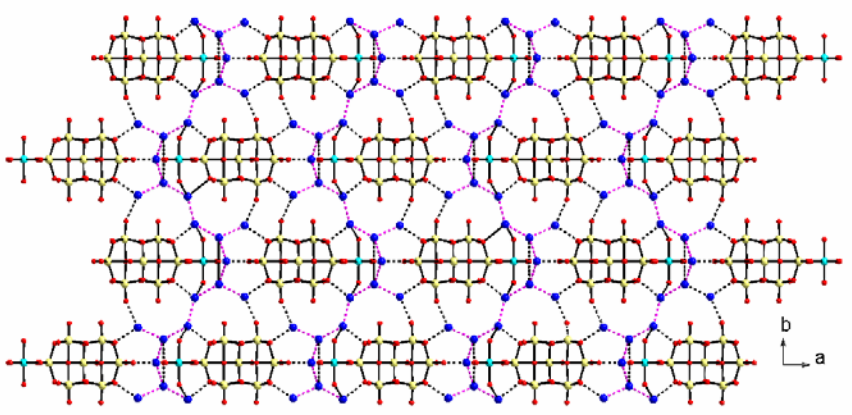

Figure 3.13. The water chain motif laterally linked by O H···O hydrogen bonding interactions with its surrounding resulting in a two-dimensional (2D) framework in compound **2**. Color codes are same as mentioned in the caption of Figure 3.12.

Both bridging and terminal oxygen atoms of the isopolyanion and zinc-coordinated water oxygens are actively involved in stabilizing this water chain. The water chain motif with its surrounding (Figure 3.12(b)) is, in turn, laterally linked by hydrogen bonding interactions resulting in an intricate supramolecular feature as shown in Figure 3.13. The ring nitrogen of 2-aminopyridine is more basic than the substituent amine group nitrogen and hence the protonation is likely to be taken place at its ring nitrogen. We tried to locate the hydrogen atoms on the protonation site, amine nitrogens and hydrogen atoms of water molecules through differential Fouriar map without success. The hydrogen bonding distances are given as O O distances (Table 3.5). The C H O hydrogen bonding parameters are listed in Table 3.6.

Crystal Structure of $[3\text{-ampH}]_4[\{Zn(3\text{-ampy})(H_2O)_4\}Mo_7O_{24}]\cdot 4H_2O$ (3)

Compound **3** crystallizes in the monoclinic system (space group *Cc*). The asymmetric unit in the crystal structure of **3** is composed of a discrete heptamolybdate anion supported zinc coordination complex $[\{Zn(3\text{-ampy})(H_2O)_4\}Mo_7O_{24}]^4$, four mono protonated 3-aminopyridine molecules and four lattice water molecules giving rise to the full molecule $[3\text{-ampH}]_4[\{Zn(3\text{-ampy})(H_2O)_4\}Mo_7O_{24}]\cdot 4H_2O$ (**3**). The relevant thermal ellipsoidal plot is shown in Figure 3.14. The crystal structure of compound **3** differs from the compound **2** in the zinc cation's coordination environment: in the crystal structure of compound **2**, Zn^{2+} ion covalently linked with POM anion but not with 2-amp molecule, whereas in the case of compound **3**, the Zn^{2+} ion is covalently coordinated with both POM anion and 3-amp molecule (Figure 3.14). The coordination site of each Zn^{2+} ion, in the crystal structure of compound **3,** is a distorted octahedron formed by one terminal oxygen atom from heptamolybdate anion, one 3-aminopyridine molecule and the rest four positions of the octahedron are co-ordinated by four aqua ligands. We believe that the less steric hindrance in 3-aminopyridine molecule, compared to 2-aminopyridine molecule in compound **2**, is the possible driving force for its coordination to zinc cation.

The molybdenum-oxygen distances in **3** can be grouped into four sets: Molybdenum-terminal oxygen (Mo O$_t$), 1.708(2) 1.731(2) Å; Mo O(μ_2) 1.736(2) 2.556(3) Å, Mo O(μ_3) 1.863(2) 2.308(2) Å, and Mo O(μ_4) 2.108(2) 2.266(2) Å.

Table 3.5. Geometrical parameters of the O H···O and N H···O / O H···N hydrogen bonds (Å) involved in supramolecular network of compound **2**

O(3) O(23)#1	2.748(14)	O(8) O(21)#2	2.811(13)
O(14) O(21)	2.817(4)	O(15) O22)	2.898(16)
O(3) N(1)#3	2.922(17)	O(11) N(2)#3	2.890(2)
O(19) O(23)#1	3.020(2)	O(21) O(8)#2	2.811(13)
O(21) O(25)#4	2.729(17)	O(21) O(14)	2.817(14)
O(22) O(15)	2.898(16)	O(23) O(23)#5	2.890(3)
O(23) O(19)#6	3.020(2)	O(23) O(25)#3	2.750(3)
O(23) O(3)#6	2.748(14)	O(25) O(23)#7	2.750(3)
O(25) O(21)#4	2.729(17)	O(25) O(24)#9	2.94(2)
O(24) O(25)#10	2.94(2)	O(21) N(2)#3	2.930(2)
N(2) O(21)#7	2.930(2)	N(2) O(11)#7	2.890(2)
N(1) O(3)#7	2.922(17)		

Symmetry transformations used to generate equivalent atoms: #1 1+x, y, z; #2 1-x, 1-y, 2-z; #3 x, y, 1+z; #4 1-x, 1-y, 1-z; #5 -x, 1-y, 2-z; #6 -1+x, y, z; #7 x, y, -1+z; #8 1.5-x, 1-y, -0.5+z; #9 0.5-x, 1-y, -0.5+z; #10 0.5-x, 1-y, 0.5+z.

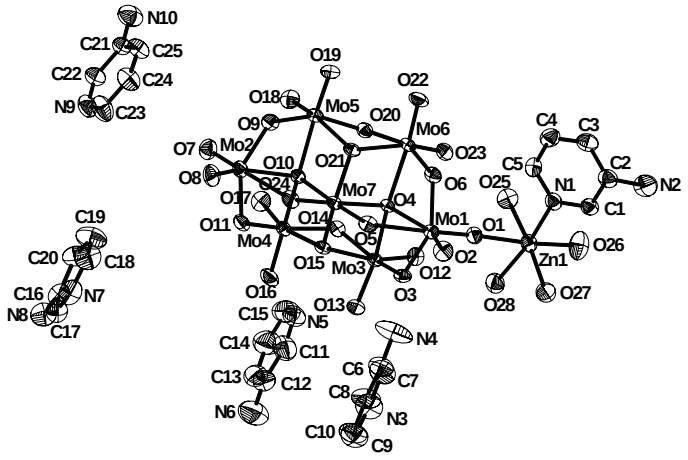

Figure 3.14. The thermal ellipsoidal plot (50% probability) of the molecular structure of compound [3-ampH]$_4$[{Zn(3-ampy)(H$_2$O)$_4$}Mo$_7$O$_{24}$] ·4H$_2$O (**3**) excluding lattice water molecules.

Table 3.6. Geometrical parameters of the C H···O hydrogen bonds (Å, °) involved in supramolecular network of compound **2**. D = donor; A = acceptor.

D H···A	d(D···H)	d(H···A)	d(D···A)	(DHA
C2 H2 O22#4	0.95	2.79	3.540(3)	136.8
C3 H3 O11#8	0.95	2.60	3.470(2)	153.6
C3 H3 O21#8	0.95	2.81	3.510(2)	131.2
C7 H7 O25	0.95	2.63	3.380(3)	136.6
C8 H8 O11#4	0.95	2.72	3.379(18)	127.3
C8 H8 O10#4	0.95	2.78	3.369(19)	121.1
C9 H9 O19#4	0.95	2.99	3.590(5)	122.7
C9 H9 O15#9	0.95	2.43	3.240(3)	143.4
C10 H10 O14#9	0.95	2.64	3.304(19)	127.5

Symmetry transformation codes are given in the footnote of Table 3.5.

Studies on Supramolecular Interactions in [3-ampH]$_4$[{Zn(3-ampy)(H$_2$O)$_4$}Mo$_7$O$_{24}$]·4H$_2$O (3): Identification of a acyclic water pentamer and three dimensional network

In the crystal structure of compound [3-ampH]$_4$[{Zn(3-ampy)(H$_2$O)$_4$}Mo$_7$O$_{24}$]·4H$_2$O (**3**) an acyclic water pentamer is found to be formed from three lattice water molecules O(30), O(31), O(32) and two zinc-coordinated water molecules O(27) and O(28) as shown Figure 3.15(a). The water pentamer in the crystal of compound **3** is stabilized through its supramolecular hydrogen bonding interactions with its surrounding three POM cluster anions via terminal oxygen atoms (Figure 3.15(b)). Crystallographic observations of different forms / conformations of water pentamers in different molecular crystalline hydrates have been reported earlier.[23] The O H O hydrogen bonding distances for the water pentamer and between the pentamer and its surrounding are presented in Table 3.7. Overall O H O / N H O and C H O hydrogen bonding parameters are given in Tables 3.7 and 3.8 respectively.

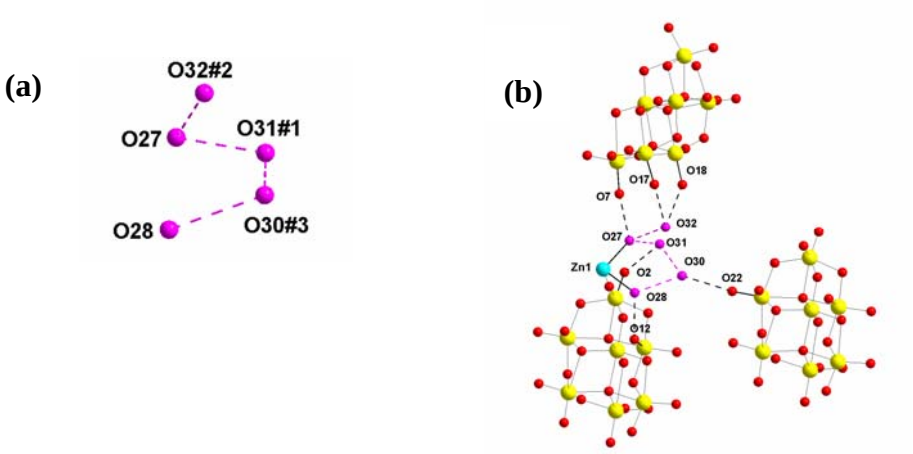

Figure 3.15. (a) An acyclic water pentamer formed by supramolecualr O H···O hydrogen bonding interactions in compound **3**; (b) An acyclic water pentamer is stabilized by O H···O hydrogen bonding interaction with its surroundings. Color code: Mo, yellow; Zn, cyan; O, red; oxygen from acyclic water pentamer, purple; purple and black dotted lines represent the O H···O hydrogen bonding interactions within the water pentamer and its surrounding respectively.

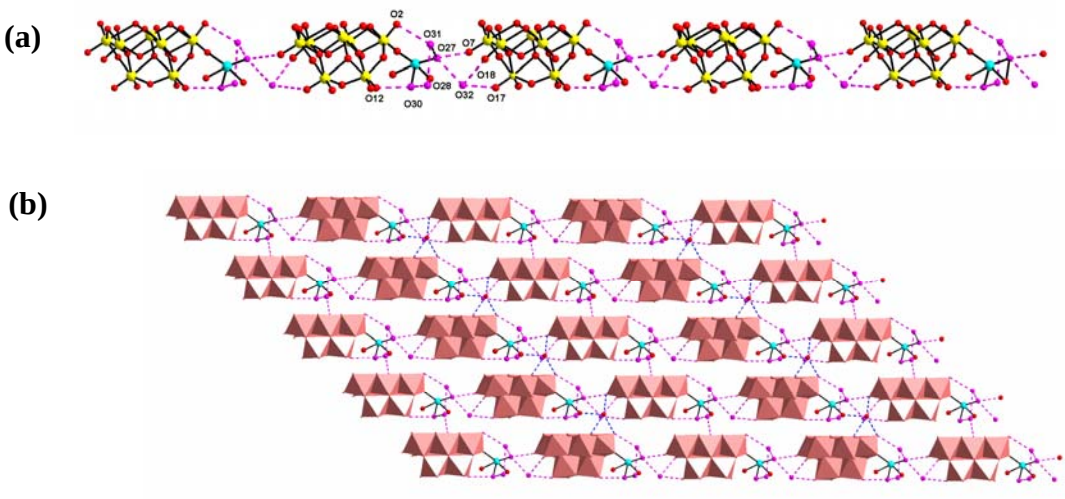

Figure 3.16. (a) The formation of one-dimensional hydrogen bonded polyoxometalate cluster anion chain in which acyclic water pentamer is the bridging unit; (b) two-dimensional hydrogen bonded framework. Color code: Mo, yellow; Zn, cyan; O, red; oxygen atom from water pentamer and a lattice water molecule involved in O H···O hydrogen bonding interactions, purple; polyhedral representation of polyoxometalate cluster anions are shown in light brown color; purple and blue dotted lines represent the O H···O hydrogen bonding interactions of polyoxometalate cluster anions with water pentamer and a lattice water molecule respectively.

Table 3.7. Geometrical parameters of the O H···O and N H···O / O H···N hydrogen bonds (Å) involved in supramolecular network of compound $[3\text{-ampH}]_4[\{Zn(3\text{-ampy})(H_2O)_4\}Mo_7O_{24}]\cdot 4H_2O$ (**3**)

O(25) O(8)#1	2.894(4)	O(25) O(23)	2.792(4)
O(26) O(24)#1	2.859(4)	O(26) O(29)#2	2.717(5)
O(27) O(31)#3	2.734(6)	O(27) O(32)#4	2.867(8)
O(27) O(7)#2	2.805(4)	O(28) O(12)	2.804(4)
O(28) O(30)#2	2.759(6)	O(29) O(26)#5	2.717(5)
O(29) O(7)	2.903(4)	O(29) O(2)#6	3.076(4)
O(29) O(5)#6	2.883(4)	O(30) O(22)#7	2.903(5)
O(30) O(31)#8	3.099(11)	O(30) O(28)#5	2.759(6)
O(31) O(30)#9	3.098(11)	O(31) O(2)#10	2.998(6)
O(31) O(27)#10	2.732(6)	O(32) O(17)#6	3.004(8)
O(32) O(18)#6	2.848(9)	O(32) O(27)#11	2.867(8)
O(2) O(29)#12	3.076(4)	O(2) O(31)#3	2.997(6)
O(12) O(28)	2.804(4)	O(17) O(32)#12	3.006(8)
O(7) O(27)#5	2.805(4)	O(7) O(29)	2.903(4)
O(8) O(25)#13	2.894(4)	O(18) O(32)#12	2.848(9)
O(22) O(30)#14	2.902(5)	O(23) O(25)	2.792(4)
O(5) O(29)#12	2.884(4)	O(24) O(26)#13	2.859(4)
O(6) N(7)#12	2.630(4)	O(19) N(3)#15	2.732(5)
O(19) N(10)#14	2.946(4)	O(9) N(6)#15	3.057(7)
O(8) N(2)#5	2.962(6)	O(17) N(4)#6	2.971(5)
O(11) N(9)#12	2.663(4)	O(15) N(5)	2.676(4)
O(12) N(10)#2	3.092(5)	O(13) N(10)#2	3.092(5)
O(3) N(4)	3.009(5)	O(31) N(8)#16	2.854(7)
N(2) O(8)#2	2.962(6)	N(3) O(19)#17	2.732(5)
N(4) O(17)#12	2.971(5)	N(6) O(9)#17	3.057(7)
N(7) O(6)#6	2.630(4)	N(9) O(11)#6	2.663(4)
N(10) O(12)#5	3.092(5)	N(10) O(13)#5	3.092(5)
N(10) O(19)#7	2.946(4)	N(8) O(31)#18	2.854(7)

Symmetry transformations used to generate equivalent atoms are given in the footnote of Table 3.8.

The water pentamer along with zinc ion acts as the supramolecular glue to link the POM cluster anions resulting in the formation of a one dimensional chain as

shown in Figure 3.16a. These chains are again laterally linked by supramolecular O H O hydrogen bonding interactions (shown in purple dot lines, Figure 3.16b) that involve O22 (terminal oxygen atom of the POM cluster anion) and O30 (part of water pentamer). Another mode of O H O hydrogen bonding interactions (shown in blue dot lines, Figure 3.16b), that are also responsible for the formation of same layer, involves a pair of hydrogen bonding interactions: (i) O2 (a terminal oxygen atom of the POM cluster anion) and O29 (a lattice water molecule) which is further hydrogen bonded to zinc-coordinated water O26 and O7, a terminal oxygen atom of POM cluster anion. These layers stack one after another and linked again by O H O hydrogen bonding interactions resulting in a three-dimensional supramolecular network having well defined irregular rectangular grid channels with an approximate inner dimension of 28.90 x 2.90 $Å^2$ (Figure 3.17(a)) occupied by the 3-aminopyridinium cations as guests (Figure 3.17(b)). The formation of three dimensional supramolecular structures arising from the stacking of the one-to-one layers can be explained by a schematic representation (Scheme 4), in which it has been stressed that the layers are linked in such a way that the boxes, that are recognizable from the front view, can also be recognizable from the side view. In the network, there are four different crystallographically independent 3-aminopyridinium cations, namely 'N3N4', 'N5N6', 'N7N8' and 'N9N10'. The 'N9N10' type cations are located in the channels (vide supra). Besides above described O H O hydrogen bonding interactions, there are significant N H···O / O H···N and C H···O hydrogen bonding interactions between all four types of 3-aminopyridinium cations, namely 'N3N4', 'N5N6', 'N7N8' and 'N9N10' and isopolyanion $[Mo_7O_{24}]^6$ resulting in an intricate supramolecular network in the crystal structure of compound **3**. The immediate C H···O and N H···O / O H···N hydrogen bonding interactions around 'N3N4', 'N5N6', 'N7N8' and 'N9N10' type cations and zinc coordinated 3-aminopyridine molecule ('N1N2' type) are shown in Figures 3.18(a) – 3.18(e) respectively.

(a)

(b)

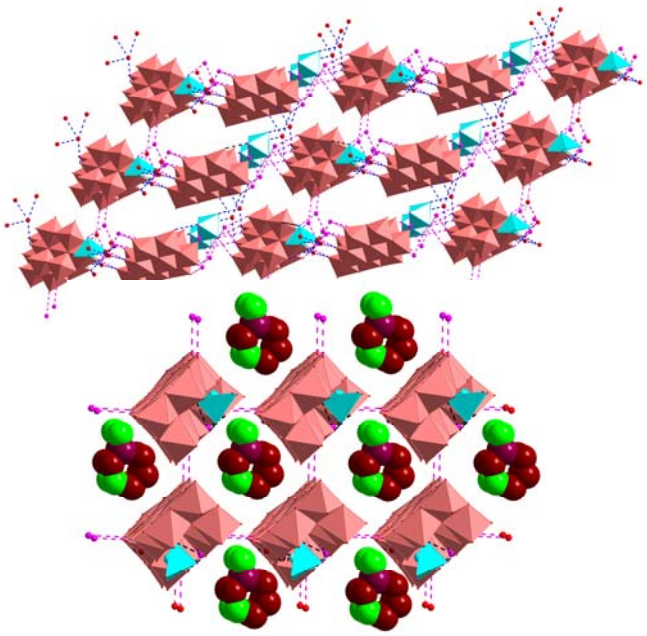

Figure 3.17. (a) The three-dimensional supramolecular network formed by O H···O hydrogen bonding interactions having well defined irregular rectangular grid channels in compound **3**. (b) View for guest 3-aminopyridine molecules which are situated in irregular rectangular grid channels. Color code: C, dark brown; N, green; polyhedral representation of polyoxometalate cluster anions and zinc-aqua complexes are shown in light brown and cyan color respectively; oxygen atom from water pentamer and a lattice water molecule are involved in O H···O hydrogen bonding interactions, purple; color codes of dotted lines are same as mentioned in Figure 3.16.

Scheme 4

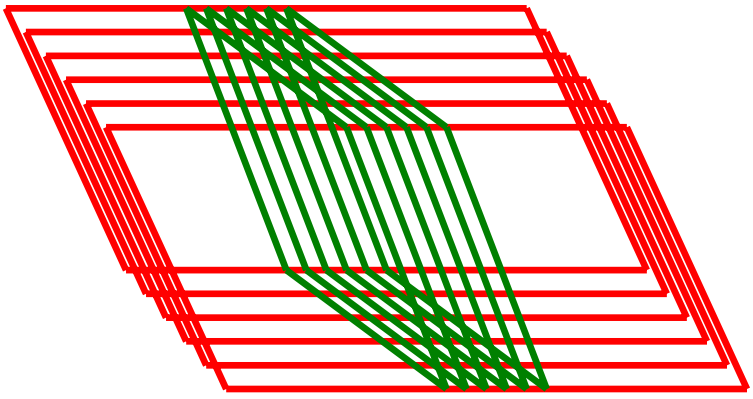

Table 3.8. Geometrical parameters of the N H···O, C H···O hydrogen bonds (Å, °) involved in supramolecular network of compound **3**. D = donor; A = acceptor.

D H···A	d(D···H)	d(H···A)	d(D···A)	(DHA
N3 H3A O19#17	0.92	2.00(6)	2.732(5)	136(5)
N7 H7A O6#6	1.00(5)	1.65(5)	2.629(4)	165(4)
N9 H9A O11#6	1.03(6)	1.67(6)	2.664(4)	162(5)
C3 H3 O20#14	0.93	2.68	3.362(4)	130.9
C3 H3 O18#14	0.93	2.72	3.413(5)	131.9
C4 H4 O32#19	0.93	2.77	3.534(9)	140.4
C5 H5 O6	0.93	2.74	3.427(4)	130.8
C1 H1 O7#2	0.93	2.57	3.482(4)	167.3
C11 H11 O13	0.93	2.79	3.381(6)	122.6
C13 H13 O23	0.93	2.43	3.284(6)	152.1
C14 H14 O30#12	0.93	2.77	3.602(9)	150.1
C14 H14 O32#3	0.93	2.46	3.160(11)	131.7
C10 H10 O9#17	0.93	2.85	3.417(6)	120.3
C6 H6 O13	0.93	2.65	3.318(5)	129.4
C6 H6 O3	0.93	2.57	3.306(5)	136.9
C8 H8 O17#12	0.93	2.56	3.302(5)	137.1
C18 H18 O5#6	0.93	2.63	3.484(5)	153.4
C18 H18 O29	0.93	2.61	3.343(7)	135.8
C20 H20 O14#13	0.93	2.46	3.383(5)	170.3
C25 H25 O20#7	0.93	2.61	3.479(5)	154.9
C23 H23 O2#10	0.93	2.51	3.074(5)	119.3
C23 H23 O16 #6	0.93	2.65	3.243(5)	122.5

Symmetry transformations used to generate equivalent atoms: #1 0.5+x, 0.5+y, z; #2 0.5+x, 1.5-y, -0.5+z; #3 x, y, -1+z; #4 0.5+x, 0.5+y, -1+z; #5 -0.5+x, 1.5-y, 0.5+z; #6 x, 1-y, 0.5+z; #7 x, 2-y, 0.5+z; #8 -0.5+x, 1.5-y, -0.5+z; #9 0.5+x, 1.5-y, 0.5+z; #10 x, y, 1+z; #11 -0.5+x, -0.5+y, 1+z; #12 x, 1-y, -0.5+z; #13 -0.5+x, -0.5+y, z; #14 x, 2-y, -0.5+z; #15 -0.5+x, 0.5+y, z; #16 0.5+x, 0.5-y, 0.5+z; #17 0.5+x, -0.5+y, z; #18 -0.5+x, 0.5-y, -0.5+z; #19 x, 1+y, -1+z; #20 x, -1+y, z.

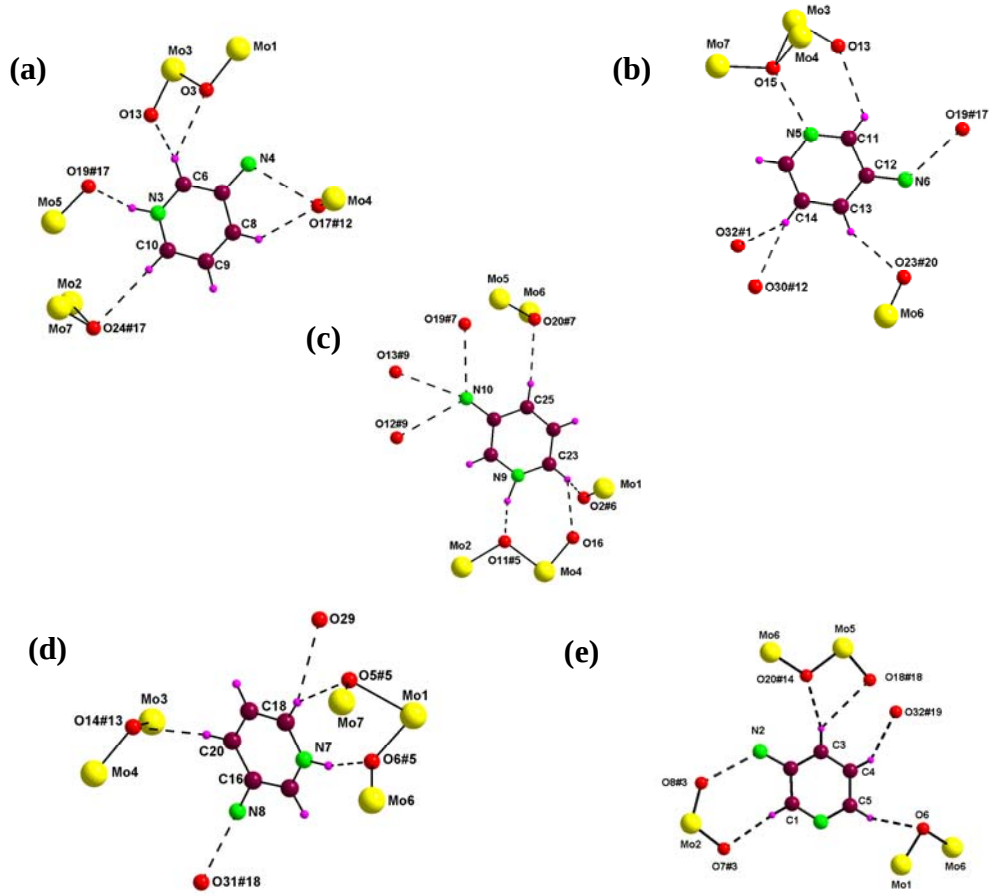

Figure 3.18. Supramolecular N H···O and C H···O hydrogen bonding interactions noticed around coordinated and non-coordinated 3-aminopyridine molecules in compound **3**. Color code: black dotted lines represent the hydrogen bonding interactions.

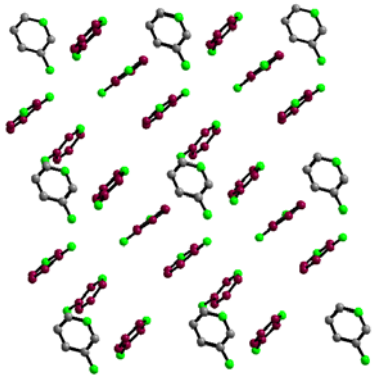

Figure 3.19. Molecular packing of the zinc-coordinated 3-aminopyridine and non-coordinated 3-aminopyridinium cations that are arrayed in perpendicular direction to each in compound **3**. Color code: N, green; carbon atoms from zinc-coordinated 3-aminopyridine, gray; carbon atoms from non-coordinated 3-aminopydinium cations, brown.

The detailed hydrogen bonding parameters are presented in Table 3.8. Since the hydrogen of amine groups are not located in the crystal structure, the N H···O / O H···N distances are presented as N···O distances. In the crystal structure of compound **3**, the view of the molecular packing of the zinc-coordinated aminopyridine molecules ('N1N2' type) and aminopyridinium cations ('N3N4', 'N5N6', 'N7N8' and 'N9N10' type) is shown in Figure 3.19, which shows that the cationic pyridines ('N3N4', 'N5N6', 'N7N8' and 'N9N10' type) are perpendicular the zinc coordinated neutral 'N1N2' type pyridine.

Structural description of compound [3-ampH]$_4$[{Co(3-ampy)(H$_2$O)$_4$}Mo$_7$O$_{24}$] 4H$_2$O (4)

As shown in Table 3.4, both compounds **3** and **4** are isostructural and accordingly the unit cell volume, cell data, space group, number of lattice water molecules etc. of **3** and **4** are identical. They differ in their metal contents, *i.e*., compound [3-ampH]$_4$[{Co(3-ampy)(H$_2$O)$_4$}Mo$_7$O$_{24}$] 4H$_2$O (**4**) is cobalt analogue of zinc-containing compound [3-ampH]$_4$[{Zn(3-ampy)(H$_2$O)$_4$}Mo$_7$O$_{24}$] 4H$_2$O (**3**). Since the molecular structure of compound **3**, including its supramolecular structure has been described in the preceding section in detail, the structural details of compound **4** is not described again here.

Crystal Structure Description of Compound [2,3-diampH]$_4$[Co(H$_2$O)$_6$][Mo$_7$O$_{24}$]·6H$_2$O (**5**)

The pink color crystals of compound **5** can be easily be grown from an aqueous solution by slow evaporation. Compound **5** crystallizes in monoclinic space group *C2/c*. The asymmetric unit contains half of the POM cluster anion $[Mo_7O_{24}]^6$, two mono protonated 2,3-diaminopyridine molecules, half of the complex cation $[Co(H_2O)_6]^{2+}$ with half occupancy of cobalt, and three solvent water molecules. The molecular structure of compound **5** is presented in the Figure 3.20**.** In the molecular structure,

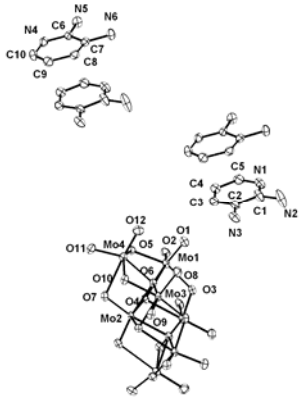

Figure 3.20. The thermal ellipsoidal plot (50% probability) of the molecular structure of compound $[2,3\text{-diampH}]_4[Co(H_2O)_6][Mo_7O_{24}]\cdot 6H_2O$ (**5**) excluding cobalt-aqua complex cation and lattice water molecules.

cobalt-aqua complex $[Co(H_2O)_6]^{2+}$ exists as a discrete entity and partially fulfill the negative charges of POM cluster anion. The residual negative charges have been compensated by four protonated 2,3-diaminopyridine molecules (Figure 3.20). The Mo O bond lengths are within the range of Mo O bond distances of other $[Mo_7O_{24}]^{6}$ clusters found in compounds **2** **4** (vide supra). The Co O bond lengths vary in the range of 1.904 – 2.229Å. The crystal data and structural parameters are given Table 3.4.

Studies on Supramolecular Interactions in $[2,3\text{-diampH}]_4[Co(H_2O)_6][Mo_7O_{24}]\cdot 6H_2O$ (5): Identification of a acyclic water tetramer

A supramolecularly hydrogen bonded water tetramer is identified crystallographically in the crystal lattice of compound **5** as shown Figure 3.21(a). This water tetramer has exclusively been formed by lattice water molecules O(17), O(18) and their symmetry equivalent atoms. A water tetramer, $(H_2O)_4$ cluster can be represented in five different ways as shown in Scheme 5.[24] On entropic grounds, two coordinate connectivities (for example, a chain or a ring in Scheme 5) are favored over three- or four coordinate networks, which are disfavored because of strongly hindered intermolecular bending or stretching modes. The present $(H_2O)_4$ cluster found in the crystal lattice of compound **5** is a near linear water tetramer (Figure 3.21(a)) and its present conformation is favored through supramolecular interactions with its surrounding POM cluster anion.

Scheme 5

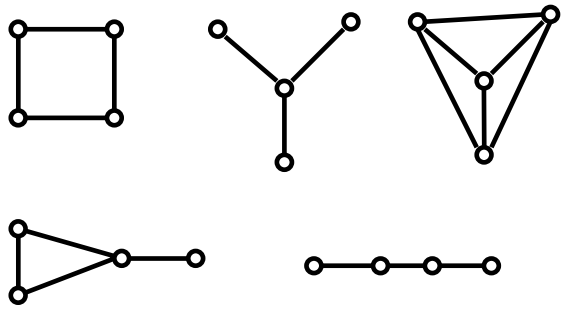

More specifically, the water molecule O(18) from the tetramer interacts with O(5) from the $[Mo_7O_{24}]^{6}$ cluster anion as shown in Figure 3.21(b). The O H O distances, in the water tetramer (based on O O) varies in the range of 2.763(13) 2.798(10) Å. Since the water molecules from cobalt-aqua complex are considerable disordered, N H···O and C H···O interactions (for this compound) will not be discussed further in this chapter.

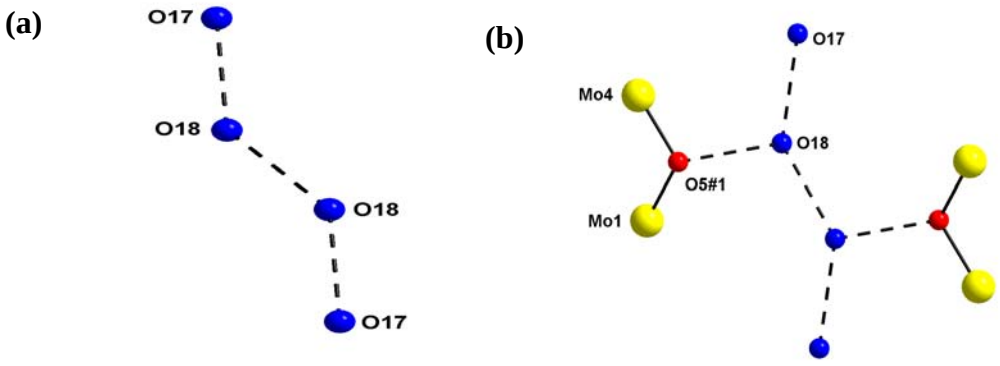

Figure 3.21. (a) The formation of water tetramer, $(H_2O)_4$ cluster by supramolecular O H···O hydrogen bonding interaction in compound **5**. (b) The immediate environment of water tetramer with its surrounding in compound **5**. The water molecule O(18) interacts with its symmetry equivalent atom O(18) by symmetry operator 0.5-x, 0.5-y, 2-z. The same water molecule O(18) from water tetramer interacts with O(5) from polyoxometalate cluster anion through O H···O hydrogen bonding interaction by the symmetry operator x, 1-y, 0.5+z. Color code: Mo, yellow; O, red; oxygen atoms from water tetramer, blue; black dotted lines represent O H···O hydrogen bonding interactions.

Crystal Structure Description of Compound [2,3-diampH]$_2$[{Zn(2,3-diampH)$_2$(H$_2$O)$_2$}Mo$_8$O$_{27}$]·2H$_2$O (6)

The yellow colored crystals of compound **6** were isolated from an aqueous solution. Compound **6** crystallizes in monoclinic space group *C2/c*. Corresponding crystal data and refinement parameters for compound **6** are given in Table 3.4. The asymmetric unit of the crystal of compound **6** (Figure 3.22) can be represented as [2,3-diampH][$Mo^{VI}_4O_{13.5}Zn^{II}_{0.5}$(H$_2$O)(2,3-diampH)] ·H$_2$O and thus the molecular formula of compound **6** is described as [2,3-diampH]$_2$[{Zn(2,3-diampH)$_2$(H$_2$O)$_2$}Mo$_8$O$_{27}$]·2H$_2$O. In the crystal structure, the zinc ion and one oxygen atom (O12, Figure 3.22) are characterized in their special positions. As shown in Figure 3.22, the coordination complex [Zn(H$_2$O)$_2$(2,3-diampH)$_2$]$^{2+}$ is coordinated by the POM cluster anion [Mo$_8$O$_{27}$]^{6} via the terminal oxygen atom (O1, Figure 3.22) giving rise to the POM supported zinc-coordination complex [{Zn(2,3-diampH)$_2$(H$_2$O)$_2$}Mo$_8$O$_{27}$]^{2} , two negative charges of which are compensated by two protonated 2,3-diaminopyridine molecules resulting in the isolation of compound **6**. Notably the zinc-coordinated 2,3-diaminopyridine molecules are mono-protonated.

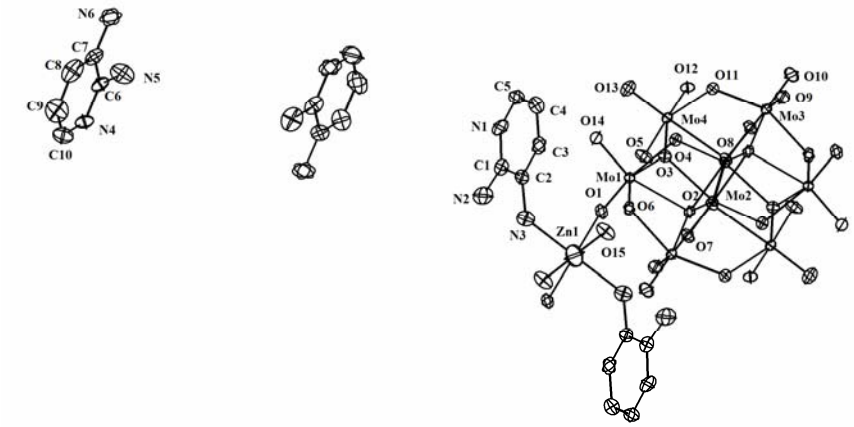

Figure 3.22. The thermal ellipsoidal plot (50% probability) of the asymmetric unit of compound [2,3-diampH][$Mo^{VI}_4O_{13.5}Zn^{II}_{0.5}$(H$_2$O)(2,3-diampH)] ·H$_2$O **(6)** excluding hydrogen atoms.

The POM $[Mo_8O_{27}]^6$ cluster anion, found in compound **6**, is similar to other reported $[Mo_8O_{26}]^4$ octamolybdate anion.[25] Both types consist of eight $\{MoO_6\}$ octahedra by edge sharing. The rare type octamolydate cluster anion $[Mo_8O_{27}]^6$, found in compound **6**, is differed from the most common octamolybdate anion $[Mo_8O_{26}]^4$ by having one extra Mo=O bond (more specifically, there are two Mo=O bonds with half occupancies, that are involved in corner sharing) in compound **6.** The Mo O groups in the crystal structure of **6** can be grouped into four categories: There are sixteen Mo-Ot with the bond lengths in the range of 1.689(5) 1.898(2) Å; six μ_2 type bridged Mo O_b bonds with distances varying in between 1.753(5) 2.309(5) Å; four μ_3 type bridging molybdenum-oxygen distances in the range of 1.857(5) 2.328(5) Å and two bridging μ_4 type molybdenum-oxygen distances in the range of 1.948(5) 2.415(5) Å. The same cluster $[Mo_8O_{27}]^6$ is known to exist in compound $[\{H_2DABCO\}_2\{H_2pipz\}][Mo_8O_{27}]$ in which the cluster anion does not support any organic cation $\{H_2DABCO\}_2$ / H_2pipz by coordinate covalent bonds[26] and is also found to exists through single common corner sharing in compounds $(NH_4)_6Mo_8O_{27}.\ 4H_2O$,[26b] and $(C_4H_{12}N_2)_3Mo_8O_{27}$.[26c] In all these compounds, the cluster anions condense via Mo O Mo bonds to a one-dimensional chain. In the present compound $[2,3\text{-diampH}]_2[\{Zn(2,3\text{-diampH})_2(H_2O)_2\}Mo_8O_{27}]\cdot 2H_2O$ (**6**), a similar chain is formed by a Mo4 O12 Mo4 bonds along the chain axis (crystallographic *c* axis), in which the each cluster is functionalized by zinc coordination complexes $[\{Zn(2,3\text{-diampH})_2(H_2O)_2\}]^{4+}$ as shown in Figure 3.23. This type of POM based chains, formed exclusively by Mo O_b Mo bonds, are vary rare in literature.[27] This chain undergoes lateral linking by coordination of adjacent POM cluster anions through Mo1=O1 Zn1 coordinate covalent bonds (Figure 3.23) resulting in the formation of a two-dimensional network having well defined honey comb cavities (Figure 3.24(a)) in which non-coordinated 2,3-diaminopyridine molecules and solvent water molecules are present (Figure 3.24(b)).

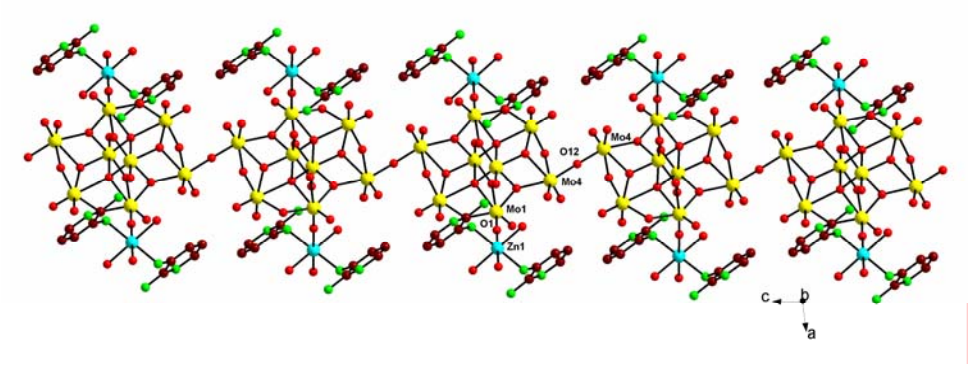

Figure 3.23. A view of one dimensional chain formed by Mo O Mo linkage along the crystallographic '*c*' axis in compound **6** in which each cluster anion is functionalized by zinc coordination complexes $[\{Zn(2,3\text{-diampH})_2(H_2O)_2\}]^{4+}$. Color code: Mo, yellow; Zn, cyan; O, red; C, brown; N, green.

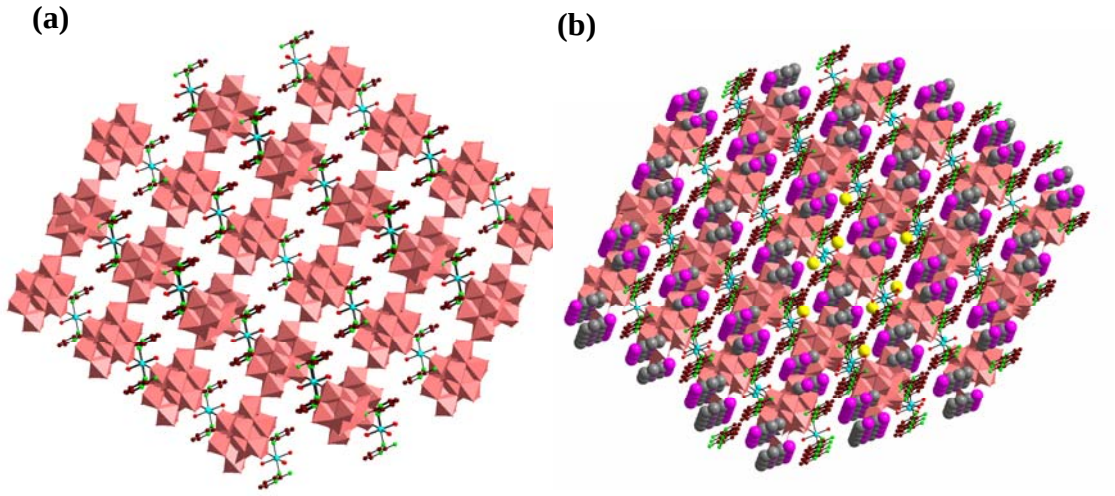

Figure 3.24. (a) Two-dimensional layered framework in which well defined honeycomb cavities also can be seen in compound $[2,3\text{- diampH}]_2[\{Zn(2,3\text{-diampH})_2(H_2O)_2\}Mo_8O_{27}]\cdot 2H_2O$ (**6**); (b) A view of the accommodation of non-coordinated 2,3-diaminopyridine molecules and lattice water molecules as guests in the honeycomb cavities. Color code: Zn, cyan; O, red; C from coordinated ligands, dark brown; N from coordinated ligands, green; C from non-coordinated guest ligands, gray; N from non-coordinated guest ligands, purple; O from lattice water molecules, yellow; polyhedral representation of polyoxometalate cluster anions are shown in light brown.

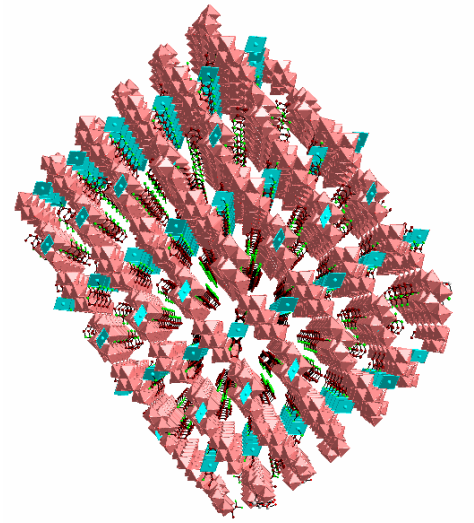

Figure 3.25. A perspective view of the packing diagram in compound **6** shows that zinc coordinated 2,3-diaminopyridine molecules are stacked over each other through π…π interactions. Color code: C, dark brown; N, green; polyhedral representation of polyoxometalate cluster anions and $[\{Zn(2,3\text{-diampH})_2(H_2O)_2\}]^{4+}$ are shown in light brown and cyan color respectively.

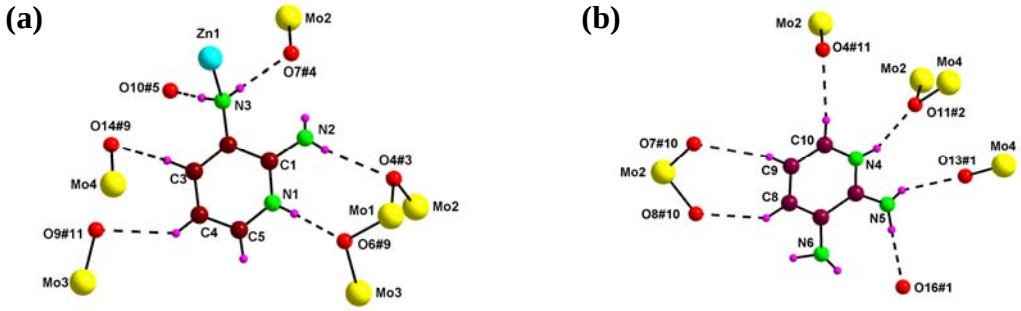

Figure 3.26. The immediate environment of coordinated and non-coordinated 2,3-diaminopyridine molecules through N H···O/O H···N and C H···O hydrogen bonding interactions. Color code: Mo, yellow; Zn, cyan; O, red; C, brown; N, green; H, purple.

The relevant packing diagram shows that the coordinated organic ligands (2,3-diaminopyridine molecules) are stacked each other through π…π interaction (Figure 3.25. The weak supramolecular hydrogen bonding interactions such as N H···O/O H···N and C H···O interactions among these two-dimensional layers (Figure 3.24) result in an intricate three-dimensional network. The immediate environment of coordinated and non-coordinated 2,3-diaminopyridine molecules through N H···O/O H···N and C H···O

interactions is shown in the Figure 3.26. The corresponding hydrogen bonding distances were given in the Table 3.9.

Table 3.9. Geometrical parameters of the N H···O/O H···N, and C H···O hydrogen bonds (Å, °) involved in supramolecular network of compound $[2,3\text{-diampH}]_2[\{Zn(2,3\text{-diampH})_2(H_2O)_2\}Mo_8O_{27}]\cdot 2H_2O$ (**6**). D=donor; A=acceptor.

D H···A	d(D···H)	d(H···A)	d(D···A)	(DHA
N5 H5B O16#1	0.83(12)	2.22(13)	3.037(12)	167(11)
N5 H5A O13#1	0.71(12)	2.22(12)	2.848(11)	148(12)
N4 H4A O11#2	0.78(10)	1.97(11)	2.700(9)	155(10)
N2 H2B O4#3	0.74(11)	2.36(11)	3.073(10)	162(10)
N3 H3A O7#4	0.82(11)	2.08(11)	2.884(9)	166(11)
N3 H3B O10#5	0.86(10)	1.97(10)	2.799(9)	161(9)
N1 H1A O6#8	0.80(10)	1.92(10)	2.712(8)	177(10)
C8 H8 O8#9	0.93	2.38	3.172(11)	143.4
C9 H9 O7#9	0.93	2.65	3.535(12)	158.6
C10 H10 O4#10	0.93	2.36	3.239(11)	157.0
C3 H3 O14	0.93	2.96	3.505(9)	118.8
C4 H4 O9#11	0.93	2.52	3.280(10)	139.4

D H···A	d(D···A)
O(11) N(4)#6	2.700(9)
O(10) N(3)#7	2.799(9)

Symmetry transformations used to generate equivalent atoms: #1 1-x, y, 0.5-z; #2 1+x, y, z; #3 0.5-x, 0.5-y, 1-z; #4 0.5-x, 1.5-y, 1-z; #5 0.5+x, 0.5+y, z; #6 -1+x, y, z; #7 -0.5+x, -0.5+y, z; #8 0.5-x, 0.5-y, 1-z; #9 1+x, -1+y, z; #10 1+x, y, z; #11 –x, y, 0.5-z.

3.3.4. Catalysis Studies

The catalytic activity of compound $[HMTAH]_2[\{Zn(H_2O)_5\}\{Zn(H_2O)_4\{Mo_7O_{24}\}]\cdot 2H_2O$ (**1**) has been studied for the oxidation of a primary alcohol in the presence of hydrogen peroxide as an oxidant. We have selected benzyl alcohol (as a substrate) for the oxidation reaction. Compound **1** selectively oxidizes benzyl alcohol to benzaldehyde with the moderate conversion percentage.

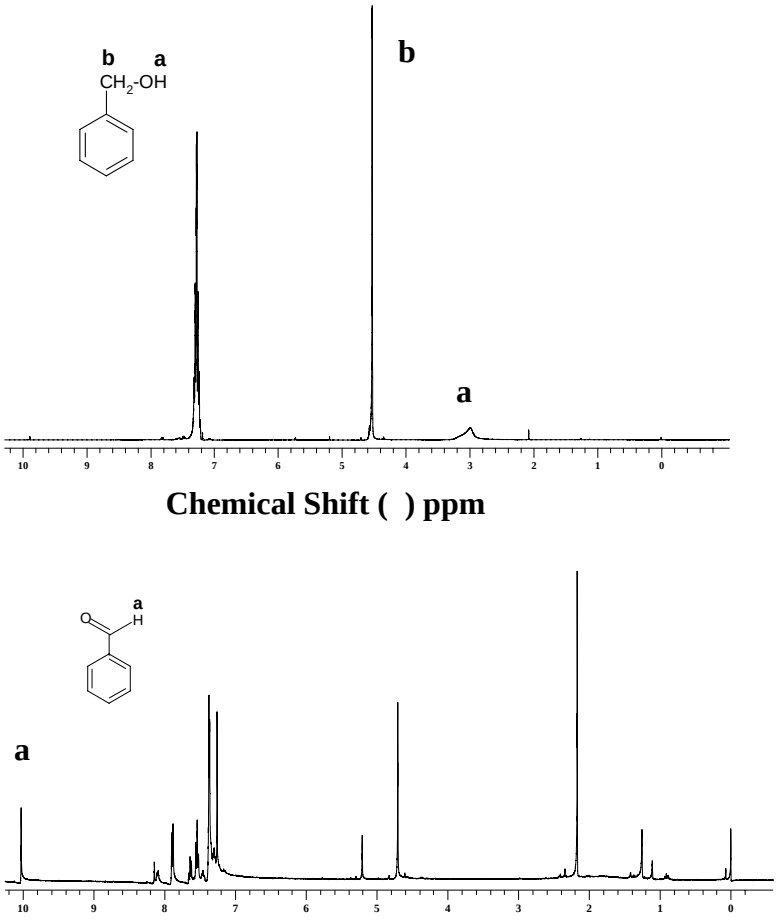

Figure 3.27. 400 MHz ^{1}H NMR spectrum of distilled benzyl alcohol in $CDCl_3$ (top) and product mixture in $CDCl_3$ (CHO peak is marked as 'a') (bottom).

In a typical experiment, the mixture of benzyl alcohol (0.052 mL, 0.5 mmol), compound **1** (0.042g, 0.025 mmol), 30% (w/v) of hydrogen peroxide (0.460 mL) were taken in screwed vial and heated at 80^{o}C for 9 hrs. The product was extracted by dichloromethane and analysis was done by ^{1}H NMR spectral studies. The result shows that, the conversion of benzyl alcohol to benzaldehyde occurs in 50%. The same reaction was checked without catalyst and without hydrogen peroxide separately that did not show any notable conversion. It clearly indicates the need of both catalyst and hydrogen peroxide for the successful oxidation. The ^{1}H NMR spectra of distilled benzyl alcohol and product mixture are given in Figure 3.27.

Characterization data for benzyl alcohol: ^{1}H NMR ($CDCl_3$) : 3.00 (s, 1H, OH), 4.51 (s, 2H, CH_2), 7.16 7.26 (m, 5H, Ar-CH).

Characterization data for benzaldehyde: ^{1}H NMR ($CDCl_3$) : 7.21 7.31 (m, 5H, Ar-CH), 10.03 (s, 1H, HC=O).

In another experiment, we have chosen compounds [2-ampH]$_4$[{Zn(H_2O)$_5$}Mo$_7$O$_{24}$] ·9H_2O (**2**) and [2-ampH]$_4$[{Co(H_2O)$_5$}Mo$_7$O$_{24}$] ·9H_2O (**2a**) as catalysts and H_2O_2 as an oxidant (oxygen source) for the conversion of a series of secondary alcohols to corresponding ketones. The basis of choosing secondary alcohols instead of primary alcohols as substrates is to avoid unwanted side reactions (for example, the formation of Schiff base that can be formed from the product aldehyde and aminopyridine of compounds **2** and **2a**). On the other hand, ketonic compounds (oxidation products of secondary alcohols) are relatively stable towards Schiff base condensation reaction. In our first attempt, we have chosen 1-phenylethanol (secondary alcohol) as a representative substrate to optimize the reaction condition towards the favorable conversion percentage. Since the rate of oxidation reactions of secondary alcohol is considerably slower, it needs drastic conditions to optimize good yield. The numbers of reactions were carried out by varying the reaction time and concentration of the oxidant (hydrogen peroxide). Finally we optimized the maximum product conversion

percentage by taking 1-phenylethanol (0.50 mmol) as a substrate, compound **2** / **2a** (0.03 mmol) as a catalyst, and 30% (w/n) hydrogen peroxide (4.86 mmol) as an oxidant in a screw type vial and subsequently it was heated at 70 80^{o}C for 9 hours.

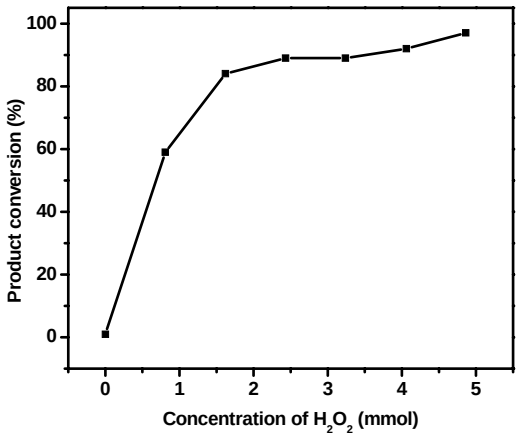

Figure 3.28. The plot shows the conversion (%) of secondary alcohols to ketone versus the concentration of hydrogen peroxide, in which amount of catalyst, temperature, reaction time and substrate concentration are kept constant.

We observed (through our experience) that the amount of oxidation is directly proportional to the amount of active oxygen content (hydrogen peroxide is the source in the present system). It has been demonstrated (Figure 3.28) that, when the amount of catalyst, temperature, reaction time and substrate concentration are kept fixed / constant and the concentration of hydrogen peroxide is varied (Figure 3.28), the conversion percentage is directly proportional to the increasing amount of hydrogen peroxide. When the same reaction was monitored in absence of either catalyst or hydrogen peroxide (in two separate experiments), it did not show any notable conversion. It clearly indicates the need of both catalyst and hydrogen peroxide for the successful oxidation. The role of catalyst here is to activate hydrogen peroxide. The peroxygen atom of H_2O_2 cannot be transferred directly to the reaction system unless it is activated in a transition metal complex or peracid or dioxirane.[28] The product was extracted in dichloromethane and the catalysts were filtered by simple filteration for and reused without any significant changein it's catalytic activity. The usage of combination of polyoxometalate cluster

(a)

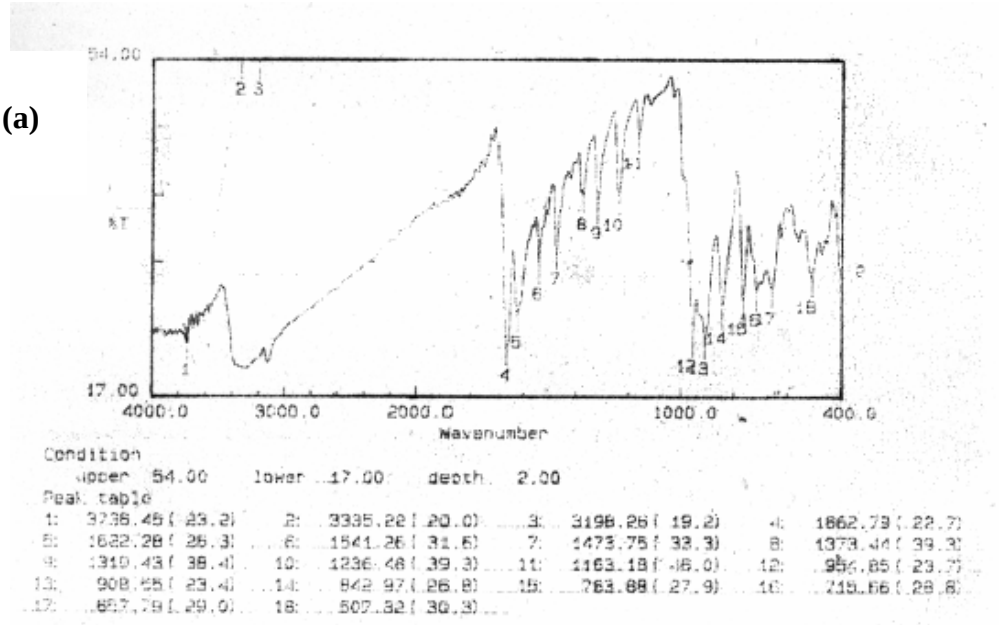

(b)

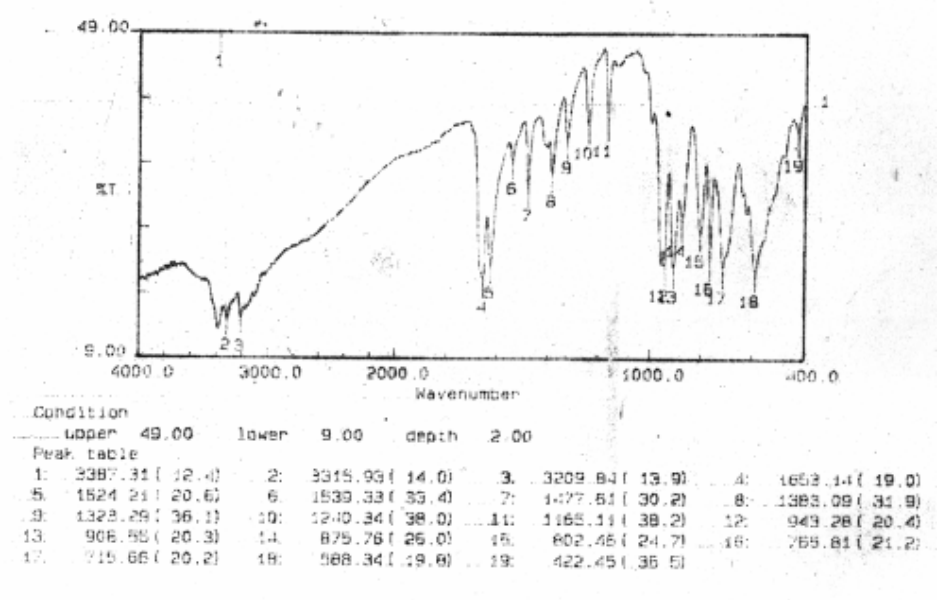

Figure 3.29. The IR spectra of catalyst compound [2-ampH]$_4$[{Zn(H$_2$O)$_5$}Mo$_7$O$_{24}$]·9H$_2$O (**2**) (a) fresh catalyst (b) recycled catalyst.

anion as catalyst and hydrogen peroxide as an oxidant is well known in the literature[29] and its various possible mechanisms were discussed elaborately.[30] Used catalysts were filtered, dried and reused for the same oxidation in identical condition in multiple cycles. It clearly indicates that the catalyst is stable even after completion of the reaction and further the presence of POM cluster in the used catalyst are proved by the existence of stretching frequency at 943 cm^{-1} which is due to the presence of Mo O_t in the IR spectrum of used catalyst, which matches with IR spectrum of compound **2** (Figure 3.29). The same conditions were applied to a series of substituted 1-phenylethanol derivatives. The catalysis results are summarized in Table 3.10. All the product analyses were done by H^1 NMR spectral studies (see Figures 3.30 3.34 for the corresponding NMR spectra).

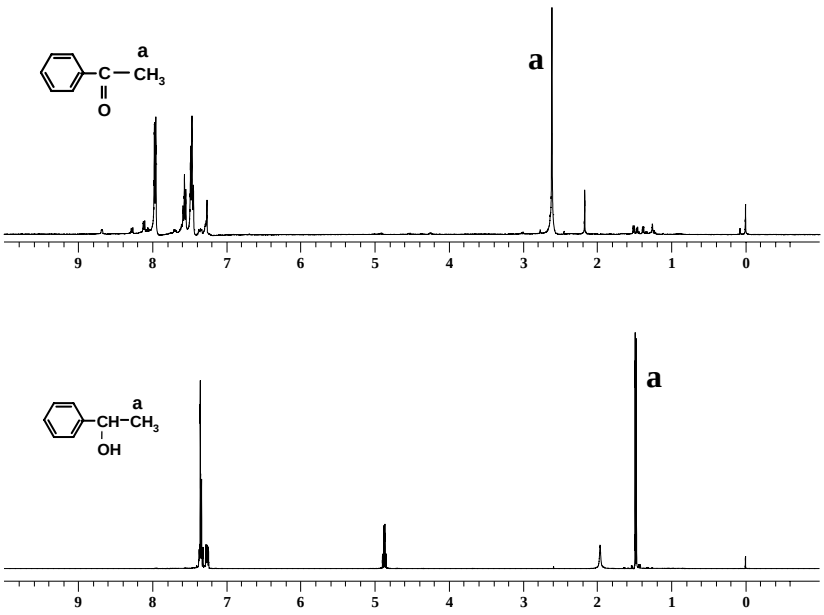

Figure 3.30. 400 MHz ^1H NMR spectra of acetophenone (top) from the product mixture in $CDCl_3$ (CH_3 peak is marked as 'a') and distilled 1-phenylethanol (bottom) in $CDCl_3$ (CH_3 peak is marked as 'a').

Table 3.10. Oxidation of secondary alcohols catalyzed by $[2\text{-ampH}]_4[\{Zn(H_2O)_5\}Mo_7O_{24}]\cdot 9H_2O$ (**2**) and $[2\text{-ampH}]_4[\{Co(H_2O)_5\}Mo_7O_{24}]\cdot 9H_2O$ (**2a**) using H_2O_2 as an oxidant[#]

Entry	Substrate	Product	Conversion (%)		Conversion (%)	
			Catalyst **2**	TON[*]	Catalyst **2a**	TON
a	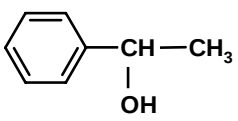	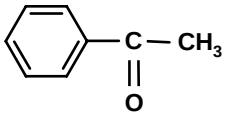	**97**	**17**	**45**	**8**
b	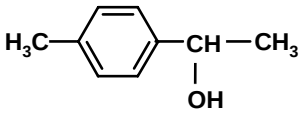	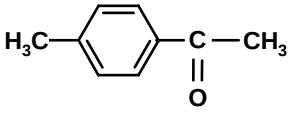	**97**	**17**	**64**	**11**
c	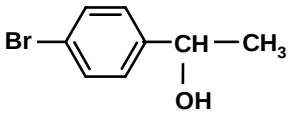	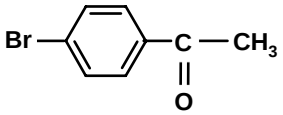	**96**	**166**	**40**	**71**
d	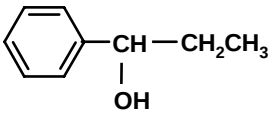	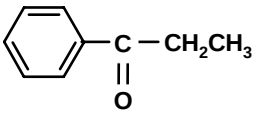	**90**	**16**	**47**	**19**
e	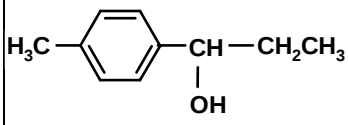	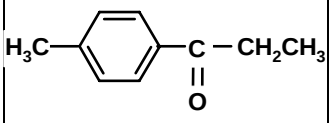	**50**	**9**	**7**	**1**

[#]Reaction conditions: 0.5 mmol of substrate for entries a, b, d and e; 5.0 mmol of substrate for entry c; 4.86 mmol of H_2O_2, compound **2** or **2a** 0.029 mmol, 80°C, 9hrs. TON[*] (Turn Over Number) is mole of products from secondary alcohol / mole of catalyst compound **2** or **2a**.

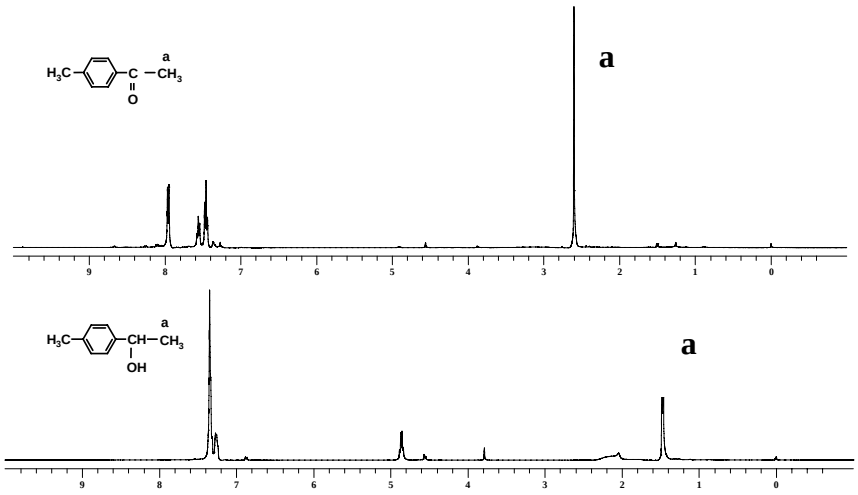

Figure 3.31. 400 MHz ^{1}H NMR spectra of 4 methyl acetophenone (top) from the product mixture in $CDCl_3$ (CH_3 peak is marked as 'a') and distilled 4-methyl phenylethanol (bottom) in $CDCl_3$ (CH_3 peak is marked as 'a').

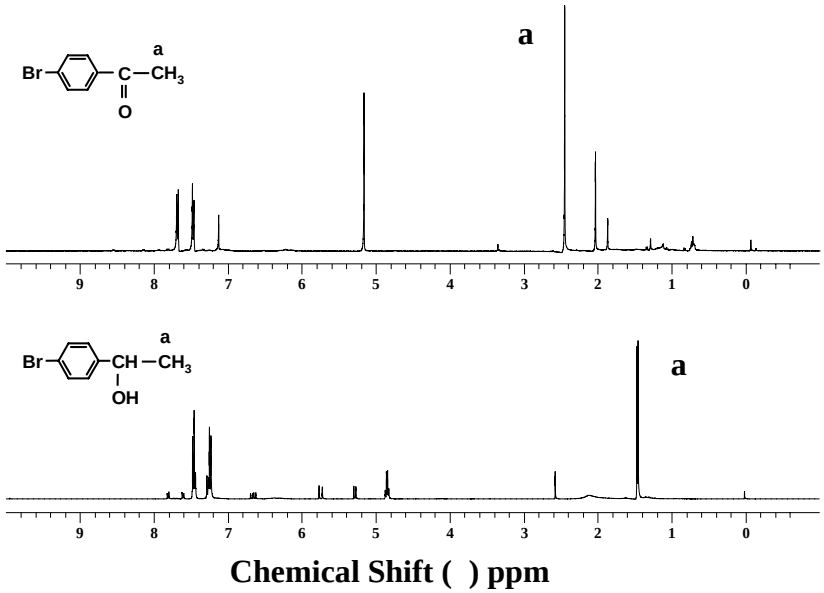

Figure 3.32. 400 MHz ^{1}H NMR spectra of 4 bromo acetophenone (top) from the product mixture in $CDCl_3$ (CH_3 peak is marked as 'a') and distilled 4-bromo phenylethanol (bottom) in $CDCl_3$ (CH_3 peak is marked as 'a')

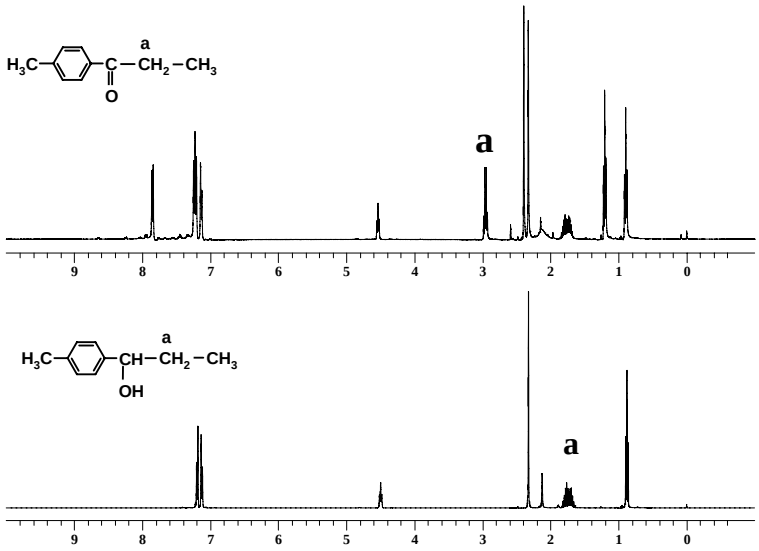

Figure 3.33. 400 MHz ^{1}H NMR spectra of propiophenone (top) from the product mixture in $CDCl_3$ (CH_2 peak is marked as 'a') and distilled 1 phenylpropanol (bottom) in $CDCl_3$ (CH_2 peak is marked as 'a').

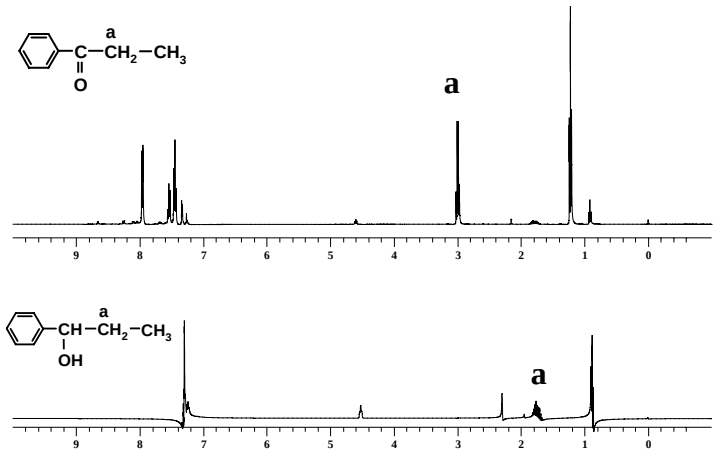

Figure 3.34. 400 MHz ^{1}H NMR spectra of 4 methyl propiophenone (top) from the product mixture in $CDCl_3$ (CH_2 peak is marked as 'a') and distilled 4 methyl phenylpropanol (bottom) in $CDCl_3$ (CH_2 peak is marked as 'a').

3.4. Conclusion

Heptamolydate (also known as paramolybdate) is the most common chemical of molybdenum (as ammonium salt), we see in any general chemical laboratory. Its crystal structure is also well-established. Ammonium heptamolybdate has been used as an oxidation catalyst in industry. Its catalytic value increases if it supports / it is functionalized by a transition metal coordination complex on its surface. However, instances of paramolybdate supported transition metal complexes (as a discrete entity) are very rare. We have described here a series of paramolydate supported zinc coordination complexes stressing their supramolecular structures. Even though, numerous POM supported transition metal complexes have been reported in recent past,[9] the catalysis aspect of these POM supported metal coordination complexes is largely unexplored.[10] The salient feature in this chapter is the catalytic activity of compound **1** and **2** / **2**a. Compound **1** catalyzes the oxidation of primary alcohol to respective aldehyde. Catalysis work has been done in solvent free and ecological benign condition, where compound **1** (catalyst) is not soluble. Thus we can utilize the used-catalyst in many cycles without loosing its catalytic activity. We have, at least, done six catalytic cycles using same used-catalyst (compound **1**) just by filtering from the reaction mixture after the completion of each experiment. We have also demonstrated here that compound **2** /**2a** catalyzes the oxidation of a series of secondary alcohols to corresponding ketones at a moderate temperature in a heterogeneous reaction, in which the catalyst (compound **2** / **2a**) is recyclable. Small water clusters such as water tetramer, pentamer and extended water structure were identified crystallographically in the crystal lattice of some of these compounds. We have described a new type of linked structure that is formed by a corner-shared condensed chain, in which the supported zinc coordination complex plays an important role to result in a coordination polymer. We are currently attempting the oxidation of other organic substrates with this and other similar POM based compounds in our laboratory, which will be published in near future.

3.5. References

1. a) M. T. Pope, *In Compre. Coord. Chem. II,* **2004**, *4*, 635; b) C. L. Hill, *In Compre. Coord. Chem. II,* **2004**, *4*, 679; c) M. T. Pope, A. Müller, *Angew. Chem. Int. Ed.* **1991**, *30*, 34; d) C. L Hill, C. M. Prosser-McCartha, *Coord. Chem. Rev.* **1995**, *143,* 407; e) C. L. Hill, *Chem. Rev.* **1998**, *98*, 1; f) *Zeolites*, *Clay and Heteropolyacid in Organic Reactions*; Y. Izumi, K. Urabe, M. Onaka, Kodansha: Tokyo, **1992**; g) M. I. Khan, E. Yohannes, R. J. Doedens, *Inorg. Chem.* **2003**, *42*, 3125; h) M. T. Pope, *Heteropoly and Isopoly Oxometalates*; Springer-Verlag: Berlin, **1983**.
2. a) A. K. Cheetham, C. N. R. Rao, *Chem. Commun.* **2006**, 4780; b) M. Dan, C. N. R. Rao, *Angew. Chem. Int. Ed.* **2006**, *45*, 281; c) W. G. Klemperer, C. G. Wack, *Chem. Rev.* **1998**, *98*, 297; d) E. Coronado, C. J. Gomez Garcia, *Chem. Rev.* **1998**, *98***,** 273; e) L. C. W. Backer, D. C. Glick, *Chem. Rev.* **1998**, *98*, 3.
3. a) V. Soghomonian, Q. Chen, R. C. Haushalter, J. Zubieta, C. O'Connor, *Science,* **1993**, *25,* 1596; b) D. Hagrman, P. J. Hagrman, J. Zubieta, *Angew. Chem. Int. Ed.* **1999**, *38,* 3165; c) P. J. Hagrman, J. Zubieta, *Inorg. Chem.* **2000**, *39,* 3252; d) D. Hagrman, C. Sangregorio, C. J. O'Connor, J. Zubieta, *J. Chem. Soc., Dalton Trans.* **1998**, 3707; f) P. J. Hagrman, D. Hagrman, J. Zubieta, *Angew. Chem. Int. Ed.* **1999**, *38*, 2638.
4. a) M. I. Khan, *J. Solid State Chem.* **2000**, *152***,** 105; b) M. I. Khan, E. Yohannes, D. Powell, *Chem. Commun.* **1999**, 23; c) M. I. Khan, E. Yohannes, D. Dödens, *Angew. Chem. Int. Ed.* **1999**, *38*, 1292; d) M. I. Khan, E. Yohannes, R. J. Dödens, S. Tabussum, S. Cevik, L. Manno, D. Powell, *Cryst. Eng.* **1999**, *2*, 171; e) M. I. Khan, E. Yohannes, D. Powell. *Inorg. Chem.* **1999**, *38*, 212.
5. a) L.-H. Bi, U. Kortz, *Inorg. Chem.* **2004**, *43*, 7961; b) B. S. Bassil, M. H. Dickman, U. Kortz, *Inorg. Chem.* **2006**, *45*, 2394; c) L. Chen, K. Zhu, L.-H. Bi, A. Suchopar, M. Reicke, G. Mathys, H. Jaensch, U. Kortz, R. M. Richards, *Inorg.*

Chem. **2007**, *46*, 8457; d) U. Kortz, A. Teze, G. Herve, *Inorg. Chem.* **1999**, *38*, 2038; e) U. Kortz, I. M. Mbomekalle, B. Keita, L. Nadjo, P. Berthet, *Inorg. Chem.* **2002**, *41*, 6412; f) B. S. Bassil, S. Nellutla, U. Kortz, A. C. Stowe, J.van Tol, N. S. Dalal, B. Keita, L. Nadjo, *Inorg. Chem.* **2005**, *44*, 2659.

6. a) I. Bar-Nahum, J. Ettedgui, L. Konstantinovski, V. Kogan, R. Neumann, *Inorg. Chem.* **2007**, *46*, 5798; b) I. Bar-Nahum, H. Cohen, R. Neumann, *Inorg. Chem.* **2003**, *42*, 3677; c) A. M. Khenkin, R. Neumann, *Inorg. Chem.* **2000**, *39*, 3455; d) E. Derat, D. Kumar, R. Neumann, S. Shaik, *Inorg. Chem.* **2006**, *45*, 8655; e) R. Neumann, A. M. Khenkin, *Inorg. Chem.* **1995**, *34*, 5753.

7. a) D. –L. Long, Y. –F. Song, E. F. Wilson, P. Kögerler, S. –X. Guo, A. M. Bond, J. S. J. Hargreaves, L. Cronin, *Angew. Chem. Int. Ed.,* **2008**, *47*, 4384; b) D. –L. Long, Y.–F. Song, E. F. Wilson, P. Kögerler, S. –X. Guo, A. M. Bond, J. S. J. Hargreaves, L. Cronin, *Angew. Chem. Int. Ed.,* **2008**, *47*, 4456.

8. a) Y. Xu, J-Q. Xu, K-L. Zhang, Y. Zhang, X-Z, You. *J. Chem. Soc., Chem. Commun.* **2000**, *2*, 153; b) C. Martin, C. Lamonier, M. Fournier, O. Mentré, V. Harlé, D. Guillaume, E. Payen, *Inorg. Chem.* **2004**, *43*, 4636; c) S. Reinoso, P. Vitoria, L. Lezama, A. Luque, J. M. Gutiérrez Zorrilla, *Inorg. Chem.* **2003**, *42*, 3709; d) W-B, Yang, C-Z. Lu, X. Lin, H-H. Zhuang, *J. Chem. Soc., Dalton Trans.* **2002**, *14*, 2879; e) C-D. Wu, C-Z. Lu, X. Lin, J-S. Huang, *Inorg. Chem. Commun.* **2002**, *5*, 664; e) C-M. Liu, D-Q. Zhang, D-B. Zhu, *Cryst. Growth Des.* **2003**, *3*, 363.

9. a) J. Wang, G. Zhang, P. Ma, J. Niu, *Inorg. Chem. Commun.* **2008**, *11*, 825; b) N. laronze, J. Marrot, G. Herve, *Inorg. Chem.* **2003**, *42*, 5857; c) S. Reinoso, P. Vitoria, L. S. Felices, L. Lezama, J. M. Gutiérrez-Zorrilla, *Inorg. Chem.* **2006**, *45*, 108; d) R- Z. Wang, J –Q. Xu, G-Y. Yang, W-M. Bu, Y-H. Xing, D-M, Li, S. –Q. Liu, L. Ye. Y. –G. Fan, *Polyhedron* **1999**, *18*, 2971; e) K. Hayashi, M. Takahashi, K. Nomiya, *J. Chem. Soc., Dalton Trans.* **2005**, 3751; f) L. Chen, Y. Wang, C. Hu, L. Feng, E. Wang, N. Hu, H. Jia, *J. Solid State Chem.* **2001**, *161*, 173; g) F.

Li, L. Xu, Y. Wei, X. Wang, W. Wang, E. Wang, *J. Mol. Struct.* **2005**, *753*, 65; h) Z. Zhang, E. Wang, Y. Li, H. An, Y. Qi, L. Xu, *J. Mol. Struct.* **2008**, *872*, 176; j) C-H. Tian, Z-G, Sun, J. Li, X-F. Zheng, H-D. Liang, L-C. Zhang, W-S,.You, Z-M. Zhu, *Inorg. Chem. Commun.* **2007**, *10*, 757; k) J. Wang, S. Li, J. Zhao, J. Niu, *Inorg. Chem. Commun.* **2006**, *9*, 599; l) X. Wei, M. H. Dickman, M. T. Pope, *Inorg. Chem.* **1997**, *36*, 130; m) Y. Lu, J. Lu, E. Wang, Y. Guo, X. Xu, L. Xu, *J. Mol. Struct.* **2005**, *740*, 159; n) J. Niu, Y. Shen, J. Wang, *J. Mol. Struct.* **2005**, *733*, 19; o) D-L. Long, P. Kögerler, L. J. Farrugia, L. Cronin, *J. Chem. Soc., Dalton Trans.* **2005**, 1372; p) D. Xiao, Y. Hou, E. Wang, S. Wang, Y. Li, L. Xu. C. Hu, *Inorg. Chim. Acta.* **2004**, *357*, 2525; q) D. Laurencin, R. Villanneau, P. Herson, R. Thouvenot, Y. Jeannin, A. Proust, *Chem. Commun.* **2005**, 5524; r) J. –W.Cui, X. –B.Cui, H. –H. Yu, J. –Q. Xu, Z. –H. Yi, W. –J. Duan, *Inorg. Chim. Acta.* **2008**, *361*, 2641; s) P. Gili, P. Lorenzo-Luis, A. Mederos, J. M. Arrieta, G. Germain, A. Castinñeiras, R. Carballo, *Inorg. Chim. Acta* **1999**, *295*, 106; t) C.-H. Tian, Z.-G. Sun, J. Li, X.-F. Zheng, H.-D. Liang, L.-C. Zhang, W.-S. You, Z.-M. Zhu, *Inorg. Chem. Commun.* **2007**, *10*, 757; u)Z. Han, H. Ma, J. Peng,Y. Chen, E. Wang, N. Hu, *Inorg. Chem. Commun.* **2004**, *7*, 182; v) R. S. Rarig, L. Bewley, Golub, C. J. O'Connor, J. Zubieta, *Inorg. Chem. Commun.* **2003**, *6*, 539; w) V. Shivaiah, S. K. Das, *Inorg. Chem.* **2005**, *44*, 8846 and references cited therein.

10. a) A. M. Khenkin, L. J. W. Shimon, R. Neumann, *Inorg. Chem.* **2003**, *42*, 3331; b) T. Arumuganathan, A. Srinivasarao, T. Vijay Kumar, S. K. Das, *J. Chem. Sci.,* **2008**, *120*, 95; c) A. R. Sidle, C. G. Markell, A. Lyon, K. O. Hodgson, A. L. Roe, *Inorg. Chem.* **1987**, *26*, 219; d) D. K. Lyon, R. G. Finke, *Inorg. Chem.* **1990**, *29*, 1789; e) Y. Lin. R. G. Finke, *J. Am. Chem. Soc.* **1994**, *116*, 8335; f) M. Pohl, D. K. Lyon, N. Mizuno, K. Nomiya, R. G. Finke, *Inorg. Chem.* **1995**, *34*, 1413.

11. a) D. H. Sell, C. S. Pybus, Eds.; *chemistry of Frangrances*; RSC Paperbacks: Cambridge, **1999**; b) R. P. Singh, H. N. Subbaraao, D. Sukh, *Tetrahedron* **1979**,

35, 1789; c) T. Fey, H. Fischer, S. Bachmann, K. Albert, C. Bolm, *J. Org. Chem.* **2001**, *66,* 8154.

12. D. B. Dess, J. C. Martin, *J. Org. Chem.* **1983**, *48*, 4155.
13. a) I. E. Marko, P. R. Giles, M. Tsukazaki, I. Chelle-Regnaut, A. Gautier, S. M. Brown, C. Urch, *J. Org. Chem.* **1999**, *64*, 2433. b) A. Haimov, R. Neumann, *Chem. Commun.* **2002**, 876. c) A. M. Khenkin, R. Neumann, *J. Org. Chem.* **2002**, *67*, 7075; d) A. M. Khenkin, L. J. W. Shimon, R. Neumann, *Eur. J. Inorg. Chem.* **2001**, 789; e) K. P. Peterson, R. C. Larock, *J. Org. Chem.* **1998**, *63*, 3185; f) S. S. Stahl, J. L. Thorman, R. C. Nelson, M. A. Kozee, *J. Am. Chem. Soc.* **2001**, *123*, 7188; g) B. A. Steinhoff, S. R. Fix, S. S. Stahl, *J. Am. Chem. Soc.* **2002**, *124*, 766; h) B. Betzemeier, M. Cavazzini, S. Quici, P. Knochel, *Tetrahedron Lett.* **2000**, *41*, 4343; i) A. Dijksman, A. Marino-Gonzalez, A. M. I. Payeras, I. W. C. E. Arends, R. A. Sheldon, *J. Am. Chem. Soc.* **2001**, *123*, 6826; k) C. Y. Lorber, S. P. Smidt, J. A. Osborn, *Eur. J. Inorg. Chem.* **2000**, 655; l) J. Muldoon, S. N. Brown, *Org. Lett.* **2002**, *4*, 1043; m) G. Csjernyik, A. H. Ell, L. Fadini, B. Pugin, J. –E. Backvall, *J. Org. Chem.* **2002**, *67*, 1657; n) K. Yamaguchi, K. Mori, T. Mizugaki, K. Ebitani, K. Kaneda, *J. Am. Chem. Soc.* **2000**, *122*, 7144; o) M. Lee, S. Chang, *Tetrahedron Lett*. **2000**, *41*, 7507; p) R. Ciriminna, M. Pagliaro, *Chem. Eur. J.* **2003**, *9*, 5067; q) B. Z. Zhan, M. A. White, T. –K. Sham, J. A. Pincock, R. J. Doucet, K. V. R. Rao, K. N. Robertson, T. S. Cameron, *J. Am. Chem. Soc.* **2003**, *125*, 2195; r) J. H. J. Kluytmans, A. P. Markusse, B. F. M. Kuster, G. B. Marin, J. C. Schouten, *Catal. Today* **2000**, *57*, 127; s) M. Besson, P. Gallezot, *Catal. Today* **2000**, *57*, 143; t) T. Mallat, A. Baiker, *Chem. Rev.* **2004**, *104*, 3037; u) Y.-C. Son,V. D. Makwana, A. R. Howell, S. L.Suib, *Angew. Chem., Int. Ed.* **2001**, *40*, 4280; v) S. Velusamy, T. Punniyamurthy, *Org. Lett.* **2004**, *6*, 217.
14. R. A. Sheldon, I. W. C. E. Arends, A. Dijksman, *Catal. Today* **2000**, *57*, 157.
15. a) *SAINT: Software for the CCD Detector System*; Bruker Analytical X-ray Systems, Inc.: Madison, WI, 1998; b) the structures were solved using *SHELXS*-

97; c) Sheldrick, G. M. *SHELXS-97*, *Program for Structure Solution of crystal structure;* University of Göttingen: Germany, 1997.

16. K. Brandenburg, *DIAMOND Version 2.1e*, Crystal Impact GbR, Bonn, Germany, **2001**.
17. H. T. Evans, B. M. Gatehouse, P. J. Leverett, *J. Chem. Soc., Dalton Trans.* **1975**, 505.
18. a) H. Jin, C. Qin, Y G. Li, E B. Wang, *Inorg. Chem. Commun.* **2006**, *9,* 482; b) J P. Wang, X D. Du, J Y. Niu, *J. Solid State Chem.* **2006**, *179,* 3260; c)H. Jin, C. Qin, Y G. Li, E.Wang, *Inorg. Chem. Commun.* **2006**, *9,* 482; d) C D.Wu, C Z. Lu, H H. Zhuang, J S. Huang, *Inorg. Chem.* **2002**, *41*, 5636; e) W. Yang, C. Lu, H. Zhuang, *J. Chem. Soc., Dalton Trans.* **2002**, 2879; f) Y. Xu, L B. Nie, D. Zhu, Y. Song, G P. Zhou, W S. You, *Cryst. Growth Des.* **2007**, *7,* 925; g) V. Soghomonian, Q. Chen, R. C. Haushalter, J. Zubieta, C. J. O'Connor, *Science,* **1993**, *259,* 1596; h) D. Hagrman, P. J. Hagrman, J. Zubieta, *Angew. Chem. Int. Ed.,* **1999**, *38,* 3165; i) P. J Hagrman, J. Zubieta, *Inorg. Chem.* **2000**, *39,* 3252; j) D. Hagrman, C. Sangregorio, C. J. O'Connor, J. Zubieta, *J. Chem. Soc., Dalton Trans.* **1998**, 3707; k) P. J. Hagrman, D. Hagrman, J. Zubieta, *Angew. Chem. Int. Ed.* **1999**, *38,* 2638; l) M. I. Khan, *J. Solid State Chem.* **2000**, *152*, 105; m) M. I. Khan, E. Yohannes, D. Powell, *Chem. Commun.* **1999**, 23; n) M. I. Khan, E. Yohannes, D. Dödens, *Angew. Chem., Int. Ed.* **1999**, *38,* 1292; o) M. I. Khan, E. Yohannes, R. J. Dödens, S. Tabussum, S. Cevik, L. Manno, D. Powell, *Cryst. Eng.* **1999**, *2*, 171; p) M. I. Khan, E. Yohannes, D. Powell, *Inorg. Chem.* **1999**, *38,* 212.
19. T. Li, J. Lü, S. Gao, R. Cao. *Inorg. Chem. Chem.* **2007**, *10*, 1342.
20. Q.Liu, Y-Z. Li, Y. Song, H. Liu, Z. Xu, *J. Solid State Chem.* **2004**, *177*, 470; b) L. Carlucci, G. Ciani, D. M. Proserpio, A. Sironi, *J. Am. Chem. Soc.,* **1995**, *117*, 12861; c) L. Carlucci, G. Ciani, D. M. V. Gudenberg, D. M. Proserpio, A. Sironi,

Chem. Commun. **1997**, *631*; d) L. Carlucci, G. Ciani, D. M. Proserpio, A. Sironi, *Inorg. Chem.* **1997**, *36*, 1736; e) L. Carlucci, G. Ciani, D. M. Proserpio, S. Rizzato, *J. Solid State Chem.* **2000**, *152*, 211; f) M. L. Tong, S. L. Zheng, X. M. Chen, *Chem. Commun.* **1999**, 561; g) S. L. Zheng, M. L. Tong, H. L. Zhu, Y. Fang, X. M. Chen, *J. Chem. Soc., Dalton Trans.* **2001**, 2049; h) S. L. Zheng, M. L. Tong, X. L. Yu, X. M. Chen, *J. Chem. Soc., Dalton Trans.* **2001**, 586; i) S. L. Zheng, M. L. Tong, R. W. Fu, X. M. Chen, *Inorg. Chem.* **2001**, *40*, 3562; j) Q. Liu, X. Q. Sun, J-Z. Zou, K-B. J. Yu, *J. Coord. Chem.* **2002**, *55*, 1021; k) Y. Zheng, J. Li, M. Nishiura, T. Imamoto, *J. Mol. Struct.* **2000**, *520*, 257; l) B. Moulton, J. Lu, M. J. Zaworotko, *J. Am. Chem. Soc.* **2001**, *123*, 9224; m) S. R. Batten, B. F. Hoskins, R. Robson, *Inorg. Chem.* **1998**, *37*, 3432; n) Q. Liu, B.L. Li, Z. Xu, X. Q. Sun, K-B. Yu, *Transition Met. Chem.* **2002**, *27*, 786; o) Q. Liu, B. L. Li, Z. Xu, K-B. Yu, *J. Coord. Chem,* **2003**, *56*, 771.

21. a) D. L. Long, P. Kögerler, L. J. Farrugia, L. Cronin, *Angew. Chem, Int. Ed.* **2003**, *42*, 4180; b) D. L. Long, Kögerler, L. J. Farrugia, L. Cronin, *J. Chem. Soc., Dalton Trans.* **2005**, 1372.

22. L. Infantes, S. Motherwell, *Cryst. Engg. Commun.* **2002**, *4*, 454.

23. M. G. Brown, F. N. Keutsch, R. J. Saykally, R. J. *J. Chem. Phys.* **1998**, *109*, 22; b) B. Q. Ma, H. L. Sun, S. Gao, *Chem. Commun*. **2004**, 2220; c) Y. Wang, J. R. Gunn, *Can. J. Chem.* **1999**, *77*, 367; d) Y. Ma, A. S. Foster, R. M. Nieminen, *J. Chem. Phys.* **2005**, *122*, 144709; e) K. Balasubramanian, *J. Phys. Chem. A.* **2004**, *108,* 5527; f) K. Liu, M. G. Brown, J. D. Cruzan, R. J. Saykally, *J. Phys. Chem. A.* **1997**, *101,* 9011; g) K. Liu, M. G. Brown, J. D. Cruzan, R. J. Saykally, *Science,* **1996**, *271*, 5245; h) J. D. Cruzan, M. R. Viant, M. G. Brown, D. D. Lucas, K. Liu, R. J. Saykally, *Chem. Phy. Lett.* **1998***, 292*, 667; i) S. K. Ghosh, P. K. Bharadwaj, *Inorg. Chim. Acta.* **2006***, 359*, 1685; k) T. Miyake, M. Aida, *Int. Elect. J. Mol. Des.* **2003**, *2*, 24; l) M. G. B. Drew, S. De, D. Datta, *J. Chem. Cryst.*

2007, *38*, 495; m) J. Q. Liu, Y. Y. Wang, P. Liu, W. P. Wu, Y. P. Wu, X. R. Zeng, F. Zhong, Q. Z. Shi, *Inorg. Chem. Commun.* **2007**, *10*, 343; n) J. F. Song, J. Lu, Y. Chen, Y. B. Lui, R. S. Zhou, X. Y. Xu, J. Q. Xu, *Inorg. Chem. Comm.* **2007,** *9*, 1079; o) G. Garberoglio, R. Vallauri, *J. Mol. Liq.* **2004**, *110*, 141; p) L. A. Burke, J. O. Jensen, J. L. Jensen, P. N. Krishnan, *Chem. Phys. Lett.* **1993**, *206*, *1-4*, 293.

24. R. Ludwig, *Angew. Chem. Int. Ed.* **2001**, *40*, 1808.

25. a) J. Luo, M. Hong, R. Wang, Q. Shi, R. Cao, J. Weng, R. Sun, H. Zhang, *Inorg. Chem. Comm.* **2003**, *6*, 702; b) D. G. Allis, R. S. Rarig, E. Burkholder, J. Zubieta, *J. Mol. Struct.* **2004**, *688*, 11; c) C. Qin, X. Wang, Y. Qi, E. Wang, C. Hu, L. Xu, *J. Solid State Chem*. **2004**, *177*, 3263 d) M. McCann, K. Maddock, *Polyhedron* **1995**, *14*, 2919; e) C. Sun, E. Wang, D. Xio, H. An, L. Xu, *J. Mol. Struct.* **2005**, *741*, 149; f) R. Q. Fang, Y. F. Zhao, X. M. Zhang, *Inorg. Chim. Acta.* **2006**, *359*, 2023; g) D. Hagrman, P. Hagrman, J. Zubieta, *Inorg. Chim. Acta***. 2000**, *300*, 212; h) A. K. Stover, J. R. Gutnick, A. N. Sarjeant, A. J. Norquist, *Inorg. Chem.* **2007**, *46*, 4389; i) X. Lu, S. Liu, X. Mao, X. Bu, *J. Mol. Struct.* **2001**, *562*, 89; j) X. B. Cui, K. Lu, Y. Fan, J. Q. Xu, L. Ye, Y. H. Sun, Y. Li, H. H. Yu, Z. H. Yi, *J. Mol. Struct.* **2005**, *743*, 151; k) X. J. Wang, B. S. Kang, C. Y. Su, K. B. Yu, H. X. Zhang, Z. N. Chen, *Polyhedron* **1999**, *18*, 3371; l) Q. Zhai, C. Lu, Q. Zhang, X. Wu, X. Xu, S. Chen, L. Chen, *Inorg. Chim. Acta, **2006***, *359*, 3875; m) Y. Chen, H. Zhang, X. Wang, C. Huang, Y. Cao, R. Sun, *J. Solid State Chem*. **2006**, *179*, 1674; n) A. J. Bridgeman, G. Cavigliasso, *Inorg. Chem.* **2002**, *41*, 3500; o) W. J. Kroenke, J. P. Jr. Fackler, A. Mazanty, *Inorg. Chem.* **1983**, *22*, 2412.

26. a) V. Coué, R. Dessapt, M. Bujoli-Doeuff, M. Evain, S. Jobic, *Inorg. Chem.* **2007**, *46*, 2824; b) R. Benchrifa, M. Leblanc, R. de Pape, *Eur. J. Solid State Inorg. Chem.* **1989**, *26*, 593; c) W. T. A. Harrison, L. L. Dussack, A. J. Jacobson, *Acta. Cryst. C.* **1996**, *52*, 1075.

27. D. Xiao, H. An, E. Wang, L. Xu, *J. Mol. Struct.* **2005**, *738*, 217.

28. a) J.-M. Brégeault, *J. Chem. Soc., Dalton Trans.* **2003**, 3289; b) J. Wang, L. Yan, G. Li, X. Wang, Y. Ding, J. Suo, *Tetrahedron Lett.* **2005**, *46*, 7023.

29. a) M. V. Vasylyev, R. Neumann, *J. Am. Chem. Soc.* **2004**, *126*, 885; b) A. Lambert, P. Plucinskib, I. V. Kozhevnikov, *Chem. Commun.* **2003**, *714*; c) T. Sakamoto. C. Pac. *Tetrahedron Lett.* **2000**, *41*, 10009.

30. a) J. Wang, L. Yan, G. Li, X. Wang. Y. Ding, J. Suo, *Terahedron Lett.* **2005***,* 46, 7023; b) A. M. Khenkin, L. J. W. Shimon, R. Neumann, *Inorg. Chem.* **2003**, *42*, 3331.

****

Chapter 4

==========

'Ionic Crystals' Consisting of Trinuclear Macrocations and Polyoxometalate Anions Exhibiting Single Crystal to Single Crystal Transformation: Breathing of Crystals

==========

4.1. Introduction

Transition metal carboxylate chemistry, in particularly trinuclear oxo centered macrocation, generally formulated as $[M_3O(OOCR)_6L_3]^+$ (where M = Fe^{3+}, Cr^{3+} etc., R = H, CH_3, CH_2Cl, etc., L = neutral ligands such as H_2O, pyridine etc.), has played vital role in the development of modern inorganic chemistry.[1] The { $_3$-O} centered trinuclear metal complexes are also known as 'basic' metal carboxylate complexes. Two basic carboxylate complexes $[Fe_3(\ _3\text{-}O)(OOCCH_3)_6(H_2O)_3]Cl \cdot 6H_2O$ and $[Cr_3(\ _3\text{-}O)(OOCCH_3)_6(H_2O)_3]Cl \cdot 6H_2O$, whose physical properties have been exhaustively studied, are known for over 50 years.[2] An interesting feature of a homonuclear 'basic carboxylate complex' (when the concerned metal centers are paramagnetic) is that the complex nearly always fails to adopt expected the 3 fold symmetry.[3] It is has been argued that net antiferromagnetic coupling distorts spontaneously to a non 3 fold symmetry as a result of spin frustration (also known as "magnetic Jahn Teller effect").[4] We have been working on basic trinuclear cluster containing compounds and exploiting their solid state properties to obtain new materials in application point of view. Recently, we have demonstrated that the basic iron trinuclear ($_3$-O) cluster containing compound is capable of sensing methanol selectively in a single crystal to single crystal transformation study.[5] Generally, basic trinuclear ($_3$-O)-bridged transition metal carboxylate clusters are well documented in the literature in three different ways: (i) discrete ($_3$-O) clusters, which are

classified either under neutral mixed metal ($_3$-O) cluster or discrete cationic ($_3$-O) clusters.[2] These basic trinuclear clusters are considered as important subclass of inorganic trinuclear compounds because of their numerous applications such as, majority of higher nuclear clusters {e.g., Fe_{10} wheel type clusters) are generated from these starting precursors.[6] This class of compounds are also important in terms of magnetism[7], and catalysis.[8] (ii) Open metal organic framework materials (MOFs), in which trinuclear ($_3$-O)-clusters, acting as building units, are interconnected by organic linkers using covalent bonds in the relevant crystal lattice having well-defined pores and cavities.[9] (iii) Ionic crystals, in which 's' block metal ions (e.g., Na^+, K^+, Rb^+, Cs^+ ions), trinuclear macrocations, polyoxometalate anions and solvent molecules are accommodated in the crystal lattice and stabilized by electrostatic interactions. Polyoxometalates are metal-oxide based molecular clusters generally observed in anionic forms that are isolated as crystalline materials with appropriate cations. The interest in this class of polyoxometalate based 'ionic crystals' has opened up a new field of research and enormous work has been done by Mizuno and co-workers, especially in terms of their applications in selective sorption and desorption of small molecules.[10] They found that the systems, showing this selective host-guest chemistry, have the maximum macrocation / polyoxometalate ratio of 2:1, where the remaining negative charges were counterbalanced by alkali metal ions. In this chapter we have discussed a series of ionic crystals consisting of macrocation / polyoxoanion ratio in the range of 1:1 4:1 without the presence of alkali metal cations. We have described here the synthesis and structural characterization of compound $[Fe_3(\ _3\text{-}O)(ClCH_2COO)_6(H_2O)_3]_4[SiW_{12}O_{40}]\cdot 18H_2O \cdot 2ClCH_2COOH$ (**1**) (ratio of macrocation / polyoxoanions is 4:1). Compound **1**, on heating at 85°C for 3.5 hours in an open oil bath, undergoes single crystal to single crystal transformation resulting in a dehydrated compound $[Fe_3(\ _3\text{-}O)(ClCH_2COO)_6(H_2O)_3]_4[SiW_{12}O_{40}]\cdot 10H_2O \cdot 2ClCH_2COOH$ (**dehydrated 1-85°**). When the crystals of compound **1** are heated at 135°C for 3.5 hours in an open oil bath,

relatively more dehydrated compound $[Fe_3(\ _3\text{-}O)(ClCH_2COO)_6(H_2O)_3]_4[SiW_{12}O_{40}]\cdot 8H_2O\cdot 2ClCH_2COOH$ (**dehydrated 1-135^o**) is obtained. Both these dehydrated compounds (**dehydrated 1-85^o, dehydrated 1-135^o**) have been characterized by crystal structure determination. One of these dehydrated compounds, **dehydrated 1-85^o** on exposing to water vapor for one week regenerates to compound **1** (**regenerated 1**). The single crystals of **regenerated 1** exhibited similar cell parameters as those of parent **1** (the single crystal structure of **regenerated 1** could not be determined due to its poor data quality. The crystals of **regenerated 1** were further characterized by routine spectroscopic analysis, TGA-Mass studies and powder X-ray diffraction studies. We have shown similar crystal to crystal transformations mediated by chromium analogue compounds as shown below (except the unlikeness that chromium analogue **2** resulted in same dehydrated compound, **dehydrated 2**, even when **2** was heated at 85^{o}C as well as 135^{o}C):

$[Cr_3(\ _3\text{-}O)(ClCH_2COO)_6(H_2O)_3]_4[SiW_{12}O_{40}]\cdot 14H_2O\cdot 2ClCH_2COOH$ (**2**)

(2) + heated 85^{o}C / 135^{o}C $[Cr_3(\ _3\text{-}O)(ClCH_2COO)_6(H_2O)_3]_4[SiW_{12}O_{40}]\cdot 8H_2O\cdot 2ClCH_2COOH$ (**dehydrated 2**)

dehydrated 2 + exposure of water vapor **regenerated 2**

Thus we have demonstrated synthesis and reversible crystal to crystal transformation studies mediated by compounds **1** and **2** through exclusion and inclusion of water molecules in respective ionic crystals. In addition, we have structurally characterized the ionic crystals $[H_2(Fe_3(\ _3\text{-}O)(OOCCH_2CN)_6(H_2O)_3)_2(SiMo_{12}O_{40})]\cdot 16H_2O$ (**3**), $[H_2(Cr_3(\ _3\text{-}O)(OOCCH_2CN)_6(H_2O)_3)_2(SiMo_{12}O_{40})]\cdot 16H_2O$ (**4**), and $[H_3(Cr_3(\ _3\text{-}O)(OOCCH_2CN)_6(H_2O)_3)(SiW_{12}O_{40})]\cdot 6H_2O$ (**5**). In compounds **3** and **4**

macrocation / polyoxometalate ratio is 2:1 whereas in compound **5** the same is 1:1. The remaining negative charges are counterbalanced by protons. The compounds are characterized by IR, UV, powder XRD, TGA analysis and unambiguously by single crystal X-ray structure determination.

4.2. Experimental Section

4.2.1. Materials

All the chemicals were reagent grade and used without any further purification. The distilled water was used throughout the work. $H_4SiW_{12}O_{40}$, hydrochloric acid and anhydrous $FeCl_3$ were acquired from Merck. $H_4SiMo_{12}O_{40}$ was synthesized by following the reported procedure.[11] $ClCH_2COOH$ and $CNCH_2COOH$ were received from S. D. Fine and Spectrochem respectively. $Cr(NO_3)_3 \cdot 9H_2O$ was obtained from Loba chemicals.

4.2.2. Physical Measurements

Infra red spectra of solid samples were obtained as KBr pellets on a JASCO – 5300 FT – IR spectrophotometer. A Cary 100 Bio UV/vis spectrophotometer was used to record the electronic absorption spectra. Thermogravimetric analyses were carried out on a STA 409 PC analyzer and corresponding masses were analyzed by QMS 403 C mass analyzer, under the flow of N_2 gas with a heating rate of $5^oC\ min^{-1}$, in the temperature range of 30-1100^{o}C. The Powder X-ray diffraction patterns were recorded using Cu-Kα (λ = 1.54 Å) radiation on a Phillips PW 3710 diffractometer at a scanning speed of $3^o\ min^{-1}$.

4.2.3. Synthesis and Characterization

$[Fe_3(\ _3\text{-}O)(ClCH_2COO)_6(H_2O)_3]_4[SiW_{12}O_{40}] \cdot 18H_2O \cdot 2ClCH_2COOH$ (1)

To a 100 mL of water, $H_4SiW_{12}O_{40}$ (0.5 g, 0.17mmol), 5 mL of 2.3M HCl were added followed by the addition of $ClCH_2COOH$ (5.5 g, 58.20 mmol). The pH of the resulting reaction mixture was adjusted to 2.0 by 5M NaOH solution. To this solution, $FeCl_3$ (0.34 g, 2.10 mmol) was added and the resulting solution was stirred for an hour, then filtered and the filtrate was kept open at room temperature. After one week, settled red colored crystals were collected, dried in room temperature and used for further studies. Yield: 0.45 g (39% based on W). IR (KBr pellet): (ν/cm^{-1}): 3342, 2945, 1734, 1614, 1431, 1392, 1259, 1016, 974, 920, 798, 692, 574, 507.

$[Fe_3(\ _3\text{-}O)(ClCH_2COO)_6(H_2O)_3]_4[SiW_{12}O_{40}] \cdot 14H_2O \cdot 2ClCH_2COOH$ (dehydrated 1-85^o)

Compound **1**, on heating in the temperature range of 80 85^{o}C for 3.5 hours produced **dehydrated 1-85^o**. IR (KBr pellet): (ν/cm^{-1}): 3296, 2945, 1728, 1610, 1431, 1394, 1259, 1016, 974, 918, 798, 690, 578, 509.

$[Fe_3(\ _3\text{-}O)(ClCH_2COO)_6(H_2O)_3]_4[SiW_{12}O_{40}] \cdot 8H_2O \cdot 2ClCH_2COOH$ (dehydrated 1-135^o)

Compound **1**, on heating in the temperature range of 130 140^{o}C for 3.5 hours produced **hehydrated 1-135^o**. IR (KBr pellet): (ν/cm^{-1}): 3306, 2949, 2334, 1738, 1614, 1550, 1429, 1398, 1259, 1016, 974, 918, 800, 690, 578, 511.

$[Fe_3(\ _3\text{-}O)(ClCH_2COO)_6(H_2O)_3]_4[SiW_{12}O_{40}] \cdot 14H_2O \cdot 2ClCH_2COOH$ (regenerated 1)

Compound **1b**, on exposure to water vapor for the period of one week provided **regenerated 1**, and was characterized by IR, PXRD and TGA / Mass analysis.

$[Cr_3(\ _3\text{-}O)(ClCH_2COO)_6(H_2O)_3]_4[SiW_{12}O_{40}] \cdot 14H_2O \cdot 2ClCH_2COOH$ (2)

To a 100 mL of water, $H_4SiW_{12}O_{40}$ (0.5 g, 0.17mmol), 5 mL of 2.3M HCl were added followed by the addition of $ClCH_2COOH$ (5.5 g, 58.20 mmol). The pH of the resulting reaction mixture was adjusted to 2.0 by 5M NaOH solution. To this solution, $Cr(NO_3)_3 \cdot 9H_2O$ (1.0 g, 2.50 mmol) was added and the resulting solution was stirred for an hour, then filtered and the filtrate was kept open at room temperature. After one week, settled green colored crystals were filtered, dried in room temperature and used for further studies. Yield: 0.52 g (46% based on W). IR (KBr pellet): (ν/cm^{-1}): 3557, 3335, 2949, 1643, 1440, 1406, 1263, 974, 920, 800, 706, 659, 441.

$[Cr_3(\ _3\text{-}O)(ClCH_2COO)_6(H_2O)_3]_4[SiW_{12}O_{40}] \cdot 8H_2O \cdot 2ClCH_2COOH$ (dehydrated 2-85^o)

A bunch of crystalline compound **2**, on heating in the temperature range of 135^{o}C for 3.5 hours produced **dehydrated 2-85^o** compound. IR (KBr pellet): (ν/cm^{-1}): 3557, 3342, 2953, 1643, 1440, 1410, 1261, 1016, 972, 920, 802, 706, 655, 588, 439.

$[Cr_3(\ _3\text{-}O)(ClCH_2COO)_6(H_2O)_3]_4[SiW_{12}O_{40}] \cdot 8H_2O \cdot 2ClCH_2COOH$ (dehydrated 2-135^o)

Compound **2**, on heating in the temperature range of 135^{o}C for 3.5 hours provided **dehydrated 2-135^o**. IR (KBr pellet): (ν/cm^{-1}): 3557, 3342, 2950, 1643, 1440, 1410, 1260, 1016, 972, 920, 802, 706, 650, 588, 439.

$[Cr_3(\ _3\text{-}O)(ClCH_2COO)_6(H_2O)_3]_4[SiW_{12}O_{40}] \cdot 4H_2O \cdot 2ClCH_2COOH$ (regenerated 2)

Compound **2**, on exposure to water vapor for the period of one week produced **regenerated 2**. It was characterized by IR, PXRD and TGA / Mass analysis. IR (KBr pellet): (ν/cm^{-1}): 3314, 2951, 1792, 1643, 1440, 1406, 1263, 1016, 974, 920, 800, 706, 655, 588, 532, 428.

$[H_2(Fe_3(\ _3\text{-}O)(OOCCH_2CN)_6(H_2O)_3)_2(SiMo_{12}O_{40})]\cdot 16H_2O$ (3)

To 100 mL of water, $H_4SiMo_{12}O_{40}$ (0.5 g, 0.27 mmol), 5 mL of 2.3M hydrochloric acid were added followed by the addition of $CNCH_2COOH$ (4 g, 34.5 mmol). The pH of the resulting solution was adjusted to 2.0 by NaOH solution. Then, anhydrous $FeCl_3$ (0.6 g, 3.70 mmol) was added and the resulting reaction mixture was stirred for two hours at room temperature and then filtered. The red colored clear filtrate was kept open in a beaker for crystallization without any disturbance. After one week, crystals formed, were filtered, washed thoroughly with water and finally dried at room temperature. One of the diamond shaped red colored crystal was characterized by single crystal X-ray diffraction. The needle shaped crystals observed in the same crystal bunch could not be characterized by single crystal X-ray diffraction study. Anal.calcd for $C_{36}H_{70}N_{12}O_{88}SiFe_6Mo_{12}$: C, 12.03; H, 2.42; N, 4.67%. Found C, 11.696; H 2.31; N, 4.45%. IR (KBr pellet): (ν/cm^{-1}): 3400(br), 2970(s), 2908(s), 2274(s), 1911(s), 1645(m), 1427(s), 1375(s), 1282(s), 956(s), 906(s), 802(s), 717(s), 586(m), 532(s), 461(s).

$[H_2(Cr_3(\ _3\text{-}O)(OOCCH_2CN)_6(H_2O)_3)_2(SiMo_{12}O_{40})]\cdot 16H_2O$ (4)

To 100 mL of water, $H_4SiMo_{12}O_{40}$ (0.5 g, 0.27 mmol), 5 mL of 2.3M hydrochloric acid were added followed by the addition of $CNCH_2COOH$ (4 g, 34.5 mmol). The pH of the resulting solution was adjusted to 2.0 by NaOH solution. Then, $Cr(NO_3)_3\cdot 9H_2O$ (1.0 g, 2.50 mmol) was added and the resulting reaction mixture was stirred for two hours at room temperature and then filtered. The green colored filtrate was kept open in a beaker for crystallization without any disturbance. After one week, crystals formed, were filtered, washed with water and finally dried at room temperature. One of the diamond shaped green colored crystal was characterized by single crystal X-ray diffraction. The green needle shaped crystals observed in the same crystal bunch could not be characterized by single crystal X-ray diffraction study. Anal. calcd for $C_{36}H_{70}N_{12}O_{88}SiCr_6Mo_{12}$: C, 12.11; H, 2.43; N, 4.71%. Found C, 11.58; H 2.35; N,

4.60%. IR (KBr pellet υ, cm^{-1}): 3422(br), 2964(s), 2922(s), 2268(s), 1728(s), 1660(m), 1620(m), 1439(s), 1377(s), 1300(s), 1016(s), 976(s), 920(s), 802(s), 594(m), 532(s).

$[H_3(Cr_3(\ _3\text{-}O)(OOCCH_2CN)_6(H_2O)_3)(SiW_{12}O_{40})]\cdot 6H_2O$ (5)

To 100 mL of water, $H_4SiW_{12}O_{40}\ .xH_2O$ (0.5 g, 0.17 mmol), 5 mL of 2.3M hydrochloric acid was added followed by the addition of $CNCH_2COOH$ (5 g, 43.1 mmol). The pH of the resulting solution was adjusted to 2.0 by NaOH solution. Then, $Cr(NO_3)_3\cdot 9H_2O$ (1.0 g, 2.50 mmol) was added and the resulting reaction mixture was stirred for two hours at room temperature and then filtered. The green colored filtrate was kept open in a beaker for crystallization without any disturbance. After one week, crystals formed, were filtered, washed with water and finally dried at room temperature. One of the diamond shaped green colored crystal was characterized by single crystal X-ray diffraction. The green needle shaped crystals observed in the same crystal bunch could not be characterized by single crystal X-ray diffraction study. Anal: calcd for $C_{18}H_{33}N_6O_{62}SiCr_3W_{12}$: C, 5.81; H, 0.68; N, 2.26%. Found C, 6.01; H, 0.69; N, 2.63%. IR (KBr pellet υ, cm^{-1}): 3431(br), 2964(s), 2924(s), 2268(s), 1660(s), 1618(s), 1439(s), 1377(s), 1298(s), 1018(s), 978(s), 920(s), 798(s), 534(m).

4.2.4. Single Crystal Structure Determination

Data were measured on a Bruker SMART APEX CCD area detector system [λ(Mo Kα) = 0.71073 Å], graphite monochromator, 2400 frames were recorded with an ω scan width of 0.3°, each for 10 second, a crystal detector distance of 60 mm, and a collimator of 0.5 mm. The data were reduced using SAINTPLUS,[12a] the structures were solved using SHELXS-97,[12b] and refined using SHELXL-97.[12c] DIAMOND[13] software was used for molecular graphics. All non hydrogen atoms were refined anisotropically. Hydrogen atoms on chloroacetate moiety from the trinuclear cluster were introduced on calculated positions and included in the refinement riding on their respective parent

atoms. We tried to locate the hydrogen atom of solvent water molecules through differential Fourier maps, but couldn't succeed. The lattice $ClCH_2COOH$ molecules are refined isotropically due to the considerable disorder. Summaries of the crystallographic data and structure determination parameters for compounds **1**, **dehydrated 1-85°** and **dehydrated 1-135°** are provided in Table 4.1. The crystal data and relevant parameters for compound **2**, **dehydrated 2-85° / 135 °** are presented in Table 4.9. The crystal data and structure refinement parameters of compounds **3–5** are provided in Tale 4.17.

4.3. Results and Discussion

4.3.1. Electronic Spectroscopy

During crystal to crystal transformations, the metal centers do not change their coordination environments and hence the physical properties of the compounds **1**, **dehydrated 1-85°**, **dehydrated 1-135°** and **2**, **dehydrated 2-85° / 135°** would not be expected to change. Therefore, UV-visible absorbance spectra have been studied by taking compound **1** and **2** as representative compound from each series. The O → Fe^{3+} charge transfer band (460 nm) in compound **1** is comparable to that of similar trinuclear iron compounds known in literature.[14] The corresponding UV-visible absorption spectra are presented in Figure 4.1.

4.3.2. Powder X-ray Diffraction (PXRD)

The powder X-ray diffraction (PXRD) patterns (Figure 4.2) of parent compound **1**, **dehydrated 1-85°** and **regenerated 1** did not show any notable change, this is because of the following reasons: The heated crystals **dehydrated 1-85°** and **dehydrated 1-135°** did not loose all the lattice water molecules. Indeed, all three systems (parent **1**, **dehydrated 1-85°** and **dehydrated 1-135°)** have identical unit cell parameters (except the volumes of the unit cells), crystal system and space group (vide infra).

Table 4.1. Crystal Data and Structural Refinement Parameters for Compounds **1**, **dehydrated 1-85°** and **dehydrated 1-135°**

	1	**dehydrated 1-85°**	**dehydrated 1-135°**
Empirical formula	$C_{52}H_{114}Cl_{26}Fe_{12}O_{126}SiW_{12}$	$C_{52}H_{98}Cl_{26}Fe_{12}O_{118}SiW_{12}$	$C_{52}H_{94}Cl_{26}Fe_{12}O_{116}SiW_{12}$
Formula weight	6581.62	6437.49	6401.46
T [K]	293(2)	293(2)	293(2)
λ [Å]	0.71073	0.71073	0.71073
Crystal system	Monoclinic	Monoclinic	Monoclinic
Space group	*C2/c*	*C2/c*	*C2/c*
a [Å]	30.283(9)	30.607(8)	30.507(13)
b [Å]	17.759(5)	17.805(5)	17.764(7)
c [Å]	32.435(9)	30.083(8)	29.939(12)
deg]	90.0000	90.000	90.000
β [deg]	101.292(4)	113.060(4)	112.941(7)
deg]	90.0000	90.000	90.000
V [Å^3]	17106(8)	15084(7)	14941(11)
Z	4	4	4
$_{Dcalc}$ [Mg m^{-3}]	2.556	2.835	2.846
μ [mm^{-1}]	9.536	10.806	10.908
F[000]	12360	12040	11960
Crystal size [mm^3]	0.36 x 0.08 x 0.06	0.28 x 0.16 x 0.04	0.18 x 0.10 x 0.06
θ range for data collection [deg]	1.28 to 26.00	1.35 to 28.37	1.40 to 26.16
Reflections Collected/unique	87670 / 16902	85120 / 17989	74774 /14813
R [int]	0.0570	0.0676	0.1314
Refinement method	Full-matrix least-squares on F^2		
Data/restraints/parameters	16902 / 0 / 1009	17989 / 0 / 1015	14813 / 0 / 953
Goodness-of-fit on F^2	1.164	1.076	0.963
R_1/wR_2 [I > 2σ(I)]	0.0503/0.1216	0.0512/0.0991	0.0531/0.1149
R_1/wR_2 (all data)	0.0596/0.1278	0.0706/0.1056	0.1028/0.1333
Largest diff. Peak/hole [e Å ^{3}]	1.978/-2.314	1.862/-1.668	2.074/-1.46

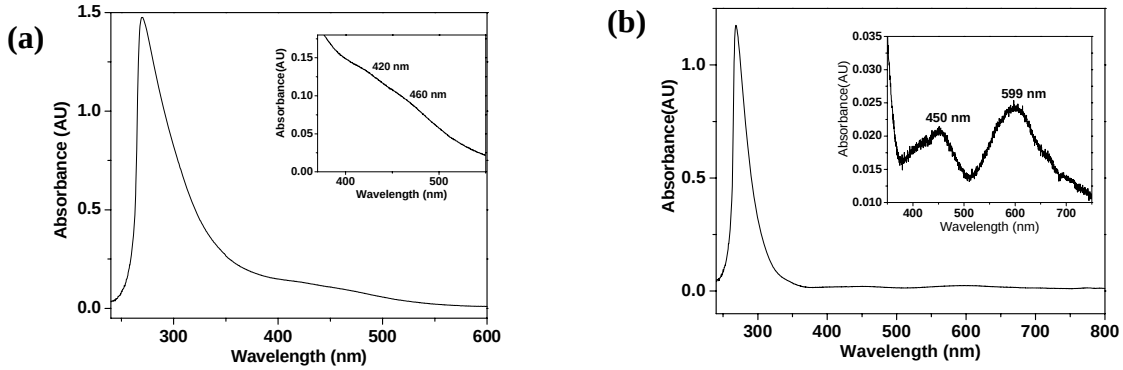

]Figure 4.1. UV-visible absorbance spectra of $[Fe_3(_3\text{-}O)(ClCH_2COO)_6(H_2O)_3]_4[SiW_{12}O_{40}] \cdot 18H_2O \cdot 2ClCH_2COOH$ (**1**) and $[Cr_3(_3\text{-}O)(ClCH_2COO)_6(H_2O)_3]_4[SiW_{12}O_{40}] \cdot 14H_2O \cdot 2ClCH_2COOH$ (**2**) in $1x10^{-4}$M.in methanol solution: For compound **1**: $_{max}$ (nm) = 460, 420 and 270 and corresponding ε_{max} ($M^{-1}cm^{-1}$) = 924, 1326 and 14510 respectively. For compound **2**: $_{max}$ (nm) = 599, 450 and 268 and corresponding ε_{max} ($M^{-1}cm^{-1}$) = 242, 211 and 11660 respectively.

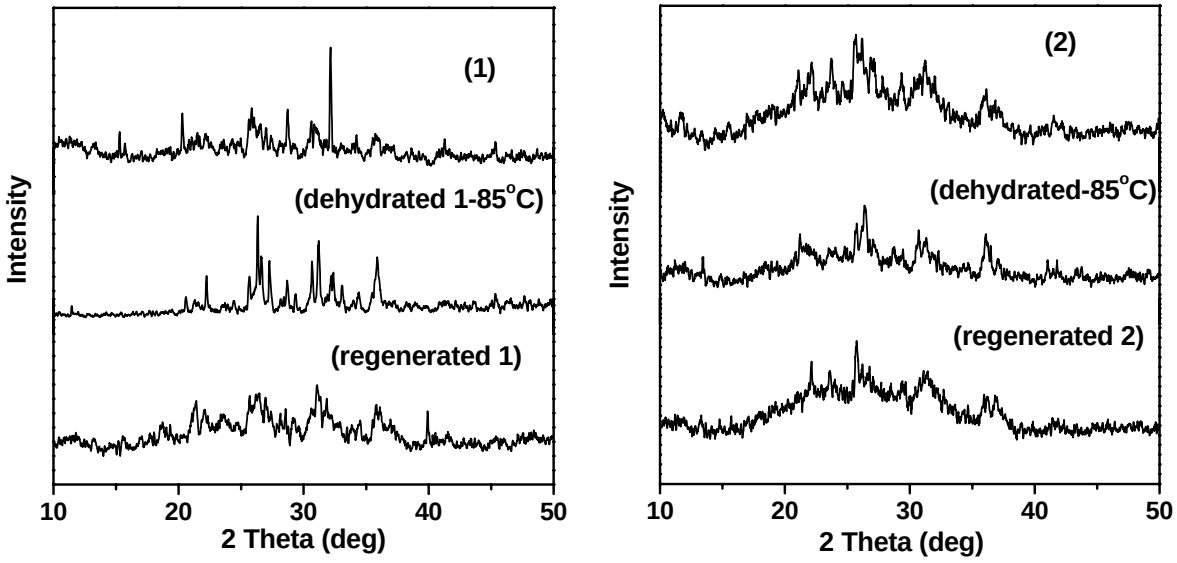

Figure 4.2. PXRD pattern of iron basic carboxylate-Keggin based ionic crystals (left): compounds **1**, **dehydrated 1-85°** and **regenerated 1**; PXRD pattern of chromium basic carboxylate-Keggin based ionic crystals (right): **2**, **dehydrated 2-85°** and **regenerated 2**.

Intentionally, we have avoided higher temperature because iron coordinated water molecules are known to leave the crystal lattice resulting in the loss of crystalline state.[15] Similarly, PXRD patterns of compound **2**, **dehydrated 2-85°**, and **regenerated 2** are also recorded and as expected they have identical powder patterns as shown in Figure 4.2(right).

4.3.3. Thermogravimetric / Mass Analyses (TGA / Mass)

The thermogravimetric analyses of all compounds were performed in flowing N_2 with a heating rate of 5°C min^{-1} in the temperature range of 30 1100°C.

$[Fe_3(\ _3\text{-}O)(ClCH_2COO)_6(H_2O)_3]_4[SiW_{12}O_{40}] \cdot 18H_2O \cdot 2ClCH_2COOH$ (1)

TGA curve of compound **1** is divided into four sets. The first weight loss is 4.18% that corresponds to the loss of fifteen lattice water molecules per formula unit in the temperature range of 50 – 120°C (calculated mass loss for fifteen water molecules is 4.18%). The second weight loss is 3.80%, which corresponds to the loss of fourteen water molecules in the temperature range of 120 – 170°C (calculated mass loss for fourteen water molecules is 3.83%). The major mass loss of 37.04% was observed in the temperature range of 170 – 585°C due to the decomposition of the cluster. The evolution of water molecules (from the lattice and iron coordination sites) and carbon dioxide gas molecules are evidenced by the TGA / Mass curves, which are shown in blue and purple color respectively in Figure 4.3(**1**).

$[Fe_3(\ _3\text{-}O)(ClCH_2COO)_6(H_2O)_3]_4[SiW_{12}O_{40}] \cdot 10H_2O \cdot 2ClCH_2COOH$ (dehydrated 1-85°)

TGA curve of compound **dehydrated 1-85°** is divided into three sets. The first weight loss 1.90%, which corresponds to the loss of seven lattice water molecules per formula unit in the temperature range of 50 – 140°C (calculated mass loss for seven water molecules is 1.96%). The second weight loss is 3.96% corresponding to the loss of

fourteen water molecules in the temperature range of 140 – 201°C (calculated mass loss for fourteen water molecules is 3.91%).

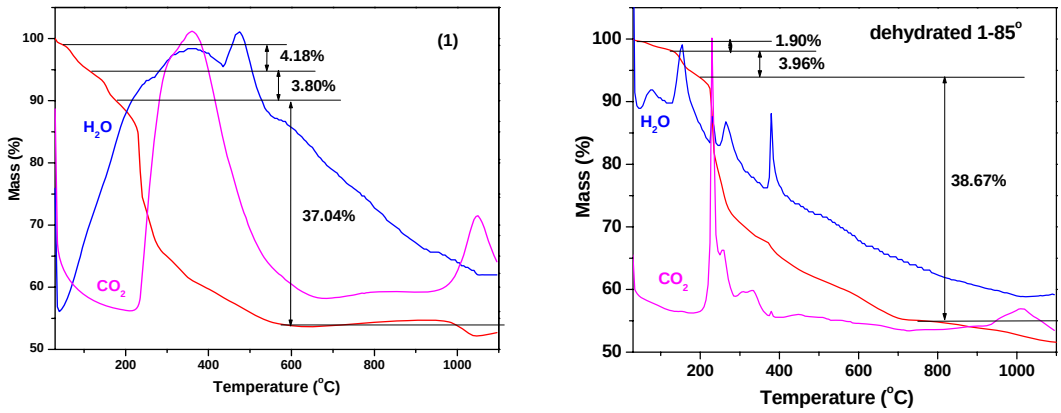

Figure 4.3. TGA / Mass spectrum of $[Fe_3(_3\text{-}O)(ClCH_2COO)_6(H_2O)_3]_4[SiW_{12}O_{40}] \cdot 18H_2O \cdot 2ClCH_2COOH$ (**1**) (left); TGA / Mass spectrum of $[Fe_3(_3\text{-}O)(ClCH_2COO)_6(H_2O)_3]_4[SiW_{12}O_{40}] \cdot 10H_2O \cdot 2ClCH_2COOH$ (**dehydrated 1-85°**) (right).

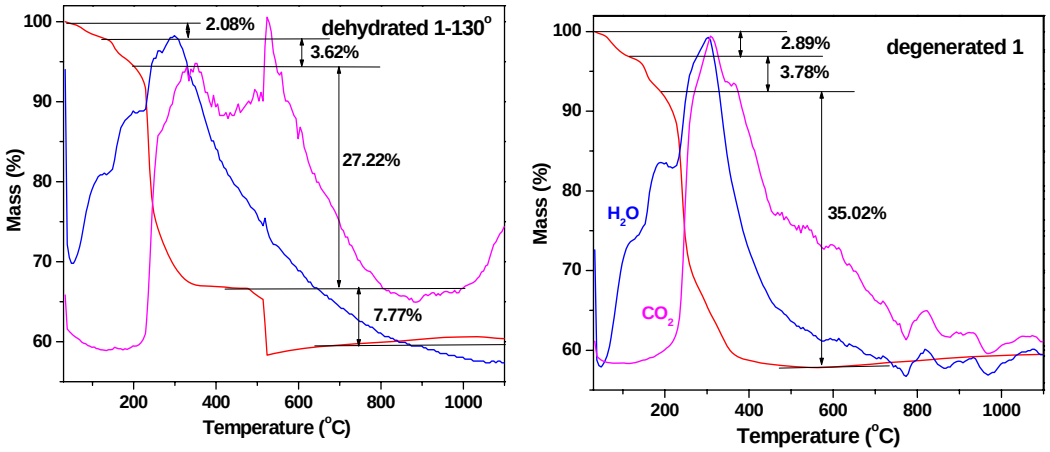

Figure 4.4. TGA / Mass spectrum of $[Fe_3(_3\text{-}O)(ClCH_2COO)_6(H_2O)_3]_4[SiW_{12}O_{40}] \cdot 8H_2O \cdot 2ClCH_2COOH$ (**dehydrated 1-85°**) (left); TGA / Mass spectrum of water regenerated compound (**regenerated 1**) (right).

The major mass loss of (38.67%) was observed in the temperature range of 201 – 748^{o}C due to the collapse of the structure of the cluster. The evolution of water molecules and carbon dioxide gas molecules are evidenced by the TGA / Mass curves, which are shown in blue and purple color respectively in the Figure 4.3(**dehydrated 1-85^{o}**).

$[Fe_3(\ _3O)(ClCH_2COO)_6(H_2O)_3]_4[SiW_{12}O_{40}] \cdot 8H_2O \cdot 2ClCH_2COOH$ (dehydrated 1-135^{o})

TGA curve of **dehydrated 1-135^{o}** can be divided into four sets. The first weight loss of 2.08% corresponds to the loss of seven lattice water molecules per formula unit in the temperature range of 50 – 140^{o}C (calculated mass loss for seven water molecules is 1.97%). The second weight loss of 3.62% corresponds to the loss of thirteen water molecules in the temperature range of 140 – 201^{o}C (calculated mass loss for thirteen water molecules is 3.66%). Two major mass losses (27.22% and 7.77%) are observed in the temperature range of 207 – 598^{o}C, due to the decomposition of the structure of the trinuclear iron cluster. The evolution of water molecules and carbon dioxide gas molecules are shown by the TGA / Mass curves, which are shown in blue and purple color respectively in the Figure 4.4 (**dehydrated 1-135^{o})**.

$[Fe_3(\ _3$-O)$(ClCH_2COO)_6(H_2O)_3]_4[SiW_{12}O_{40}] \cdot 18H_2O \cdot 2ClCH_2COOH$ (regenerated 1)

The bunch of crystals of **regenerated 1** were dried in room temperature and then loaded in to thermogravimetric crucible for TGA / Mass analysis. The typical TGA curve has been divided into three groups. The first weight loss of 2.89% corresponds to the loss of eleven lattice water molecules per formula unit in the temperature range of 50 – 120^{o}C (calculated mass loss for eleven water molecules is 3.01%). The water mass loss in this stage is significantly lesser than the expected 4.18% (from parent compound **1**, Figure 4.3(**1**)). This might be due to the removal of some water molecules (approximately four water molecules) during the drying process of the relevant crystals at room temperature. The second weight loss of 3.78% corresponds to the loss of fourteen water molecules in

the temperature range of 120 – 181°C (calculated mass loss for fourteen water molecules is 3.83%). The major mass loss (35.02%) is observed in the temperature range of 181 – 506°C due to the decomposition of the pertinent cluster. The evolution of water molecules and carbon dioxide gas molecules are observed by the TGA / Mass curves which are shown in blue and purple color respectively in the Figure 4.4(**degenerated 1**)

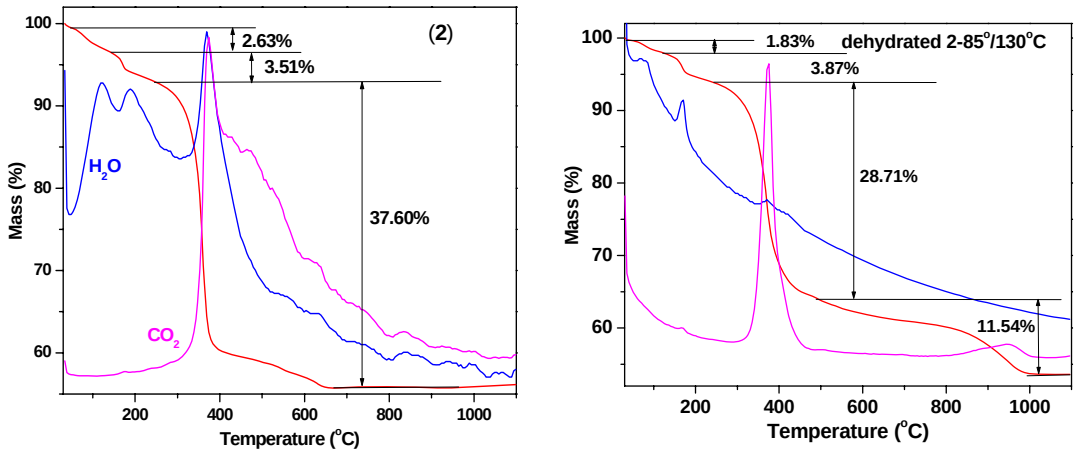

Figure 4.5. TGA / Mass spectrum of $[Cr_3(_3\text{-}O)(ClCH_2COO)_6(H_2O)_3]_4[SiW_{12}O_{40}]\cdot 14H_2O\cdot 2ClCH_2COOH$ (**2**) (left) ; TGA / Mass spectrum of $[Cr_3(_3\text{-}O)(ClCH_2COO)_6(H_2O)_3]_4[SiW_{12}O_{40}]\cdot 8H_2O\cdot 2ClCH_2COOH$ (**dehydrated 2-85°C**).

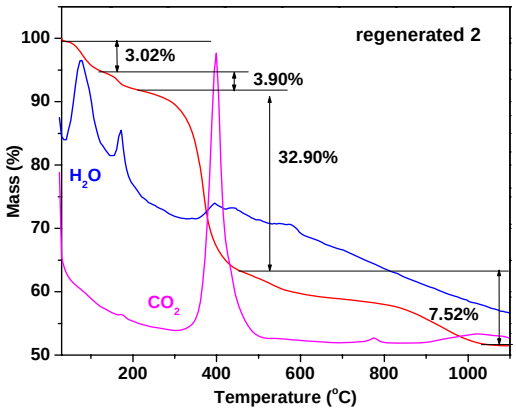

Figure 4.6. TGA / Mass spectrum of water regenerated compound (**degenerated 2**).

$[Cr_3(\ _3\text{-}O)(ClCH_2COO)_6(H_2O)_3]_4[SiW_{12}O_{40}]\cdot 14H_2O\cdot 2ClCH_2COOH$ (2)

TGA curve of compound **2** is divided into three sets. The first weight loss of 2.63% corresponds to the loss of nine lattice water molecules per formula unit in the temperature range of 50 – 130°C (calculated mass loss for nine water molecules is 2.51%). The second weight loss of 3.51%, which corresponds to the loss of thirteen water molecules (five water molecules from lattice and eight water molecules from iron coordination sites), occurred in the temperature range of 130 – 220°C (calculated mass loss for fifteen water molecules is 3.62%). The major weight loss of 37.60% was observed in the temperature range of 220 – 670°C showing the decomposition of the concerned cluster. The evolution of water molecules and carbon dioxide gas molecules are evidenced by the TGA / Mass curves, which are shown in blue and purple color respectively in the Figure 4.5(**2**).

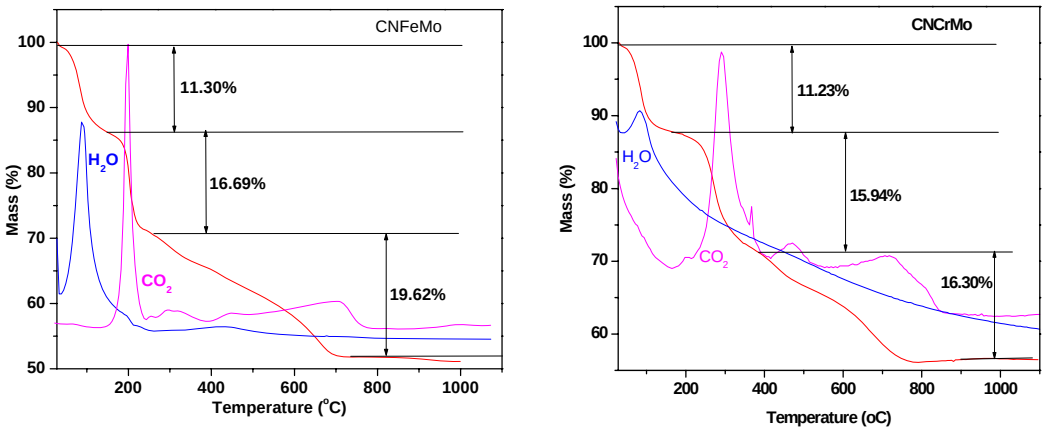

Figure 4.7. TGA / Mass spectrum of $[H_2(Fe_3O(OOCCH_2CN)_6(H_2O)_3)_2(SiMo_{12}O_{40})]\cdot 16H_2O$ (**3**) (left); TGA / Mass spectrum of $[H_2(Cr_3O(OOCCH_2CN)_6(H_2O)_3)_2(SiMo_{12}O_{40})]\cdot 16H_2O$ (**4**).

$[Cr_3(\ _3\text{-}O)(ClCH_2COO)_6(H_2O)_3]_4[SiW_{12}O_{40}]\cdot 8H_2O\cdot 2ClCH_2COOH$ (dehydrated 2 85°C / 130°C)

TGA curve of **dehydrated 2 85°C / 130°C** is divided into four groups. The first weight loss of 1.83%, which corresponds to the loss of six lattice water molecules per formula unit, occurred in the temperature range of 50 – 130°C (calculated mass loss for six water molecules is 1.70%). The second weight loss of 3.87% corresponds to the loss of fourteen water molecules (eight water molecules from lattice and six water molecules from iron coordination sites) in the temperature range of 142 – 191°C (calculated mass loss for fourteen water molecules is 3.97%). Two major weight losses (28.71% and 11.54%) were observed in the temperature range of 240 – 1017°C due to the decomposition of the cluster. The evolution of water molecules and carbon dioxide gas molecules are evidenced in the TGA / Mass curves that are shown in blue and purple colors respectively as shown in the Figure 4.5 (**dehydrated 2-85°/130°**).

$[Cr_3(\ _3\text{-}O)(ClCH_2COO)_6(H_2O)_3]_4[SiW_{12}O_{40}]\cdot 14H_2O\cdot 2ClCH_2COOH$ (regenerated 2)

The **regenerated 2** bunch of crystals were dried in room temperature and then powdered sample was loaded in thermogravimetric crucible for TGA / Mass analysis. The typical TGA curve has been divided into four groups (Figure 4.6). The first weight loss of 3.02% corresponds to the loss of eleven lattice water molecules per formula unit in the temperature range of 50 – 100°C (calculated mass loss for eleven water molecules is 3.06%). The mass loss in **regenerated 2** (3.02% for eleven lattice water molecules) in this stage is approximately comparable to the mass loss obtained in parent compound **2** where the same was 2.63% for nine lattice water molecules). The second weight loss of 3.90% corresponds to the loss of fourteen water molecules in the temperature range of 100 – 190°C (calculated mass loss for fourteen water molecules is 3.90%). The major mass losses 32.90% and 7.52%, observed in the temperature range of 190 – 1100°C, are

due to the decomposition of the cluster structure. The evolution of water molecules and carbon dioxide gas molecules are confirmed by the TGA / Mass curves that are shown in blue and purple color respectively as shown in the Figure 4.6.

$[H_2(Fe_3(\ _3\text{-}O)(OOCCH_2CN)_6(H_2O)_3)_2(SiMo_{12}O_{40})]\cdot 16H_2O$ (3)

The typical TGA / Mass loss of curve of compound **3** can be divided in to three stages. The first weight loss of 11.30% in the temperature range of 35 90^oC is due to the loss of twenty two water molecules (sixteen lattice and six metal coordinated water molecules). The calculated mass loss for twenty two water molecules is 10.99%. The relevant TGA / Mass graph is presented in Figure 4.7(**CNFeMo**). The second loss (16.69%) and third loss (19.62%) in the temperature range of 130 235^oC are due to decomposition of cluster structure. The evolution of water and carbon dioxide is shown in blue and purple color respectively in the TGA / Mass spectra.

$[H_2(Cr_3(\ _3\text{-}O)(OOCCH_2CN)_6(H_2O)_3)_2(SiMo_{12}O_{40})]\cdot 16H_2O$ (4)

TGA / Mass loss curve of compound **4** can be divided in three stages. The first weight loss of 11.23% in the temperature range 35 130^oC corresponds to the loss of twenty two water molecules (sixteen lattice and six metal coordinated water molecules). The calculated mass loss for twenty two water molecules is 11.06%. The TGA / Mass curve is given in the Figure 4.7(**CNCrMo**). The second loss (15.94%) and third loss (16.30%) in the temperature range of 130 345^oC are due to structural decomposition. The evolution of water and carbon dioxide gas molecules are shown in blue and purple color respectively.

4.3.4. X-ray Crystallographic Studies

$[Fe_3(\ _3\text{-}O)(ClCH_2COO)_6(H_2O)_3]_4[SiW_{12}O_{40}]\cdot 18H_2O\cdot 2ClCH_2COOH$ (1)

Compound **1** crystallizes in monoclinic system with space group *C2/c* and single crystal X-ray data, obtained at 298 K, are summarized in Table 4.1. In compound **1**, the asymmetric unit contains half part of Keggin anion (in which Si atom has half occupancy), two basic trinuclear iron oxo macrocations, one lattice $ClCH_2COOH$ and nine non coordinated (lattice) water molecules. Accordingly, compound **1** can be formulated as $[Fe_3(\ _3\text{-}O)(ClCH_2COO)_6(H_2O)_3]_4[SiW_{12}O_{40}]\cdot 18H_2O\cdot 2ClCH_2COOH$ (**1**). The thermal ellipsoidal plot of the asymmetric unit of compound **1** is presented in Figure 4.8(a) (the solvent water molecules and lattice chloroaceticacid are not shown). The molecular structure of compound **1** is shown in Figure 4.8(b). The structure of keggin anion can be described as four W_3O_{13} groups surrounding the central hetero atom Si. Each W_3O_{13} group is formed by three WO_6 octahedra sharing edges and having a common oxygen atom which is also shared by the central hetero atom. On the whole, the oxygen bonding modes in Keggin (POM) anion can be grouped into four different categories: (i) W O_t (O_t is terminal oxygen) 1.694(7) 1.716(7) Å; (ii) W $O(\mu_2)$, 1.894(7) 1.950(7) Å; (iii) W $O(\mu_4)$, 2.333(6) 2.360(6) Å; (iv) Si $O(\mu_4)$, 1.625(6) 1.627(6) Å.

The structure of $[Fe_3(\ _3\text{-}O)(ClCH_2COO)_6(H_2O)_3]^{1+}$ macrocation can be described as follows: Each $ClCH_2COOH$ bridges two adjacent iron metal centers in bidentate fashion through carboxylate functionality and every two adjacent iron metal centers are bridged by two such bidentate ligands. Further the terminal position of each metal center is occupied by a monodentate water molecule. All three iron metal ions (Fe^{3+}) are bridged by a triply bridging oxygen atom. The geometry around each iron metal center is octahedral and overall charge of each macrocation is +1. In molecular structure of compound **1**, four macrocations neutralize the charge of a Keggin anion $[SiW_{12}O_{40}]^4$.

(a)

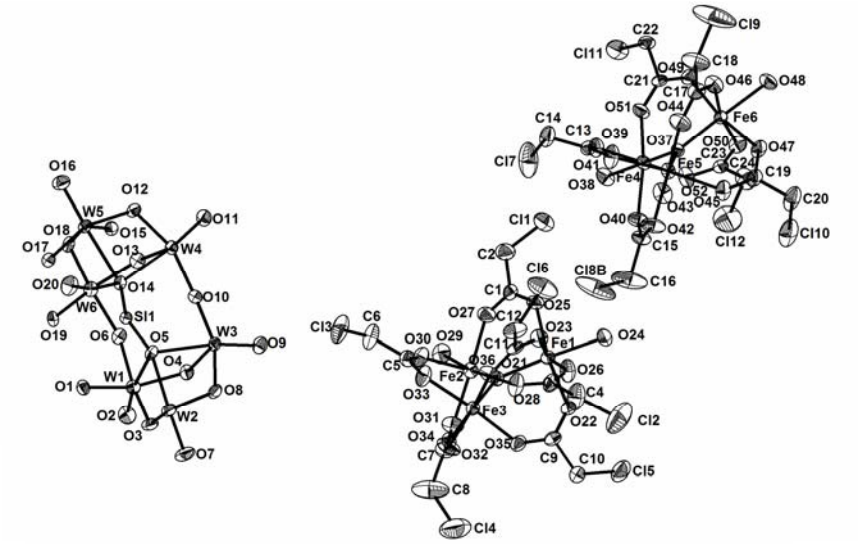

(b)

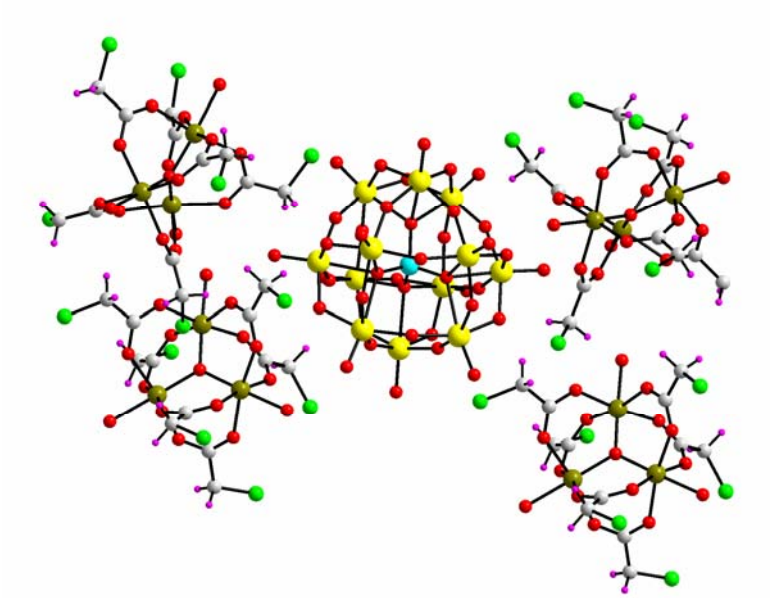

Figure 4.8. (a) Thermal ellipsoidal representation (50 % probability level) of the asymmetric unit of $[Fe_3(\ _3\text{-}O)(ClCH_2COO)_6(H_2O)_3]_4[SiW_{12}O_{40}] \cdot 18H_2O \cdot 2ClCH_2COOH$ (**1**) excluding lattice solvent water and chloroacetic acid and hydrogen atoms; (b) The molecular structure of compound **1,** excluding lattice water and chloroacetic acid molecules. Color code: Mo, yellow; Si, cyan; O, red; Fe, dark green; C, gray; Cl, light green; H, purple.

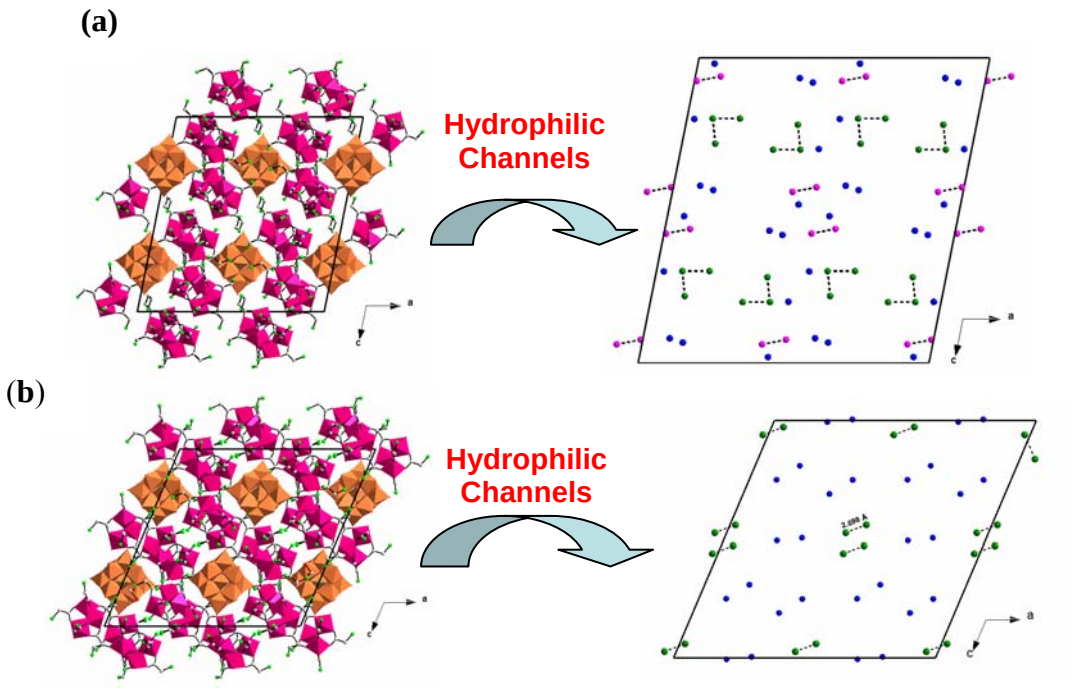

Figure 4.9. (a) The unit cell packing diagram of $[Fe_3(\ _3\text{-}O)(ClCH_2COO)_6(H_2O)_3]_4[SiW_{12}O_{40}] \cdot 18H_2O \cdot 2ClCH_2COOH$ (**1**) in which the arrangement of lattice water molecules in hydrophilic channels; (b) The unit cell packing diagram of $[Fe_3(\ _3\text{-}O)(ClCH_2COO)_6(H_2O)_3]_4[SiW_{12}O_{40}] \cdot 10H_2O \cdot 2ClCH_2COOH$ (**dehydrated 1-85°**) in which the arrangement of lattice water molecules in hydrophilic channels.

Compound **1** contains, two lattice $ClCH_2COOH$ and eighteen lattice water molecules per formula unit. Out of these lattice water molecules, two types of water clusters, namely water trimer (water molecules O53, O56 and O58, O···O separation distance is in the range of 2.820(3) 2.910(3) Å) and water dimer (water molecules O57 and O60, O···O separation distance is 3.030(5) Å) are observed in the crystal lattice of compound **1** (located in hydrophilic channels) as shown in Figure 4.9(a). Lattice $ClCH_2COOH$ is considerably disordered and hence refined isotorpically only. The Overall structure is stabilized by the electrostatic interactions between $[Fe_3(\ _3\text{-}O)(ClCH_2COO)_6(H_2O)_3]^{1+}$ macrocation and $[SiW_{12}O_{40}]^4$ cluster anion. Further the

supramolecular C H···O and O H···O hydrogen bonding interactions offer extra stability in obtaining this ion pair system. The possible C H···O and O H···O hydrogen bonding interactions are shown in Figure 4.10. The relevant hydrogen bonding parameters (for C H···O interactions, D···A distance is considered up to 3.6 Å, whereas for O H···O interactions, the same is considered up to 3.1 Å) are presented in Tables 4.2 and 4.3.

Table 4.2. Geometrical parameters of the C H···O hydrogen bonds (Å, °) involved in supramolecular network of compound $[Fe_3(\ _3\text{-}O)(ClCH_2COO)_6(H_2O)_3]_4[SiW_{12}O_{40}] \cdot 18H_2O \cdot 2ClCH_2COOH$ (**1**), where D=donor; A=acceptor.

D H···A	d(D···H)	d(H···A)	d(D···A)	(DHA
C2 H2A O54	0.97	2.59	3.558(19)	174.6
C2 H2B O9#1	0.97	2.61	3.315(15)	129.9
C2 H2B O17#2	0.97	2.56	3.349(14)	138.7
C4 H4B O41#3	0.97	2.80	3.500(16)	129.8
C6 H6A O11#1	0.97	2.63	3.506(17)	150.0
C10 H10A O4#4	0.97	3.02	3.569(15)	117.2
C10 H10A O6#4	0.97	2.81	3.494(15)	128.6
C10 H10A O13#4	0.97	2.62	3.428(14)	141.4
C10 H10A O49#5	0.97	2.60	3.412(13)	141.0
C12 H12B O8#6	0.97	2.40	3.368(13)	178.4
C12 H12A O39#7	0.97	2.67	3.541(14)	150.2
C14 H14A O8#1	0.97	2.56	3.366(13)	140.6
C20 H20A O47#8	0.97	2.59	3.378(15)	138.2
C22 H22A O9#9	0.97	2.88	3.471(12)	120.0
C22 H22B O34#10	0.97	2.65	3.272(12)	122.6
C24 H24B O11#9	0.97	2.71	3.318(16)	121.3
C24 H24B O12#9	0.97	2.67	3.530(15)	148.3

Symmetric transformations used to generate equivalent atoms: #1 x, 1-y, 0.5+z; #2 -x, 1-y, 1-z; #3 0.5-x, 1.5-y, 2-z; #4 0.5-x, 0.5-y, 1-z; #5 x, -1+y, z; #6 0.5-x, 0.5-y, 1-z; #7 0.5-x, -0.5+y, 1.5-z; #8 1-x, 2-y, 2-z; #9 0.5-x, 1.5-y, 1-z; #10 x, 1+y, z; #11 0.5-x, 0.5+y, 1.5-z; #12 x, 1+y, 1+z.

Table 4.3. Geometrical parameters of the O H···O hydrogen bonds (Å) involved in supramolecular network of compound $[Fe_3(\ _3\text{-}O)(ClCH_2COO)_6(H_2O)_3]_4[SiW_{12}O_{40}] \cdot 18H_2O \cdot 2ClCH_2COOH$ (**1**).

O(16) O(27)#2	3.019(10)	O(16) O(29)#2	3.039(11)
O(18) O(54)#2	3.071(14)	O(13) O(48)#9	2.898(10)
O(11) O(49)#9	2.906(10)	O(11) O(50)#9	2.909(10)
O(9) O(34)#4	2.723(9)	O(2) O(24)#4	2.909(10)
O(24) O(57)	2.636(18)	O(24) O(2)#4	2.909(10)
O(34) O(9)#4	2.723(9)	O(34) O(56)#7	2.738(11)
O(29) O(16)#2	3.039(11)	O(29) O(55)	2.686(18)
O(33) O(38)#7	2.867(10)	O(27) O(16)#2	3.019(10)
O(38) O(56)	2.709(12)	O(38) O(33)#11	2.867(10)
O(48) O(13)#9	2.898(10)	O(48) O(62)#12	3.000(9)
O(43) O(54)#3	2.775(15)	O(49) O(11)#9	2.909(10)
O(53) O(58)#7	2.820(3)	O(54) O(18)#2	3.071(14)
O(54) O(43)#3	2.775(15)	O(55) O(29)	2.686(18)
O(56) O(34)#11	2.738(11)	O(56) O(38)	2.709(12)
O(56) O(58)	2.910(3)	O(57) O(24)	2.636(18)
O(57) O(60)	3.030(5)	O(58) O(53)#11	2.820(3)

Symmetric codes are already specified in the footnote of Table 4.3.

Water Exclusion (dehydration) and Inclusion (regeneration) Experiments in Compound 1

Compound **1** originally contains eighteen lattice water molecules. When the crystals of compound **1** are heated at 85°C and 135°C for the period of 3.5 hours, they loose considerable number of lattice water molecules and generate the dehydrated analogues $[Fe_3(\ _3\text{-}O)(ClCH_2COO)_6(H_2O)_3]_4[SiW_{12}O_{40}] \cdot 10H_2O \cdot 2ClCH_2COOH$ (**dehydrated 1-85°**) and $[Fe_3(\ _3\text{-}O)(ClCH_2COO)_6(H_2O)_3]_4[SiW_{12}O_{40}] \cdot 8H_2O \cdot 2ClCH_2COOH$ (**dehydrated 1-135°**) respectively

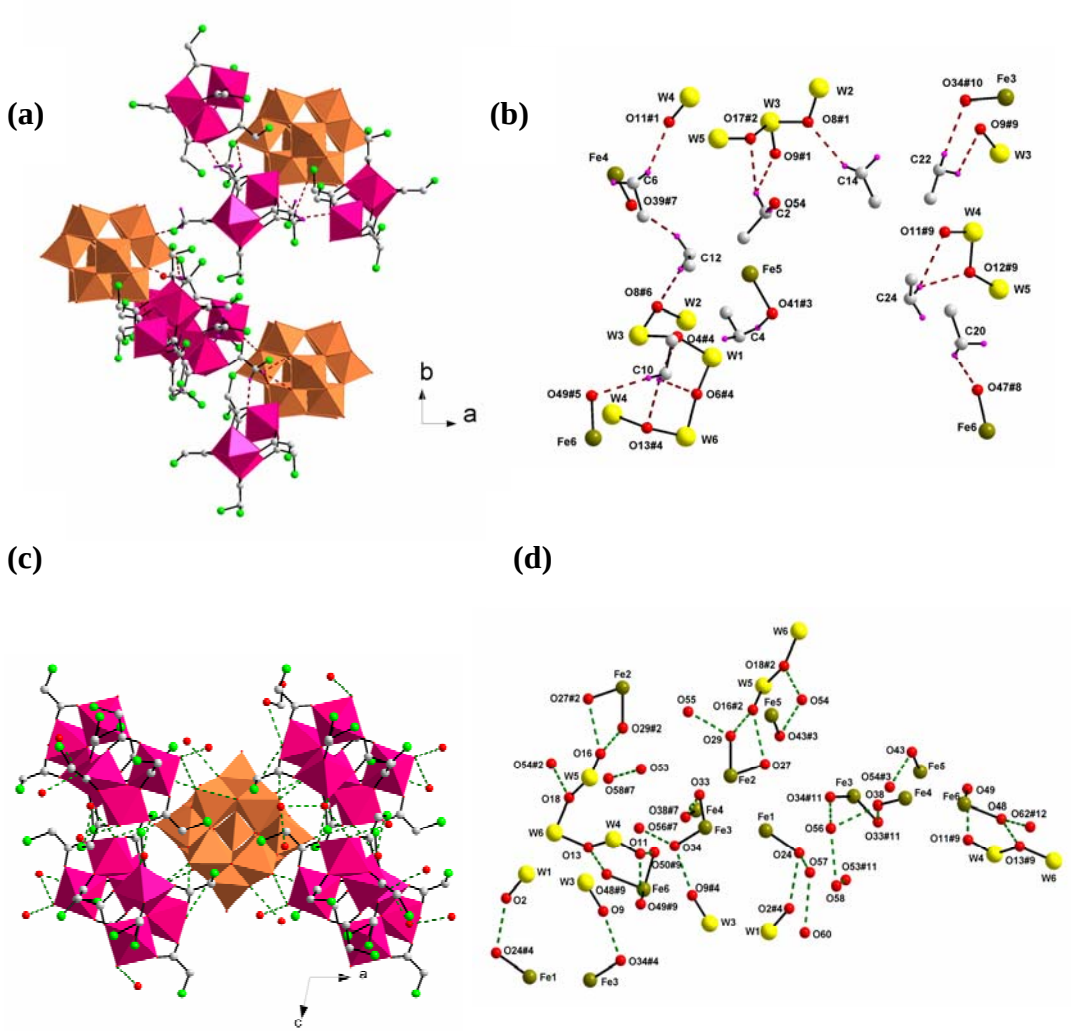

Figure 4.10. (a) C H···O hydrogen bonding interactions in $[Fe_3(\mu_3\text{-}O)(ClCH_2COO)_6(H_2O)_3]_4[SiW_{12}O_{40}] \cdot 18H_2O \cdot 2ClCH_2COOH$ (**1**); (b) C H···O hydrogen bonding interactions with relevant symmetry codes in compound **1**; (c) O H···O hydrogen bonding interactions in compound **1**; (d) O H···O hydrogen bonding interactions with relevant symmetry codes in compound **1**. Color code: W, yellow; O, red; Fe, dark green; Cl, light green; C, gray; H, purple; $[Fe_3(\mu_3\text{-}O)(ClCH_2COO)_6(H_2O)_3]^{1+}$ cluster, purple polyhedra; $[SiW_{12}O_{40}]^{4}$ cluster, golden yellow polyhedra; C H···O hydrogen bonding interactions, brown dotted lines; O H···O hydrogen bonding interactions green dotted lines.

Table 4.4. The inter nuclear distances between two $[SiW_{12}O_{40}]^4$ cluster anions along c axis in compound **1** and **dehydrated 1-85°**

$[Fe_3(\ _3\text{-}O)(ClCH_2COO)_6(H_2O)_3]_4$ $[SiW_{12}O_{40}] \cdot 18H_2O \cdot 2ClCH_2COOH$ (**1**) Internulear distance (Å) between two $[SiW_{12}O_{40}]^4$ cluster anions			$[Fe_3(\ _3\text{-}O)(ClCH_2COO)_6(H_2O)_3]_4$ $[SiW_{12}O_{40}] \cdot 10H_2O \cdot 2ClCH_2COOH$ **(dehydrated 1-85°)** Internulear distance (Å) between two $[SiW_{12}O_{40}]^4$ cluster anions	
Si	Si	17.78	Si	Si	15.35
W1	W1	13.15	W1A	W1A	11.31
W1	W1	20.31	W1A	W1B	19.53
W2	W2	14.02	W2A	W2A	13.67
W2	W2	19.76	W2A	W2B	17.98
W3	W3	18.37	W3	W3	14.92
W3	W3	19.67	W3	W3	18.55
W4	W4	17.66	W4A	W4A	13.63
W4	W4	23.81	W4B	W4A	21.12
W5	W5	18.14	W5A	W5B	15.34
W5	W5	23.44	W5A	W5B	19.95
W6	W6	11.91	W6A	W6A	9.05
W6	W6	24.43	W6A	W6B	22.18

The compounds **dehydrated 1-85°** and **dehydrated 1-135°** are structurally characterized. The relevant crystal data and refinement parameters are given in the Table 4.1. Crystal structure of compounds **dehydrated 1-85°** and **dehydrated 1-135°** contains ten and eight lattice water molecules per formula unit respectively. The regular arrangement of lattice water molecules in hydrophilic channels (that include water dimer) of the crystal structure of compound **dehydrated 1-85°** is depicted in Figure 4.9(b). The less number of hydrogen bonded lattice water molecules compared to those in parent compound **1** are expected in a dehydrated crystal. We have chosen 135°C as maximum

temperature for reversible water exclusion experiment because if we heat the crystals beyond this temperature range, the pertinent crystals do not difract in the X-ray diffractometer. The metal coordinated water molecules are supposed to leave at high temperature resulting in the formation of polycrystalline material. The release of lattice water molecules from **1** to **dehydrated 1-135°** leads to the shrinkage of the unit cell volume gradually as **1** (V 17106(8) $Å^3$) **dehydrated 1-85°** (V 15084(7) $Å^3$) **dehydrated 1-135°** (V 14941(11) $Å^3$). The shrinkage of unit cell occurred in the crystallographic 'c' axis (Table 4.1 for unit cell data), which confirms that the water molecules accommodated in the crystallographic 'c' axis readily released from the crystal lattice.

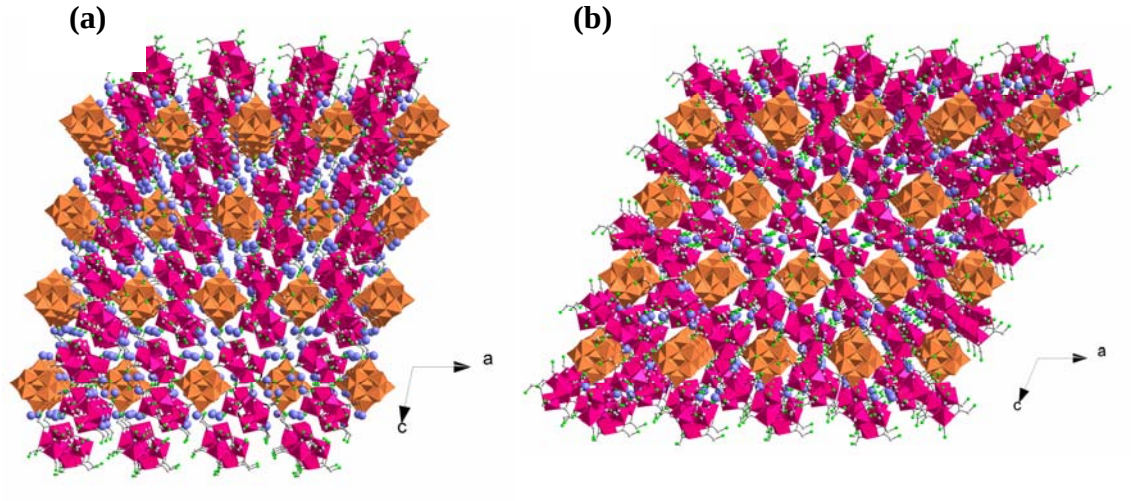

Figure 4.11. A perspective view of packing diagram along the crystallographic *b* axis: (a) $[Fe_3(\ _3\text{-}O)(ClCH_2COO)_6(H_2O)_3]_4[SiW_{12}O_{40}] \cdot 18H_2O \cdot 2ClCH_2COOH$ (**1**); (b) $[Fe_3(\ _3\text{-}O)(ClCH_2COO)_6(H_2O)_3]_4[SiW_{12}O_{40}] \cdot 10H_2O \cdot 2ClCH_2COOH$ (**dehydrated 1-85°**); Color code: $[Fe_3(\ _3\text{-}O)(ClCH_2COO)_6(H_2O)_3]^{1+}$ cluster, purple polyhedra; $[SiW_{12}O_{40}]^4$ cluster, golden yellow polyhedra; non-coordinated water molecules, blue; Cl, light green.

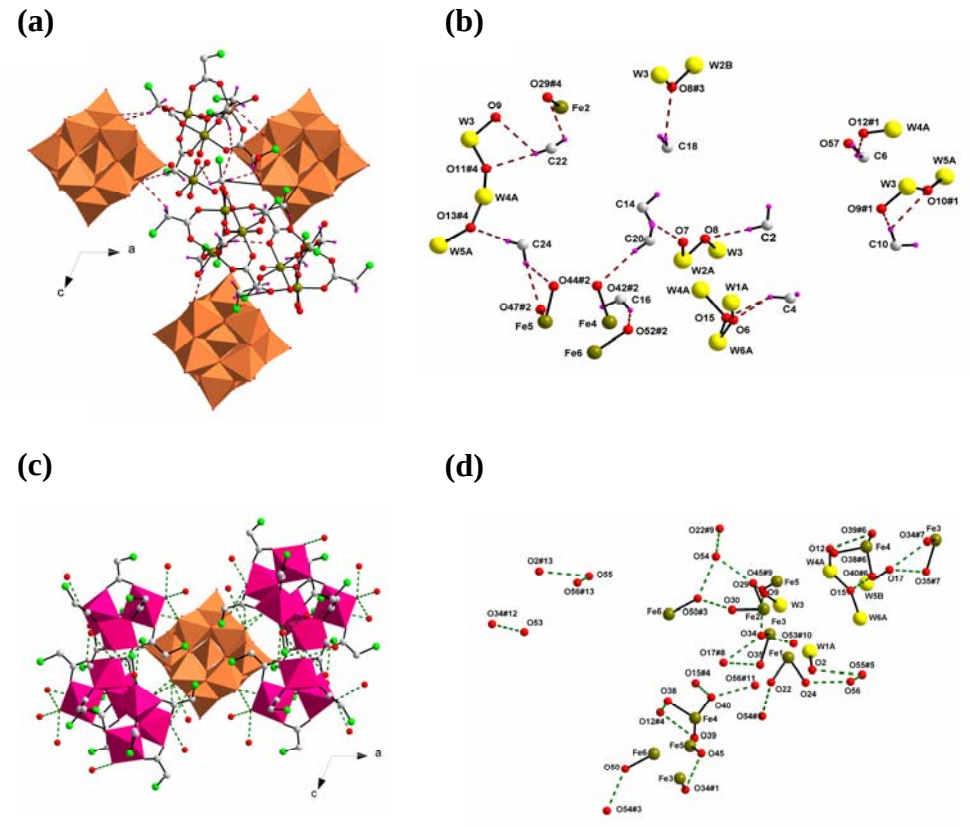

Figure 4.12. The C H···O hydrogen bonding interactions in $[Fe_3(\ _3\text{-}O)(ClCH_2COO)_6(H_2O)_3]_4[SiW_{12}O_{40}] \cdot 10H_2O \cdot 2ClCH_2COOH$ (**dehydrated 1-85^o**); (b) C H···O hydrogen bonding interactions with relevant symmetry codes in compound **1b**; (c) O H···O hydrogen bonding interactions in compound **1b**; (d) O H···O hydrogen bonding interactions with relevant symmetry codes in compound **dehydrated 1-85^o** Color code: same as described in Figure 4.10 caption.

The packing diagrams of compounds **1** and **dehydrated 1-85^o** view down the crystallographic 'b' axis are presented in Figure 4.11. For an assessment of unit cell volume shrinkage, the corresponding internuclear distances between two keggin anion cluster (For compound **1** and **dehydrated 1-85^o**) along the 'c' axis are measured and represented in Table 4.4. The C H···O and O H···O hydrogen bonding interactions observed in the crystal structure of compound **dehydrated 1-85^o** are shown in Figure 4.12 and the relevant parameters are given in Tables 4.5 and 4.6 respectively. Similarly in

compound **dehydrated 1-135°**, C H···O and O H···O hydrogen bonding interactions are shown in Figure 4.13 and appropriate parameters are presented in Tables 4.7 and 4.8 respectively. Crystals of compounds **dehydrated 1-85°** (heated compound) on exposure to water vapor at ambient condition for two weeks, crystals get moistened

Table 4.5. Geometrical parameters of the C H···O hydrogen bonds (Å, °) involved in supramolecular network of compound $[Fe_3(\ _3\text{-}O)(ClCH_2COO)_6(H_2O)_3]_4[SiW_{12}O_{40}] \cdot 10H_2O \cdot 2ClCH_2COOH$ (**dehydrated 1-85°**), where D=donor; A=acceptor.

D H···A	d(D···H)	d(H···A)	d(D···A)	(DHA
C2 H2A O8	0.97	2.47	3.442(13)	179.1
C4 H4B O6	0.97	2.82	3.480(12)	126.1
C4 H4B O15	0.97	2.57	3.395(11)	142.9
C6 H6A O12#1	0.97	2.58	3.444(15)	148.0
C6 H6B O57	0.97	2.71	3.410(3)	129.9
C10 H10A O9#1	0.97	2.31	3.122(13)	140.3
C10 H10A O10#1	0.97	2.75	3.387(12)	123.6
C14 H14A O7	0.97	2.53	3.401(15)	150.2
C16 H16B O52#2	0.97	2.69	3.510(2)	143.2
C18 H18A O8#3	0.97	2.83	3.554(12)	131.8
C20 H20A O42#2	0.97	2.57	3.492(15)	158.2
C22 H22A O9#4	0.97	2.95	3.588(12)	124.3
C22 H22A O11#4	0.97	2.61	3.522(11)	157.5
C22 H22B O29#4	0.97	2.79	3.364(11)	119.0
C24 H24B O13#4	0.97	2.44	3.409(11)	173.9
C24 H24B O44#2	0.97	2.87	3.442(13)	118.5
C24 H24A O47#2	0.97	2.55	3.509(13)	170.2

Symmetry transformations used to generate equivalent atoms: #1 0.5-x, -0.5+y, 0.5-z; #2 -x, -y, 1-z; #3 0.5-x, 0.5-y, 1-z; #4 x, 1-y, 0.5+z; #5 -1+x, y, z; #6 x, 1-y, -0.5+z; #7 -0.5+x, 0.5+y, z; #8 0.5+x, -0.5+y, z; #9 0.5-x, 0.5+y, 0.5-z; #10 x, y, -1+z; #11 -x, y, 0.5-z; #12 x, y, 1+z; #13 1+x, y, z.

without their dissolution reverts back to the parent compound **degenerated 1**. The color of the heated crystals (light red) became dark red after exposing to the water vapor. A single crystal with suitable size from this water regenerated bunch of the crystals has been mounted in X-ray diffractometer for data collection. Re-entering of the water molecules in the crystal lattice leads to expansion of the unit cell volume as **dehydrated 1-85°** (V 15084.00 Å^3) **degenerated 1 (**V = 17039Å^3). The obtained cell data for compound **degenerated 1** exactly match to that of parent compound **1**; however, we have not succeeded to solve the crystal structure of water regenerated compound **degenerated 1** because of the poor quality of reflection data.

Table 4.6. Geometrical parameters of the O H···O hydrogen bonds (Å) involved in supramolecular network of compound $[Fe_3(\ _3\text{-}O)(ClCH_2COO)_6(H_2O)_3]_4[SiW_{12}O_{40}] \cdot 10H_2O \cdot 2ClCH_2COOH$ (**dehydrated 1-85°**).

O(2) O(24)	2.886(9)	O(2) O(55)#5	3.098(13)
O(9) O(29)	2.733(9)	O(12) O(38)#6	2.913(9)
O(12) O(39)#6	3.026(10)	O(15) O(40)#6	2.753(8)
O(17) O(34)#7	2.840(9)	O(17) O(35)#7	3.052(9)
O(22) O(54)#1	3.079(11)	O(24) O(56)	2.738(10)
O(29) O(54)	2.773(10)	O(30) O(50)#3	2.878(9)
O(34) O(17)#8	2.840(9)	O(34) O(45)#9	3.061(10)
O(34) O(53)#10	2.560(18)	O(35) O(17)#8	3.052(9)
O(38) O(12)#4	2.913(9)	O(39) O(12)#4	3.026(10)
O(40) O(15)#4	2.753(8)	O(40) O(56)#11	2.746(9)
O(45) O(34)#1	3.061(10)	O(50) O(54)#3	2.793(10)
O(53) O(34)#12	2.560(18)	O(54) O(22)#9	3.079(11)
O(55) O(2)#13	3.098(13)	O(5) O(56)#13	2.702(15)
O(56) O(55)#5	2.702(15)		

Symmetry codes are already specified in the footnote Table 4.5.

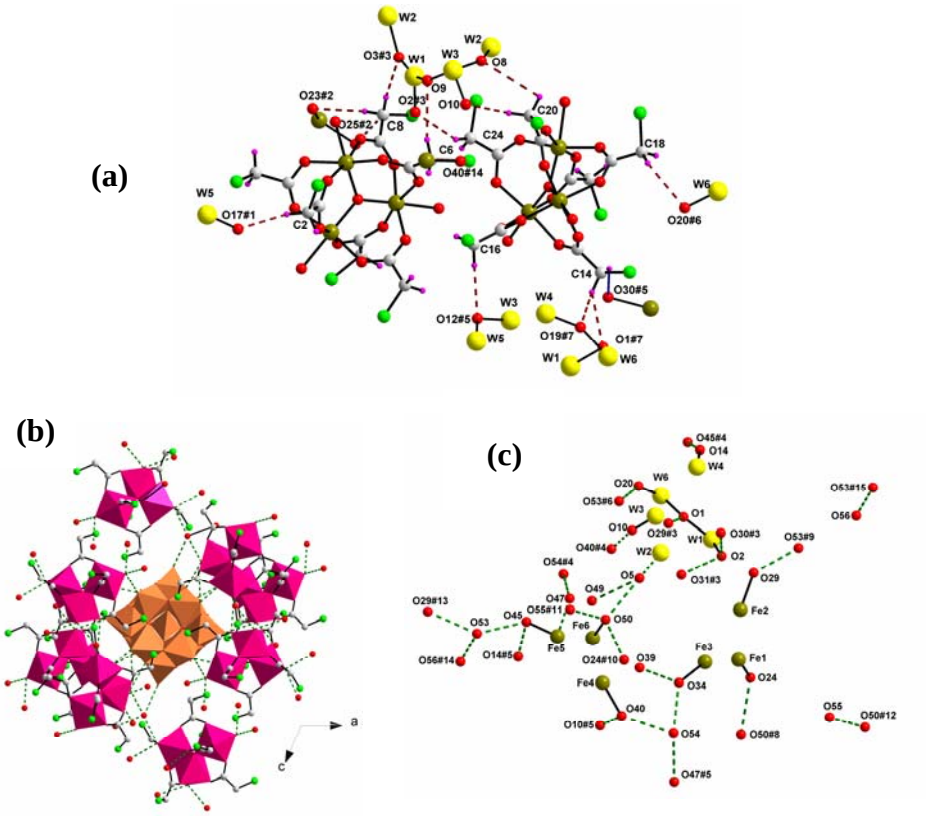

Figure 4.13. The C H···O hydrogen bonding interactions in $[Fe_3(\ _3\text{-}O)(ClCH_2COO)_6(H_2O)_3]_4[SiW_{12}O_{40}] \cdot 8H_2O \cdot 2ClCH_2COOH$ (**dehydrated 1-135°**) with relevant symmetry code; (b) The O H···O hydrogen bonding interactions in compound **dehydrated 1-135°**; (c) The O H···O hydrogen bonding interactions with relevant symmetry codes in compound **dehydrated 1-135°** Color code: same as described in Figure 4.10 caption.

$[Cr_3(\ _3\text{-}O)(ClCH_2COO)_6(H_2O)_3]_4[SiW_{12}O_{40}] \cdot 14H_2O \cdot 2ClCH_2COOH$ (2)

Dark green colored crystals of compound **2** were grown from an acidic aqueous medium containing $H_4SiW_{12}O_{40}$, $ClCH_2COOH$ and $Cr(NO)_3{\cdot}9H_2O$. Compound **2** crystallizes in monoclinic system with space group *C2/c* and single crystal X-ray data obtained at 298 K are summarized in Table 4.9. The asymmetrical unit contains half part of Keggin anion (in which Si atom is in half occupancy), two basic trinuclear

Table 4.7. Geometrical parameters of the C H···O hydrogen bonds (Å, °) involved in supramolecular network of compound $[Fe_3(\ _3\text{-}O)(ClCH_2COO)_6(H_2O)_3]_4[SiW_{12}O_{40}] \cdot 8H_2O \cdot 2ClCH_2COOH$ (**dehydrated 1-135°**). D=donor; A=acceptor.

D H···A	d(D···H)	d(H···A)	d(D···A)	(DHA
C2 H2B O17#1	0.97	2.52	3.400(2)	151.5
C6 H6B O9	0.97	2.64	3.545(16)	156.3
C6 H6A O40#4	0.97	2.79	3.358(18)	118.0
C8 H8A O3#3	0.97	2.41	3.375(16)	173.2
C8 H8B O23#2	0.97	2.54	3.498(19)	170.5
C8 H8B O25#2	0.97	2.84	3.410(19)	118.1
C14 H14B O19#7	0.97	2.82	3.480(17)	125.6
C14 H14B O1#7	0.97	2.56	3.385(17)	143.5
C14 H14A O30#5	0.97	2.57	3.328(16)	134.7
C16 H16A O12#5	0.97	2.47	3.438(17)	177.8
C18 H18B O20#6	0.97	2.61	3.221(18)	120.7
C20 H20A O10	0.97	2.29	3.116(17)	142.1
C20 H20A O8	0.97	2.73	3.387(16)	125.5
C24 H24A O2#3	0.97	2.63	3.490(2)	147.8

Symmetry transformations used to generate equivalent atoms: #1 x, -y, 0.5+z; #2 1-x, 1-y, 1-z; #3 1-x, y, 0.5-z; #4 0.5-x, -0.5+y, 0.5-z; #5 0.5-x, 0.5+y, 0.5-z; #6 0.5-x, 0.5-y, -z; #7 -0.5+x, 0.5+y, z; #8 x, 1-y, 0.5+z; #9 0.5+x, 0.5-y, 0.5+z; #10 x, 1-y, -0.5+z; #11 x, y, -1+z; #12 x, y, 1+z; #13 -0.5+x, 0.5-y, -0.5+z; #14 -1+x, y, z; #15 1+x, y, z.

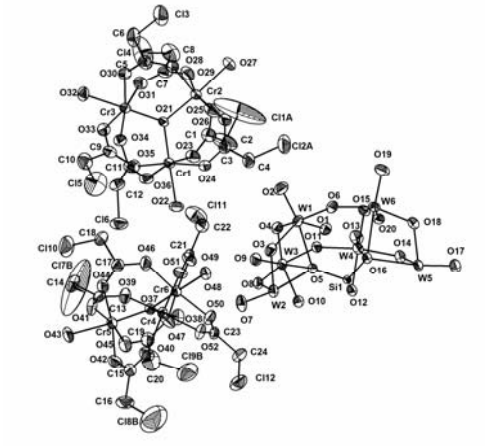

Figure 4.14. Thermal ellipsoidal plot of compound **2** in asymmetric unit (50% probability). Hydrogen atoms, lattice water molecules and lattice chloroacetic acid were omitted for clarity.

Table 4.8. Geometrical parameters of the O H···O hydrogen bonds (Å) involved in supramolecular network of compound $[Fe_3(\ _3\text{-}O)(ClCH_2COO)_6(H_2O)_3]_4[SiW_{12}O_{40}] \cdot 8H_2O \cdot 2ClCH_2COOH$ (**dehydrated 1-135°**).

O(2) O(30)#3	2.900(12)	O(2) O(31)#3	3.035(14)
O(1) O(29)#3	2.727(12)	O(5) O(49)	3.087(13)
O(5) O(50)	2.849(13)	O(10) O(40)#4	2.734(12)
O(14) O(45)#4	2.898(12)	O(20) O(53)#6	3.069(14)
O(24) O(50)#8	3.038(14)	O(29) O(53)#9	2.733(13)
O(34) O(39)	2.866(14)	O(34) O(54)	2.773(14)
O(40) O(10)#5	2.734(12)	O(40) O(54)	2.768(14)
O(45) O(14)#5	2.898(12)	O(45) O(53)	2.717(14)
O(47) O(54)#4	3.048(14)	O(50) O(24)#10	3.038(14)
O(50) O(55)#11	2.500(3)	O(55) O(50)#12	2.500(3)
O(53) O(29)#13	2.733(13)	O(53) O(56)#14	2.710(2)
O(54) O(47)#5	3.048(14)	O(56) O(53)#15	2.710(2)

Symmetry codes are already specified in the footnote of Table 4.7.

chromium oxo macrocations, one lattice $ClCH_2COOH$ and seven non-coordinated water molecules. Thermal ellipsoidal plot of compound $[Cr_3(\ _3\text{-}O)(ClCH_2COO)_6(H_2O)_3]_4[SiW_{12}O_{40}] \cdot 14H_2O \cdot 2ClCH_2COOH$ (**2**) with atom labeling scheme is presented in Figure 4.14. Compound **2** is isostructural to compound **1** and hence coordination bonding environments around metal centers are similar. In the crystal structure two non-coordinated $ClCH_2COOH$ were located in the lattice and those were refined isotropically due to considerable disorder. Crystal structure of compound **2** contains fourteen lattice water molecules. A water dimer, exclusively formed by lattice water molecules, O53 and O54 is crytallographically characterized. The O H···O hydrogen bonding distance is 2.68(5) Å Overall, C H···O and O H···O hydrogen

bonding interactions are shown in Figure 4.15. The relevant hydrogen bonding parameters are presented in Tables 4.10 and 4.11 respectively.

Table 4.9. Crystal Data and Structural Refinement for Compounds **2**, **dehydrated 2-85°** and **dehydrated 2-135°**

	2	**dehydrated 2-85°**	**dehydrated 2-135°**
Empirical formula	$C_{52}H_{106}Cl_{26}Cr_{12}O_{122}SiW_{12}$	$C_{52}H_{94}Cl_{26}Cr_{12}O_{116}SiW_{12}$	$C_{52}H_{94}Cl_{26}Cr_{12}O_{116}SiW_{12}$
Formula weight	6463.36	6355.26	6355.26
T [K]	293(2)	293(2)	293(2)
λ [Å]	0.71073	0.71073	0.71073
Crystal system	Monoclinic	Monoclinic	Monoclinic
Space group	*C2/c*	*C2/c*	*C2/c*
a [Å]	30.1958(17)	30.539(6)	30.569(8)
b [Å]	17.7025(10)	17.777(3)	17.778(4)
c [Å]	32.2944(18)	29.880(6)	29.823(7)
deg]	90.0000	90.000	90.000
β [deg]	101.6470(10)	112.962(3)	112.809(4)
deg]	90.0000	90.000	90.000
V [Å^3]	16907.2(16)	14936(5)	14940(6)
Z	4	4	4
D_{calc} [Mg m^{-3}]	2.539	2.826	2.825
μ [mm^{-1}]	9.386	10.619	10.616
F[000]	12104	11864	11864
Crystal size [mm^3]	0.26 x 0.10 x 0.06	0.22 x 0.10 x 0.06	0.30 x 0.10 x 0.02
θ range for data collection [deg]	1.34 to 26.05	1.48 to 28.36	1.45 to 26.54
Reflections Collected/unique	87235 / 16671	85248 / 17891	69592 /14651
R [int]	0.0473	0.0674	0.1329
Refinement method	Full-matrix least-squares on F^2		
Data/restraints/parameters	16671 / 0 / 1029	17891 / 0 / 964	14651 / 0 / 953
Goodness-of-fit on F^2	1.048	1.182	0.962
R_1/wR_2 [I > 2σ(I)]	0.0354/0.0911	0.0619/0.1226	0.0470/0.0946
R_1/wR_2 (all data)	0.0452/0.0959	0.0779/0.1286	0.0809/0.1048
Largest diff. Peak/hole [e Å ^{3}]	2.125/-1.308	2.711/-2.473	2.038/-1.843

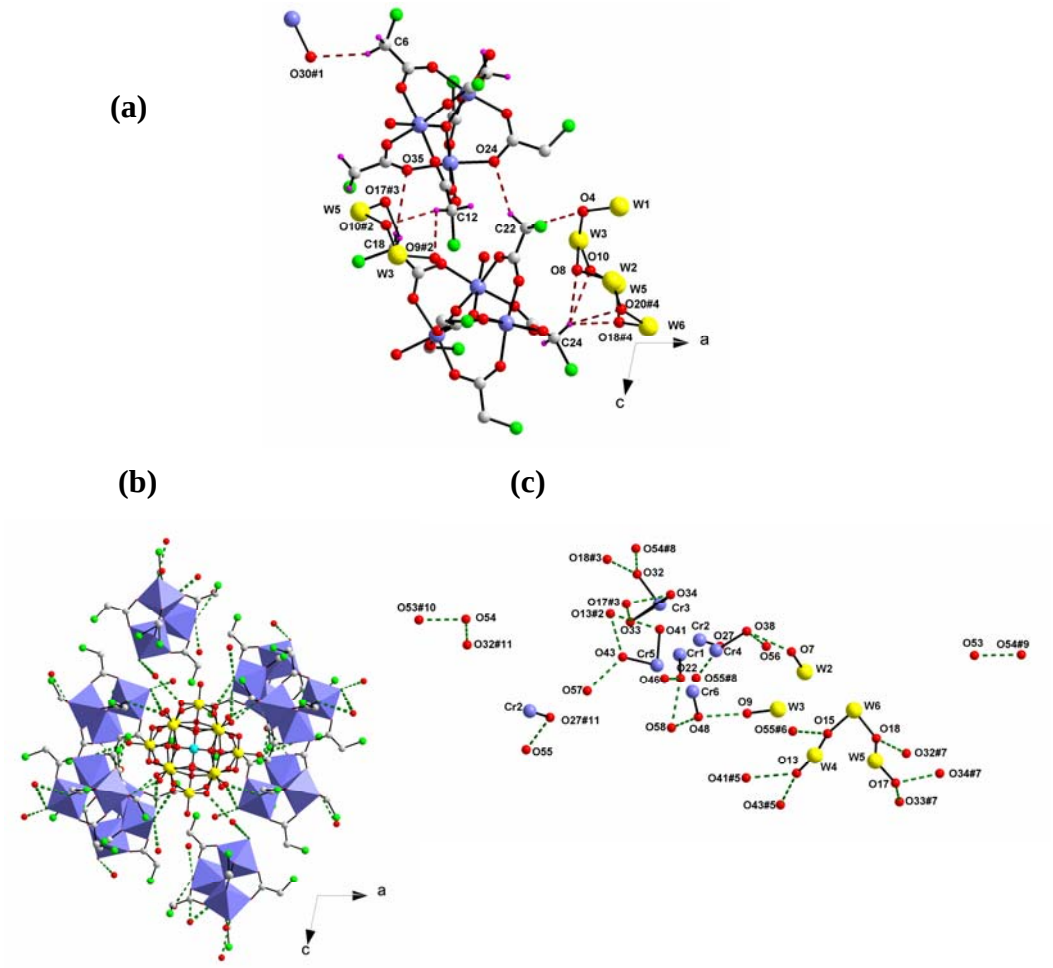

Figure 4.15. (a) C H···O hydrogen bonding interactions in $[Cr_3(\ _3\text{-}O)(ClCH_2COO)_6(H_2O)_3]_4[SiW_{12}O_{40}] \cdot 14H_2O \cdot 2ClCH_2COOH$ (**2**) along with relevant symmetry code; (b) O H···O hydrogen bonding interactions in compound **2**; (c) O H···O hydrogen bonding interactions with relevant symmetry codes in compound **2**. Color code: W, yellow; Si, cyan; O, red; Cr, violet; Cl, light green; C, gray; H, purple; $[Cr_3(\ _3\text{-}O)(ClCH_2COO)_6(H_2O)_3]^{1+}$ cluster, violet polyhedra; C H···O hydrogen bonding interactions, brown dotted lines; O H···O hydrogen bonding interactions green dotted lines.

Water Exclusion (dehydration) and Inclusion (regeneration) Experiments in Compound 2

The similar heating experiments are repeated for compound **2**. Heating the crystals bunch of compound **2** at 85°C and 135°C for the period of 3.5 hours looses considerable number of lattice water molecules and generate corresponding dehydrated analogues $[Cr_3(\ _3\text{-}O)(ClCH_2COO)_6(H_2O)_3]_4[SiW_{12}O_{40}] \cdot 8H_2O \cdot 2ClCH_2COOH$ (**dehydrated 2-85°/135°**). The same number of lattice water molecules characterized in both **dehydrated 2-85°** and **dehydrated 2-135°**.

Table 4.10. Geometrical parameters of the C H···O hydrogen bonds (Å, °) involved in supramolecular network of compound $[Cr_3(\ _3\text{-}O)(ClCH_2COO)_6(H_2O)_3]_4[SiW_{12}O_{40}] \cdot 14H_2O \cdot 2ClCH_2COOH$ (**2**). D=donor; A=acceptor.

D H···A	d(D···H)	d(H···A)	d(D···A)	(DHA
C6 H6B O30#1	0.97	2.60	3.383(11)	137.9
C12 H12A O9#2	0.97	2.90	3.472(9)	118.8
C12 H12A O10#2	0.97	2.57	3.475(10)	155.9
C18 H18B O17#3	0.97	2.62	3.494(12)	150.7
C18 H18A O35	0.97	2.96	3.587(11)	123.3
C22 H22B O4	0.97	2.41	3.382(9)	177.2
C22 H22A O24	0.97	2.70	3.547(10)	145.7
C24 H24A O8	0.97	2.95	3.527(10)	118.9
C24 H24A O10	0.97	2.69	3.594(10)	154.4
C24 H24A O18#4	0.97	2.59	3.374(10)	138.6
C24 H24A O20#4	0.97	2.74	3.444(10)	130.3

Symmetry transformations used to generate equivalent atoms: #1 -x, 1-y, -z; #2 0.5-x, 0.5+y, 0.5-z; #3 -0.5+x, 0.5+y, z; #4 1-x, y, 0.5-z; #5 0.5-x, -0.5+y, 0.5-z; #6 0.5-x, 0.5-y, 1-z; #7 0.5+x, -0.5+y, z; #8 x, y, -1+z; #9 1+x, y, z; #10 -1+x, y, z; #11 x, y, 1+z.

The dehydrated compounds **dehydrated 2-85°** and **dehydrated 2-135°** is structurally characterized and crystal data and refinement parameters are presented in the Table 4.9. The C H···O and O H···O hydrogen bonding interactions observed in the crystal structure of compound **2b** is shown in Figure 4.16 and the relevant parameters are given in Tables 4.12 and 4.13 respectively. The compounds **dehydrated 2-85°** and **dehydrated 2-135°** are practically identical and hence the hydrogen bonding interactions in compound **dehydrated 2-135°** is not discussed here. The release of lattice water molecules (water exclusion) from **2** to **dehydrated 2-85°/135°** leads to the shrinkage of the unit cell volume as follows: **2** (V 176907(16) Å^3) **dehydrated 2-85°** (V 14936(5) Å^3) ≡ **dehydrated 2-135°** (V 14940(11) Å^3). **degenerated 2**. A single crystal with suitable size from this water regenerated bunch of the crystals has been mounted in X-ray diffractometer for data collection.

Table 4.11. Geometrical parameters of the O H···O hydrogen bonds (Å) involved in supramolecular network of compound $[Cr_3(\ _3\text{-}O)(ClCH_2COO)_6(H_2O)_3]_4[SiW_{12}O_{40}] \cdot 14H_2O \cdot 2ClCH_2COOH$ (**2**).

O(7) O(38)	2.912(7)	O(9) O(48)	2.726(7)
O(13) O(41)#5	2.992(7)	O(13) O(43)#5	3.003(8)
O(15) O(55)#6	3.069(10)	O(17) O(33)#7	2.899(7)
O(17) O(34)#7	2.890(7)	O(18) O(32)#7	2.909(7)
O(22) O(46)	2.900(8)	O(22) O(58)	2.712(9)
O(27) O(55)#8	2.715(11)	O(32) O(54)#8	2.740(2)
O(32) O(18)#3	2.909(7)	O(33) O(17)#3	2.899(7)
O(34) O(17)#3	2.890(7)	O(38) O(56)	2.638(12)
O(41) O(13)#2	2.992(7)	O(43) O(13)#2	3.003(8)
O(43) O(57)	2.677(13)	O(48) O(58)	2.749(9)
O(53) O(54)#9	2.680(5)	O(54) O(53)#10	2.680(5)
O(54) O(32)#11	2.740(2)	O(55) O(27)#11	2.715(11)

Symmetric codes are already specified in the footnote of Table 4.10.

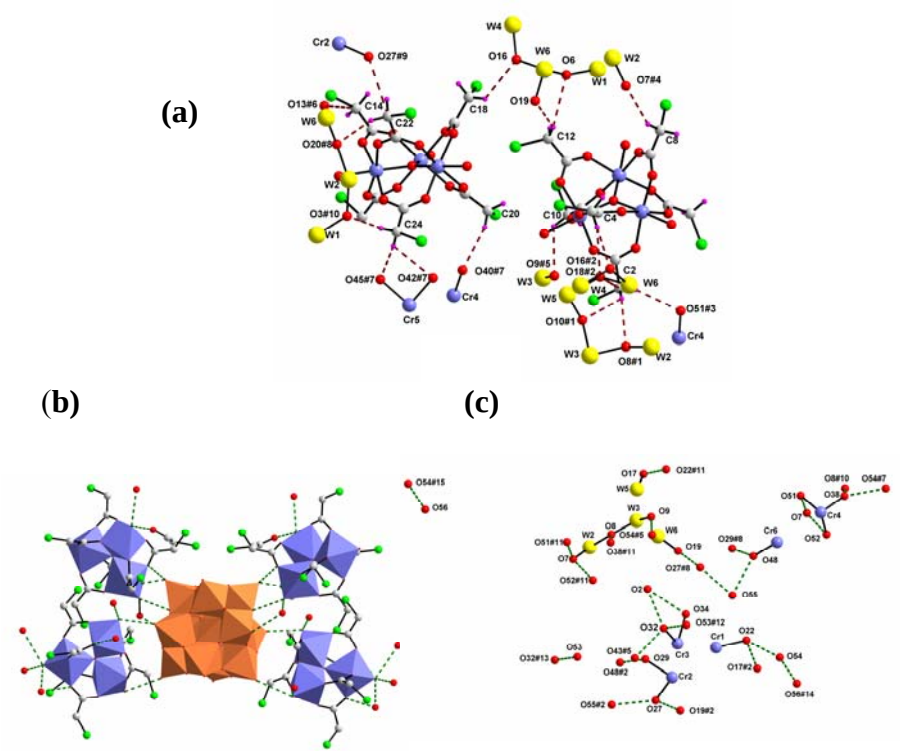

Figure 4.16. (a) C H···O hydrogen bonding interactions in $[Cr_3(\ _3\text{-}O)(ClCH_2COO)_6(H_2O)_3]_4[SiW_{12}O_{40}] \cdot 8H_2O \cdot 2ClCH_2COOH$ (**dehydrated 2-85^o**) along with relevant symmetry code; (b) O H···O hydrogen bonding interactions in compound **dehydrated 2-85^o**; (c) O H···O hydrogen bonding interactions with relevant symmetry codes in compound **dehydrated 2-85^o**. Color code: W, yellow; O, red; Cr, violet; Cl, light green; C, gray; H, purple; $[Cr_3(\ _3\text{-}O)(ClCH_2COO)_6(H_2O)_3]^{1+}$ cluster, violet polyhedra; $[SiW_{12}O_{40}]^4$ cluster, golden yellow polyhedra; C H···O hydrogen bonding interactions, brown dotted lines; O H···O hydrogen bonding interactions green dotted

When dehydrated compound **dehydrated 2-85^o** exposed to water vapor for the period of one week, it regenerates to parent compound. the water regenerated compound The unit cell parameter of water regenerated compound **degenerated 2** is as follows: a = 30.319 Å, b = 17.655 Å, c = 32.771 Å and β = 102.588^o, V = 17120.53 Å^3. The obtained unit cell volume exactly matches to the parent compound **2**, it clearly indicates the expansion of unit cell as **dehydrated 2-85^o** (V 14936(5) Å^3) **dehydrated 2-135^o (**V = 17120.53 Å^3).

Although the water regenerated compound diffracted in X-ray diffractometer, their corresponding structure couldn't be solve because of the poor quality of reflection data.

Table 4.12. Geometrical parameters of the C H···O hydrogen bonds (Å, °) involved in supramolecular network of compound $[Cr_3(\ _3O)(ClCH_2COO)_6(H_2O)_3]_4[SiW_{12}O_{40}] \cdot 8H_2O \cdot 2ClCH_2COOH$ (**dehydrated 2-85°**). D=donor; A=acceptor.

D H···A	d(D···H)	d(H···A)	d(D···A)	(DHA
C2 H2A O8#1	0.97	2.58	3.386(14)	140.8
C2 H2A O10#1	0.97	2.77	3.440(15)	127.0
C2 H2A O18#2	0.97	3.04	3.592(15)	117.4
C2 H2B O51#3	0.97	2.56	3.352(14)	138.3
C4 H4B O16#2	0.97	2.47	3.444(15)	179.2
C4 H4B O18#2	0.97	2.98	3.597(16)	122.6
C8 H8B O7#4	0.97	2.56	3.429(17)	149.2
C10 H10A O9#5	0.97	2.57	3.222(15)	124.7
C12 H12B O6	0.97	2.75	3.391(14)	123.8
C12 H12B O19	0.97	2.30	3.116(16)	140.8
C14 H14A O13#6	0.97	2.52	3.392(17)	149.9
C18 H18A O16	0.97	2.85	3.541(16)	129.1
C20 H20A O40#7	0.97	2.57	3.500(2)	162.5
C22 H22A O20#8	0.97	2.61	3.520(14)	157.1
C22 H22B O27#9	0.97	2.75	3.337(14)	119.5
C24 H24B O3#10	0.97	2.43	3.383(14)	168.6
C24 H24B O42#7	0.97	2.81	3.443(16)	123.2
C24 H24A O45#7	0.97	2.56	3.518(16)	171.5

Symmetry transformations used to generate equivalent atoms: #1 -0.5+x, -0.5+y, z; #2 0.5-x, -0.5+y, 0.5-z; #3 x, -1+y, z; #4 1-x, y, 0.5-z; #5 0.5-x, 0.5-y, -z; #6 0.5-x, 1.5-y, -z; #7 -x, 1-y, -z; #8 0.5-x, 0.5+y, 0.5-z; #9 x, 1+y, z; #10 -0.5+x, 0.5+y, z; #11 0.5+x, -0.5+y, z; #12 x, y, -1+z; #13 x, y, 1+z; #14 -1+x, y, z; #15 1+x, y, z.

Table 4.13. Geometrical parameters of the O H···O hydrogen bonds (Å) involved in supramolecular network of compound **dehydrated 2-85°**.

O(7) O(51)#11	2.919(11)	O(7) O(52)#11	3.006(11)
O(8) O(38)#11	2.765(10)	O(9) O(54)#5	3.073(13)
O(17) O(22)#8	2.905(11)	O(19) O(27)#8	2.736(10)
O(22) O(17)#2	2.905(11)	O(22) O(54)	2.717(12)
O(27) O(19)#2	2.736(10)	O(27) O(55)#2	2.793(13)
O(29) O(48)#2	2.913(12)	O(32) O(2)	2.856(11)
O(32) O(43)#5	3.049(13)	O(32) O(53)#12	2.540(2)
O(34) O(2)	3.036(11)	O(38) O(8)#10	2.765(10)
O(38) O(54)#7	2.750(12)	O(48) O(29)#8	2.913(12)
O(48) O(55)	2.795(13)	O(51) O(7)#10	2.919(11)
O(52) O(7)#10	3.006(11)	O(53) O(32)#13	2.540(2)
O(54) O(56)#14	2.735(18)	O(55) O(27)#8	2.793(13)
O(56) O(54)#15	2.735(18)		

Symmetric codes are already specified in the footnote of Table 4.12.

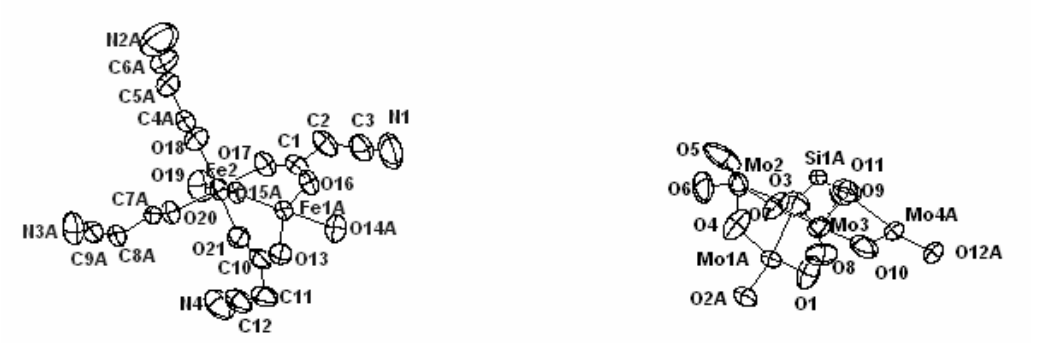

Figure 4.17. Thermal ellipsoidal representation of (50 % probability level) of the asymmetric unit of $[H_2(Fe_3O(OOCCH_2CN)_6(H_2O)_3)_2(SiMo_{12}O_{40})]\cdot 16H_2O$ (**3**) excluding lattice solvent water and hydrogen atoms.

$[H_2(Fe_3O(OOCCH_2CN)_6(H_2O)_3)_2(SiMo_{12}O_{40})]\cdot 16H_2O$ (3)

Single crystal X-ray structure analysis of compound **3** revealed the presence of one fourth of the silicomolybdate cluster anion, half of the iron trinuclear macrocation, four lattice water molecules in asymmetric unit. The starting precursor to synthesize compound **3** is $H_4SiMo_{12}O_{40}$ and hence the remaining charge of the resulting compound **3**

Table 4.17. Crystal Data and Structural Refinement for Compounds **3 5.**

	3	**4**	**5**
Empirical formula	$C_{36}H_{16}Fe_6Mo_{12}N_{12}O_{92}Si$	$C_{36}H_{16}Cr_6Mo_{12}N_{12}O_{92}Si$	$C_{18}H_8Cr_3W_{12}N_6O_{62}Si$
Formula weight	3603.08	3579.98	3690.59
T [K]	293(2)	293(2)	293(2)
λ [Å]	0.71073	0.71073	0.71073
Crystal system	Monoclinic	Monoclinic	Orthorhombic
Space group	*C2/m*	*C2/m*	*Pnma*
a [Å]	27.692(6)	27.419(12)	18.901(2)
b [Å]	18.955(4)	18.993(8)	15.852(2)
c [Å]	13.265(3)	13.278(6)	27.375(3)
deg]	90	90	90
β [deg]	116.726(3)	116.694(6)	90
deg]	90	90	90
V [Å^3]	6219(2)	6178(5)	8202.1(16)
Z	2	2	4
D_{calc} [Mg m^{-3}]	1.924	1.924	2.989
μ [mm^{-1}]	1.958	1.795	17.244
F[000]	3452	3428	6512
Crystal size [mm^3]	0.40 x 0.22 x 0.20	0.38 x 0.22 x 0.22	0.36 x 0.22 x 0.20
θ range for data collection [deg]	1.35 to 28.55	1.36 to 28.25	1.31 to 28.33
Reflections Collected/unique	35430 / 7749	27615 / 6554	93029 / 10342
R (int)	0.0511	0.0612	0.05
Refinement method	Full-matrix least-squares on F^2		
Data/restraints/ parameters	7749 / 0 / 405	6554 / 0 / 404	10342 / 3 / 505
Goodness-of-fit on F^2	1.047	1.086	1.078
R_1/wR_2 [I > 2σ(I)]	0.0745/0.2326	0.0813/0.2492	0.0383/0.1056
R_1/wR_2 (all data)	0.0965/0.2613	0.1073/0.2708	0.0570/0.1170
Largest diff. Peak/hole [e· Å^3]	1.741/-1.637	1.856/-1.448	1.824/-1.175

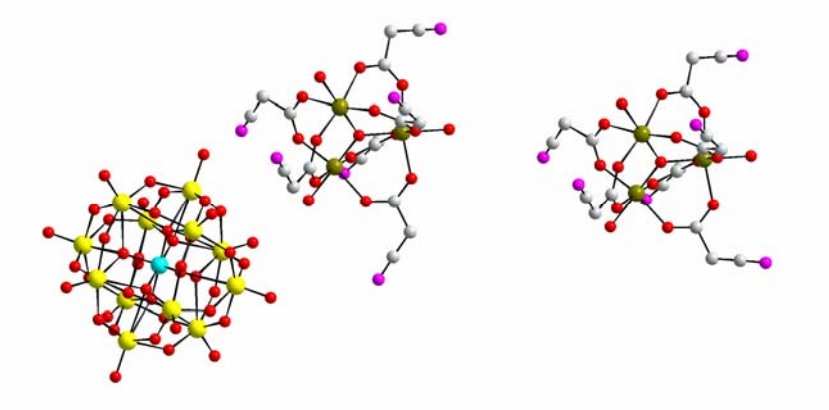

Figure 4.18. The molecular structure of $[H_2(Fe_3O(OOCCH_2CN)_6(H_2O)_3)_2(SiMo_{12}O_{40})]$ $\cdot 16H_2O$ (**3**) excluding hydrogen atoms; Color code: W, yellow; Si, cyan; Fe, green; C, gray; N, purple; O, red.

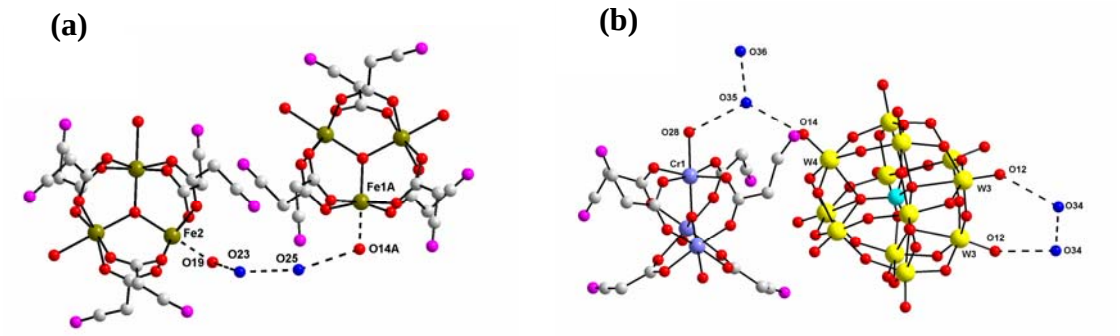

Figure 4.19. The immediate environment of supramolecularly hydrogen bonded water dimer excluding hydrogen atoms: (a) in compound $[H_2(Fe_3O(OOCCH_2CN)_6(H_2O)_3)_2(SiMo_{12}O_{40})]$ $\cdot 16H_2O$ (**3**); (b) in compound $[H_3(Cr_3O(OOCCH_2CN)_6(H_2O)_3)(SiW_{12}O_{40})]$ $\cdot 6H_2O$ (**5**); Color code: W, yellow; Si, cyan; Fe, green; Cr, violet; C, gray; N, purple; O, red; oxygen from water dimer, blue, O H···O hydrogen bonding interactions, black dotted lines.

is counter balanced by H^+ ions. And hence compound **3** can be formulated as $[H_2(Fe_3O(OOCCH_2CN)_6(H_2O)_3)_2(SiMo_{12}O_{40})]$ $\cdot 16H_2O$ (**3**). The thermal ellipsoidal representation of compound **3** is depicted in Figure 4.17 and crystal data parameters are presented in Table 4.17. The molecular structure of $[H_2(Fe_3O(OOCCH_2CN)_6(H_2O)_3)_2(SiMo_{12}O_{40})]$ $\cdot 16H_2O$ (**3**) is depicted in Figure 4.18.

The atoms labeled with O14, Fe1, O15, C7, C8, C4, and C5 are located in crystallographic special position. The atoms C6, N2 and C9, N3 from cyanoacitic acid are in considerable disorder and refined with half occupancy. Supramolecularly hydrogen bonded water dimer (exclusively formed by lattice water molecules O23 and O25) is characterized crystallographically. The hydrogen bonding surrounding of water dimer is shown in Figure 4.19(a).

$[H_2(Cr_3O(OOCCH_2CN)_6(H_2O)_3)_2(SiMo_{12}O_{40})] \cdot 16H_2O$ (4)

As shown in Table 4.17, both compounds **3** and **4** are iso-structural (varies only in the place of metal center from trinuclear cluster) and accordingly the unit cell volume, cell data, space group, number of lattice water molecules etc. of **3** and **4** are identical.

$[H_3(Cr_3O(OOCCH_2CN)_6(H_2O)_3)(SiW_{12}O_{40})] \cdot 6H_2O$ (5)

Crystal structure of compound **5** contains half unit of the chromium trinuclear cluster, half unit of the silicotungstate cluster, and three lattice water molecules in asymmetric unit. The remaining charge of the molecular unit is neutralized by protons (H^+). We couldn't locate H^+ ions in the crystal lattice. The starting precursor to synthesize compound **5** is $H_4SiW_{12}O_{40}$, and hence, we assumed three protons (H^+) in molecular unit for charge compensation. The compound **5** can be formulated as $[H_3(Cr_3O(OOCCH_2CN)_6(H_2O)_3)(SiW_{12}O_{40})] \cdot 6H_2O$ (**5**). The thermal ellipsoidal plot of compound **5** is illustrated in Figure 4.20. The atoms labeled as O31, Cr2, O25, C7, C8, C10, and C11 are located in the special position. The atoms labeled with C9, N3 and C12, N4 are in considerable disorder and refined with half occupancy. In the crystal structure of compound **5**, two supramolecularly hydrogen bonded water dimers (O35 and O36, O34 and its symmetry equivalent atom) are found within the O H···O hydrogen bonding distance. The supramolecular environment around water dimers is presented in Figure 4.19(b).

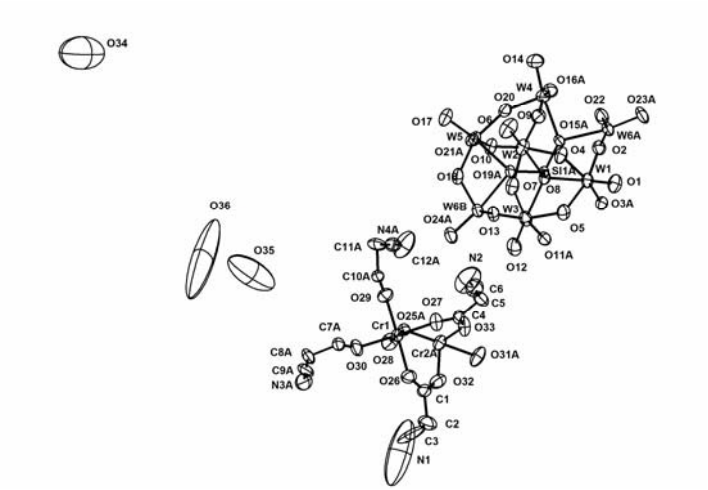

Figure 4.20. The thermal ellipsoidal representation of (50 % probability level) $[H_3(Cr_3O(OOCCH_2CN)_6(H_2O)_3)(SiW_{12}O_{40})]\cdot 6H_2O$ (**5**) excluding hydrogen atoms.

4.4. Conclusion

In summary, we have isolated the ionic crystals **1** **5** from an aqueous medium and structurally characterized. The solid state properties of compound **1** and **dehydrated 1-85°** are described in the view of exclusion (shrinkage of unit cell volume) and inclusion (expansion of unit cell volume) of water molecules in the crystal lattice. We report here the first example of 'ionic crystal' in which macrocation / polyoxometalate ratio is 4:1, without the presence of alkali metal ions. To the best of our knowledge, 4:1 is the highest trinuclear macrocation / polyoxoanion ratio observed in the crystal structure. The axial coordinated monodentate ligand in basic trinuclear cluster is more labile for substitution by Lewis base such as pyridine etc..[16] An attempt to replace the terminal coordinated aqua ligands by pyridine molecule in compounds **1** and **2** is in progress in our laboratory. The macrocation / polyoxometalate ratio in compounds **3** and **4** is 2:1 whereas in compound **5** the same is 1:1. The remaining negative charges are counterbalanced by protons (H^+). The supramolecular O H···O and C H···O hydrogen bonding interactions

of all the compounds are discussed elaborately. The adsorption and desorption properties of trinuclear macrocation and polyoxometalate based ion pair complexes systems will be an interesting study. The macrocations with similar coordination functionalities will be prepared and corresponding ionic crystal's adsorption properties and their related studies will be done in near future.

4.5. References

1. a) A. Vlachos, V. Psycharis, C. P. Paptopoulou, N. Lalioti, Y. Sanakis, G. Diamantopoulos, M. Fardis, M. Karayanni, G. Papavassiliou, A. Terzis, *Inorg. Chim. Acta.* **2004**, *357*, 3162; b) T. Fujihara, J. Anonahata, S. Kumakura, A. Nagasawa, K. Murakami, T. Ito, *Inorg. Chem.* **1998**, *37*, 3779; c) C. E. Anson, J. P. Bourke, R. D. Cannon, U. A. Jayasooriya, M. Molinier, A. K. Powell, *Inorg. Chem.* **1997**, *36*, 1265; d) R. D. Cannon, U. Jayasooriya, F. E. Sowrey, C. Tilford, A. Little, J. P. Bourke, R. D. Rogers, J. B. Vincent, G. J. Kearley, *Inorg. Chem,* **1998**, *37*, 5675; d) L. Keeney, M. J. Hynes, *J. Chem. Soc. Dalton Trans.,* **2005**, 1524.
2. R. D. Cannon, R. P. White, *Prog. Inorg. Chem.* **1988**, *36* 195.
3. a) R. D. Cannon, R P. White, *Progr. Inorg. Chem.* **1988**, *36*, 195; b) S. P. Pali, D. E. Richardson, M. L. Hansen, B. B. Iversen, F. K. Larsen, L. Singerean, G. A. Timco, N. V. Gerbeleu, K. R. Jennings, J. R. Eyler, *Inorg. Chim. Acta,* **2001**, *319,* 23 and references cited therein; c) F. E. Sowrey, C. Tilford, S. Wocadlo, C. E. Anson, A. K. Powell, S. M. Bennington, W. Montfrooij, U. A. Jayasooriya, R. K. D. Cannon, *J. Chem. Soc. Dalton Trans.* **2001**, 862.
4. T. Murao, *Phys. Lett.* **1974**, *49A*, 33.
5. S. Supriya, S. K. Das, *J. Am. Chem. Soc.* **2006**, *129*, 3464.

6. a) S. M. Gorun, S. J. Lippard, *Nature,* **1986**, *319,* 666; b) S. M. Gorun, G. C.Papaefthymiou, R. B. Frankel, S. J. Lippard, *J. Am. Chem. Soc.* **1987**, *109*, 3337.
7. a) L. A. Welo, *Phys. Rev.* **1923**, *32*, 320; b) L. A. Welo, *Philos. Mag.* **1928**, *6*, 481.
8. H. E. Toma, K. Araki, A. D. P. Alexiou, S. Nikolaou, S. Dovidauskas, *Coord. Chem. Rev.* **2001**, *217–219*, 187.
9. A. C. Sudik, A. P. Côté, A. G. Wong-Foy, M. O'Keeffe, O. M. Yaghi, *Angew. Chem. Int. Ed.* **2006**, *45*, 2528.
10. a) S. Uchida, R. Kawamoto, N. Mizuno, *Inorg. Chem.* **2006**, *45*, 5136; b) N. Mizuno, S. Uchida, *Chem. Lett.* **2006**, *35*, 688; c) S. Uchida, M. Hashimoto, N. Mizuno. *Angew. Chem. Int. Ed.* **2002**, *41*, 2814; d) S. Uchida, N. Mizuno, *Chem. Eur. J.* **2003**, *9*, 5850; e) S. Uchida, N. Mizuno, *J. Am. Chem. Soc.* **2004**, *126*, 1602; f) S. Uchida, R. Kawamoto, T. Akatsuka, S. Hikichi, N. Mizuno, *Chem. Mater.* **2005**, *17*, 1367; g) R. Kawamoto, S. Uchida, N. Mizuno, *J. Am. Chem. Soc.* **2005**, *127*, 10560; h) Y. Ogasawara, S. Uchida, N. Mizuno, *J. Phys. Chem. C.* **2007**, *111*, 8218; i) A. Lesbani, R. Kawamoto, S. Uchida, N. Mizuno, *Inorg. Chem.* **2008**, *47*, 3349.
11. C. Rocchiccioli-Deltcheff, M. Fournier, R. Franck, R. Thouvenot, *Inorg. Chem.* **1983**, *22*, 207.
12. a) *SAINT: Software for the CCD Detector System*; Bruker Analytical X-ray Systems, Inc.: Madison, WI, 1998; b) the structures were solved using *SHELXS-97*; c) Sheldrick, G. M. *SHELXS-97*, *Program for Structure Solution of crystal structure;* University of Göttingen: Germany, 1997.
13. K. Brandenburg, *DIAMOND Version 2.1e*, Crystal Impact GbR, Bonn, Germany, 2001.

14. a) C. Nozaki, I. Kiyoto, Y. Minai, M. Misono, N. Mizuno, *Inorg. Chem.* **1999**, *38*, 5724.; b) F. Zonnevijille, C. M. Tourné, G.. F. Tourné, *Inorg. Chem.* **1982**, *21*, 2751.

15. S. Supriya, S. Manikumari, P. Ragahvaiah, S. K. Das, *New. J. Chem*,. **2003**, *27*, 218.

16. a) N. Puri, R. O. Asplund, W. F. Tucker, *Inorg. Chim. Acta*, **1982**, *66*, 7; b) A. B. P. Lever, *Inorganic Electronic Spectroscopy*, Elsevier, Amsterdam, 2nd edn., **1984**, 751.

****

Chapter 5

==========

Co-existence of Polyoxometalate Cluster Anion and Manganese (III) Based Schiff-base Complex Cations: Syntheses and Structural Characterizations

==========

5.1. Introduction

Schiff-bases can be synthesized from amine and carbonyl compound by nucleophilic addition forming a hemiaminal followed by the dehydration to form an imine, which is first reported by Hugo Schiff in 1864.[1a] Schiff-base is a functional group that contains carbon-nitrogen double bond with the nitrogen atom connected to an aryl or alkyl group but not with hydrogen. In general, Schiff-bases are formulated as $R_1R_2C{=}NR_3$, where R_3 is aryl or alkyl group that makes the Schiff-bases stable imine. When two equivalents of salicylaldehyde are combined with a diamine, a particular chelating Schiff-base, popularly known as 'salen', is produced. The literature based on transition metal coordinated Schiff-base complexes is huge. The first salen ligand and its copper complex were discovered in 1889.[1b] Salen ligands are able to coordinate a range of different metals, and to stabilize them in their various oxidation states, enabling the use of metal salen complexes as a potential catalysts for the large variety of industrially important organic transformations.[2] Salen ligand contains four coordination sites described as [O, N, N, O] and two axial sites open to ancillary ligands. The coordination feature of a salen ligand is quite similar to that of porphyrins, but salens are more easily prepared compared to the multi-step synthesis of porphyrins. Schiff-base metal complex cations associated with polyoxometalate cluster anions have attracted considerable interest in recent years because of their importance in designing and developing novel materials.[3] Keggin type of heteropolyanions exhibit remarkable redox chemistry because

of their ability to act as electron reservoir. This unique property makes POM cluster anions important in various applicable research areas such as catalysis, magnetism, medicinal chemistry and materials science.[4] In this regard, the combination of Mn(III) Salen transition metal coordination complexes and polyoxometalate anionic clusters (namely Keggin, formulated as $H_4SiM_{12}O_{40}$ where M = Mo^{6+} or W^{6+}) would be interesting as far as molecule based materials (that could show novel magnetic, optical and catalytic properties) are concerned. Keeping this view in mind, a series of ion pair complexes $[DMFMn^{III}L_1(CH_3COO)(Mn^{III}L_1)_2(CH_3COO)Mn^{III}L_1DMF][Mn^{III}L_1(DMF)_2]_2[SiMo_{12}O_{40}]\cdot 6DMF\cdot 2H_2O$ (**1**), $[DMF\{Mn^{III}L_2\}_2DMF]_2[SiMo_{12}O_{40}]\cdot 2DMF$ (**2**), $[Mn^{III}L_3(DMF)_2]_4[SiMo_{12}O_{40}]\cdot 2DMF\cdot 4H_2O$ (**3**), $[Mn^{III}L_3(DMF)_2]_4[SiW_{12}O_{40}]\cdot 2DMF$ (**4**) have been prepared and structurally characterized. The Schiff-base ligands *N,N′*-bis(salicylaldehydo)ethylenediamine (H_2L_1 for compound **1**), *N,N′*-bis(2-hydroxyacetophenone)ethylenediamine (H_2L_2 for compound **2**) and *N,N′*-bis(5-bromosalicylidene)ethylenediamine (H_2L_3 for compounds **3** and **4**) are prepared by following the conventional preparative procedure and used in the above mentioned synthesis. In all compounds the oxidation state of manganese is +3, that is further confirmed by EPR spectroscopy, CV studies and BVS calculations. These compounds 1 4 are also important in the sense that manganese(III) is found to play an important biochemical role in oxygen-evolving complex (OEC) of photosystem-II (PS-II) in green plants.[5] Moreover, Mn(III) is very commonly found in many metallo-enzyme systems like conalbumin,[6a] tranferrin,[6b] avinmanganin,[6c] concanvalin A,[6d] pyruvate carboxylase,[6e] and superoxide dismutase from E. Coli,[6f]. We have introduced a rational synthetic strategy for preparing compounds **1 4** and characterized them by usual spectroscopic techniques such as IR, UV spectroscopy, elemental analysis, ESR studies and unambiguously by single crystal X-ray crystallography.

5.2. Experimental Section

5.2.1. Materials

The starting precursor $H_4SiMo_{12}O_{40}$ was prepared by slight modification of the reported procedure.[7] Another precursor $H_4SiW_{12}O_{40}$ was purchased from Merck and used without any further purification. $Mn(CH_3COO)_2{\cdot}4H_2O$, Salicylaldehyde, 2 hydroxyacetophenone, 5 bromosalicylaldehyde, ethylenediamine and solvent dimethlyformamide were obtained as commercial reagent grade. HPLC grade dimethylformamide solvent was used for spectroscopic measurements.

5.2.2. Physical Measurements

Micro-analytical (C, H, and N) data were obtained with Perkin-Elmer Model 240C elemental analyzer and FLASH EA 1112 Series CHNS analyzer. Infrared spectra (IR) were recorded by using KBr pellets on a JASCO-5300 FT-IR spectrophotometer in the region of 400 4000 cm^{-1}. A Cary 100 Bio UV/vis spectrophotometer was used to record the electronic absorption spectra. ESR spectra were recorded on a Bruker ECS 106 spectrometer. A CH-Instruments model 620A electrochemical analyzer was used for cyclic voltammetric experiments with dimethylformamide solutions of the compounds containing $[Bu_4N][ClO_4]$ (TBAP) as supporting electrolyte. The three electrode measurements were carried out at 298 K under a dinitrogen atmosphere with a platinum working electrode, a platinum wire auxiliary electrode and Ag/AgCl as reference electrode. The potentials reported in this work are uncorrected for junction contributions.

5.2.3. Synthesis and Characterization

Synthesis of H_2L_1

5.0 mL (46.92 mmol) of salicylaldehyde and 1.57 mL (23.48 mmol) of ethylenediamine were mixed in 20 mL of ethanol and this mixture was stirred for an hour. The yellow colored solid thus obtained was filtered and dried by washing with diethylether.

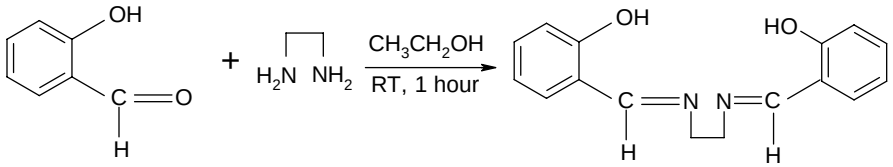

H_2L_1

Synthesis of H_2L_2

0.85 mL (7.06 mmol) of 2-hydroxyacetophenone and 0.24 mL (3.60 mmol) of ethylenediamine were mixed in 15 mL of ethanol and this mixture was stirred for one hour. The yellow colored solid thus obtained was filtered and dried by washing with diethylether.

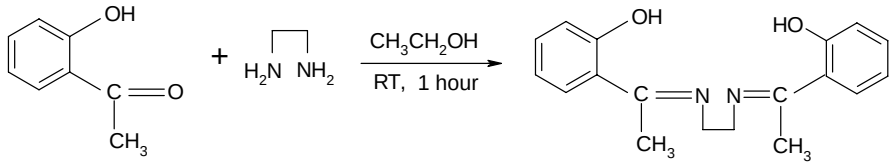

H_2L_2

Synthesis of H_2L_3

0.65g (3.23 mmol) of 5-bromosalicylaldehyde and 0.11 mL (1.65 mmol) of ethylenediamine were mixed in 15 mL of ethanol and the resulting mixture was stirred for an hour. The resulting yellow color solid was filtered and dried by washing with diethylether.

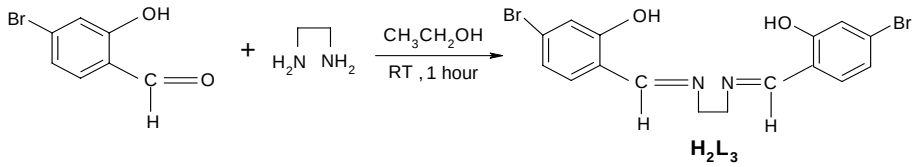

H_2L_3

[DMFMn^{III}L$_1$(CH$_3$COO)(Mn^{III}L$_1$)$_2$(CH$_3$COO)Mn^{III}L$_1$DMF][Mn^{III}L$_1$(DMF)$_2$]$_2$ [SiMo$_{12}$O$_{40}$] ·6DMF ·2H$_2$O (1)

H_2L_1 (0.18 g, 0.67 mmol), synthesized by the procedure as described above, was suspended in 50 mL of methanol. To this reaction mixture $Mn(CH_3COO)_2$ $4H_2O$ (0.4 g, 1.63 mmol) was added. The resulting reaction mixture was stirred until a clear solution was obtained. The color of the reaction mixture turned to brown during the course of the reaction. Then $H_4SiMo_{12}O_{40}$ (0.3 g, 0.16 mmol) was added and it was further stirred for another 24 hours. The solvent was evaporated by using rotary evaporator and the resulting brown precipitate was kept open in air for 3 days. The product was dissolved in minimum amount of DMF and filtered in to a small beaker that was kept in a big beaker containing diethylether, whereby the big beaker was kept closed by aluminum foil for 24 hours. Subsequently the small beaker (in which ether got diffused) was kept open at room temperature for slow evaporation. Dark brown colored crystals, obtained were separated and washed with Et_2O. Crystals were good enough for single crystal X-ray structure analysis. Yield 0.15g (19% based on Mo). Anal. calcd for $C_{136}H_{178}N_{24}O_{74}Mn_6SiMo_{12}$ (4842.03 g mol^{-1}): C, 38.74; H, 3.71; N, 6.94; Found: C, 38.90; H, 3.60; N, 6.88; IR (KBr pellet) (υ/cm^{-1}): 3435, 2924, 1651, 1622, 1599, 1541, 1442, 1386, 1334, 1292, 1201, 1151, 1089, 985, 943, 900, 794, 628, 594, 464.

[DMF{Mn^{III}L$_2$}$_2$DMF]$_2$[SiMo$_{12}$O$_{40}$] ·2DMF (2)

H_2L_2 (0.15 g, 0.56 mmol), synthesized by the procedure as described above, was suspended in 50 mL of methanol. To this reaction mixture $Mn(CH_3COO)_2$ $4H_2O$ (0.4 g, 1.63 mmol) was added. The resulting reaction mixture was stirred until a clear solution was obtained. The color of the reaction mixture turned to brown during the course of the reaction. Then $H_4SiMo_{12}O_{40}$ (0.3 g, 0.16 mmol) was added and it was further stirred for another 43 hours. The solvent was evaporated by using rotary evaporator and the resulting brown precipitate was kept open in air for 3 days. The product was dissolved in

minimum amount of DMF and filtered in to a small beaker that was kept in a big beaker containing diethylether, whereby the big beaker was kept closed by aluminum foil for 24 hours. Subsequently the small beaker (in which ether got diffused) was kept open at room temperature for slow evaporation. Dark brown colored crystals, obtained were separated and washed with Et_2O. Crystals were good enough for single crystal X-ray structure analysis. Yield: 0.205g (34% based on Mo). Anal. calcd for $C_{90}H_{114}N_{14}O_{58}Mn_4SiMo_{12}$ (3719.08 g mol^{-1}): C, 29.07; H, 3.09; N, 5.27; Found: C, 29.01; H, 2.92; N, 5.35. IR (KBr pellet) (υ/cm^{-1}): 3439, 2922, 1674, 1645, 1597, 1537, 1435, 1379, 1321, 1234, 1138, 1091, 985, 945, 900, 794, 601, 507, 453.

$[Mn^{III}L_3(DMF)_2]_4[SiMo_{12}O_{40}]\cdot 2DMF\cdot 4H_2O$ (3)

H_2L_3 (0.18 g, 0.42 mmol), synthesized by the procedure as described above, was suspended in 50 mL of methanol. To this reaction mixture $Mn(CH_3COO)_2\ 4H_2O$ (0.4 g, 1.63 mmol) was added. The resulting reaction mixture was stirred until a clear solution was obtained. The color of the reaction mixture turned to brown during the course of the reaction. Then $H_4SiMo_{12}O_{40}$ (0.32 g, 0.18 mmol) was added and it was further stirred for another 38 hours. The solvent was evaporated by using rotary evaporator and the resulting brown precipitate was kept open in air for 3 days. The product was dissolved in minimum amount of DMF and filtered in to a small beaker that was kept in a big beaker containing diethylether, whereby the big beaker was kept closed by aluminum foil for 24 hours. Subsequently the small beaker (in which ether got diffused) was kept open at room temperature for slow evaporation. Dark reddish brown colored crystals, obtained were separated and washed with Et_2O. Crystals were good enough for single crystal X-ray structure analysis. Yield: 0.35 g (43% based on Mo). Anal. calcd for $C_{94}H_{126}N_{18}O_{66}Br_8Mn_4SiMo_{12}$ (4602.54 g mol^{-1}): C, 24.53; H, 2.76; N, 5.48; Found: C, 24.38; H. 2.72. N, 5.40; IR (KBr pellet) (υ/cm^{-1}): 3051, 2930, 1655, 1626, 1525, 1452, 1373, 1284, 1178, 1109, 945, 900, 800, 684, 653, 532, 482.

[{$Mn^{III}(L_3)(DMF)_2\}_2][SiW_{12}O_{40}]$ ·2DMF (4)

H_2L_3 (0.18 g, 0.42 mmol), synthesized by the procedure as described above, was suspended in 50 mL of methanol. To this reaction mixture $Mn(CH_3COO)_2$ $4H_2O$ (0.4 g, 1.63 mmol) was added. The resulting reaction mixture was stirred until a clear solution was obtained. The color of the reaction mixture was turned to brown during the course of the reaction. Then $H_4SiW_{12}O_{40}$ (0.5 g, 0.17 mmol) was added and further it was stirred for another 44 hours. The solvent was evaporated by using rotary evaporator and the resulting brown precipitate was kept open in air for 3 days. The product was dissolved in minimum amount of DMF and filtered in to a small beaker that was kept in a big beaker containing diethylether, whereby the big beaker was kept closed by aluminum foil for 24 hours. Subsequently the small beaker (in which ether got diffused) was kept open at room temperature for slow evaporation. Dark reddish brown colored crystals, obtained were separated and washed with Et_2O. Yield: 0.39 g (40% based on Mo). Anal. calcd for $C_{94}H_{118}N_{18}O_{61}Br_8Mn_4SiW_{12}$ (5569.39 g mol^{-1}): C, 20.27; H, 2.14; N, 4.53; Found: C, 20.21; H, 2.18; N, 4.50; IR (KBr pellet) (υ/cm^{-1}): 3472, 3057, 2926, 1653, 1626, 1525, 1448, 1371, 1282, 1178, 1111, 1012, 968, 920, 800, 684, 652, 532, 482.

5.2.4. Single Crystal Structure Determination

The crystallographic data for compounds **1** **4** have been collected at 293 K on Bruker SMART APEX CCD, area detector system [λ(Mo Kα) = 0.7103 Å], graphite monochromator, 2400 frames were recorded with an ω scan width of 0.3°, each for 10 s, crystal-detector distance 60 mm, collimator 0.5 mm. Data reduction by SAINTPLUS,[8a] structure solution using SHELXS-97,[8b] and refined using SHELXL-97.[8c] All non hydrogen atoms were refined anisotropically. For compounds **1** and **3**, the water hydrogen atoms are not located in its crystal structure analyses. Thus, hydrogen bonding interactions were discussed in terms of O···O, and C···O contacts. The DIAMOND[9] software was used for molecular graphics.

5.3. Results and Discussion

5.3.1. Infrared Spectroscopy

The IR spectra of compounds **1** **4** exhibit the characteristic features for the metal-bonded $_{str}$(C=N) imine stretching frequency, that appear in the 1590 1640 cm^{-1} region. The phenolic $_{str}$(C O) stretching frequency appears in the range of 1270 1290 cm^{-1}. The IR bands, appear in the range of 450 480 cm^{-1}, can be assigned to the ligand coordination to the Mn(III) centre through Mn N and Mn O bonds. Two strong bands appear in the range of 900 960 cm^{-1} that are characteristic stretching frequencies for the M = O_t (where M = Mo^{6+} or W^{6+}) of the polyoxometalate cluster anion. The detailed infrared data for all the compounds are given in the Experimental Section. The IR data strongly support the association of polyoxometalate anions with Mn(III) salen cations in respective compounds.

5.3.2. Electronic Spectroscopy

In general, the metalation of salen ligands with $Mn^{II}(OAC)_2$ yields the respective Mn(III) salen compounds that can be well characterized by UV visible absorbance spectra.[10] The electronic absorbance spectra (Figure 5.1) of compounds **1** **4** (1.0 x 10^{-5} M) were recorded in HPLC grade dimethylformamide (DMF). The obtained absorption maximum values are presented in the caption of Figure 5.1. The inset pictures, shown in Figure 5.1, are recorded in comparatively higher concentrations (1.0 x 10^{-4} M). The following moderately strong absorption bands are assigned for (N imine) → Mn(III)

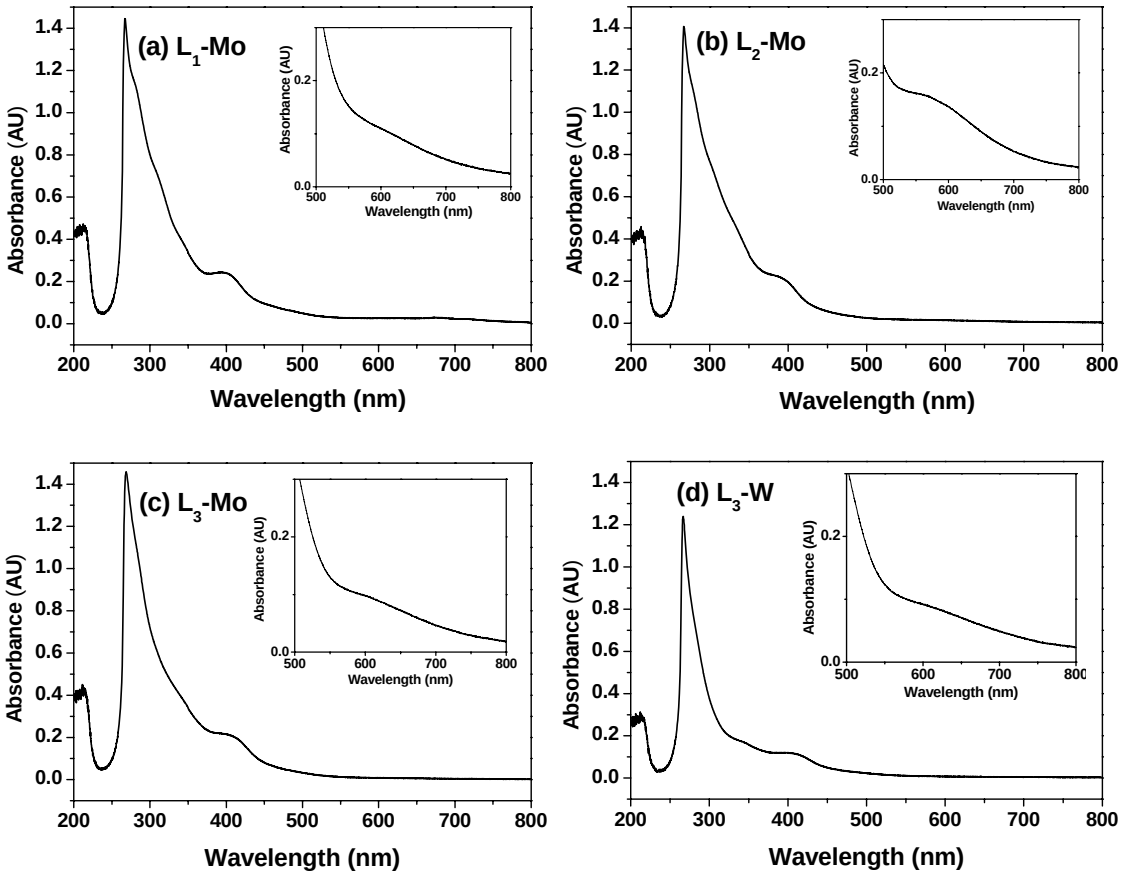

Figure 5.1. The UV-visible absorbance spectra of compounds **1** **4** in DMF: (a) For compound **1**: $_{max}$ (nm) = 608, 392, 343, 312, 283, 265 and their corresponding ε_{max} (M ^{1}cm ^{1}) = 1050, 25000, 38500, 67900, 109200, and 122400 respectively; (b) For compound **2**: $_{max}$ (nm) = 592, 393, 332, 305, 281, 266 and their corresponding ε_{max} (M ^{1}cm ^{1}) = 1400, 21200, 46800, 71600, 106300 and 136200 respectively; (c) For compound **3**: $_{max}$ (nm) = 604, 401, 339, 285, 270 and their corresponding ε_{max} (M ^{1}cm ^{1}) = 952, 21300, 40100, 103600 and 142600 respectively; (d) For compound **4**: $_{max}$ (nm) = 607, 405, 342, 288, 268 and their corresponding ε_{max} (M ^{1}cm ^{1}) = 884, 11800, 17200, 58600 and 118300 respectively.

ligand to metal charge transfer (LMCT) transitions: $_{max}$ (nm) = 392 with ε_{max} (25000 M ^{1}cm ^{1}) for **1**; $_{max}$ (nm) = 393 with ε_{max} (21200 M ^{1}cm ^{1}) for **2**; $_{max}$ (nm) = 401 with ε_{max} (21300 M ^{1}cm ^{1}) for **3** and $_{max}$ (nm) = 405 with ε_{max} (11800 M ^{1}cm ^{1}) for **4**. The

N(imine)→Mn(III) charge transfer absorption maxima values are consistent with the similar values of Mn(III)-salen systems reported in the literature.[10b] The following very strong $_{max}$ values are assigned for O→M(VI) (M= Mo, W) charge transfer transition which are characteristic absorption peaks for a polyoxometalate (POM) cluster anion: $_{max}$ (nm) = 265 (ε_{max} = 122400 M ^{1}cm ^{1}) for **1**; $_{max}$ (nm) = 266 (ε_{max} = 136200 M ^{1}cm ^{1}) for **2**; $_{max}$ (nm) = 270 with (ε_{max} = 142600 M ^{1}cm ^{1}) for **3** and $_{max}$ (nm) = 268 with (ε_{max} = 118300 M ^{1}cm ^{1}) for **4**. These values are comparable to those of other POM clusters.[3]

5.3.3. Electron Paramagnetic Resonance (EPR) Spectroscopy

The EPR measurements of compounds **1** **4** were performed in X-band frequency at 150^{o}C in dimethylformamide solution. In general, Mn(III) ion (d^4, integer spin S = 2) is EPR silent in traditional perpendicular polarization EPR spectroscopy at normal X-band frequency, whereas it is EPR active at g = 8 in the high field EPR spectrometers.[10b, 11]

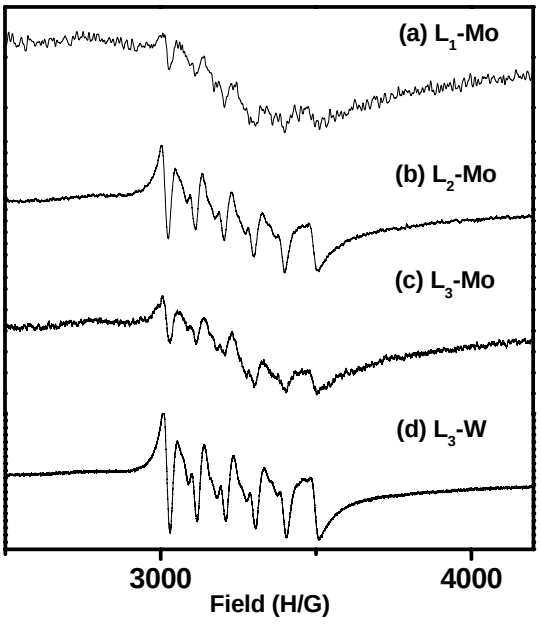

Figure 5.2. EPR spectra of compounds **1** **4** at 150^{o}C in dimethylformamide.
(a) Compound **1**;
(b) Compound **2**;
(c) Compound **3** and
(d) Compound **4.**

Those type of integer spin paramagnetic species (S = 1, 2, etc.,) can be investigated only in parallel-mode EPR (microwave field H_1 is parallel to the static field H_0) spectroscopy. However, Mn(III) salen POM compounds are EPR active at the normal X-band frequency and the resulting spectra of compounds **1** **4** are given in Figure 5.2. The resulting EPR spectra show the resonance at g 2 with a six-lines hyperfine coupling, which is corresponds to the presence of manganese species (I = 5/2).

5.3.4. Electrochemistry

The electrochemical behavior of compounds **1** **4** were studied in DMF (1 x 10^{-3} M) solution containing $[Bu_4N][ClO_4]$ (0.1 M) as supporting electrolyte, with the help of cyclic voltammetry. The typical cyclic voltammograms are presented in the Figure 5.3. Compounds **1** and **2** show irreversible one electron reduction wave, $E_{1/2}(Mn^{III}/Mn^{II})$, at 0.271 and 0.455 V respectively, whereas compounds **3** and **4** show quasi-reversible one electron reduction wave $E_{1/2}(Mn^{III}/Mn^{II})$, at 0.198 and 0.183 V respectively. All reduction potentials are characterized versus Ag/AgCl reference electrode with scan rate of 0.05 V. The electrochemical data of all compounds are presented in Table 5.1. Compounds **1** **4** do not exhibit any oxidative response. The similar complexes that show only Mn(III) Mn(II) reduction are known in the literature.[12]

5.3.5. X-ray Crystallographic Studies

Crystal Structure Description of Compound $[DMFMn^{III}L_1(CH_3COO)(Mn^{III}L_1)_2(CH_3COO)Mn^{III}L_1DMF][Mn^{III}L_1(DMF)_2]_2[SiMo_{12}O_{40}]\cdot 6DMF\cdot 2H_2O$ (1)

X-ray quality crystals of compound **1** were grown from the DMF solution by ether diffusion method. The compound **1** crystallizes in triclinic system with space group *P 1* and single crystal X-ray data, obtained at 293 K, are summarized in Table 5.2.

The asymmetric unit contains a Mn_2 dimer complex, a Mn_1 monomer complex, $[SiMo_6O_{20}]^2$ (half of the Keggin POM cluster anion, in which Si atom has half occupancy), one non coordinated water molecule and three lattice solvent DMF molecules.

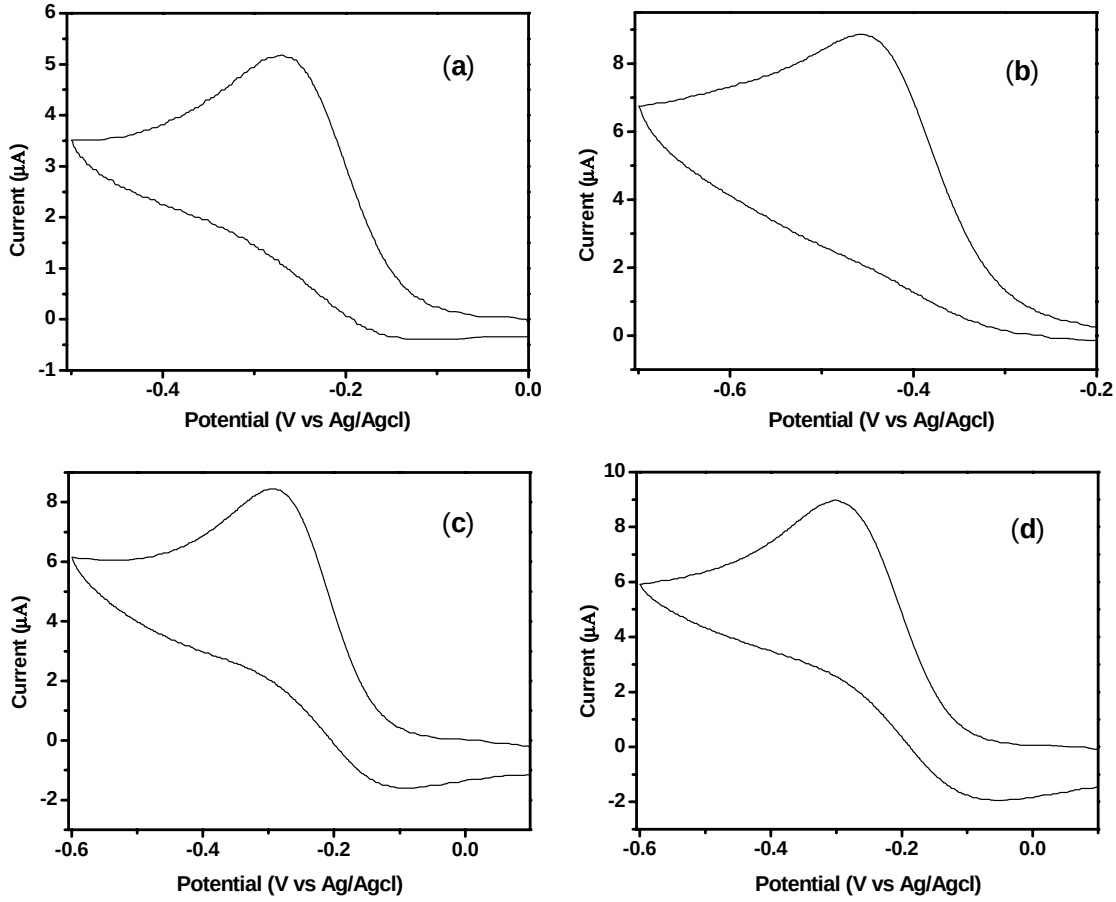

Figure 5.3. Cyclic voltammograms in DMF (1 x 10^3 M) solution containing $[Bu_4N][ClO_4]$ (0.1 M), scan rate 0.05 V s^{-1} at room temperature: (a) $[DMFMn^{III}L_1(CH_3COO)(Mn^{III}L_1)_2(CH_3COO)Mn^{III}L_1DMF][Mn^{III}L_1(DMF)_2]_2$ $[SiMo_{12}O_{40}]$ ·6DMF ·$2H_2O$ (**1**); (b) $[DMF\{Mn^{III}L_2\}_2DMF]_2[SiMo_{12}O_{40}]$ ·2DMF (**2**); (c) $[Mn^{III}L_3(DMF)_2]_4[SiMo_{12}O_{40}]$ ·2DMF ·$4H_2O$ (**3**); (d) $[Mn^{III}L_3(DMF)_2]_4[SiW_{12}O_{40}]$ ·2DMF (**4**).

The relevant thermal ellipsoidal plot with labeling scheme is depicted in Figure 5.4. The asymmetric Mn_2 dimer unit $[\{Mn^{III}_2(L_1)_2\}(CH_3COO)(DMF)]^{1+}$ core, consisting of two Mn(III) centers that are bridged by a acetate ligand through its carboxylate functional group via O(25) and O(26). The axial position of one of the metal center Mn(2) of this moiety is coordinated by a DMF molecule, whereby the apical position of the other metal

Table 5.1. Electrochemical data of compounds **1 4**

Compound	$E_{1/2}$ (Mn^{III}/Mn^{II}) V, (Ep) V
$[DMFMn^{III}L_1(CH_3COO)(Mn^{III}L_1)_2(CH_3COO)Mn^{III}L_1DMF]$ $[Mn^{III}L_1(DMF)_2]_2[SiMo_{12}O_{40}] \cdot 6DMF \cdot 2H_2O$ (**1**)	0.271 (irreversible)
$[DMF\{Mn^{III}L_2\}_2DMF]_2[SiMo_{12}O_{40}] \cdot 2DMF$ (**2**)	0.455 (irreversible)
$[Mn^{III}L_3(DMF)_2]_4[SiMo_{12}O_{40}] \cdot 2DMF \cdot 4H_2O$ (**3**)	0.198 (0.096) (quasi reversible)
$[Mn^{III}L_3(DMF)_2]_4[SiW_{12}O_{40}] \cdot 2DMF$ (**4**)	0.183 (0.237) (quasi reversible)

$E_{1/2} = (E_{pa} + E_{pc})/2$ V, $E_p = E_{pa}$ E_{pc} V, where E_{pa} and E_{pc} are anodic and cathodic peak potentials, respectively.

center Mn(1) remains unoccupied. In the molecular structure, two Mn(1) centers are bridged by two ($_3$-O) oxygen atoms (hydroxyl oxygen from each salen ligand) resulting in an unusual Mn_4 tetramer, which can be described as Mn(2) O(26) C(17) O(25) Mn(1) 2 $_3$(O) Mn(1) O(25) C(17) O(26) Mn(2) as

shown in Figure 5.5. In the molecular structure Mn_4 tetramer unit can be formulated as $[DMFMnL_1(CH_3COO)(MnL_1)_2(CH_3COO)MnL_1DMF]^{2+}$. The coordination geometry around Mn(1) and Mn(2) is octahedral, in which the equatorial positions are satisfied by N_2O_4 core from the salen ligand.

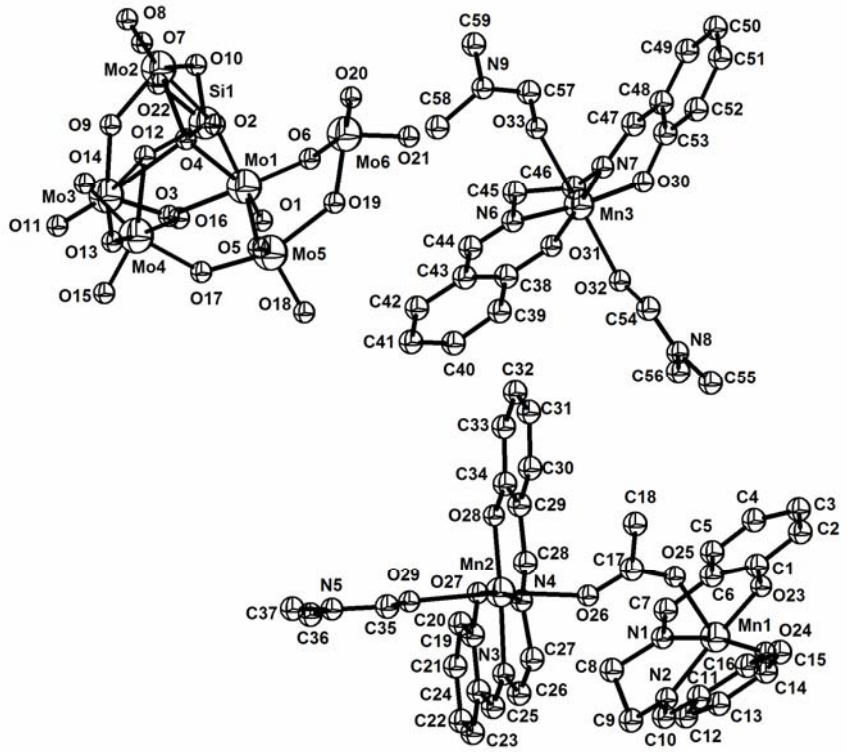

Figure 5.4. Thermal ellipsoidal plot (50 % probability level) of the asymmetric unit of $[DMFMn^{III}L_1(CH_3COO)(Mn^{III}L_1)_2(CH_3COO)Mn^{III}L_1DMF][Mn^{III}L_1(DMF)_2]_2$ $[SiMo_{12}O_{40}]\cdot 6DMF\cdot 2H_2O$ (**1**) excluding lattice solvent molecules and hydrogen atoms.

The salen moiety acts as dianionic tetradentate ligand for each Mn(III) ion which resides in an approximately square planar coordination environment. The structural environment around Mn_1 monomer moiety in asymmetric unit can be explained as follows. The four equatorial positions of the Mn(3) metal center is coordinated by N_2O_4 core unit from the salen ligand; remaining two apical positions of the same metal center Mn(3) is satisfied by two solvent DMF molecules.

Table 5.2. Crystal Data and Structural Refinement for Compounds **1** **2**

	1	**2**
Empirical formula	$C_{136}H_{178}N_{24}O_{74}Mn_6SiMo_{12}$	$C_{90}H_{114}N_{14}O_{58}Mn_4SiMo_{12}$
Formula weight	4842.03	3719.08
T [K]	293(2)	298(2)
λ [Å]	0.71073	0.71073
Crystal system	Triclinic	Triclinic
Space group	P–1	P–1
a [Å]	14.4448(8)	12.580(3)
b [Å]	15.5126(8)	15.480(3)
c [Å]	19.9360(11)	16.744(4)
deg]	71.1650(10)	96.037(4)
β [deg]	85.7350(10)	99.770(4)
deg)	89.6420	90.039(4)
V [Å^3]	4215.5(4)	3195.1(12)
Z	1	1
D_{calc} [Mg m^{-3}]	1.907	1.933
μ [mm^{-1}]	1.399	1.617
F[000]	2422	1834
Crystal size [mm^3]	0.40 x 0.20 x 0.04	0.40 x 0.20 x 0.04
θ range for data collection [deg]	1.39 to 25.00	1.24 to 24.99
Reflections collected/unique	40713 / 14804	30092 / 11089
R [int]	0.0344	0.0731
Refinement method	Full-matrix least-squares on F^2	
Data/restraints/parameters	14804 / 0 / 1190	11089 / 0 / 772
Goodness-of-fit on F^2	1.335	1.169
R_1/wR_2 [$I > 2\sigma(I)$]	0.0865/0.1896	0.1230/0.3037
R_1/wR_2 [all data]	0.0900/0.1910	0.1556/0.3194
Largest diff. Peak/hole [e$^-$ Å ^{3}]	1.281/-1.414	2.742/-1.403

In the crystal structure of compound **1**, one Mn_4 tetramer unit $[DMFMnL_1(CH_3COO)(MnL_1)_2(CH_3COO)MnL_1DMF]^{2+}$ and two Mn_1 monomer units $[MnL_1(DMF)_2]^{2+}$ totally generates four positive charges which is balanced by a

polyoxometalate cluster anion $[SiMo_{12}O_{40}]^{4}$. The molecular structure of the compound **1** is depicted in Figure 5.5. The bond lengths of Si O, Mo O_t, and Mo O_b (O_t = terminal, O_b = bridging oxygen) in the crystal structure of **1** are in the usual range. The packing diagram depicted in Figure 5.6 evidence the formation of channels in which polyoxometalate cluster anion is accommodated. In MnN_2O_4 coordination sphere, the Mn N and Mn O bond lengths for compound **1** are in the range of 1.974(8) 1.997(8) and 1.874(7) 1.929(7) Å respectively. The average Mn N and Mn O bond distances are comparable to those of various reported Mn(III) complexes with similar ligation.[13]

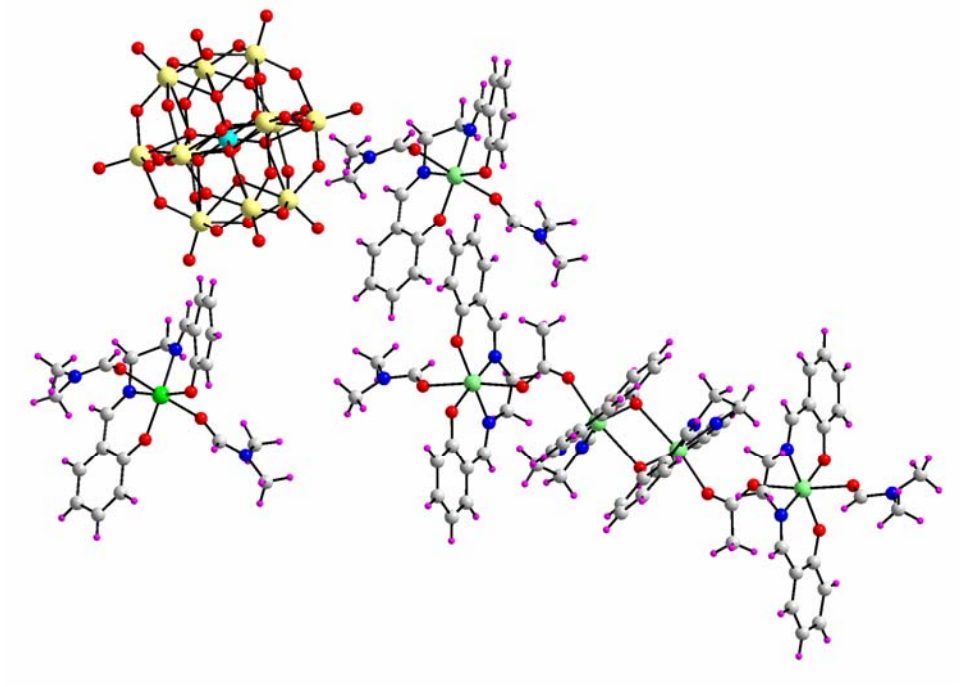

Figure 5.5. The molecular structure of compound **1** is in ball & stick representation. Color code: Mo, yellow; Mn, green; Si, cyan; O, red; C, gray; N, blue; H, purple.

In MnN_2O_4 coordination sphere, the O Mn O and O Mn N angles are close to 90^{o} (within 5^{o}). The oxidation state of manganese centers (Mn(1), Mn(2) and Mn(3)) are assigned as +3, which is consistent with their coordination geometries and confirmed

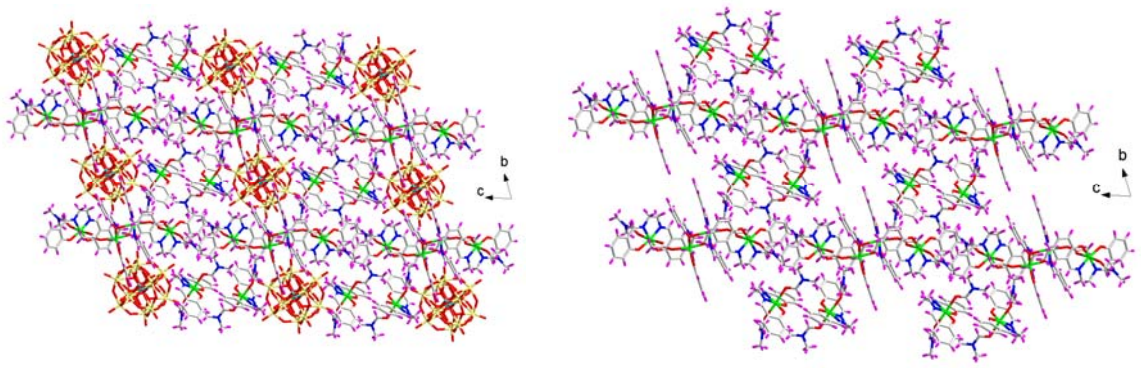

Figure 5.6. The view of packing along '*a*' axis (wire-frame representation) of compound **1** displaying both $[[DMFMn^{III}L_1(CH_3COO)(Mn^{III}L_1)_2(CH_3COO)Mn^{III}L_1DMF][Mn^{III}L_1(DMF)_2]_2]^{4+}$ and $[SiMo_{12}O_{40}]^4$ anions (left); The display of only $[[DMFMn^{III}L_1(CH_3COO)(Mn^{III}L_1)_2(CH_3COO)Mn^{III}L_1DMF][Mn^{III}L_1(DMF)_2]_2]^{4+}$ cations (right); Color code: Mo, yellow; Mn, green; Si, cyan; O, red; C, gray; N, blue; H, purple.

by Bond Valence Sum calculation (BVS). BVS result gives the value for Mn(1), Mn(2) and Mn(3) are 3.31, 3.33 and 3.39 respectively. It is well known that in the literature "Oxygen-Evolving Complex (OEC)" contains a cluster of four manganese atoms which induces the oxidation of water to dioxygen.[14] It is worthwhile to mention here that, the similar synthesized manganese tetrameric model complexes[15] are not many. In the crystal structure of compound **1**, we noticed considerable weak supramolecular O H···O and C H···O hydrogen bonding interactions. One of the lattice solvent DMF molecules interacts with lattice water molecule through O H···O hydrogen bonding interaction. The corresponding symmetry operator is 1+x, y, z. The supramolecular interactions from the remaining lattice DMF molecules are not considered because of high disorder in the molecule. The weak C H···O hydrogen bonding interactions noticed in the crystal structure of compound **1** are propagate through the crystal lattice resulting in the formation of complicated three dimensional structure. The relevant hydrogen bonding parameters are listed in Table 5.3.

Crystal Structure Description of Compound $[DMF\{Mn^{III}L_2\}_2DMF]_2[SiMo_{12}O_{40}]\cdot 2DMF$ (2)

Compound $[DMF\{Mn^{III}L_2\}_2DMF]_2[SiMo_{12}O_{40}]\cdot 2DMF$ (**2**) was synthesized starting from $Mn(CH_3COO)_2\cdot 4H_2O$, H_2L_2 and $H_4SiMo_{12}O_{40}$ in methanol solvent. Dark brown crystals of **2** were obtained from DMF solvent by diffusing ether over a period of 24 hours. The compound **2** crystallizes in triclinic system with space group *P-1* and crystal data obtained at 293 K are summarized in Table 5.2. ORTEP projections of 'cations' and 'anions', in the crystal structure of compound **2** are displayed in Figure 5.7. The asymmetric unit of the crystal structure of compound **2** consists of two $[DMF\{Mn^{III}L_2\}_2DMF]^{2+}$ cations and half of $[SiMo_{12}O_{40}]^{4}$ anion and one lattice DMF solvent molecule, accordingly the molecular structure of compound **2** is depicted in Figure 5.8.

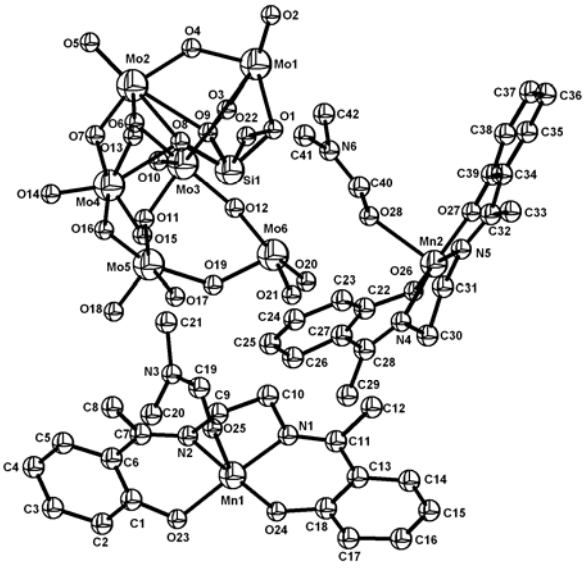

Figure 5.7. Thermal ellipsoidal plot (50 % probability level) of the asymmetric unit of $[DMF\{Mn^{III}L_2\}_2DMF]_2$ $[SiMo_{12}O_{40}]\cdot 2DMF$ (**2**) excluding lattice solvent molecules and hydrogen atoms.

Table 5.3. Geometrical parameters of the C H···O hydrogen bonds (Å, °) involved in supramolecular network of compound $[DMFMn^{III}L_1(CH_3COO)(Mn^{III}L_1)_2(CH_3COO)Mn^{III}L_1DMF][Mn^{III}L_1(DMF)_2]_2$ $[SiMo_{12}O_{40}]\cdot 6DMF\cdot 2H_2O$ (**1**) where D=donor; A=acceptor.

D H···A	d(D···H)	d(H···A)	d(D···A)	(DHA
C2 H2···O11 #2	0.93	2.68	3.584(14)	165.5
C3 H3···O21 #3	0.93	2.45	3.331(13)	157.4
C4 H4···O14 #4	0.93	2.80	3.301(17)	115.0
C5 H5···O6 #5	0.93	2.83	3.484(15)	128.6
C5 H5···O14 #4	0.93	2.51	3.175(14)	128.8
C7 H7···O1 #5	0.93	2.84	3.409(13)	120.5
C7 H7···O2 #5	0.93	2.62	3.537(14)	170.5
C8 H8B···O1 #1	0.97	2.64	3.469(15)	143.6
C9 H9B···O11 #6	0.97	2.88	3.503(13)	123.2
C10 H10···O11 #6	0.93	2.60	3.378(14)	141.5
C13 H13···O21 #7	0.93	2.58	3.234(14)	127.7
C14 H14···O6 #7	0.93	2.69	3.39(2)	133.6
C14 H14···O21 #7	0.93	2.89	3.389(14)	115.2
C20 H20···O7 #5	0.93	2.83	3.494(15)	128.9
C23 H23···O1 #6	0.93	2.61	3.308(14)	132.8
C25 H25···O3 #6	0.93	2.64	3.542(15)	164.2
C26 H26B···O17#6	0.97	2.21	3.03(2)	141.5
C26 H26A···O13 #6	0.97	2.63	3.36(2)	132.5
C27 H27A···O36 #6	0.97	2.39	3.22(2)	143.4
C27 H27B···O37	0.97	2.77	3.47(3)	129.4
C18 H18A···O37	0.96	2.65	3.557(17)	157.9
C35 H35···O36 #6	0.93	2.61	3.52(4)	166.0
C42 H42···O18	0.93	2.60	3.519(15)	171.8
C44 H44···O34 #6	0.93	2.74	3.299(14)	119.8
C45 H45B···O34 #6	0.97	2.54	3.396(15)	147.3
C45 H45A···O21	0.97	2.34	2.988(14)	123.3
C45 H45B···O37 #7	0.97	2.86	3.523(16)	126.1

continued

D H···A	d(D···H)	d(H···A)	d(D···A)	(DHA
C46 H46A···O37 #7	0.97	2.74	3.327(16)	119.6
C46 H46B···O15 #1	0.97	2.48	3.397(13)	158.3
C47 H47···O15 #1	0.93	2.63	3.485(13)	153.0
C50 H50···O27 #3	0.93	2.90	3.495(13)	122.7
C51 H51···O27 #3	0.93	2.79	3.451(13)	129.4
C51 H51···O26 #3	0.93	2.94	3.451(13)	116.2
C51 H51···O28 #3	0.93	2.40	3.314(13)	166.1
C55 H55C···O31 #3	0.96	2.46	3.414(14)	170.8
C55 H55A···O35 #1	0.96	2.60	3.49(2)	155.7
C56 H56B···O35 #1	0.96	2.68	3.557(18)	152.4
C60 H60···O18 #6	0.93	2.61	3.452(16)	151.1
C61 H61A···O5 #6	0.96	2.73	3.59(2)	150.7
C61 H61B···O1 #6	0.96	2.92	3.50(2)	119.8
C62 H62A···O37 #8	0.96	2.94	3.565(18)	124.1
C62 H62B···O35	0.96	2.53	3.460(18)	164.1

Symmetry transformations used to generate equivalent atoms: #1 1+x, y, z; #2 1+x, y, -1+z; #3 2-x, -y, 1-z; #4 1-x, -y, 1-z; #5 x, y, -1+z; #6 1-x, 1-y, 1-z; #7 2-x, 1-y, 1-z; #8 -1+x, y, z.

The lattice DMF molecules have been removed from the crystal lattice by using SQUEEZ procedure of the PLATON package,[16] because appropriate atoms couldn't be located properly due to high disorderness. But identification of two DMF molecules per formula unit has been confirmed by elemental analysis technique. The molecular structure of compound **2** shows the presence of two $[DMF\{Mn^{III}L_2\}_2DMF]^{2+}$ dimer moieties as cations and $[SiMo_{12}O_{40}]^{4}$ as anion . In each dimer entity, two Mn(III) ions are bridged by two $_3$ oxygen atoms. The oxygen atoms (from salicylate ligand) labeled as O(23) and its symmetry equivalent atom (from one dimer), O(26) and its symmetry

equivalent atom (from another dimer) are involved in the above mentioned bridging formation (Figure 5.8). In dimer entities, the internuclear distances between Mn(1)···Mn(1) and Mn(2)···Mn(2) are 3.374 and 3.331 Å respectively. Each Mn(III) is additionally coordinated by N_2O_4 core from L_2^2 ligand in the equatorial plane and sixth coordination is completed by DMF ligands. In the crystal structure of **2,** geometry around each Mn(III) is distorted octahedron. The trans bond angles in the distorted octahedron geometry are O(23) Mn(1) N(1), O(24) Mn(1) N(2), O(27) Mn(2) N(4) and O(26) Mn(2) N(5) 165.7(6)°, 176.5(6)°, 173.7(7)° and 168.1(6)° respectively, which are slightly deviated from linear bond angle 180°. The axial Mn O bond distances Mn(1) O(25) and Mn(2) O(28) are 2.147(14) Å and 2.142(15) Å respectively, which are significantly longer than the equatorial Mn O distances that are in the range of 1.853 1.929 Å, as expected for a Jahn-Teller elongation of a Mn^{III} ion.

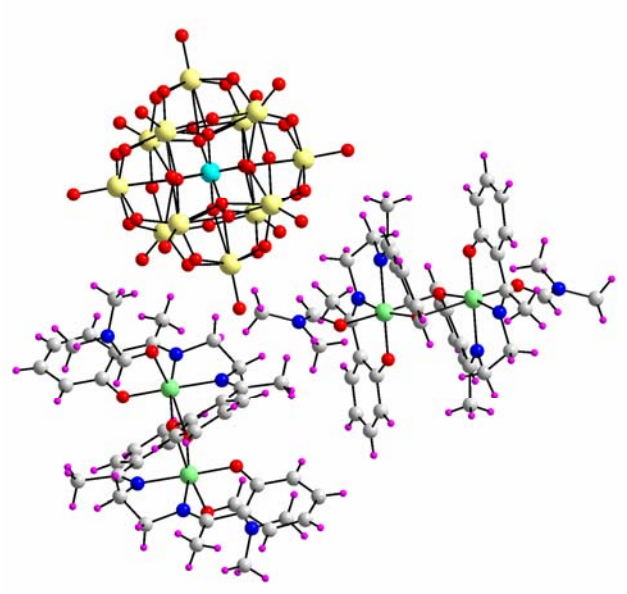

Figure 5.8. The molecular structure of compound **2** is in ball & stick representation. Color code is same as discussed in Figure 5.5.

The high spin d^4 Mn(III) system is a correct example for Jahn Teller distortion which are evidenced in the text book also. The oxidation state of manganese centers Mn(1) and Mn(2) in the crystal structure of compound **2** are assigned as +3, which is consistent with

their coordination geometries and bond valence sum calculation (BVS). BVS results give the value for Mn(1) and Mn(2) are 3.31 and 3.33 respectively. The crystal packing shows that, the dimer moieties $[DMF\{Mn^{III}L_2\}_2DMF]^{2+}$ exist as cationic and $[SiMo_{12}O_{40}]^4$ polyoxometalate cluster as anionic in nature (Figure 5.9). The cations and anions are stabilized by electrostatic interaction in the crystal lattice.

Apart from the above discussion, the weak supramolecular O H···O and C H···O hydrogen bonding interactions are also observed crystallographically in stabilizing the crystal packing. The terminal oxygen atom O(5) from the polyoxometalate cluster anion interacts through O H···O hydrogen bonding interaction with another oxygen atom O(5) from the adjacent polyoxometalate cluster. The corresponding symmetry operator is -x, 1-y, 1-z. Since the cluster anion in the crystal structure is asymmetric, the O H···O interaction propagates throughout the crystal lattice resulting in the formation of one dimensional chain (Figure 5.10). Similarly, we have found weak supramolecular C H···O interaction affords additional stability in crystal packing. The relevant C H···O hydrogen bonding interaction parameters are listed in Table 5.4.

Crystal Stucture Description of $[Mn^{III}L_3(DMF)_2]_4[SiMo_{12}O_{40}]\cdot 2DMF\cdot 4H_2O$ (3)

Compound $[Mn^{III}L_3(DMF)_2]_4[SiMo_{12}O_{40}]\cdot 2DMF\cdot 4H_2O$ (**3**) was synthesized, starting from $Mn(CH_3COO)_2\cdot 4H_2O$, H_2L_3 and $H_4SiMo_{12}O_{40}$ in methanol solvent. Dark reddish-brown crystals of **3** were obtained from DMF solvent diffused by ether over a period of 24 hours. The Thermal ellipsoidal plot of the asymmetric unit of compound **3** is shown in the Figure 5.11. The compound **3** crystallizes in the triclinic system with space group *P-1* and crystal data obtained at 293 K are summarized in Table 5.5. The asymmetric unit of the crystal structure of compound **3** consists of two $[Mn^{III}L_3(DMF)_2]^{1+}$ cation and half of $[SiMo_{12}O_{40}]^4$ anion, one lattice DMF solvent molecule and two water molecules, accordingly the molecular structure of compound **3** is

depicted in Figure 5.12. The molecular structure of compound **3** shows the presence of four $[Mn^{III}L_3(DMF)_2]^{1+}$ mono-cations and $[SiMo_{12}O_{40}]^{4}$ as anion. Each Mn^{III} ion is coordinated by N_2O_4 core of the L_3^{2} ligand in the equatorial plane and two apical positions are satisfied by two DMF molecules. In the crystal structure of compound **3** each Mn^{III} ion is in distorted octahedron geometry. The trans bond angles in the distorted octahedron geometry are O(23) Mn(1) N(1), O(24) Mn(1) N(2), O(27) Mn(2) N(5) and O(28) Mn(2) N(6) 173.9(6)^o, 174.1(5)^o, 173.6(5)^o and 173.7(5)^o respectively, which slightly deviate from linear bond angle 180^o. The axial Mn O bond distances are listed as follows: Mn(1) O(25) = 2.200(12) Å, Mn(1) O(26) = 2.241(12) Å, Mn(2) O(29) = 2.256(12) Å, and Mn(2) O(30) = 2.248(12) Å, which are significantly longer than the equatorial Mn O distances those are in the range of 1.874(11) 1.897(11) Å, as expected for a Jahn-Teller distorted Mn^{III} ions. The oxidation state of manganese centers Mn(1) and Mn(2) in the crystal structure of compound **3** are assigned as +3, which is consistent with their coordination geometries and confirmed by bond valence sum calculations (BVS). BVS result gives the value for Mn(1) and Mn(2) are 2.76 and 3.35 respectively. The packing diagram for compound **3** is depicted in Figure 5.13. The packing diagram shows the co-existence of cations and anions in which the cations are stacked each other and interacted each other through weak π π interactions. Interesting supramolecular interactions are observed in the crystal structure of compound **3**. The terminal oxygen atom O(12) and bridging oxygen atom O(9) from the same polyoxometalate cluster anion interacts individually with the lattice water molecule O(33) through O H···O hydrogen bonding interaction. The respective hydrogen bonding interaction has been extended from O(33) to O(12) and O(9) throughout the crystal lattice. Since the crystal structure is asymmetric, the respective symmetry equivalent atoms are also involved in the above discussed hydrogen bonding interactions, resulting in the formation of one dimensional chain, which is shown in Figure 5.14**.** The weak interactions like C H···O hydrogen

bonding interactions affords the additional stability to the framework. The pertinent O H···O and C H···O hydrogen bonding interaction parameters are listed in Tables 5.6 and 5.7 respectively.

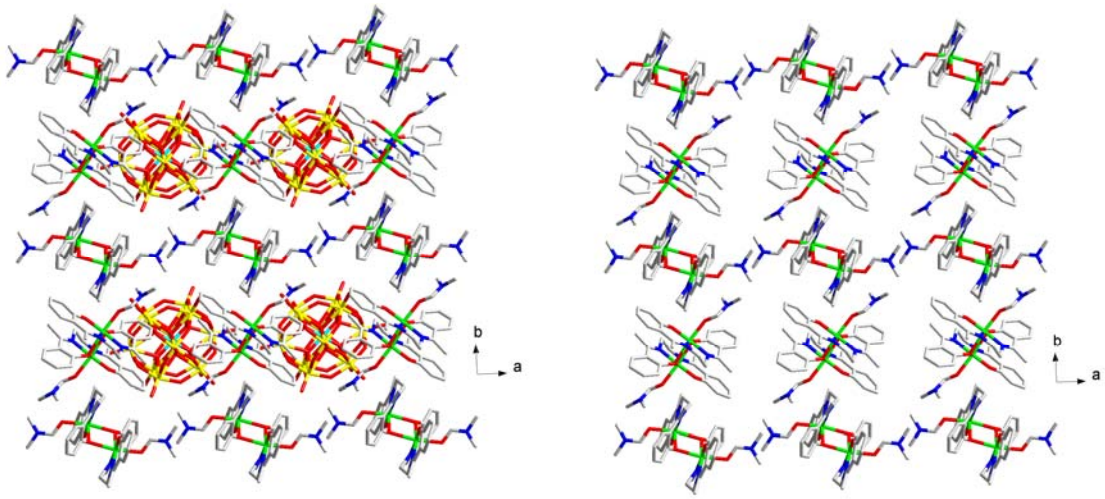

Figure 5.9. The view of packing along '*c*' axis (wire-frame representation) of compound **2** displaying both $[(DMF\{Mn^{III}L_2\}_2DMF)_2]^{4+}$ and $[SiMo_{12}O_{40}]^4$ anions (left); The display of only the $[(DMF\{Mn^{III}L_2\}_2DMF)_2]^{4+}$ cations (right); Color code: Mo, yellow; Mn, green; Si, cyan; O, red; C, gray; N, blue; H, purple.

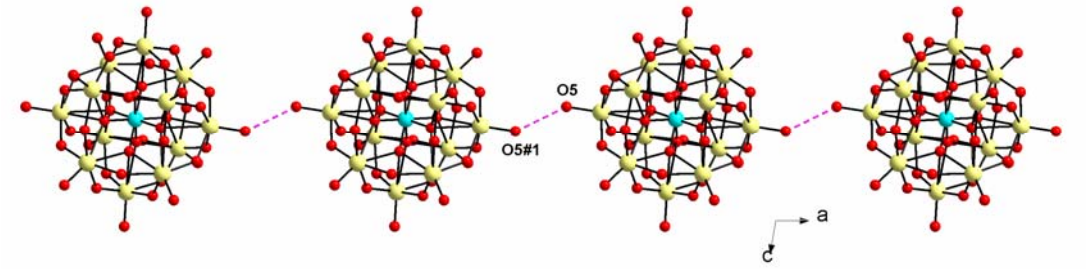

Figure 5.10. One dimensional chain propagates through O H···O hydrogen bonding interaction along the '*ac*' plane. Color code: Mo, yellow; Si, cyan; O, red.

Crystal Stucture Description of $[Mn^{III}L_3(DMF)_2]_4[SiW_{12}O_{40}]$ ·2DMF (4)

The synthesis procedure of compound $[Mn^{III}L_3(DMF)_2]_4[SiW_{12}O_{40}]$ ·2DMF (**4**) is similar to compound **3** except the polyoxometalate precursor used. Dark reddish-brown crystals of **4** were obtained from DMF solvent diffused by ether over a period of 24 hours. The crystal structure of compound **4** is isostructural to compound **3**.

Table 5.4. Geometrical parameters of the C H···O hydrogen bonds (Å, °) involved in supramolecular network of compound $[DMF\{Mn^{III}L_2\}_2DMF]_2[SiMo_{12}O_{40}]$ ·2DMF (**2**) where D=donor; A=acceptor.

D H···A	d(D···H)	d(H···A)	d(D···A)	(DHA
C3 H3···O14 #2	0.93	2.44	3.33(3)	158.7
C4 H4···O18 #2	0.93	2.72	3.33(3)	129.3
C8 H8C···O18	0.96	2.67	3.46(3)	140.0
C9 H9B···O2 #3	0.97	2.62	3.48(2)	148.5
C9 H9B···O17	0.97	2.54	3.34(2)	139.4
C10 H10A···O20	0.97	2.57	3.37(2)	140.1
C12 H12A···O5 #3	0.96	2.56	3.34(3)	137.6
C14 H14···O11 #4	0.93	2.69	3.29(2)	123.1
C15 H15···O11 #4	0.93	2.75	3.32(3)	120.0
C19 H19···O19	0.93	2.43	3.32(3)	159.6
C19 H19···O21	0.93	2.81	3.51(3)	132.4
C24 H24···O2 #5	0.93	2.43	3.33(3)	160.9
C29 H29C···O21	0.96	2.64	3.28(3)	125.0
C31 H31B···O5 #4	0.97	2.58	3.34(3)	135.5
C33 H33A···O14 #3	0.96	2.58	3.26(4)	127.5
C41 H41C···O12	0.96	2.89	3.40(5)	114.1
C42 H42A···O10 #5	0.96	2.60	3.39(4)	139.5

Symmetry transformations used to generate equivalent atoms: #1 -x, 1-y, 1-z; #2 1-x, 1-y, 2-z; #3 1-x, 1-y, 1-z; #4 1+x, y, z; #5 1-x, -y, 1-z

The thermal ellipsoidal plot of the asymmetric unit of compound **4** is shown in the Figure 5.15. The compound **4** crystallizes in the triclinic system with space group *P-1* and crystal data obtained at 293 K are summarized in Table 5.5. The asymmetric unit in the crystal structure of compound **4** consists of two $[Mn^{III}L_3(DMF)_2]^{1+}$ cation and half of

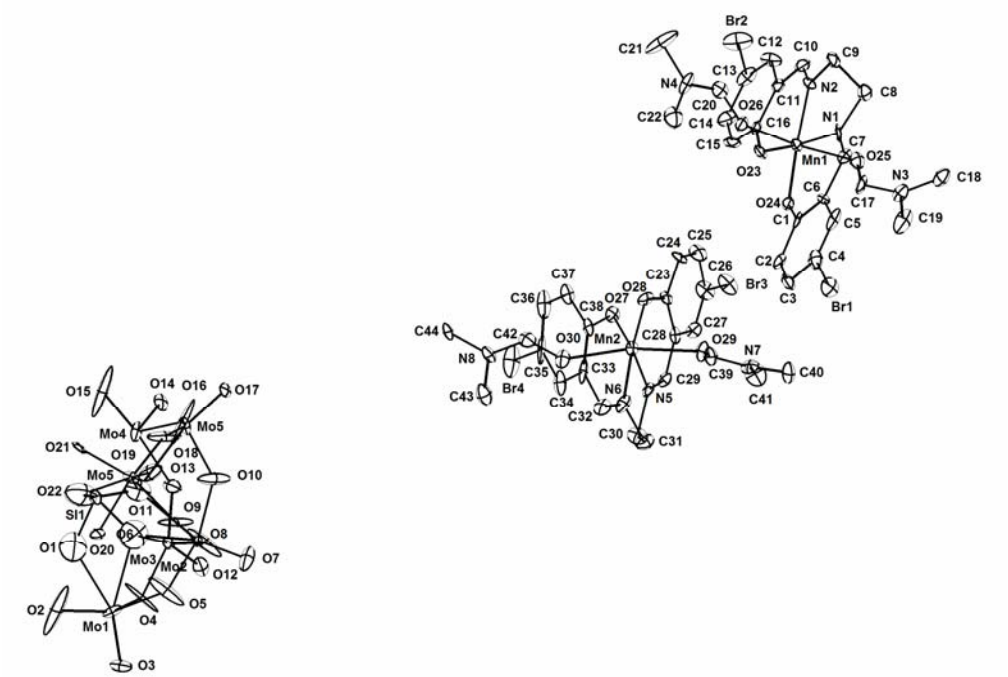

Figure 5.11. Thermal ellipsoidal plot (50 % probability level) of the asymmetric unit of compound $[Mn^{III}L_3(DMF)_2]_4[SiMo_{12}O_{40}]$ ·2DMF ·4H_2O (**3**) excluding lattice solvent molecules and hydrogen atoms.

$[SiW_{12}O_{40}]^4$ anion, one lattice DMF solvent molecule, accordingly the molecular structure of compound **4** is depicted in Figure 5.15. The molecular structure of compound **4** shows the presence of four $[Mn^{III}L_3(DMF)_2]^{1+}$ mono-cations and $[SiW_{12}O_{40}]^4$ as an anion . Each Mn^{III} ion is coordinated by N_2O_4 core of the L_3^2 ligand in the equatorial plane and two apical positions are satisfied by two DMF molecules. In the crystal structure of compound **4** each Mn^{III} ion is in distorted octahedron geometry. The trans bond angles in the distorted octahedron geometry are O23(1) Mn(1) N(2), O(24) Mn(1) N(1), O(27) Mn(2) N(6) and O(28) Mn(2) N(5) 174.7(7)^o, 175.3(7)^o,

174.1(7)^{o} and 172.2(7)^{o} respectively, which are slightly deviating from linear bond angle 180^{o}.

Table 5.5. Crystal Data and Structural Refinement for Compounds **3** **4**

	3	**4**
Empirical formula	$C_{94}H_{126}N_{18}O_{66}Br_8Mn_4SiMo_{12}$	$C_{94}H_{118}N_{18}O_{61}Br_8Mn_4SiW_{12}$
Formula weight	4602.54	5569.39
T [K]	293(2)	293(2)
λ [Å]	0.71073	0.71073
Crystal system	Triclinic	Triclinic
Space group	*P–1*	*P–1*
a [Å]	10.996(2)	11.193(5)
b [Å]	17.753(4)	17.723(8)
c [Å]	19.200(4)	19.328(9)
deg]	111.64(3)	110.694(7)
β [deg]	95.66(3)	96.885(8)
deg)	93.66(3)	94.195(8)
V [Å^3]	3446.5(12)	3533(3)
Z	1	1
D_{calc} [Mg m^{-3}]	2.218	2.617
μ [mm^{-1}]	3.831	12.427
F[000]	2242	2578
Crystal size [mm^3]	0.40 x 0.30 x 0.04	0.20 x 0.08 x 0.04
θ range for data collection [deg]	1.24 to 28.27	1.14 to 26.24
Reflections collected/unique	40182 / 16046	36918 / 13987
R [int]	0.0358	0.0613
Refinement method	Full-matrix least-squares on F^2	
Data/restraints/parameters	16046 / 0 / 928	13987 / 0 / 909
Goodness-of-fit on F^2	1.359	1.208
R_1/wR_2 [I > 2σ(I)]	0.1237/0.2857	0.0760/0.1831
R_1/wR_2 [all data]	0.1270/0.2870	0.1097/0.2021
Largest diff. Peak/hole [e· Å ^{3}]	2.338/-2.238	1.770/-2.396

The axial Mn O bond distances are listed as follows: Mn(1) O(25) = 2.273(17) Å, Mn(1) O(26) = 2.164(18) Å, Mn(2) O(29) = 2.239(14) Å, and Mn(2) O(30) =

2.263(15) Å, which are significantly longer than the equatorial Mn O distances those are in the range of 1.851(14) 1.892(14) Å, as expected for a Jahn-Teller distorted Mn^{III} ions.

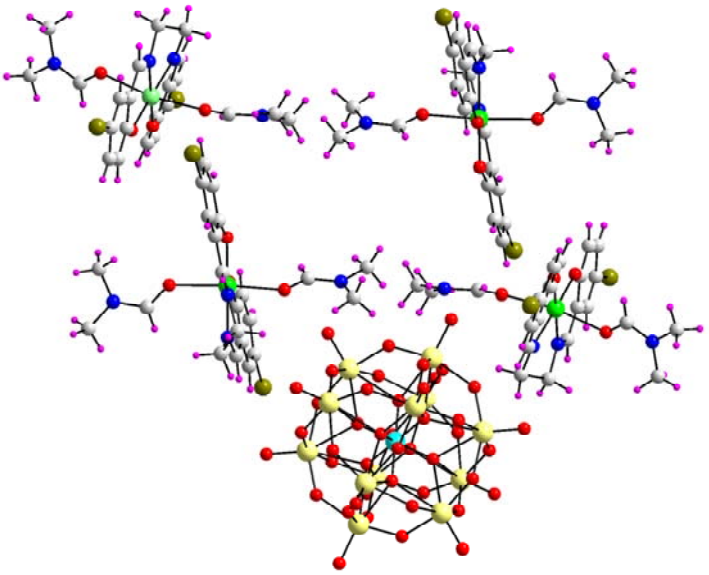

Figure 5.12. The molecular structure of **3** is in ball & stick representation. Color code: Mo, yellow; Mn, light green; Si, cyan; Br, dark green; O, red; C, gray; N, blue; H, purple.

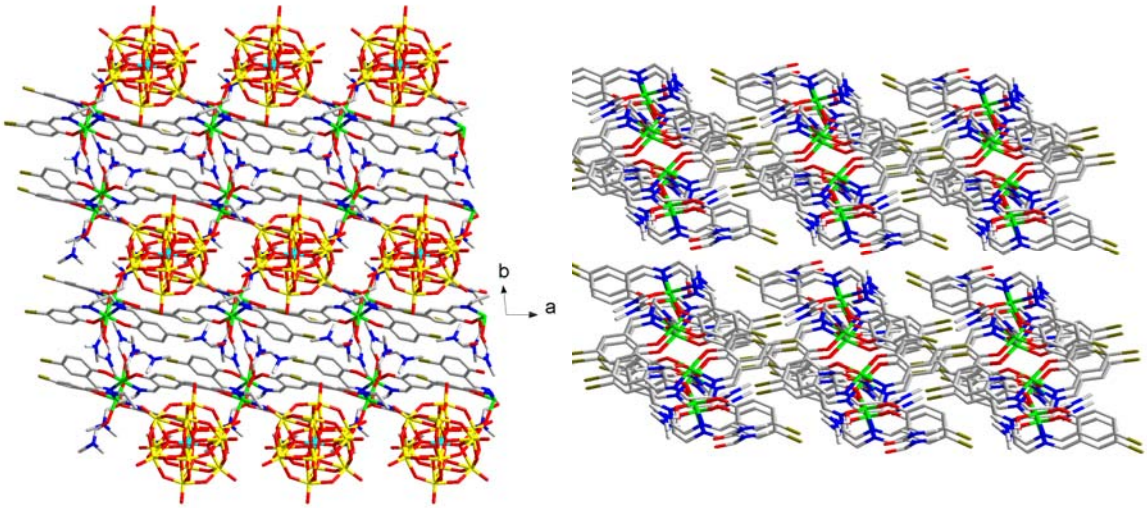

Figure 5.13. The packing diagram of compound **3** illustrating the alignment of $[\{Mn^{III}L_3(DMF)_2\}_4]^{4+}$ cations and $[SiMo_{12}O_{40}]^4$ anions in a view along '*c*' axis (left); Stacking of $[\{Mn^{III}L_3(DMF)_2\}_4]^{4+}$ cations by π···π interactions in the crystal structure of compound **3** (right); Color code: Mo, yellow; Mn, light green; Si, cyan; Br, dark green; O, red; C, gray; N, blue. (hydrogen atoms were omitted for clarity).

Table 5.6. Geometrical parameters of the O H···O hydrogen bonds (Å, °) involved in supramolecular network of compound $[Mn^{III}L_3(DMF)_2]_4[SiMo_{12}O_{40}]$ ·2DMF ·$4H_2O$ (**3**) where D=donor; A=acceptor.

D H···A	d(D···A)	D H···A	d(D···A)
O9···O33 #1	2.78(5)	O12···O33 #2	2.95(5)
O32···O24	2.81(4)	O33···O9 #3	2.78(5)
O33···O12 #3	2.95(5)		

Symmetry operators used to generate equivalent atoms are given in footnote of Table 5.7.

The oxidation state of manganese centers Mn(1) and Mn(2) in the crystal structure of compound **4** are assigned as +3, which is consistent with their coordination geometries and confirmed by bond valence sum calculations (BVS). BVS result gives the value for Mn(1) and Mn(2) are 3.43 and 3.43 respectively. The crystal packing of compound **4** is similar as described in Figure 5.13 (For compound **3**). The packing diagram shows the co-existence of cations and anions in which the cations are stacked each other and interacted by weak π π interactions. Since the compound **4** is isostructural to compound **3**, the similar O H···O and C H···O hydrogen bonding interactions have been observed. In compound **3**, two adjacent polyoxometalate clusters are interacted by O H···O hydrogen bonding interaction through lattice water molecule, whereas in compound **4**, two adjacent clusters are directly interacted by O H···O hydrogen bonding interactions. It results in the formation of one dimensional chain (Figure 5.16) in which the terminal oxygen atoms O(6) and O(11) from the same cluster made hydrogen bonding with O(11) and O(6) from the adjacent clusters respectively.

Table 5.7. Geometrical parameters of the C H···O hydrogen bonds (Å, °) involved in supramolecular network of compound $[Mn^{III}L_3(DMF)_2]_4[SiMo_{12}O_{40}]$ ·2DMF ·4H_2O (**3**) where D=donor; A=acceptor.

D H···A	d(D···H)	d(H···A)	d(D···A)	(DHA
C5 H5···O17 #4	0.93	2.45	3.36(2)	167.3
C7 H7···O16 #4	0.93	2.57	3.40(3)	147.9
C8 H8B···O16 #4	0.97	2.96	3.56(2)	120.9
C8 H8A···O14 #4	0.97	2.75	3.49(2)	133.7
C8 H8A···O19 #5	0.97	2.59	3.29(2)	125.7
C9 H9B···O19 #5	0.97	2.56	3.20(2)	123.3
C12 H12···O7 #5	0.93	2.60	3.52(2)	169.3
C17 H17···O32	0.93	2.83	3.45(5)	125.5
C18 H18B···O2 #6	0.96	2.75	3.45(3)	130.3
C21 H21A···O31 #5	0.96	2.48	3.27(3)	138.7
C27 H27···O3 #7	0.93	2.44	3.30(2)	155.0
C29 H29···O3 #7	0.93	2.53	3.38(2)	152.8
C30 H30B···O4 #7	0.97	2.58	3.49(3)	156.9
C31 H31B···O33 #5	0.97	2.29	3.11(5)	141.5
C31 H31B···O20 #8	0.97	2.74	3.42(2)	127.6
C31 H31A···O14 #9	0.97	2.51	3.37(2)	148.5
C32 H32···O5 #8	0.93	2.51	3.31(2)	144.2
C34 H34···O5#8	0.93	2.46	3.24(3)	141.0
C41 H41C···O32	0.96	2.87	3.49(5)	123.4
C42 H42···O27 #4	0.97	2.72	3.30(2)	121.2
C44 H44A···O28 #4	0.96	2.44	3.395(19)	172.5
C44 H44C···O24#4	0.96	2.78	3.301(18)	115.1
C44 H44C···O26 #4	0.96	2.55	3.42(2)	151.6
C45 H45C···O7 #8	0.96	2.68	3.22(2)	115.8
C46 H46A···O8 #8	0.96	2.59	3.44(4)	147.5
C46 H46A···O12#8	0.96	2.57	3.11(3)	115.8
C46 H46C···O33 #10	0.96	2.78	3.53(6)	136.0

Symmetric transformations used to generate equivalent atoms: #1 x, y, 1+z; #2 -1+x, y, 1+z; #3 1+x, y, -1+z; #4 -x, 1-y, 1-z; #5 1-x, 1-y, 1-z; #6 x, 1+y, -1+z; #7 -x, 1-y, 2-z; #8 1-x, 1-y, 2-z; #9 x, 1+y, z; #10 x, 1+y, z.

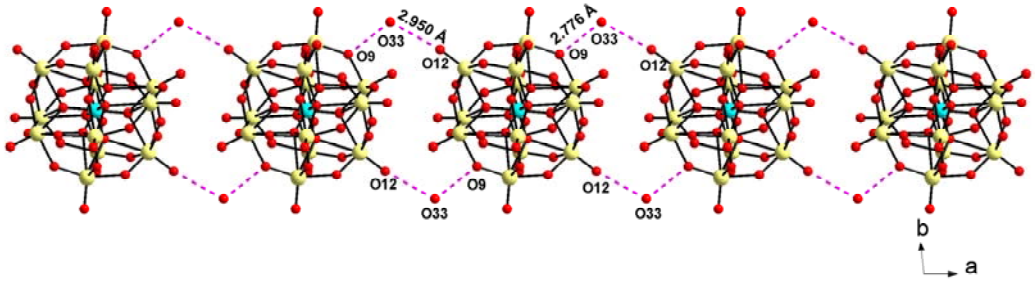

Figure 5.14. One dimensional chain propagates through O H···O hydrogen bonding interactions along the '*ab*' plane. Color code: Mo, yellow; Si, cyan; O, red.

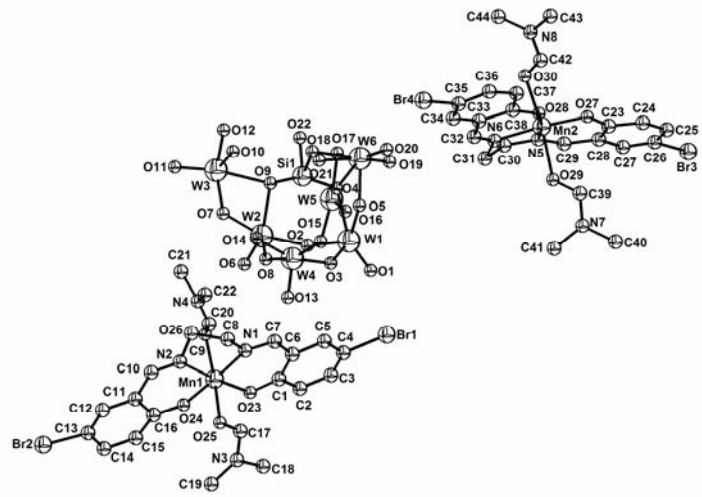

Figure 5.15. Thermal ellipsoidal plot (50 % probability level) of the asymmetric unit of compound $[Mn^{III}L_3(DMF)_2]_4[SiW_{12}O_{40}]\cdot 2DMF$ (**4**) excluding lattice solvent molecules and hydrogen atoms.

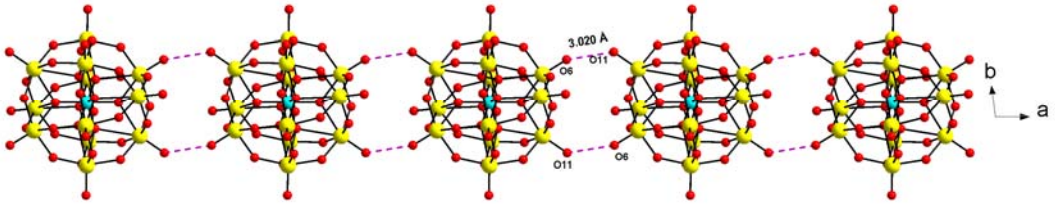

Figure 5.16. The view along the crystallographic '*c*' axis represent, one dimensional chain propagates through O H···O hydrogen bonding interactions. Color code: Mo, yellow; Si, cyan; O, red.

Table 5.8. Geometrical parameters of the C H···O hydrogen bonds (Å, °) involved in supramolecular network of compound $[Mn^{III}L_3(DMF)_2]_4[SiW_{12}O_{40}]$ ·2DMF (**4**) where D=donor; A=acceptor.

D H···A	d(D···H)	d(H···A)	d(D···A)	(DHA
C8 H8B···O6	0.97	2.47	3.18(3)	129.4
C9 H9A···O6	0 97	2.94	3.51(3)	118.1
C10 H10···O15 #2	0.93	2.59	3.39(3)	144.7
C12 H12···O13 #2	0.93	2.46	3.36(2)	162.7
C17 H17···O31 #3	0.93	2.64	3.34(7)	132.9
C18 H18C···O31 #3	0.96	2.31	3.17(10)	148.1
C18 H18A···O1 #4	0.96	2.79	3.36(5)	119.1
C21 H21A···O14	0.96	2.82	3.54(3)	132.7
C21 H21C···O16 #2	0.96	2.51	3.38(3)	149.7
C21 H21A···O19 #5	0.96	2.70	3.58(4)	151.3
C27 H27···O5 #6	0.93	2.61	3.34(3)	136.6
C29 H29···O5 #6	0.93	2.59	3.39(2)	144.3
C30 H30A···O16 #7	0.97	2.58	3.53(3)	165.3
C31 H31B···O11 #5	0.97	2.41	3.07(3)	124.9
C34 H34···O20	0.93	2.40	3.29(3)	159.9
C39 H39···O27 #8	0.93	2.80	3.35(3)	119.0
C40 H40C···O28 #8	0.96	2.54	3.44(3)	156.2
C40 H40B···O24#3	0.96	2.58	3.35(3)	136.9
C41 H41B···O23 #3	0.96	2.57	3.50(3)	165.7
C44 H44C···O16 #7	0.96	2.74	3.47(4)	133.9
C46 H46A···O11 #5	0.97	2.74	3.32(4)	119.1
C47 H47B···O1	0.96	2.89	3.40(7)	114.6

Symmetry transformations used to generate equivalent atoms: #1 -x, 1-y, 1-z; #2 -1+x, y, z; #3 1-x, -y, 1-z; #4 -x, -y, 1-z; #5 1-x, 1-y, 1-z; #6 1+x, y, z; #7 2-x, 1-y, 2-z; #8 2-x, -y, -z.

The symmetry operator involved in generating the equivalent atom is –x, 1–y, 1–z. The weak C H···O hydrogen bonding interactions affords the additional stability to the framework. The relevant C H···O hydrogen bonding interaction parameters are listed in Table 5.8.

5.4. Conclusion

A series of (compounds **1** **4**) polyoxometalate cluster anion and Mn(III) ion-pair complexes were synthesized from salen Schiff-base derivatives with N_2O_4 coordination environment. The oxidation state of manganese was confirmed by EPR, CV and BVS calculations. The combination of UV-visible absorbance studies evidences the inter molecular charge transfer transitions (LMCT) from imine nitrogen to Mn(III) ion. The EPR spectral features (g 2) are consistent with a Mn(III) complex. The title compounds exhibit a irreversible (compounds **1** and **2**) and quasi reversible (compounds **3** and **4**) negative redox wave in the cyclic voltammograms corresponding to Mn(III) / Mn(II) couple. This behavior indicating the ability of the Schiff-bases H_2L_1, H_2L_2 and H_2L_3 to stabilize the higher oxidation states of manganese ions. All the compounds are unambiguously characterized by single crystal X-ray diffractometer. Interestingly, mononuclear (compounds **1**, **3** and **4**), dinuclear (compound **2**) and tetranuclear (compound **1**) of Mn(III) ions are observed in the crystal structures. In all the compounds, Mn(III) ions are in octahedron geometry, and terminal coordination positions are satisfied by *N,N*-dimethyformamide ligand. We have also demonstrated weak supramolecular O H···O and C H···O hydrogen bonding interactions noticed in the crystal structures. These supramolecular interactions are responsible for the formation of one dimensional chains, channels etc., in the crystal structures. Manganese coordination complexes are well known as "Single Molecule Magnet" in the literature and pioneer work has been done by George Christou and co-workers[17] in this area of research. The above mentioned

compounds (**1 4**) are varied in the number of manganese metal centers, the relevant low temperature magnetic susceptibility measurement will be an interesting study, which will be made in near future. Mn(III)-Salen complexes[18] and polyoxometalate clusters[19]are known as potential catalyst for the epoxidation of olefins. Subsequently the combination of Mn(III) salen complexes and POM cluster anion may show an interesting catalytic applications in the area of epoxidation of olefins and related further studies are in progress.

5.5. References

1. a) H. Schiff, *Ann. Suppl*., **1864**, *3*, 343; b) A. Combes, *C. R. Acad. Fr.* **1889**, *108*, 1252.
2. a) R. A. Sheldon, J. K. Kochi, *Metal Catalysed Oxidations of Organi Compounds*, Academic Press, New York, **1981**, p. 97, 102 and 105; b) P. G. Cozzi, *Chem. Soc. Rev*., **2004**, *33*, 410 and references cited therein.
3. I. Bar Narhum, H. Cohen, R. Neumann, *Inorg. Chem.* **2003**, *42*, 3677.
4. a) M. T. Pope, *Heteropoly and Isopoly Oxometalates*; Springer-Verlag: Berlin, **1983**; b) M. T. Pope, In *Comprehensive Coordination Chemistry* II, Vol 4; Wedd, A. G., Ed.; Elsvier: Oxford, U. K., **2004**; p 635-678; c) C. L. Hill, In *Comprehensive Coordination Chemistry II, Vol 4*; Wedd, A. G., Ed; Elsevier: Oxford, UK, 2**004**, pp 679-758; d) M. T. Pope, A. Müeller, *Angew. Chem., Int. Ed*., **1991**, *30*, 34; e) C. L. Hill, C. M. Prosser-McCartha, *Coord. Chem. Rev*., **1995**, *143*, 407; f) C. L. Hill, (ed.) *Chem. Rev.,* **1998**, *98*, 1; g) Y. Izumi, K. Urabe, M. Onaka., *Zeolites*, *Clay and Heteropolyacid in Organic Reactions. Kondashal. Tokyo*, **1992**; h) M. I. Khan, E. Yohannes, R. J. Doedens, *Inorg. Chem.*, **2003**, *42*, 3125.
5. a) S. Biswas, K. Mitra, C. H. Schqalbe, C. R. Lucas, S. K. Chattopadhyay, B. Adhikary, *Inorg. Chim. Acta,* **2005**, *358*, 2473; b) J. E. Penner-Hahn, *Metal sites*

in proteins and models, H. A. O. Hill, P. J. Sadler, A J., Ed: Thomson: Springer-Verlag, **1998**; c) J. Limburg, V. A. Szalai, G. W. Brudvig, *J. Chem. Soc., Dalton Trans.* **1999**, 1353.

6. a) A. T. Tan, R. C. Woodworth, *J. Polym. Sci (C)* **1970**, *599*, 22; b) P. R. Aisen, A. G. Aasa, J. Redfield, *J. Biol. Chem.* **1969**, *244*, 4628; c) M. C. J. Scrutton, *J. Biol. Chem.* **1971**, *10*, 3897; d) G. H. Reed, M. Cohn, *J. Biol. Chem.* **1970**, *245*, 662; e) M. C. Scrutton, M. F. Utter, A. J. Mildvan, *J. Biol. Chem.* **1966**, *241*, 348; f) B. B. Keele, J. McCord, I. Fridovich, *J. Biol. Chem,* **1970**, *245*, 6176.
7. C. Rocchiccioli Deltcheff, M. Fournier, R. Franck, R. Thouvenot, *Inorg. Chem.* **1983**, *22*, 207.
8. a) *SAINT: Software for the CCD Detector System*; Bruker Analytical X-ray Systems, Inc.: Madison, WI, 1998; b) G. M. Sheldrick, *SHELXS-97*, *Program for Structure Solution*; University of Göttingen: Göttingen, Germany, 1997; c) G. M. Sheldrick, *SHELXL-97*, *Program for Crystal Structure Analysis*; University of Göttingen: Göttingen, Germany, 1997.
9. K. Brandenburg, *DIAMOND Version 2.1e*, Crystal Impact GbR, Bonn, Germany, **2001**.
10. a) L. Boucher, *J. Inorg. Nucl. Chem*. **1974**, *36*, 531; b) J. Chakraborty, B. Samanta, G. Pilet, S. Mitra, *Struct. Chem* **2006**, *17*, 585.
11. a) K. P. Bryliakov, O. A. Kholdeeva, M. P. Vanina, E. P. Talsi, *J. Mol. Catal. A*: *Chem*. **2002**. *178*. 47; b) K. A. Campbell, M. R. Lashley, J. K. Wyatt, M. H. Nantz, R. D. Britt, *J. Am. Chem. Soc*. **2001**, *123*, 5710
12. a) M. R Bermejo, A. Castiñeiras, J. C. G. Monteagudo, M. Rey, A. Sousa, M. Walkinson, C. A. McAuliffe, R. G. Pritchard, R. L. Beddoes, *J. Chem. Soc., Dalton Trans.* **1996**, 2935; b) M. Maneiro, M. R. Bermejo, A. Sousa, M. Fondo, A. M. González, A. S. Pedrares, C. A. McAuliffe, *Polyhedron*, **2000**, *19*, 47; c)

A. Panja, N. Shaikh, M. Ali, P. Vojtišek, P. Banerjee, *Polyhedron*, **2003**, *22*, 1191.

13. M. Maneiro, M. R. Bermejo, A. Sousa, M. Fondo, A. M. Gonzalez, A. Sousa-Pedrares, C. A. McAuliffe, *Polyhedron*, **2000**, *19*, 47.
14. a) K. Wieghardt, *Angew. Chem., Int. Ed. Engl.* **1989**, *28*, 1153; b) V. K. Yachandra, K. Sauer, M. P. Klein, *Chem. Reg.* **1996**, *96*, 2927.
15. a) W. F. Ruttinger, C. Campana, G. C. Dismukes, *J. Am. Chem. Soc.* **1997**, 119, 28, 6670; b) M. N. C. Dunand-Sauthier, A. Deronzier, A. Piron, X. Pradon, S. Menage, *J. Am. Chem. Soc.* **1998**, *120*, 5373; c) L. Stelzig, A. Steiner, B. Chansou, J. P. Tuchages, *Chem. Commun.* **1998**, 771.
16. a) H. Sommer, R. Hoppe, *Z. Anorg. Allg. Chem.* **1977**, *429*, 118; b) M. Schulz-Dobrick, M. Jansen, *Inorg. Chem.* **2007**, *46*, 4380.
17. a) A. Mishra, W. Wernsdorfer, K. A. Abboud, G. Christou, *Inorg. Chem.* **2006**, *45*, 10197; b) J. Yoo, E. K. Brechin, A. Yamaguchi, M. Nakano, J. C. Huffman, A. L. Maniero, L C. Brunel, K. Awaga, H. Ishimoto, G. Christou, D. N. Hendrickson, *Inorg. Chem.* **2000**, *39*, 3615; c) E. Libby, R. J. Webb, W. E. Streib, K. Folting, J. C. Huffman, D. N. Hendrickson, G. Christou, *Inorg. Chem.* **1989**, *28*, 4037; d) S. M. J. Aubin, M. W. Wemple, D. M. Adams, H L. Tsai, G. Christou, D. N. Hendrickson, *J. Am. Chem. Soc.* **1996**, *118*, 7746; e) A. Sieber, D. Foguet Albiol, O. Waldmann, S. T. Ochsenbein, R. Bircher, G. Christou, F. Fernandez Alonso, H. Mutka, H. U. Gudel, *Inorg. Chem.* **2005**, *44*, 6771; f) G. Aromí, M. J. Knapp, J P. Claude, J. C. Huffman, D. N. Hendrickson, G. Christou, *J. Am. Chem. Soc.* **1999**, *121*, 5489; g) C. J. Milios, R. Inglis, A. Vinslava, R. Bagai, W. Wernsdorfer, S. Parsons, S. P. Perlepes, G. Christou, E. K. Brechin, *J. Am. Chem. Soc.* **2007**, *129*, 12505.
18. a) T. Katsuki, *J. Mol. Catal. A.* **1996**, *113*, 87; b) E. N. Jacobsen, *Asymmetric Catalytic Epoxidation of Unfunctionalized Olefins*. In Catalytic Asymmetric

Synthesis; Ojima, I., Ed.; VCH Publishers: New York, **1993**; pp 159-202; c) G. R. Stephenson, *Asymmetric Oxidation. In Advanced Asymmetric Synthesis;* G. R., Stephenson, Ed.; Chapman & Hall: New York, **1996**, pp 367-391; d) K. A. Jørgensen, *Chem. Rev*. **1989**, *89*, 431.

19. a) T. Sakamoto, C. Pac, *Tetrahedron Lett.* **2000**, *41*, 10009; b) A. Lambert, P. Plucinski, I. V. Kozhevnikov, *Chem. Commun.* **2003**, 714; c) R. Prabhakar, K. Morokuma, C. Hill, D. G, Musaev, *Inorg. Chem.* **2006**, *45*, 5703.

****

==========

Influences of Supramolecular Interactions in Polyoxometalate Chemistry

==========

6.1. Introduction

The rational design of novel polyoxometalate (POM) based solid state materials fascinates synthetic chemists because of their potential applications in diverse research areas, such as catalysis, medicinal chemistry, and materials science.[1] Since the POM clusters are anionic in nature, simply by changing the counter cation, novel materials can be achieved from an aqueous medium. For example, an isolated derivative of ammonium heptamolybdate $[NH_3Pr^i]_6[Mo_7O_{24}]$. $3H_2O$ has been found to have potent antitumor activity, and synthesized Keggin derivative $K_3[Cr_3O(OOCH)_6(H_2O)_3][SiW_{12}O_{40}]$. $16H_2O$ shows applications in adsorption of small alcohols.[2] One of the applicable strategies to obtain the POM-based hybrid materials is to exploit the organic molecules as cations that can act as structure-directing components.[3] POM–based organic-inorganic hybrid solids have been constructed either by electrostatic interactions between inorganic and organic components or by the formation of covalent bonds between organic and inorganic moieties.[4] The introduced structure directing organic components are mostly organic amines that can easily act as cations (by protonation) for charge compensation and hence stabilize the POM cluster through supramolecular interactions.[5] Previously reported pyridine 'N' ligands based POMs were mostly synthesized by hydrothermal techniques.[6] In this chapter, we have introduced 2-aminopyrimidine (for compound **1**) and (*R,R*)-*trans*-1,2-cyclohexyldiamine (for compound **2**) as an organic component which not only acts as the cation (on protonation) to stabilize an isopolyanion but also plays a significant role in assembling the isopolyanions (POM) leading to a multi dimensional

supramolelcular arrangement offering N H···O and C H···O hydrogen bonds. We have also observed non-covalent O···O interactions among the POM anions using a cis-{MoO_2} moiety. The non-covalent O···O interactions are well-established in the literature including their theoretical aspects. There are reports on O···O contacts that are a consequence of the N···O contacts in aromatic nitro derivatives.[7] O···O non-covalent interactions are also known to be responsible for the sulfate anion helices.[8] However, inter-POM cluster O···O contacts were not surveyed prior to this work.[9] We describe here a new type of multi dimensional supramolecular structures of an organic-inorganic hybrid compounds $[2\text{-AmpH}]_4[Mo_8O_{26}]$ (**1**) and $[CyclohexH_2]_2[Mo_8O_{26}]$ (**2**) which are formed by supramolecular self assembly. We have emphasized the O···O interactions among POM anions and stress the role of N H···O and C H···O hydrogen bonds. We have also demonstrated the helical features, observed in the crystal structure of compound **1**.

Chiral polyoxometalates are playing an important role in biomedical chemistry and catalysis.[10] An excellent review was published very recently, whereby an outline on chirality in polyoxometalate chemistry from historical to the present have been discussed well.[11] Eventhough, the number of polyoxometalates with chiral structures[12] is not limited, only a limited number of studies have focused on polyoxometalate-chirality.[13] This is because, many of these chiral structures undergo rapid racemization via water exchange, partial hydrolysis, or fluxional behavior.[12a]

In this chapter we also report the optical resolution of a Strandberg type heteropolyanion $[S_2Mo_5O_{23}]^4$ by using Pfeiffer effect, an effect in which, the displacement of a racemate equilibrium occurs in favor of one enantiomer on treating with an enantiopure optically active compounds *l*- or *d*- forms of arabinose (known as environment substance). For a Pfeiffer effect[14] to be observed, the racemic mixture must be optically labile in the presence of an environment substance. In Pfeiffer-active heteropolyanion-systems, which have been reported as yet, only one enantiomer has been

observed depending on *l*- or *d*- form of an environment substance, used in the relevant chiral discrimination reactions.[13b,c,d]

6.2. Experimental Section

6.2.1. Materials

Sodium molybdate dihydrate was purchased from Finar and used as such. (*R,R)-trans*-1,2-diaminocyclohexane was resolved from the cis-trans mixture of 1,2-diaminocyclohexane by following the reported procedure[15]. Arabinose (*l*- and *d*- forms) were purchased as analytical grade and used without any further purification. The distilled water was used throughout the crystallization experiments and acetonitrile solvent obtained as laboratory grade. Spectroscopic analysis was carried out by using HPLC grade DMSO solvent.

6.2.2. Physical Measurements

Micro-analytical (C, H, N and S) data were obtained with Perkin-Elmer Model 240C elemental analyzer and FLASH EA 1112 Series CHNS analyzer. Infrared spectra (IR) were recorded by using KBr pellets on a JASCO-5300 FT-IR spectrophotometer in the region of 400 4000 cm^{-1}. The TGA-Mass analysis were performed on a NETZSCH – STA 409PC with NETZSCH-QMS 403C (Aëolos) mass setup at a scan rate of 5^{o}C. The CD spectra were measured on a JASCO J – 810 spectropolarimeter.

6.2.3. Synthesis and Characterization

The compounds described in this chapter are:

1. $[2\text{-AmpH}]_4[Mo_8O_{26}]$ (**1**)
2. $[CyclohexH_2]_2[Mo_8O_{26}]$ (**2**)
3. Spectroscopic observation for the displacement of a racemate equilibrium in Strandberg-type heteropolyanion $[S_2Mo_5O_{23}]^4$ by a Pfeiffer effect using *l*- and *d*-forms of arabinose as enantiopure environment substances.

Synthesis of $[2\text{-AmpH}]_4[Mo_8O_{26}]$ (1)

Sodium molybdate dihydrate (1 g, 4.13 mmol) was dissolved in 20 mL of water, in which 10 mL of acetic acid was added. To this, a mixture of 0.5 g zinc(II) nitrate hexahydrate (1.68 mmol) and 0.22 g of 2-aminopyrimidine (2.31 mmol) in 20 mL of acetonitrile was added slowly and its pH was adjusted to 2 by conc. HCl. The final reaction mixture was stirred for 6 hours at room temperature. During this time, little turbidity appeared in the reaction mixture, which on heating at around 50 60^oC was dissolved and stirring was continued for another 15 hours. The clear solution was kept open in beaker at room temperature for 2 3 days, whereby colorless crystals appeared were collected by filtration and washed with cold water and finally dried at room temperature. Yield 0.25 g (31 % based on Mo). Anal. calcd. for $C_{16}H_{24}Mo_8N_{12}O_{26}$: C, 12.25; H, 1.54; N, 10.72%. Found: C, 12.22; H, 1.52; N, 10.85%.

IR (KBr pellet): (υ/cm^{-1}): 3327(s), 3229(s), 3163(s), 3107(m), 1865(s), 1662(m), 1622(s), 1539(s), 1456(s), 1342(s), 1203(s), 1068(s), 945(m), 902(m), 688(m), 501(s).

Resolution of 1,2-diaminocyclohexane

A reported procedure was followed for the resolution of the of cis-trans mixture of 1,2-diaminocyclohexane.[15] A 250 mL beaker was charged with *L*(+)-tartaric acid (37.5 g, 250 mmol) and distilled water (100 mL). The mixture was stirred at room temperature

until complete dissolution occurred. At this point, a mixture of *cis/trans*-1,2-diaminocyclohexane (60 mL, 500 mmol) was added at a rate such that the reaction temperature is below 70˚C. To the resulting solution, glacial acetic acid (25 mL) was added at a rate such that the reaction temperature is below 90˚C. The precipitate formed immediately upon the addition of glacial acetic acid and the slurry was vigorously stirred. It was cooled to 25˚C over a period of 2 hours. The mixture was cooled to 5˚C for 2 hours and the precipitate was collected by suction filtration. The wet cake was washed with cold water (25 mL) followed by cold methanol till the cake turned to white solid. The product was dried to obtain (*R,R*)-*trans*-1,2-diammoniumcyclohexane mono-(+)-tartrate salt. Yield: 111 g (85%).

The (*R,R*)-*trans*-1,2-diammoniumcyclohexane mono-(+)-tartarate salt (42 g, 159 mmol) was taken in a separatory funnel. Approximately, 30 g of KOH dissolved in water (20 mL) was added. It was shaken well and the amine layer was separated. The (*R,R*)-*trans*-1,2-diaminocyclohexane was distilled under reduced pressure.

Synthesis of [CyclohexH$_2$]$_2$[Mo$_8$O$_{26}$] (2)

Copper nitrate dihydrate (0.5 g, 2.06 mmol) was dissolved in 50 mL of acetonitrile in which 0.35 g (3.07 mmol) of (*R,R*)-*trans*-1,2-cyclohexyldiamine was added drop wise and the resulting violet color turbid solution was stirred for half an hour. To this, a mixture of 1.0 g Sodium molybdate dihydrate (4.13 mmol) and 10 mL of acetic acid in 20 mL of water was added quickly. The resulting reaction mixture was stirred for one hour and later pH was adjusted to 2.50 by Conc. H_2SO_4 and stirring was continued for another half an hour with occasional heating at 80^{o}C. The light blue color turbid solution was filtered and kept open for crystallization without any external disturbance. The colorless crystals grown from the mother liquor was filtered and washed with cold water and finally dried at room temperature, one among the suitable quality crystal was

selected for X-ray diffractometer study. Yield 0.20 g (26 % based on Mo). Anal. calcd. for $C_{12}H_{40}N_4Mo_8O_{30}$: C, 9.69; H, 2.71; N, 3.77 %. Found: C, 9.71; H, 2.68; N, 3.70 %. IR (KBr pellet): (υ/cm^{-1}): 3303(br), 3113(br), 2934(m), 1716(s), 1649(s), 1612(s), 1521(s), 1489(s), 1140(s), 1082(s), 1020(s), 949(s), 898(s), 837(s), 671(m), 557(s), 516(s).

6.2.4. Single Crystal Structure Determination

The crystallographic data for compound **1** and **2** have been collected at 293 K on Bruker SMART APEX CCD, area detector system [λ(Mo Kα) = 0.7103 Å], graphite monochromator, 2400 frames were recorded with an ω scan width of 0.3°, each for 10s, crystal-detector distance 60 mm, collimator 0.5 mm. Data reduction by SAINTPLUS,[16a] absorption correction using an empirical method SADABS,[16b] structure solution using SHELXS-97,[16c] and refined using SHELXL-97.[16d] All non hydrogen atoms were refined anisotropically. The hydrogen atoms of the protonated nitrogen were located in the differential Fourier maps and were refined using isotropic thermal parameters. The DIAMOND[17] software was used for molecular graphics. For compounds **1** and **2**, the water hydrogen atoms are not located in its crystal structure analyses. Hydrogen bonding interactions were discussed based on O···O, C···O and N···O contacts. A summary of the crystallographic data and structural determination for compounds **1** and **2** is provided in Table 6.1.

6.3. Results and Discussion

6.3.1. Infrared Spectroscopy

Generally, inorganic-organic hybrid compounds are obtained through the hydrothermal synthesis route. But we have synthesized the title compound $[2\text{-AmpH}]_4[Mo_8O_{26}]$ (**1**) from a simple wet synthesis that includes a low pH aqueous

solution of sodium molybdate, acetic acid, zinc nitrate and the organic molecule, 2-aminopyrimidine. The formation of the cluster anion $[Mo_8O_{26}]^4$ in the acidic aqueous molybdate solution is not surprising but surprisingly, the isolated compound **1** does not contain zinc ion; instead the cluster anion is stabilized by the 2-aminopyrimidinium cation. The protonation on pyrimidine molecule is expected in this low pH. We could not isolate compound **1**, without using Zn^{2+} ion in the relevant synthesis. In this synthesis, the role of zinc ion is not clear. However, we speculate that, first the cluster anion is stabilized by Zn^{2+} ions in the solution state and then during isolation / crystallization the Zn^{2+} ions are replaced by 2-aminopyrimidinium cations. The infrared spectrum of compound **1** exhibited characteristic broad feature of (Mo O Mo) in the region of 650 700 cm^{-1}. The strong peaks at 902 and 945 cm^{-1} are attributed to the vibrations of Mo=O bonds. Comparison of the IR spectra of 2-aminopyrimidine and compound $[2\text{-AmpH}]_4[Mo_8O_{26}]$ (**1**) clearly shows the presence of 2-aminopyrimidinium cation in compound **1.**

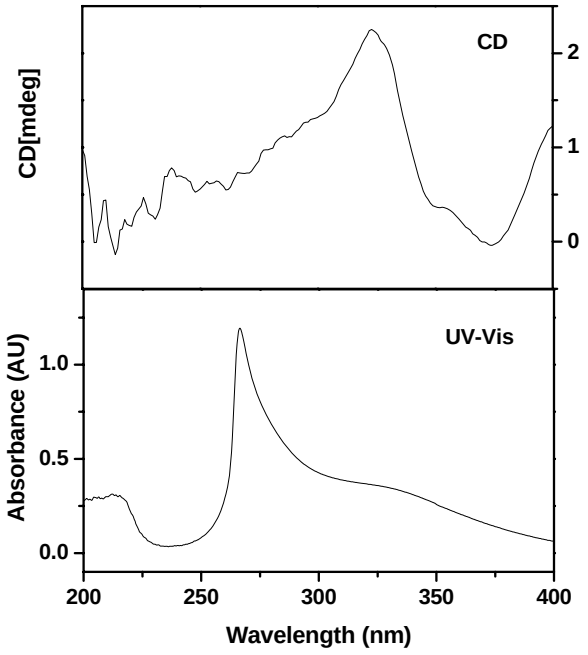

Figure 6.1. The solid state circular dichroism spectrum of compound **2** (top) and electronic absorbance spectrum (bottom) of compound **2** in DMF solution (1.0 x 10^{-4}M).

The IR data for compound (**2**) are given in the experimental section. The stretching frequencies obtained in the range of 3000 3150 cm^{-1} are mostly due to the N H stretching of NH_3^+ group. Broad peaks in the region of 3500 cm^{-1} are assigned to the O H stretching from water molecules. The aliphatic C H stretching appeared at 2934 cm^{-1}. The strong peaks in the range of 900 945 cm^{-1} are mainly due to the vibrations of Mo=O bonds. The isolated compound **2** does not contain copper ion, however we could not isolate compound **2**, without using Cu^{2+} ion in the relevant synthesis. In this synthesis, the role of copper ion is not clear.

6.3.2. Electronic absorbance and Circular Dichroism Spectroscopy

The electronic absorbance spectrum of compound **2** in DMF solution shows two electronic absorption bands around 325 nm (ε =3573) and 266 nm (ε =11890). The shoulder around 325 nm assigned to charge transfer transition from (*R,R)-trans*-1,2-diaminocyclohexane to $[Mo_8O_{26}]^4$ cluster anion. The strong absorbance peak at 266 nm is characteristic peak for oxygen to molybdenum charge transfer transition (LMCT).

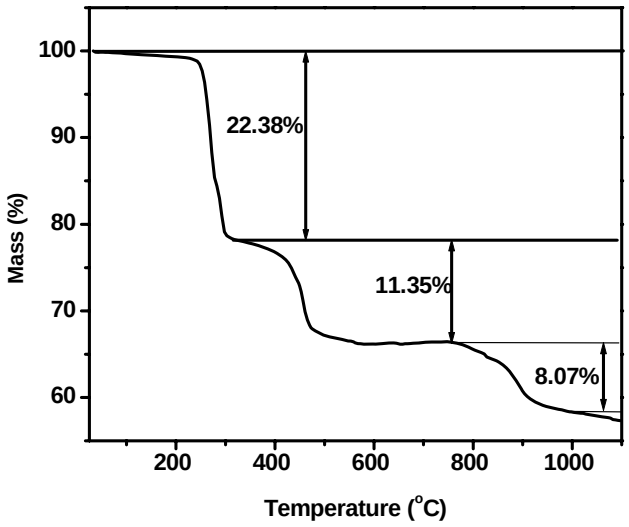

Figure 6.2. TGA plot of compound $[2\text{-AmpH}]_4[Mo_8O_{26}]$ (**1**).

The corresponding solid state circular dichroism spectrum of compound **2** shows positive Cotton effect, corresponding to the electronic (charge transfer) transition at 322 nm. The corresponding electronic absorbance and circular dichroism spectra of compound **2** is presented in the Figure 6.1.

6.3.3. Thermogravimetric / Mass Analyses (TGA /Mass)

The thermogravimetric analysis for compound **1** was performed in flowing nitrogen with a heating rate of 5^{o}C per minute in the temperature range from 30 to 1100^{o}C. The TGA curve (Figure 6.2.) shows the first weight loss of 22.38% in the temperature range of 200 ─ 300^{o}C. This corresponds to the loss of four 2-aminopyrimidine molecules (calculated 24.26%) per formula unit. Since the compound $[2\text{-AmpH}]_4[Mo_8O_{26}]$ (**1**) has four 2-aminopyrimidium cations per formula unit, the remaining two stages of the TG curve, that occur between 350 to 1100^{o}C, have been assigned due to the decomposition of the POM cluster anion, which we did not attempt to take into account.

6.3.4. X-ray Crystallographic Studies

Crystal Structure Description of $[2\text{-AmpH}]_4[Mo_8O_{26}]$ (1)

Single-crystal X-ray diffraction analysis of **1** revealed the presence of half of the octamolybdate isopolyanion and two mono-protonated 2-aminopyrimidinium cations in

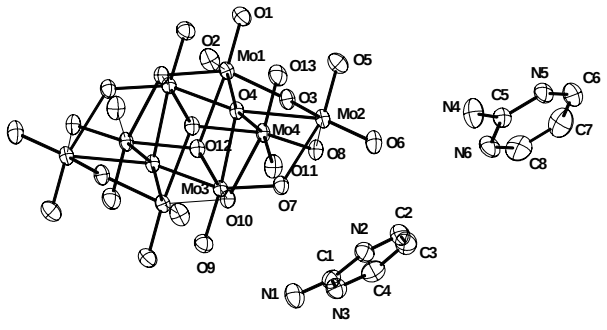

Figure 6.3. Thermal ellipsoid plot of the asymmetric unit of compound $[2\text{-AmpH}]_4[Mo_8O_{26}]$ (**1**) with 50% probability. Full molecule of octamolybdate (half of this is in the asymmetric unit) is shown in which hydrogen atoms were omitted for clarity.

its asymmetric unit. Thus the formula unit contains one full cluster anion and four mono-protonated 2-aminopyrimidinium cations and accordingly it is formulated as $[(2\text{-AmpH})_4][Mo_8O_{26}]$ (**1**). The thermal ellipsoidal representation of compound **1** is shown in Figure 6.3**.**

Table 6.1. Crystal Data and Structural Refinement for Compounds **1** and **2**

	1	**2**
Empirical formula	$C_{16}H_{24}Mo_8N_{12}O_{26}$	$C_{12}H_{40}Mo_8N_4O_{30}$
Formula weight	1567.99	1488.00
T [K]	293(2)	293(2)
λ [Å]	0.71073	0.71073
Crystal system	Triclinic	Monoclinic
Space group	*P 1*	*P2(1)*
a [Å]	9.925(3)	8.7472(6)
b [Å]	10.020(3)	20.3478(14)
c [Å]	10.414(3)	9.9677(7)
deg]	88.811(4)	90.000
β [deg]	64.907(4)	91.2880(10)
deg]	89. 506(4)	90.000
V [Å^3]	937.7(5)	1773.7(2)
Z	2	2
D_{calc} [Mg m^{-3}]	2.777	2.786
μ [mm^{-1}]	2.696	2.843
F[000]	748	1432
Crystal size [mm^3]	0.44 x 0.32 x 0.22	0.18 x 0.12 x 0.06
θ range for data collection [deg]	2.03 to 28.17	2.00 to 26.03
Reflections collected/unique	10693 / 4309	18605 / 6918
R [int]	0.0183	0.0287
Refinement method	Full-matrix least-squares on F^2	
Data/restraints/parameters	4309 / 0 / 324	6918 / 1 / 527
Goodness-of-fit on F^2	1.125	1.059
R_1/wR_2 [$I > 2\sigma(I)$]	0.0231/0.0590	0.0287/0.0622
R_1/wR_2 (all data)	0.0251/0.0601	0.0320/0.0636
Largest diff. Peak/hole [e Å ^{3}]	0.470/-0.975	0.510/-0.494

In the crystal structure, the octamolybdate cluster anion $[Mo_8O_{26}]^{4-}$ is composed of eight edge-sharing $\{MoO_6\}$ octahedra, in which a $\{Mo_6O_6\}$ ring is capped on opposite faces by two MoO_6 octahedra. Generally in such POM cluster, the {Mo O} groups can be classified into four categories: 14Mo O_t (O_t = terminal oxygen) with the bond lengths in the range of 1.687 1.715 Å; six μ_2-type bridged Mo O_b (O_b = bridging oxygen) with bond distances in the range of 1.747 2.263 Å; four μ_3-type Mo-O_b bonds that are in the range of 1.940 2.342 Å and two μ_5-type of Mo O_b with the bond lengths in the range of 2.158 2.501 Å.

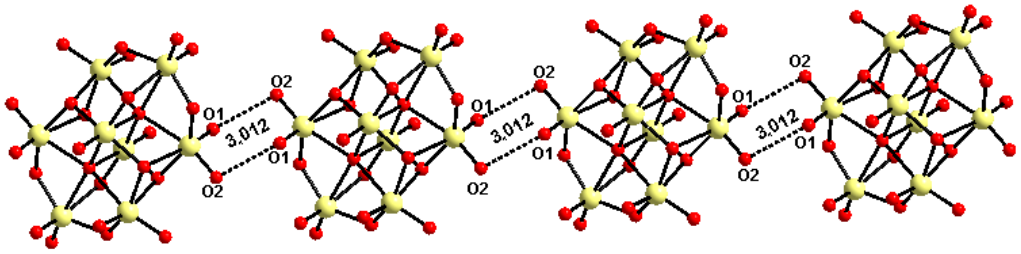

Figure 6.4. O···O non-covalent interactions among the isopolyanions $[Mo_8O_{26}]^4$ leading to a chain like structure.

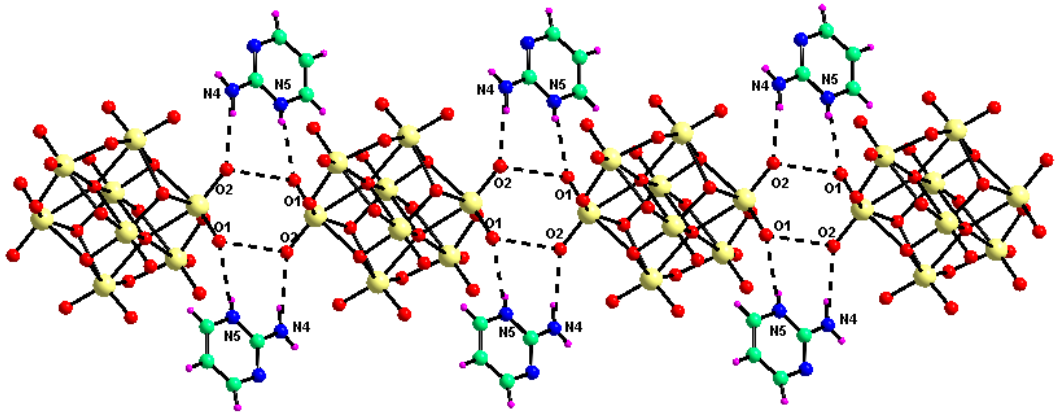

Figure 6.5. 2-aminopyrimidinium cations (named as 'N4N5N6') assist the formation of the chain by exerting N H···O hydrogen bonds. Color code: O, red; Mo, yellow; C, green; H, purple; N, blue; dotted lines represent the hydrogen bonding interactions.

Interestingly, in the crystal structure, the *cis* dioxo group (O1 and O2) of Mo1 (there are two Mo1, because it is a centro-symmetric cluster) of one $[Mo_8O_{26}]^{4-}$ cluster anion directly interacts to its two adjacent neighboring $[Mo_8O_{26}]^{4-}$ cluster anion using same *cis*- $\{MoO_2\}$ leading to a chainlike arrangement (Figure 6.4). In the linking region, O1 faces O2 and O2 faces O1 and so on as shown in Figure 6.5. This O···O interaction is characterized by the O/O separation of 3.012 Å, which is in the range of hydrogen bonding distance. The careful examination of packing of the molecules in the crystal structure of compound **1** demonstrates that 2-aminopyrimidinium cation, $[2\text{-AmpH}]^+$ plays a significant role in bringing the isopolyanions closer (in the range of hydrogen bonding distance) to accomplish O···O non-covalent interaction involving the above mentioned *cis* $\{MoO_2\}$ moieties of the adjacent isopolyanions. The role of the 2-aminopyrimidinium cation on isopolyanion --- isopolyanion O···O interaction is schematically presented in Scheme 1. This clearly shows how a pyrimidinium cation, using its two arms (X^+─H and Y─H) separated by two C─N bonds, fetches two POM anions nearer by forming strong hydrogen bonds with the oxo groupsthat are involved in O···O contact (Scheme 1). Figure 6.5 shows the real situation of the chainlike arrangement that is formed by the assistance of the 2-aminopyrimidinium cation, $[2\text{-AmpH}]^+$. The linking region involves two $[2\text{-AmpH}]^+$ cations (from two sides of the chain). It is interesting to note that O1 is hydrogen bonded to the ring nitrogen and O2 is linked to NH_2 hydrogen by N H···O hydrogen bonds. The ring nitrogen atom is more basic in nature than the amine group nitrogen, hence it is not surprising that protonation occurs on the ring nitrogen atom only. It is worth mentioning that $[Mo_8O_{26}]^4$ cluster anion rarely gets protonate and less competes for hydrogen bonding. Bond valence calculation confirmed that, all the molybdenum atoms are in fully oxidized state (+6). In the present study, the structure directing role is mainly dominated by the organic cations. In the crystal structure, we have observed that there are two crystallographically independent $[2\text{-AmpyH}]^+$. One of these (can be named as 'N4N5N6') is involved in

forming hydrogen bonds (N H···O) involving O1 and O2 that assist the chain formation through non-covalent O···O contacts (Scheme 1 and Figure 6.5). The other crystallographically independent organic cation (named as 'N1N2N3') is attached to the cluster anion in unique manner, i.e., both N3 (ring nitrogen) and N1 (from NH_2 group) of the organic cation undergo hydrogen bonding interactions with O13 terminal oxygen atom of the isopoly anion in a bifurcated fashion (Figure 6.6(a)) This cation is not involved in forming extended hydrogen bonding structure. The immediate hydrogen bonding surrounding / environment of 'N4N5N6' cation is presented in Figure 6.6(b). Figure 6.7 shows an interesting hydrogen bonding environment around a $[Mo_8O_{26}]^4$ cluster anion in the crystal structure.

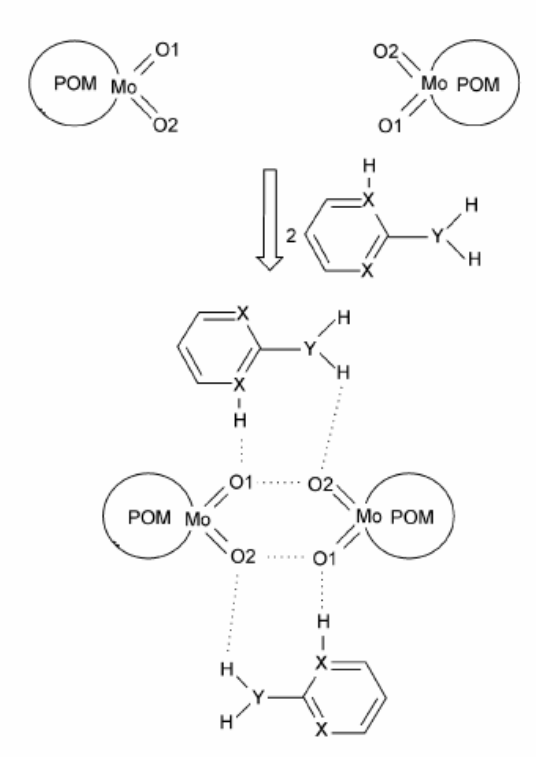

Scheme 1. Depiction of pyrimidinium cations that show the influence on the isopolyanions to come closer and achieve non-covalent O···O interactions among isopolyanions.

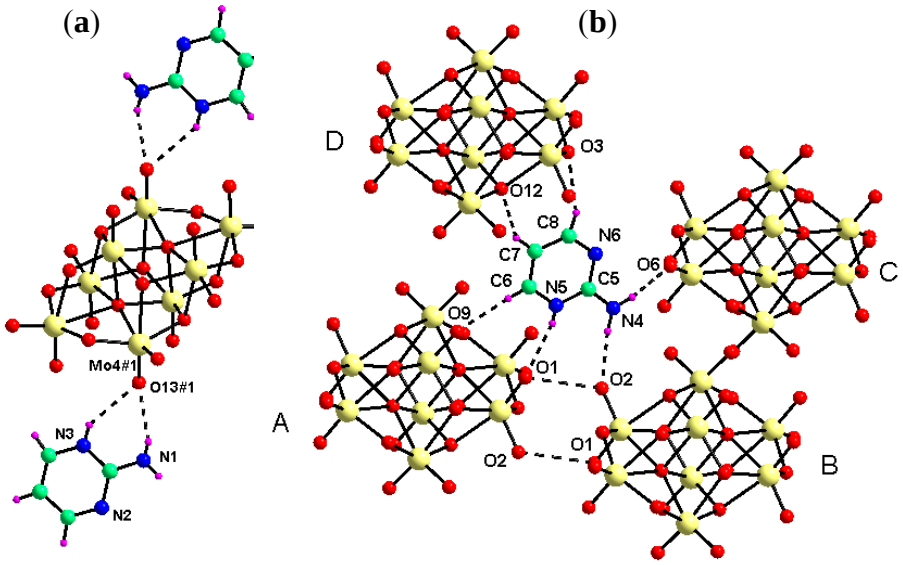

Figure 6.6. (a) One of the cystallographically independent organic cation namely'N1N2N3' exhibiting hydrogen bonding interactions to the cluster anion in a bifurcated manner. (b) The immediate hydrogen bonding environment around 'N4N5N6' cation is presented. Color code: O, red; Mo, yellow; C, green; H, purple; N, blue; dotted lines represent the hydrogen bonding interactions.

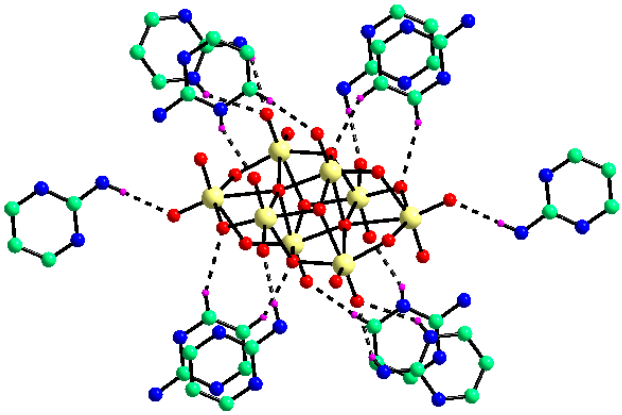

Figure 6.7. Hydrogen bonding environment around a $[Mo_8O_{26}]^4$ cluster anion in the crystal structure of $[2\text{-AmpH}]_4[Mo_8O_{26}]$ (**1**). Color code is same as mentioned in Figure 6.6.

It is remarkable that an isopolyanion interacts with its ten surrounding organic cations (Figure 6.7). Repeating of this motif (Figure 6.7) and the pattern (Figure 6.6b) or combination of both results in the formation of a new type of three-dimensional supramolecular structure having well-defined channels (Figure 6.8).

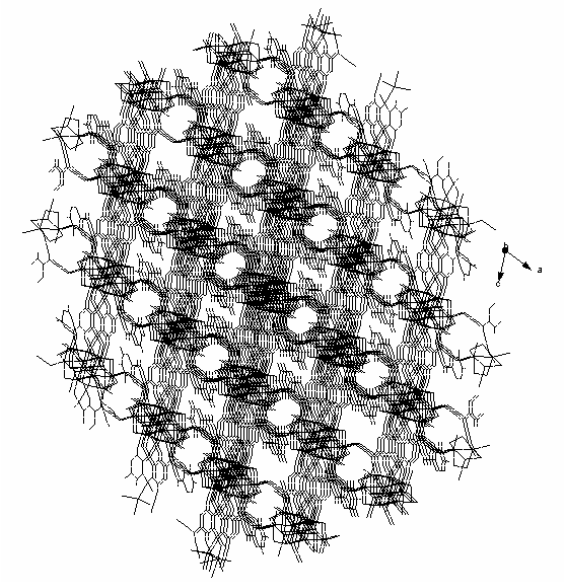

Figure 6.8. The Wire frame representation of the three-dimensional supramolecular structure of [2-AmpH]$_4$[Mo_8O_{26}] (**1**) having well-defined channels.

Careful examination of crystal structure of the title compound shows an interesting helical pattern. Both left and right handed helices are observed, whereby both handed helices are formed by hydrogen bonding interactions between 'N4N5N6' cation and the isopolyanion involving N4 H4A···O2 and N5─H5A···O1 hydrogen bonds (Figures 6.9(a) and 6.9(c)).

Table 6.2. Hydrogen bonding parameters in compound [2-AmpH]$_4$[Mo_8O_{26}] (**1**)

D H···A	d(D···H)	d(H···A)	d(D···A)	(DHA
N4-H4B...O6	0.84(5)	2.10(5)	2.917(3)	166(4)
N1-H1B...O13 #1	0.69(4)	2.21(4)	2.852(3)	155(4)
N3-H3A...O13 #1	0.77(3)	2.35(3)	3.021(3)	146(3)
C7-H7...O12 #2	0.94(4)	2.34(4)	3.180(3)	148(3)
C8-H8...O3 #3	0.93(4)	2.47(4)	3.339(3)	155(3)
N4-H4A...O2 #4	0.86(4)	2.07(4)	2.925(3)	170(4)
N5-H5A...O1 #5	0.70(3)	2.20(3)	2.823(3)	149(3)
C6-H6...O9 #6	0.87(3)	2.20(4)	3.076(4)	176(3)

Symmetry transformations used to generate equivalent atoms: #1 x, y, -1+z; #2 1+x, 1+y, -1+z; #3 1-x, 1-y, 1-z; #4 1+x, y, z; #5 1-x, 1-y, 2-z; #6 1+x, 1+y, z.

Interestingly, both handed helices cross through a common atom (Mo1) resulting in double helical feature (Figure 6.9(b)). The relevant N H···O and C H···O interactions are presented in Table 6.2. These helices run along the chainlike arrangement that is formed by O···O contacts (Figure 6.4), thereby the O···O interactions are naturally observable in the double helical structure (Figure 6.9(b)). Molecular and supramolecular helical arrangements based on inorganic complex / cluster fragments are well documented in literature.[18]

Crystal Structure Description of $[CyclohexH_2]_2[Mo_8O_{26}]$ (2)

Colorless needle shaped crystals of compound **2** were synthesized from an acidic solution containing (*R,R*)-*trans*-1,2-diaminocyclohexane, $Na_2MoO_4 \cdot 2H_2O$ and $Cu(NO_3) \cdot 3H_2O$. Compound **2** is crystallized in monoclinic chiral spacegroup *P2(1)* with all atoms located in the general position. The X-ray crystal structure of **2** shows two diprotonated (*R,R*)-*trans*-1,2-diaminocyclohexane as cation and $[Mo_8O_{26}]^4$ cluster as anion and four lattice water molecules, and there are two such components in the unit cell (Z = 2) and the relevant crystal parameters are given in Table 6.1. Thermal ellipsoidal plot of compound **2** is shown in the Figure 6.10. In crystal structure all the three hydrogen atoms (includes protonation and amine hydrogen) on N2 and N3 are nicely located from difference Fourier maps and their positions were isotropically refined. These located hydrogen atoms are remained stable during successive refinement stages. We couldn't locate hydrogen atoms on N1 and N2 due to the unstablity throughout the successive refinement. Interestingly, amine nitrogen atoms interacts with oxygen atoms (from lattice water molecules and the cluster anion) through strong N H···O hydrogen bonds. Further, weak C H···O hydrogen bonding interactions offer extra stability to the supramolecular framework. It is noteworthy to mention here that the understanding of nature and strength of intermolecular interactions is of fundamental importance in supramolecular chemistry.

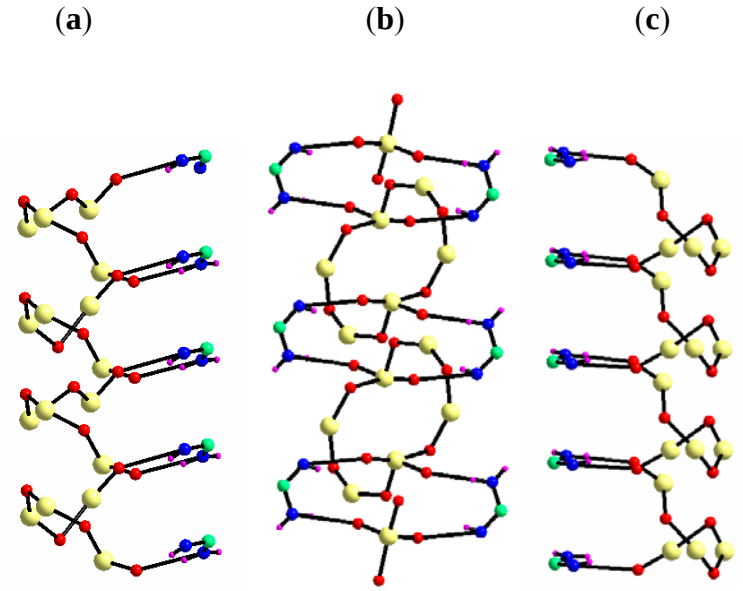

Figure 6.9. Helical arrangement formed from the isopolyanion and 'N4N5N6' organic cation: (a) the ball-and-stick model of the supramolecular left-handed helical backbone. (b) double helical arrangement formed from both left- and right-handed helices (helical backbone is shown). (c) ball-and-stick model of the supramolecular right-handed helical backbone. Color code as shown in Figure 6.6 caption.

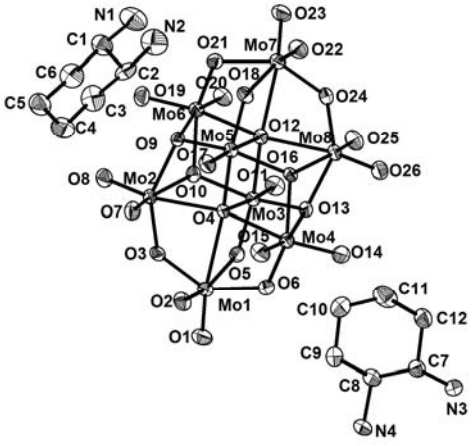

Figure 6.10. Thermal ellipsoidal plot of the compound $[CyclohexH_2]_2[Mo_8O_{26}]$ (**2**) with atom labeling scheme is drawn in 50% probability level. Hydrogen atoms were omitted for clarity.

It is interesting to note that in the crystal structure N1 (amine nitrogen atom from (*R,R*)-*trans*-1,2-diaminocyclohexane) undergoes hydrogen bonding interaction in bifurcation manner with O21 and O25 from two different polyoxomolybdate anionic clusters.

Another amine nitrogen atom N2 from same (*R,R*)-*trans*-1,2-diaminocyclohexane interacts with $[Mo_8O_{26}]^4$ cluster anion through O26. This (*R,R*)-*trans*-1,2-diaminocyclohexane in turn donates its amine hydrogens (via N1 and N2) to oxygen atoms of $[Mo_8O_{26}]^4$ cluster anion and consequently acts as a connecting link between the polyoxometalate cluster anions to form a layered framework as shown in the Figure 6.11. Apart from the above mentioned interactions, the nitrogen N1 and N2 interacted with lattice water molecules O29, O30 and O30, O28, O29 respectively through N H···O hydrogen bonds. The immediate hydrogen bonded environment around N1 and N2 is shown in the Figure 6.12. The second protonated (*R,R*)-*trans*-1,2-diaminocyclohexane nitrogen atom N3 donates its H3D to polyoxometalate cluster oxygen O22 (via N3 H3D···O22) and the same nitrogen atom donates its second hydrogen (H3C) to the adjacent polyoxometalate cluster oxygen atom O2 (via N3 H3C···O2). Another protonated amine nitrogen atom N4 from the same amine undergoes N H···O hydrogen bonding interactions in bifurcation fashion with O7 and O17 from the same polyoxometalate cluster anion. This diprotonated (*R,R*)-*trans*-1,2-diaminocyclohexane (via N3 and N4) acts as a linker in between two adjacent polyoxometalate cluster anion. As a result of this, the formation of supramolecularly hydrogen bonded one dimensional polyoxometalate chain via N H···O hydrogen bonding interaction is shown in Figure 6.13. The protonated amine nitrogen N3 and N4 further interacted with lattice water molecules O28 and O27 respectively. The immediate environment of protonated amine nitrogen atoms N3 and N4 via N H···O hydrogen bonding is presented in Figure 6.12(b). The guest water molecules (non-coordinated water molecules) O27 and O29 interacted with host (polyoxometalate cluster anion) via O3, O15 and O1, O19 respectively by O H···O hydrogen bonding. The other two lattice water molecules O28 and O30 bridged by oxygen atoms O14 and O11 (from host cluster) by supramolecular interaction.

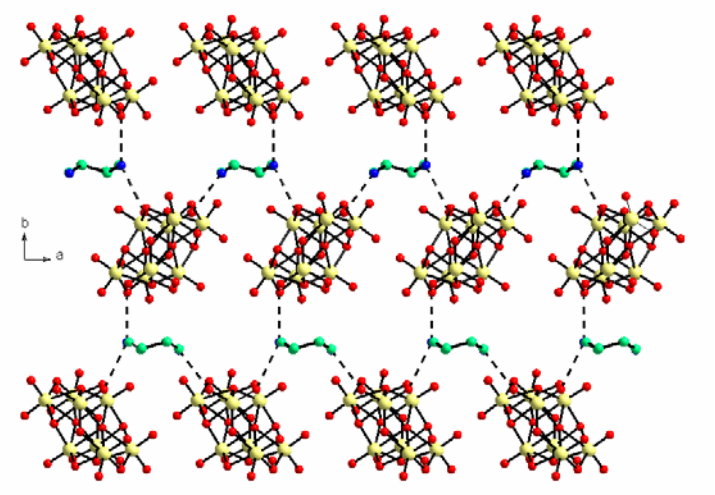

Figure 6.11 Formation of layered framework along *ab* plane via N H···O hydrogen bonds. Color code: Mo, yellow; O, red; C, green; N, blue; black dotted lines represent N H···O hydrogen bonding interactions with $[Mo_8O_{26}]^{4}$.

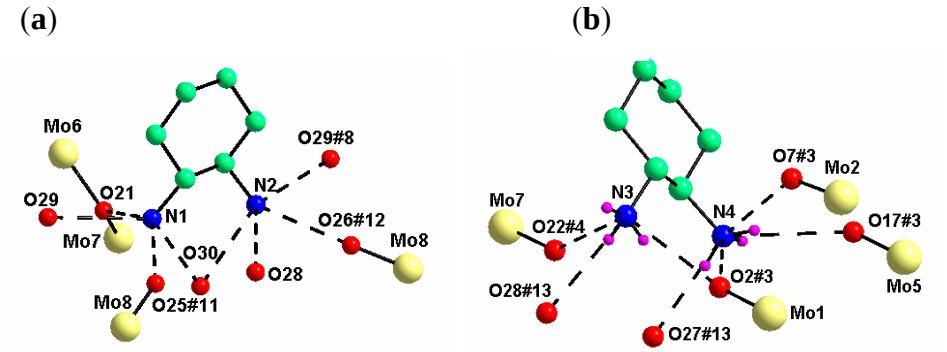

Figure 6.12. (a) N H···O hydrogen bonding environment around N1 and N2 with symmetry codes; (b) N H···O hydrogen bonding environment around N3 and N4 with symmetry codes. Color codes: Mo, yellow; O, red; C, green; N, blue; H, purple; black dotted lines represent N H···O hydrogen bonding interactions.

In addition to these lattice water molecules O28 and O30 made O H···O hydrogen bond with host through O20, O25, O26 and O23 respectively. The relevant N H···O and O H···O (donar to acceptor distance is within 3.1 Å) hydrogen bonding parameters are described in Table 6.3. Along with N H···O and O H···O interactions, C H···O also

offers extra stability to the supramolecular framework and resulting in the formation of complicated three dimensional network. The immediate surrounding of two (*R,R*)-*trans*-1,2-diaminocyclohexane with their C H···O interactions is shown in the Figure 6.14. The overall geometrical parameters of possible C H···O (donor to acceptor distance within

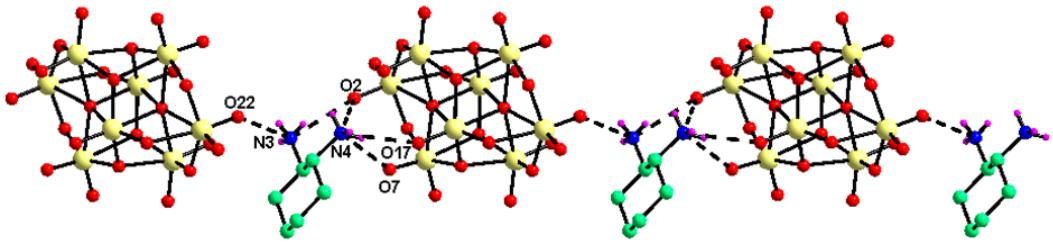

3.6 Å) hydrogen bonding interactions are provided in the Table 6.4.

Figure 6.13. Formation of one dimentional polyoxometalate chain through N H···O hydrogen bonds. Color code: Mo, yellow; O, red; C, green; N, blue; H, purple; black dotted lines represent N H···O hydrogen bonding interactions.

(**a**) (**b**)

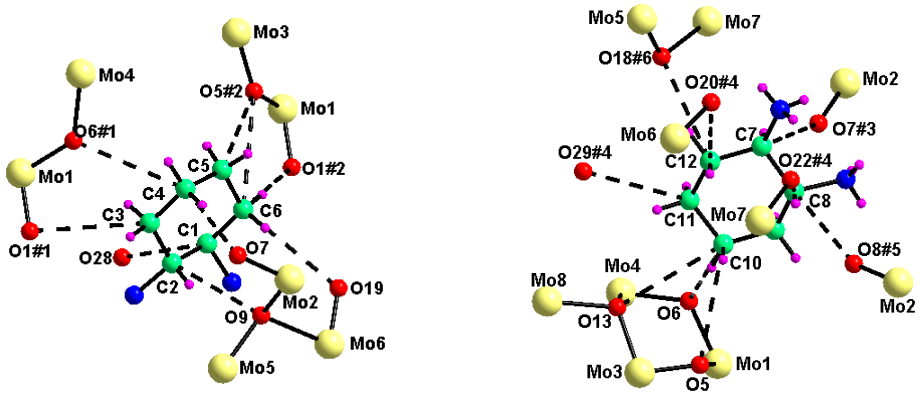

Figure 6.14. (a) C H···O hydrogen bonding environment around (*R,R*)-1,2-*trans*-diaminocyclohexane (**1**); (b) C H···O hydrogen bonding environment around (*R,R*)- (*R,R*)-*trans*-1,2-diaminocyclohexane (**2**). Color code as shown in Figure 6.13 caption.

Table 6.3. Geometrical parameters of N H···O and O H···O hydrogen bonds (Å, °) in compound **2**.

D H···A	d(D···H)	d(H···A)	d(D···A)	(DHA
N3-H3C...O2#3	0.72(7)	2.22(8)	2.905(9)	158(8)
N3-H3D···O28#13	0.83(8)	2.43(9)	2.973(9)	124(7)
N3-H3D...O22#4	0.83(8)	2.32(9)	3.026(10)	144(8)
N4-H4C...O27#13	0.84(8)	2.06(8)	2.877(9)	166(7)
N4-H4E...O7#3	0.83(6)	2.30(6)	2.972(9)	139(6)
N4-H4E···O17#3	0.83(6)	2.41(6)	3.072(8)	138(5)

D H···A	d(D···A)	D H···A	d(D···A)
O(2) N(3)#1	2.905(9)	O(2) N(4)#1	2.982(9)
N(4) O(2)#3	2.982(9)	O(1) O(26)#7	3.066(6)
O(1) O(29)#5	2.782(7)	O(3) O(27)#5	2.913(7)
O(15) O(27)#3	3.082(7)	O(28) N(3)#14	2.973(9)
O(15) O(20)#8	2.950(5)	O(14) O(30)#6	2.909(7)
O(14) O(28)#6	3.052(7)	O(26) O(28)#6	3.079(7)
O(26) (N2)#6	2.939(8)	O(26) O(1)#9	3.066(6)
O(25) O(28)#4	2.989(7)	O(25) N(1)#4	3.059(9)
O(22) N(3)#11	3.026(10)	O(23) O(30)	2.756(7)
O(23) O(8)#9	3.052(6)	O(20) O(15)#10	2.950(5)
O(20) O(28)#4	3.054(7)	O(11) O(28)#4	2.938(7)
O(11) O(30)#4	2.974(7)	O(21) N(1)	3.027(9)
O(19) O(29)	2.959(7)	O(19) O(17)#10	3.086(6)
O(8) O(23)#7	3.052(6)	O(17) O(19)#8	3.086(6)
O(29) O(1)#2	2.782(7)	O(27) O(3)#2	2.913(7)
O(27) O(15)#2	3.082(7)	O(28) O(25)#11	2.989(7)
O(28) O(26)#12	3.079(7)	O(28) O(20)#11	3.054(7)
O(28) O(14)#12	3.052(7)	O(28) O(11)#11	2.938(7)
O(30) O(11)#11	2.974(7)	O(30) O(14)#12	2.909(7)
O(30) O(23)	2.756(7)	O(29) N(2)#10	2.965(8)
O(27) N(4)#14	2.877(9)	N(1) O(21)	3.027(9)
N(1) O(29)	3.054(9)	N(1) O(30)	2.794(9)
N(1) O25)#11	3.059(9)	N(2) O(30)	2.779(10)
N(2) O(28)	2.912(9)	N(2) O(26)#12	2.939(8)
N(2) O(29)#8	2.965(8)		

Symmetric transformations used are specified in footnote of Table 6.4.

Table 6.4. C H···O hydrogen bonding parameters for compound $[CyclohexH_2]_2[Mo_8O_{26}]$ (**2**)

D H···A	d(D···H)	d(H···A)	d(D···A)	(DHA
C1 H1A O28	1.30(8)	2.45(9)	3.288(10)	119(5)
C2 H2A O9	0.89	2.58	3.406(8)	156.0
C3 H3B O1#1	0.97	2.81	3.365(9)	117.0
C4 H4A O6#1	0.97	2.71	3.388(9)	127.8
C4 H4B O7	0.97	2.50	3.463(9)	173.2
C5 H5B O5#2	0.97	2.55	3.186(9)	123.3
C6 H6B O5#2	0.97	2.94	3.539(9)	121.0
C6 H6B O1#2	0.97	2.45	3.395(9)	163.7
C6 H6A O19	0.97	2.64	3.455(9)	142.4
C7 H7A O7#3	1.03	2.44	3.330(7)	144.0
C8 H8A O22#4	0.80	2.67	3.318(8)	140.0
C8 H8A O8#5	0.80	2.49	3.083(8)	132.0
C10 H10B O5	0.97	2.71	3.523(9)	141.9
C10 H10B O6	0.97	2.56	3.475(10)	157.3
C10 H10B O13	0.97	2.82	3.511(9)	128.9
C11 H11A O29#4	0.97	2.70	3.479(9)	137.4
C12 H12A O18#6	0.97	2.49	3.360(8)	149.8
C12 H12B O20#4	0.97	2.96	3.518(8)	117.4

Symmetry transformations used to generate equivalent atoms: #1 -x, -0.5+y, -z; #2 1-x, -0.5+y, -z; #3 -x, 0.5+y, -z; #4 1-x, 0.5+y, 1-z; #5 1-x, 0.5+y, -z; #6 -x, 0.5+y, 1-z; #7 x, y, -1+z; #8 -1+x, y, z; #9 x, y, 1+z; #10 1+x, y, z; #11 1-x, -0.5+y, 1-z; #12 -x, -0.5+y, 1-z; #13 x, 1+y, z; #14 x, -1+y, z.

6.3.5. Spectroscopic Observation for the Displacement of a Racemate Equilibrium in Strandberg-Type Heteropolyanion $[S_2Mo_5O_{23}]^4$ by a Pfeiffer Effect

Strandberg-type heteropolyanion, formulated as, $[X_2M_5O_{23}]^n$ (where M = Mo^{VI} or W^{VI}; n = 6 when X = P(V) and n = 4 when X = S(VI))[12j] can be viewed as two XO_4 tetrahedra capping either side of an irregular ring of five MoO_6 octahedra linked by one corner-shared and four edge-shared contacts (Figure 6.15(a). The highest possible

symmetry in Strandberg type heteropolyanion is C_2, thus the structure is chiral. Spontaneous resolution was observed in one system of its phosphate (Strandberg type) analogue.[19]

Pfeiffer effect can be described as "the optical phenonmenon whereby the optically active solute influences the optical rotation of a racemic mixture". In general, racemic mixture do not rotate plane polarized light but the equilibrium concentration of the two enantiomers can shift from unity in the presence of strongly interacting chiral species. This effect was first observed by scientist Pfeiffer (student of Alfred Werner and the inventor of salen ligand) and so, named as Pfeiffer effect. In this context, a systematic study of Pfeiffer effect has been examined on Strandberg heteropolyanion (racemate equilibrium) system whereby *l*- and *d*- arabinose used as enantiomerically pure chiral environmental substance. The structural configurations of *l*- and *d*- arabinose, used in the present study, are shown in Scheme 2.

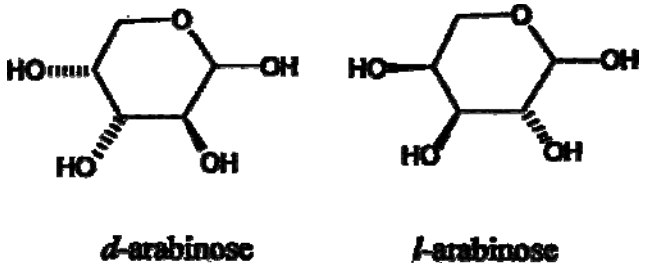

d-arabinose *l*-arabinose

Scheme 2.

The Strandberg-type heteropoly (racemic) complex $[NMe_4]_4[S_2Mo_5O_{23}]$ was synthesized by published method.[12j] The circular dichroism (CD) spectra of the compound $[NMe_4]_4[S_2Mo_5O_{23}]$ enriched by the Pfeiffer effect when *l*- and *d*- arabinose are employed as environment substances in DMSO, are presented in Figure 6.15(b). It can be seen that the CD spectra of $[S_2Mo_5O_{23}]^4$ in the presence of *l*- and *d*- arabinose are enantiomeric. A cotton effect at ca. 290 nm is clearly associated with the chromophores of the enatiomeric heteropolyanions $[S_2Mo_5O_{23}]^4$ that have lowest energy electronic absorption at ca. 260 nm. Absorption spectra of the racemic complex $[S_2Mo_5O_{23}]^4$ and

that of the racemic complex together with *l*- arabinose (as an environment substance) in DMSO solutions are shown in Figure 6.15(b) (inset). The sharp absorption at 260 nm for the racemate shifts to ca. 290 nm with the broadening of the peak on addition of *l*-arabinose. This is consistent with cotton effects observed in the CD spectra obtained with the addition of *l*- and *d*- arabinose in corresponding DMSO solutions of $[NMe_4]_4[S_2Mo_5O_{23}]$ (Figure 6.15(b)). The cotton effect at 290 nm is corresponding to the electronic absorption bands (at 260 nm) that have been assigned as oxygen to molybdenum charge transfer transitions. When *l*- arabinose is added to the DMSO solution of $[NMe_4]_4[S_2Mo_5O_{23}]$ conversion to $(+)_{300}$ enantiomer takes place. On the other hand, addition of *d*- arabinose shifts the equilibrium to $(\ )_{300}$ enantiomer (Figure 6.15b).

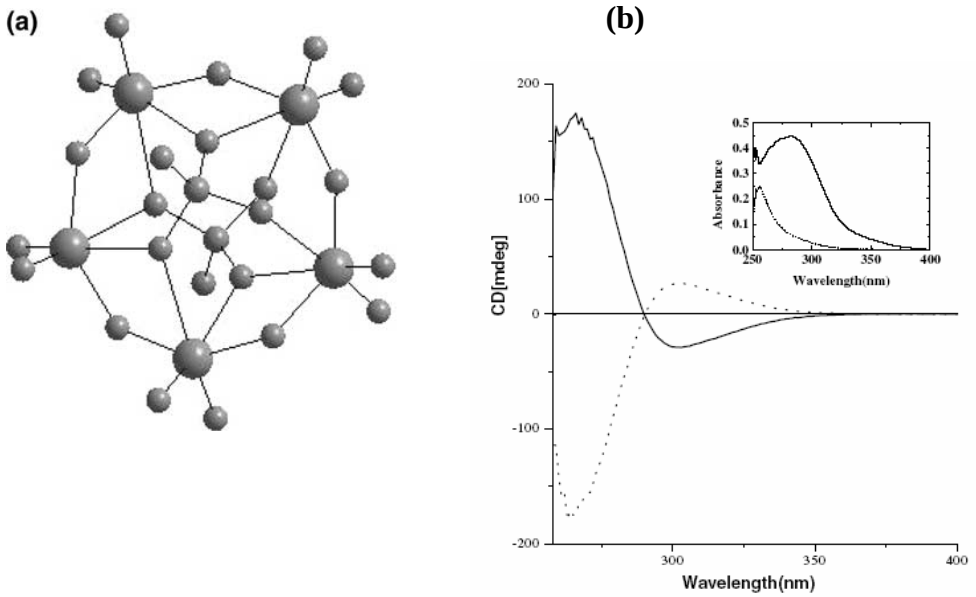

Figure 6.15. (a) Ball Stick representation of $[S_2Mo_5O_{23}]^4$; (b) Solid line (—): the CD spectrum of the solution, which was made by dissolving *d*-arabinose (0.1 g) into 35 mL of 3.55 x 10^{-3} M DMSO solution of racemic strandberg compound, $[NMe_4]_4[S_2Mo_5O_{23}]$; dotted line (····): the CD spectrum of the solution, which was made by dissolving *l*-arabinose (0.1 g) into 35 mL of 3.55 x 10^{-3} M DMSO solution of racemic strandberg compound, $[NMe_4]_4[S_2Mo_5O_{23}]$; Inset: Dotted line (····): the UV spectrum of 3.94 x 10^{-6} M DMSO solution of Standberg compound; solid line (—): UV vis spectrum obtained when 0.06 g of *l*-arabinose was added to 4.2 ml of 3.94 x 10^{-3} M DMSO solution of Strandberg compound, $[NMe_4]_4[S_2Mo_5O_{23}]$.

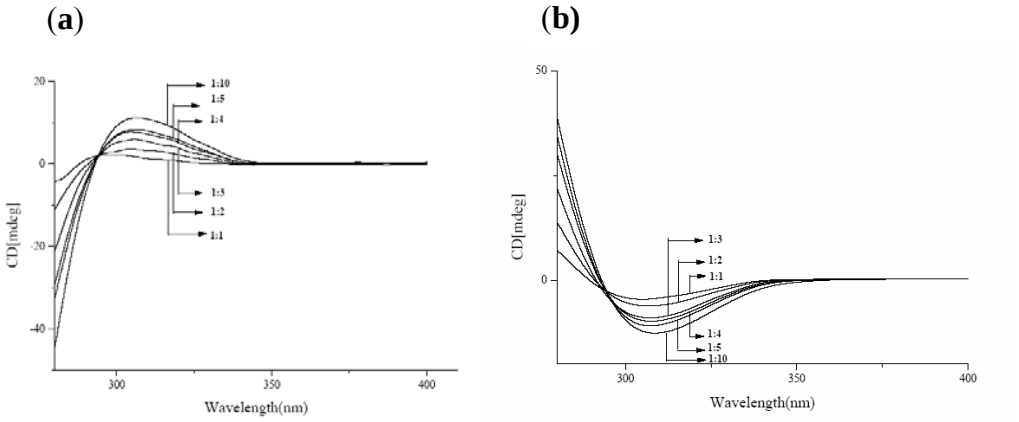

Figure 6.16. Concentration dependent CD spectra of enantiomerically pure environment substances with $[NMe_4]_4[S_2Mo_5O_{23}]$ in DMSO solution whereby the ratio of environment substances and $[NMe_4]_4[S_2Mo_5O_{23}]$ are 1:1, 1:2, 1:3, 1:4, 1:5 and 1:10; (a) with *l*-arabinose; (b) with *d*- arabinose.

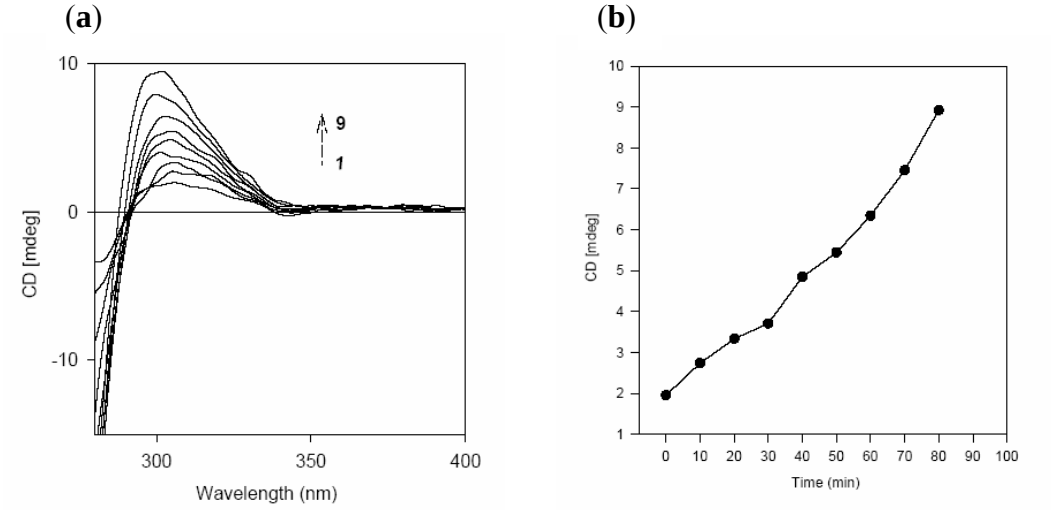

Figure 6.17. (a) Time dependent CD spectra: 0.0097 g of *l*-arabinose was added to 25 mL of DMSO solution (1.32 x 10^{-3}M) of $[NMe_4]_4[S_2Mo_5O_{23}]$; (b) The time dependent plot of the optical rotations at 300 nm induced in the Strandberg compound (1.32 x 10^{-3}M) *l*-arabinose (2.58 x 10^{-3}M) system in DMSO. Relevant CD spectra (1 7) are recorded at 10 minutes interval of time and last two are at 15 minutes interval of time.

Concentration dependent studies (with respect to environment substances) were performed for both enantiomers, whereby consistent CD spectra were obtained for solutions of $[NMe_4]_4[S_2Mo_5O_{23}]$ in DMSO that contain varying proportions of *l*- and *d*-arabinose separately. These experiments show that the molar rotations at the maximum of cotton effect centered at 290 nm (Figure 6.16). It can be supposed that the source of the Pfeiffer effect for the present system is attributed to the hydrogen bonding between O H proton of arabinose (Scheme 6.2) and terminal oxo groups of Strandberg heteropolyanion (Figure 6.15(a)). This is supported by the fact that the Pfeiffer rotation in $[S_2Mo_5O_{23}]^4$ arabinose system decreases dramatically in aqueous medium. This is because, water (a protic solvent) disfavors the formation of hydrogen bonding aggregates composed of the Strandberg complex and the chiral environment compound (*l*- and *d*- arabinose), thereby diminishing the Pfeiffer effect. When *l*- and *d*- arabinose is added as an environment substance, the Pfeiffer circular dichroism spectra, developed are time dependent. This must be associated with the dynamics for the formation of heteropolyanion enantiomer arabinose (hydrogen bonded) complex in solution. The representative time-dependent plot for the CD spectra induced for a system of racemic $[S_2Mo_5O_{23}]^4$ with *l*-arabinose as an environment substance in DMSO is provided in Figure 6.17. The time dependent increase in the intensity of CD spectra for a given concentration of *l*- arabinose reflects the formation of heteropolyanion enantiomer arabinose complex more and more with time in solution.

6.4. Conclusion

In this chapter, we have discussed the influence of strong and weak supramolecular interactions in the polyoxometalate chemistry. In conclusion, we used protonated 2-aminopyrimidine and (*R,R*)-*trans*-1,2-diaminocyclohexane as amine templates to isolate the inorganic organic hybrid compounds **1** and **2** respectively. In the

crystal structure of compound **1**, novel cis-dioxo O···O non-covalent interactions have been observed forming a chain like arrangement. The similar type of non-covalent interactions (cis-dioxo O···O) in polyoxometalate chemistry is surveyed from the literature and documented in the reference section.[9] We have argued that one of the crystallographically independent organic cations assist to achieve such O···O non-covalent interactions resulting in a supramolecular chain. Interesting helical arrangement, formed from isopolyanion and organic cation, has been demonstrated. Moreover, amino-pyrimidine derivatives are supposed to be biologically important compounds because they occur in nature as components of nucleic acids.[20] Indeed, some amino-pyrimidine compounds have been shown to have potential to act as antifolate drugs.[21] Compound **1** is the unique combination, in which both individual components are potential candidates for drug activity. Compound **1** is a rare example in which a pyrimidine type molecule interacts with a polyoxometalate cluster anion. The combination of supramolecular non-covalent interactions such as O···O, O H···O, N H···O and C H···O hydrogen bonding interactions that involve both cationic and anionic components leads to a new type of supramolelcular three-dimensional structure that has well-defined channels. We have shown, for the first time that a Strandberg-type heteropolyanion undergoes chiral discrimination with *l*- or *d*- arabinose (as an environment substance). We have succeeded to observe both enantiomers of $[S_2Mo_5O_{23}]^4$ through Pfeiffer effect a rare phenomenon in heteropolyanion chemistry. We believe that the source of the Pfeiffer effect for the present system is attributed to the O H···O hydrogen bonding between O H proton of arabinose and terminal oxo groups of Strandberg type heteropolyanion. The present work of supramolecular non-covalent interactions (namely, O···O, O H···O, N H···O and C-H···O) open a new route for the study of cluster-cluster interaction in polyoxometalate chemistry.

6.5. References

1. a) A. M. Cheetham, *Science* **1994**, *264*, 794; b) M. T. Pope, A. Müller, *Angew. Chem., Int. Ed.* **1991**, *30*, 34; c) L. Xu, C. Qin, X. L. Wang, Y. G. Wei, E. B. Wang, *Inorg. Chem.* **2003**, *42,* 7342; d) A. Müller, H. Reuter, S. Dillinger, *Angew.Chem., Int. Ed.* **1995**, *34,* 2328; e) O. M. Yaghi, ***N****ature* **1999**, *402,* 276; O. M. Yaghi, *J. Am. Chem. Soc*. **1998**, *120*, 8571.
2. a) T. Yamase, *Mol. Eng.* **1993**, *3,* 241; b) S. Uchida, M. Hashimoto, N. Mizuno, *Angew. Chem., Int. Ed.* **2002**, *41*, 2814.
3. a) R L. Jr. LaDuca, M. Desciak, M. Laskoski, R. S. Jr. Rarig, J. Zubieta, *J. Chem. Soc., Dalton Trans.* **2000**, 2255; b) P. J. Hagrman, J. Zubieta *Inorg. Chem.* **2000**, *39*, 5218; c) P. J. Zapf, R.C. Haushalter, J. Zubieta, *Chem. Commun*. **1997**, 321.
4. a) P. J. Hagman, D. Hagraman, J. Zubieta, *Angew. Chem., Int. Ed.* **1999**, *38*, 2638; b) Z. Peng, M. Lu, B. Xu, L. Xu, Y. Wei, B. Xie, N. R. Katabathini, *Polym. Prepr.* **2003**, *44,* 671; c) C. D. Wu, C. Z. Lu, H. H. Zhuang, J. S. Huang, *Inorg. Chem.* **2002**, *41,* 563; d) W. Yang, C. Lu, H. Zhuang, *Dalton Trans.* **2002**, *14*, 2879; e) R. S. Rarig, J. Zubieta, *Inorg. Chim. Acta*. **2000**, *312,* 188; f) C. D. Wu, C. Z. Lu, H. H. Zhuang, J. S. Huang, *Inorg. Chem.* **2002**, *41,* 5636.
5. a) V. Soghomonian, Q. Chen, R. C. Haushalter, J. Zubieta, C. J. O'Connor, Y-S, Lee, *Chem. Mater.* **1993**, *5,* 1690; b) V. Soghomonian, R. C. Haushalter, Q. Chen, Z. Zubieta, C. J. O'Connor, *Angew. Chem., Int. Ed.* **1993**, *32,* 610; c) J. W. Kroenke Jr, P. F. John, M. M. Anthony, *Inorg. Chem.* **1983**, *22,* 2412; d) A. J. Wilson, V. Mckee, B. R. Penfold, C. J. Wilkins, *Acta Crystallogr, Sec. C.* **1984**, *40,* 2027.
6. a) E. M. McCarron, J. F. Whitney, D. B. Chase, *Inorg. Chem*. **1984**, *23,* 3275; b) C. L. Pan, J. Q. Xu, K. X. Wang, X. B. Cui, L. Ye, Z. L. Lu, D. Q. Chu, T. G. Wang, *Inorg. Chem. Commun.* **2003**, *6,* 370; c) J. Y. Niu, M. L. Wei, J. P. Wang, D. B. Dang, *J. Mol. Struct.* **2003**, *655*, 171; d) C. L. Pan, J. F.

Song, J. Q. Xu, G. H. Li, L. Ye, T. G. Wang, *Inorg. Chem. Commun.* **2003**, *6,* 535.

7. a) K. Wozniak, H. He, J. Klinowski, W. Jones, E. Grech, *J Phys.Chem*. **1994**, *98,* 13755; b) B. Ni, K. H. Lee, S. B. Sinnott, *J. Phys. Condens. Matter* **2004**, *16*, 7261; c) M. Breza, S. Biskupic, A. Manova, *Polyhedron* **2003**, *22*, 2863; d) S. Jenkins, I. Morrison, *Chem. Phys. Lett.* **2000**, *317,* 97; e) M. C. Lemos, J. J. Luque, F. Jimenez- Morales, *J. Chem. Phys.* **1998**, *109*, 8069; f) N. P. Blake, P. C. Weakliem, H. Metiu, *J. Phys. Chem.* **1998**, *102*, 67; g) K. Igarashi, K. Tajiri, S. Tanemura, R. Nanbu, T. Fukunaga, *Z. Phys. D: At.,Mol. Clusters* **1997**, *40,* 562; h) L. X. Dang, *J. Chem. Phys.* **1992**, *97*, 2659.
8. P. Raghavaiah, S. Supriya, S. K. Das, *Chem. Commun.* **2006**, 2762.
9. According to our Cambridge Structural Database (CSD) search, no O O interactions among polyoxometalate anions were explored prior to this work. We could observe the O O interactions among polyoxometalate anions in few structures; however the relevant references did not talk about such interactions. Some of these references are: a) J. Do, X. Wang, A. J. Jacobson, *J. Solid State Chem.* **1999**, *143*, 77; b) Shu–Meichen, C–Z. Lu, Y–Q. Yu, Q–Z. Zhang, X. He, *Acta. Crystallogr., Sect. E; Struct. Rep. Online* **2004**, *60,* m723; c) Z–P. Deng, S. Gao, L–H. Huo, H. Zhao, *Acta Crystallogr. Sect. E: Struct. Rep. Online* **2005**, *61*, 2553; d) S. Chakrabarti, S. Natarajan, *Cryst. Growth Des.* **2002**, *2*, 333; e) P. Gili, P. Nunez, P. Martin–Zarza, P. A. Lorenzo–Luis, *Acta. Crystallogr., Sect. C: Cryst. Struct. Commun.* **2000**, *56,* e441; f) M. Cindric, N. Strukan, B. Kamenar, *Polyhedron* **1999**, *18,* 2781; g) S. Upreti, A. Ramanan, *Cryst. Growth. Des.* **2006**, *6*, 2066; h) U. Kortz, M. G. Savelieff, F. Y. A. Ghali, L. M. Khalil, S. A. Maalouf, D. I. Sinno, *Angew. Chem., Int. Ed.* **2002**, *41,* 4070; i) H. Liu, H. Wang, D. Shi, Z. Lu, *J. Coord. Chem.* **2006**, *59*, 1703; j) A. Aranzabe, A. S. J. Wery, S. Martin,

J. M. Gutierrez–Zorrila, A. Luque, M. Martinez–Ripoll, P. Roman, *Inorg. Chim. Acta,* **1997**, *255*, 35.

10. a) M. T. Pope, *Heteropoly and Isopoly oxometalates*, *Springer-Verlag, Berlin*, 1983; b) M.T. Pope, A. Müller, *Angew. Chem., Int. Ed.* **1991**, *30*, 34 c) C. L. Hill, C. M. Prosser-McCartha, *Coord. Chem. Rev.* **1995**, *143*, 407; d) J. T. Rhule, C. L. Hill, D. A. Judd, *Chem. Rev.* **1998**, *98*, 327; e) R. Neumann, *Prog. Inorg. Chem.* **1998**, *47,* 317.
11. B. Hasenknopf, K. Micoine, E. Lacôte, S. Thorimbert, M. Malacria, R. Thouvenot, *Eur. J. Inorg. Chem.* (in press)
12. a) F. Xin, M. T. Pope, *J. Am. Chem. Soc.* **1996**, *118*, 7731; b) M. T. Pope, *Inorg. Chem.* **1976**, *15*, 2008; c) J. C. T. Waugh D. P. Schoemaker, L. Pauling, *Acta. Crystallogr.* **1954**, *7*, 438; d) W. H. Knoth, R. L. Harlw, *J. Am. Chem. Soc.* **1981**, *103*, 1865; e) C. M. Tourne, G. F. Tourne, F. J. Zonnevijlle, *J. Chem. Soc., Dalton Trans.* **1991**, 143; f) R. Strandberg, *Acta. Chem. Scand.* **1973**, *27*, 1004; g) L. C. W. Baker, T. J. R. Weakly, *J. Inorg. Nucl. Chem.* **1966**, *28*, 447; h) H. T. Evans Jr., J. S. Showell, *J. Am .Chem. Soc.* **1969**, *91*, 6881; i) S. C. Termes, M. T. Pope, *Transit. Metal Chem.* **1978**, *3*, 103; j) T. Hori, S. Himeno, O. Tamada, *J. Chem. Soc., Dalton Trans.* **1992**, 275.
13. a) R. Acerete, J. Server-Carrio, A. Vegas, M. Martinez-Ripoll, *J. Am. Chem. Soc.* **1990**, *112*, 9386; b) T. Ama, J. Hidaka, Y. Shimura, *Bull. Chem. Soc. Jpn.* **1970**, *43*, 2654; c) J. F. Garvey, M. T. Pope, *Inorg. Chem.* **1978**, *17*, 1115; d) K. Nomiya, R. Kobayashi, M. Miwa, *Bull. Chem. Soc. Jpn.* **1983**, *56*, 3505; e) M. Inoue, T. Yamase, *Bull. Chem. Soc. Jpn.* **1996**, 69, 2863
14. a) P. Pfeiffer, K. Quehl*, Ber.* **1931**, *64*, 2667; b) P. Pfeiffer, K. Quehl, *Ber*. **1932**, *65*, 460.
15. J. F. Larrow, E. N. Jacobsen, Y. Gao, Y, Hong, X. Nie, C. M. Zepp, *J. Org. Chem.* **1994**, *59*, 1939.

16. a) *SAINT: Software for the CCD Detector System;* Bruker analytical X-ray systems Inc., Madison, WI, **1998**; b) Sheldrick G. M. *SADABS*, *A program for absorption correction with the Siemens, SMART area-detector system,* University of Göttingen, Germany, **1996**; c) G. M. Sheldrick, *SHELXS 97*, *A program for solution of crystal structures*, University of Göttingen, Germany, **1997**; d) G. M. Sheldrick, *SHELXL 97*, *A program for solution of crystal structures,* University of Göttingen, Germany, **1997**.

17. K. Brandenburg, *DIAMOND Version 2.1e*, Crystal Impact GbR, Bonn, Germany, **2001**.

18. a) L. Carlucci, G. Ciani, D. W. V. Gudenberg, D. M. Proserpio, *Inorg. Chem.* **1997**, *36,* 3812; b) V. Amendola, L. Fabbrizzi, C. Mangano, P. Pallavivini, E. Roboli, M. Zema, *Inorg. Chem.* **2000**, *39,* 5803; c) C. Z. Lu, C. D. Wu, S. F. Lu, J. C. Liu, Q. J. Wu, H. H. Zhuang, J. S. Huang, *Chem. Commun.* **2002**, 152; d) K. A. Hirsch, S. R. Wilson, J. S. Moore, *Chem. Commun.* **1998**, 13; e) T. M. Garrett, *J. Chem. Soc., Chem. Commun.* **1990**, 557; f) J M. Lehn, A. Riganlt *Angew. Chem., Int. Ed.* **1988**, *27,* 1095; g) Z. Shi, S. H. Feng, S. Gao, L. Zhang, G. Yang, J. Hua, *Angew. Chem.,Int. Ed.* **2000**, *39* 2325; h) J. Liang, Y. Wang, J. H. Yu, Y. Li, R. R. Xu, *Chem. Commun.* **2003**, 882; i) R. Kniep, H. G. Will, I. Boy, C. Röhr, *Angew. Chem., Int. Ed.* **1997**, *36*, 1013; j) S. Neeraj, S. Natarajan, C. N. R. Rao, *Chem.Commun.* **1999**, 165.

19. C. Qin, X. L. Wang, L. Yuan, E. B. Wang, *Cryst. Growth Des.* **2008**, *8*, 2093.

20. a) M. Hemamalini, P. T. Muthiah, R. J. Butcher, D. E. Lynch, *Inorg. Chem. Commun.* **2006**, *9*, 1155; b) D. J. Brown, S. F. Mason, *The Pyrimidines*, Interscience Publishers John Wiley & Sons, New York, **1962**; c) C. B. Brouillette, C. T. Chang, M. P. Mertes, *J. Med. Chem.* **1979**, *22*, 1541; d) E. D. Dlercq, J. Descamps, G. Huang, P. Torrence, *Mol. Pharmacol.* **1978**, *14*, 422; e) P. V. Danenberg, *Biochim. Biophys. Acta* **1977**, *497*, 73; f) A. D. D. Silva, A. S.

Machado, C. Tempete, M. Robert-Gero, *Eur. J. Med. Chem. Chim. Ther.* **1994**, *29,* 1149; g) S. M.. Sondhi, M. Johar, S. Rajvanshi, S, G. Dastidar, R. Shukla, R. Raghubir, J. W. Lown, *Aust. J. Chem.* **2001**, *54*, 169; h) M. Kidwai, S. Saxena, S. Rastogi, R. Venkataramanan, *Curr. Med. Chem. Ant-Infective Agents* **2004**, *2*, 269.

21. S. Huang, R. Li, P. J. Connolly, G. Xu, M. D. Gaul, S. L. Emanuel, K. R. LaMontagne, L. M. Greenberger, *Bioorg. Med. Chem. Lett.* **2006**, *16*, 6063.

****

SYNOPSIS

This thesis work entitled with "**Polyoxometalate Cluster-Based Functional Materials: Syntheses, Characterizations and Application Studies",** consists of six chapters: (**1**) Introduction, (**2**) Functionalization of Polyoxovanadate Clusters by Rare Earth Metal Ions: Syntheses, Characterization, Magnetic and Thermal Properties, (**3**) Polyoxometalate Supported Transition Metal Complexes: Syntheses, Supramolecular Structures and Catalysis, (**4**) 'Ionic Crystals' Consisting of Trinuclear Macrocations and Polyoxometalate Anions Exhibiting Single Crystal to Single Crystal Transformation: Breathing of Crystals, (**5**) Co-existence of Polyoxometalate Cluster Anion and Manganese (III) Based Schiff-base Complex Cations: Syntheses and Structural Characterizations, (**6**) Influences of Supramolecular Interactions in Polyoxometalate chemistry. The work described in this thesis, is in the direction of the synthesis and characterization of inner-transition metal (Mo, W and V) oxide clusters and providing its possible applications. Apart from the first chapter (introduction), all the chapters are sub-divided into Introduction, Experimental Section, Results and Discussion and Conclusion followed by References.

Chapter 1

Introduction

This chapter begins with more fundamental ideas about inner transition metal (Mo, W and V) oxo clusters, known as polyoxometalate (POM) cluster anions, starting from its history. It also exposes the basic principles involved in POM clusters syntheses, structural characterization and properties. Some of the polyoxometalate cluster anions, that are more relevance to various chapters of this thesis, are picked up from the literature and their structural topologies, various properties, such as host guest interactions,

magnetic, catalysis, medicinal applications and supramolecular interactions are discussed briefly. Finally, a brief note on the main objectives of this thesis work conversed shortly.

Chapter 2

Functionalization of Polyoxovanadate Clusters by Rare Earth Metal Ions: Syntheses, Characterization, Magnetic and Thermal Properties

Polyoxovanadate (POV) clusters are a sub-class of polyoxometalate (POM) chemistry. Syntheses, characterizations and properties of novel series of polyoxovanadate cluster anions functionalized by f-block elements are discussed in this chapter. Water molecule encapsulated High Nuclearity Spin Cluster (HNSC) $[As_6V_{15}O_{42}(H_2O)]^6$ is well studied in the literature as far as magnetism is concerned. Protonated salt of the same $[H_6As_6V_{15}O_{42}(H_2O)]$ $9H_2O$ (**1**) is synthesized and taken as one of the starting precursor for this chapter work. Compounds $[\{Ln(H_2O)_7\}_2(As_6V_{15}O_{42}(H_2O))]$ $\cdot nH_2O$ (n = 12 and Ln = La^{3+} (**2**), n = 13 and Ln = Sm^{3+} (**3**), n = 11 and Ln = Ce^{3+} (**4**) are synthesized and characterized crystallographically. All three compounds (**2 4**) are isostructural and crystallize in orthorhombic space group *Pna2(1)*. The crystal structure illustrates the compounds **2 4** exist as 2D coordination polymer. Each $[V_{15}As_6O_{42}(H_2O)]^6$ anion is coordinated by four $\{Ln(H_2O)_7\}^{3+}$ complexes and every $\{Ln(H_2O)_7\}^{3+}$ complex is coordinated with two $[As_6V_{15}O_{42}(H_2O)]^6$ cluster anions. Compound **2** features an interesting water pentamer exclusively comprising of the lattice water molecules. The supramolecular interactions around water pentamer with its surrounding leads to 3D hydrogen bonded supramolecular network. An aqueous reaction of $[H_6As_6V_{15}O_{42}(H_2O)]$ $\cdot 9H_2O$ (**1**) with ammonium cericnitrate results in the formation of strongly hydrated compound $[\{\{Ce(H_2O)_5\}_6As^{v}V_{12}{}^{V}O_{38}\}(V_6{}^{iv}V_6{}^{v}As_8O_{40}(NO3)^3$ $(V_7{}^{iv}V_5{}^{v}As_8O_{40}(NO_3)^4$]. $52H_2O$ (**5**) Compound **5** depicts the co-existence of Ce^{3+} ion capped polyoxovanadate cation and polyoxovanadate anions together for charge complement in the crystal

structure. The negative charge of POV cluster counterbalanced by POV cation is very rarely known in the literature. The contraction of $\{As_6V_{15}\}$ cluster in to $\{As_8V_{12}\}$ cluster along with encapsulation of nitrate anion is an unusual phenomenon in polyoxometalate chemistry. We have isolated an another series of compounds $[\{Ln(H_2O)_6\}_2(As_8V_{14}O_{42}(SO_3))] \cdot 8H_2O$ (Ln = La^{3+} (**6**), Sm^{3+} (**7**) and Ce^{3+} (**8**) by the reaction of $[NH_4]_6[As_8V_{14}O_{42}(SO_3)]$ with lanthanide ions. All three compounds (**6** **8**) are isostructural and crystallize in monoclinic space group *P2₁/n*. The crystal structure of compounds **6** **8** demonstrates the existence of 2D coordination polymer. Each $[(As_8V_{14}O_{42}(SO_3)]^6$ cluster anion is surrounded by six $[Ln(H_2O)_6]^{3+}$ complexes and each $[Ln(H_2O)_6]^{3+}$ complex is coordinated to three of its surrounding $[(As_8V_{14}O_{42}(SO_3)]^6$ cluster anions. In the crystal structure of compound **6**, we observed a "Z" shaped of water hexamer $(H_2O)_6$, which is formed exclusively from lattice water molecules O31, O32 and O33 and their symmetry equivalent atoms by O–H···O non-covalent hydrogen bonding interactions. This water hexamer, in turn, is hydrogen bonded with its surrounding water molecules resulting in a $(H_2O)_{16}$ cluster. The resulting water cluster $(H_2O)_{16}$ is further hydrogen bonded to its six surrounding $\{V_{14}\}$ clusters resulting in an intricate three-dimensional supramolecular network. Compounds are characterized by usual techniques such as UV, IR, PXRD, ESR, TGA, Bond Valence Sum calculation (BVS), magnetic susceptibility measurement and unambiguously by single crystal X-ray diffraction study. Low temperature (2 300 K) magnetic measurement of compounds **7** **8** shows the existence of strong anti-ferromagnetic coupling between V^{4+} ($3d^1$, S = ½) ions. The magnetically active Sm^{3+} ($4f^5$, S = 5/2) and Ce^{3+} ($4f^1$, S = ½) also affords significant contributions in anti-ferromagnetic coupling. Thermal properties of compounds **6** **8** are relatively interest. All compounds have additionally been characterized by TGA / Mass studies.

Chapter 3

Polyoxometalate Supported Transition Metal Complexes: Syntheses, Supramolecular Structures and Catalysis

This chapter describes the polyoxometalate (POM) supported transition metal complexes (TMCs) including their syntheses, structural characterizations, non-covalent surpramolecular hydrogen bonding interactions, and their catalytic activities. The crystal structure of an inorganic organic hybrid material, $[HMTAH]_2[\{Zn(H_2O)_5\}\{Zn(H_2O)_4\}\{Mo_7O_{24}\}]\cdot 2H_2O$ (**1**) (where HMTAH = protonated hexamethylenetetramine) shows that two different Zn(II)-aqua complexes, $[Zn(H_2O)_5]^{2+}$ and $[Zn(H_2O)_4]^{2+}$ are covalently coordinated to a heptamolybdate anion $[Mo_7O_{24}]^{6}$. In the crystal structure, N H···O / O H···N, O H···O, C H···O and N H···N hydrogen bonding interactions are observed. The catalytic activity of compound $[HMTAH]_2[\{Zn(H_2O)_5\}\{Zn(H_2O)_4\{Mo_7O_{24}\}]\cdot 2H_2O$ (**1**) in a heterogeneous reaction, at moderate temperature has been studied for the oxidation of a primary alcohol in the presence of hydrogen peroxide as an oxidant, in which the catalyst (compound **1**) is recyclable. Thermogravimetric analysis study of compound **1** pointed out that five water molecules from $[Zn(H_2O)_5]^{2+}$ complex evolved in the first weight loss. Whereas evolution of four water molecules from $[Zn(H_2O)_4]^{2+}$ complex noticed in second weight loss. This discussion is logical because polyoxometalate cluster acts as bidentate ligand to $[Zn(H_2O)_4]^{2+}$ complex and hence affords extra stability. A new series of polyoxometalate supported transition metal complexes namely, $[2\text{-ampH}]_4[\{Zn(H_2O)_5\}Mo_7O_{24}]\cdot 9H_2O$ (**2**), $[3\text{-ampH}]_4[\{Zn(3\text{-ampy})(H_2O)_4\}Mo_7O_{24}]\cdot 4H_2O$ (**3**), $[3\text{-ampH}]_4[\{Co(3\text{-ampy})(H_2O)_4\}Mo_7O_{24}]\cdot 4H_2O$ (**4**), $[2,3\text{-diampH}]_4[Co(H_2O)_6][Mo_7O_{24}]\cdot 6H_2O$ (**5**) and $[2,3\text{-diampH}]_2[\{Zn(2,3\text{-diampH})_2(H_2O)_2\}Mo_8O_{27}]\cdot 2H_2O$ (**6**) have been synthesized (where amp = aminopyridine, and diamp = diaminopyridine) from the corresponding aqueous sodium molybdate solution, by varying the transition metal salts and aminopyridine

derivatives in an acidic medium. We have demonstrated the catalytic activity of [2-ampH]$_4$[{Zn(H_2O)$_5$}Mo$_7$O$_{24}$] ·9H_2O (**2**) towards the oxidation of a series of secondary alcohols to their corresponding ketones using hydrogen peroxide as an oxidant at moderate temperature. All the oxidation reactions were carried out in solvent free, environmentally benign conditions, in which compound **1** is used as heterogeneous catalyst (in catalytic amount). All the product analyses were done by H^1 NMR spectral studies. The structural diversities in respective crystal structures make this discussion rich in supramolecular chemistry. Supramolecularly hydrogen bonded water chain in compound **2**, acyclic water pentamer in compound **3** and water tetramer in compound **5** are crystallographically characterized in their respective crystal structures. In compound **6**, one dimensional chain is formed by Mo4 O12 Mo4 bonds along the chain axis (crystallographic *c* axis), in which each cluster is functionalized by zinc coordination complexes [{Zn(2,3-diampH)$_2$(H_2O)$_2$}]$^{4+}$ resulting in the formation of 2D coordination polymer. Polymeric 2D network having well defined honeycomb cavities, is found to accommodate non-coordinated 2,3-diaminopyridine molecules and solvent water molecules in their cavities.

Chapter 4

‘Ionic Crystals’ Consisting of Trinuclear Macrocations and Polyoxometalate Anions Exhibiting Single Crystal to Single Crystal Transformation: Breathing of Crystals

This chapter mainly focused on the solid state characterization of ionic crystals isolated by ion pairing of trinuclear cluster macrocation (known as basic carboxylate), [M$_3$($_3$-O)(ClCH$_2$COO)$_6$(H_2O)$_3$]$^{1+}$ [where M Fe^{3+} (**1**) and Cr^{3+} (**2**)] and a Keggin type polyoxometalate anion [SiW$_{12}$O$_{40}$]^4 . These ionic crystals are stabilized with a number of crystal water molecules in composite type compounds [Fe$_3$($_3$-

O)($ClCH_2COO)_6(H_2O)_3]_4[SiW_{12}O_{40}]$ ·$18H_2O$ ·$2ClCH_2COOH$ (**1**), and [Cr_3($_3$-O)($ClCH_2COO)_6(H_2O)_3]_4[SiW_{12}O_{40}]$ ·$14H_2O$ ·$2ClCH_2COOH$ (**2**). It is remarkable that, crystals of **1** upon heating at 85°C and 135°C, in an open atmospheric condition, loose considerable number of lattice water molecules resulting in respective dehydrated analogues [Fe_3($_3$-O)($ClCH_2COO)_6(H_2O)_3]_4[SiW_{12}O_{40}]$ ·$10H_2O$ ·$2ClCH_2COOH$ (**dehydrated 1-85°**), and [Fe_3($_3$-O)($ClCH_2COO)_6(H_2O)_3]_4[SiW_{12}O_{40}]$ ·$8H_2O$ ·$2ClCH_2COOH$ (**dehydrated 1-135°**) respectively. Compound **2** upon heating at 85°C and 135°C produced the respective dehydrated analogue [Cr_3($_3$-O)($ClCH_2COO)_6(H_2O)_3]_4[SiW_{12}O_{40}]$ · $8H_2O$ · $2ClCH_2COOH$ (**dehydrated 2-85°/135°**) (where the dehydrated compounds at 85°C and 135°C are identical). The shrinkage of the unit cell occurred in the crystallographic '*c*' axis, which confirms that the water molecules accommodated in the '*c*' axis are readily released from the crystal lattice. These dehydrated crystals regain the water molecules (**degenerated 1**) from water vapor in a crystal to crystal transformation. The unit cell data for water regenerated sample: For compound **degenerated 1**, a = 30.4365Å, b = 17.7235Å, c = 32.3941Å, β = 105.235°, V = 17039Å^3. Degeneration of the water molecules in the crystal lattice leads to expansion of the unit cell volume as **dehydrated 1-85°** (V 15084.00 Å^3) **degenerated 1 (**V = 17039Å^3). The obtained cell data for compound **degenerated 1** exactly match with the parent compound **1**. The same experiment was repeated for compounds **2** and its dehydrated analogues **dehydrated 2-85°/135°C**. The unit cell volume of water regenerated compound (**degenerated 2**) matches to the parent compound **2**. The results are consistent with earlier. Ionic crystals produced from the combination of trinuclear macrocations and polyoxometalate cluster anions are well known in the literature. Many of them are show applications on the adsorption and desorption of smaller molecules. The lattice water molecules are arranged in hydrophilic channels. Another series of ionic crystals [$H_2(Fe_3O(OOCCH_2CN)_6(H_2O)_3)_2(SiMo_{12}O_{40})$] ·$16H_2O$ (**3**), [$H_2(Cr_3O(OOCCH_2CN)_6(H_2O)_3)_2(SiMo_{12}O_{40})$] ·$16H_2O$ (**4**), and

$[H_3(Cr_3O(OOCCH_2CN)_6(H_2O)_3)(SiW_{12}O_{40})]$ ·$6H_2O$ (**5**) are characterized by single-crystal X ray crystallography. The compounds **3** and **4** are crystallized in the monoclinic space group *C2/m* and compound **5** in orthorhombic space group *Pnma*. In compounds **3** **4** and compound **5** macrocation / polyoxometalate ratio is 2:1 and 1:1 respectively. The remaining negative charges are neutralized by protons (H^+). All the compounds are characterized by IR, PXRD, TGA, electronic absorption spectroscopy, and unambiguously by single crystal X-ray diffraction studies.

Chapter 5

Co-existence of Polyoxometalate Cluster Anion and Manganese (III) Based Schiff-base Complex Cations: Syntheses and Structural Characterization

The fifth chapter describes syntheses, structural characterization of compounds $[DMFMn^{III}L_1(CH_3COO)(Mn^{III}L_1)_2(CH_3COO)Mn^{III}L_1DMF][Mn^{III}L_1(DMF)_2]_2$ $[SiMo_{12}O_{40}]$ ·6DMF ·$2H_2O$ (**1**), $[DMF\{Mn^{III}L_2\}_2DMF]_2[SiMo_{12}O_{40}]$ ·2DMF (**2**), $[Mn^{III}L_3(DMF)_2]_4[SiMo_{12}O_{40}]$ ·2DMF ·$4H_2O$ (**3**), $[Mn^{III}L_3(DMF)_2]_4[SiW_{12}O_{40}]$ ·2DMF (**4**) (where L_1 = *N,N*^{1}-bis(salicylaldehydo)ethylenediamine, L_2 = *N,N*^{1}-bis(2-hydroxyacetophenone)ethylenediamine and L_3 = *N,N*^{1}-bis(5-bromosalicylidene)ethylenediamine in which keggin type of polyoxometalate cluster as anion and Mn(III) Schiff base complexes are act as cation. The literature based on transition metal coordinated Schiff base complexes is huge. Salen or its derivative ligands are able to coordinate many different transition metals, and to stabilize them in various oxidation states. In this present discussion Manganese exist in +3 oxidation state. The oxidation state of Manganese is confirmed by BVS calculation, and also consistent with EPR, Cyclic Voltammetry result. Crystal structure of compound **1** consists of a Mn_4

tetramer complex, two Mn-monomer complexes and a $[SiMo_{12}O_{40}]^4$ cluster anion in a molecular unit. The formation of Mn_4 tetramer unit can be described as follows: two Mn_2 dimer units are bridged together by two ($_3$-O) atoms and in each Mn_2 dimer unit, two Mn centers are bridged by a acetate ligand. Compound **2** contains two Mn_2 dimer moieties in which the internuclear distance between Mn(1)···Mn(1) and Mn(2)···Mn(2) are 3.374 and 3.331 Å respectively. The axial Mn O bond distances Mn(1) O(25) and Mn(2) O(28) are 2.147(14) Å and 2.142(15) Å respectively, which are significantly longer than the equatorial Mn O distances those are in the range of 1.853 1.929 Å, as expected for a Jahn-Teller elongation of d^4 Mn^{III} ions. In compounds **3** and **4**, Mn-salen complexes are exist as monomer. The apical position of Mn(III) center in compounds **1** **4** is coordinated by DMF molecule. Salen or its derivatives not only serve as coordination ligands but also play a significant role in the construction of multi dimensional framework by the hydrogen bonding interactions e.g., C H···O and O H···O. We found the formation of one dimensional chains by O H···O hydrogen bonding interactions in compound **2** and **3**. The molecular packing of $[\{Mn^{III}L_3(DMF)_2\}_4][SiMo_{12}O_{40}]$ ·2DMF ·$4H_2O$ (**3**) is characterized by $\pi \cdots \pi$ interactions. The IR data strongly support the association of polyoxometalate anions and Mn(III) salen cations in respective compounds. Electronic absorption spectroscopy furnishes an idea of (N imine) → M(III) ligand to metal charge transfer (LMCT) transitions, those strong absorption bands observed in the range of 390 400 nm.The Mn(III) salen POM compounds are EPR active at the normal X-band frequency. The resulting EPR spectra show the resonance at g 2 with a six-line hyperfine coupling, which is corresponds to the presence of manganese species (I = 5/2). The redox properties of this series of compounds (**1** **4**) have been investigated by electrochemical study.

Chapter 6

Influences of Supramolecular Interactions in Polyoxometalate Chemistry

In this chapter, two different aspects of supramolecular interactions of polyoxometalate cluster anions will be discussed. The first part will be described by N H···O, C H···O and O···O non-covalent interactions exist in the crystal structure of compounds $[2\text{-AmpH}]_4[Mo_8O_{26}]$ (**1**) and $[CyclohexH_2]_2[Mo_8O_{26}]$ (**2**) (where amp = aminopyrimidine, Cyclohex = (*R,R*)-*trans*-1,2-cyclohexyldiamine). Organic components which not only acts as the cation (on protonation) to stabilize an isopolyanion but also plays a significant role in assembling the isopolyanions (POM) leading to a multi dimensional supramolelcular arrangement. We have emphasized the O···O interactions among POM anions and stress the role of N─H···O hydrogen bonds for its assistance to form a chain like arrangement. We have also demonstrated the helical features, observed in the crystal structure of compound $[2\text{-AmpH}]_4[Mo_8O_{26}]$ (**1**). Compound $[CyclohexH_2]_2[Mo_8O_{26}]$ (**2**) is characterized by electronic absorbance and solid circular dichroism spectroscopy along with N H···O, O H···O and C H···O interactions. In second part of this chapter, a systematic study of spectroscopic observation for the displacement of a racemate equilibrium (Pfeiffer effect) has been examined on Strandberg heteropolyanion $[S_2Mo_5O_{23}]^4$ system (racemate equilibrium) whereby *l*- and *d*- arabinose used as enantiomerically pure chiral environmental substances. A cotton effect at ca. 290 nm is clearly associated with the chromophores of the enatiomeric heteropolyanios $[S_2Mo_5O_{23}]^4$ that have lowest energy electronic absorption at ca. 260 nm. When *l*- and *d*- arabinose is added as an environment substance, the Pfeiffer circular dichroism spectra, developed are time dependent. This must be associated with the dynamics for the formation of heteropolyanion enantiomer arabinose (hydrogen bonded)

complex in solution. It can be supposed that the source of Pffeiffer effect for the present system is attributed to the hydrogen bonding between O H proton of arabinose and terminal oxo groups of Strandberg heteropolyanion $[S_2Mo_5O_{23}]^4$. The present work of supramolecular non-covalent interactions (namely, O···O, O H···O, N H···O and C H···O) open a new route for the study of cluster-cluster interactions in polyoxometalate chemistry.

Summary: Future Scope

This chapter will demonstrate the future scope of this thesis work. In second chapter of this thesis, we have described the crystal structures and properties of lanthanide ion (Ln^{3+} = La^{3+}, Sm^{3+} and Ce^{3+}) functionalized $[As_6V_{15}O_{42}(H_2O)]^6$ and $[As_8V_{14}O_{42}(SO_3)]^6$ POV cluster anions stressing their magnetic properties. In order to achieve a new series of such materials, the other lanthanide ions (e.g., Eu^{3+}, Tb^{3+}, Gd^{3+} etc.) can be used. In our laboratory, this project has been initiated already. In chapter 4, the chemistry of tinuclear iron / chromium clusters with POM anions have been discussed. Solid state physical properties of these systems have not yet been explored. The terminal aquo ligands of trinuclear clusters are labile and can easily be substituted by other neutral ligands such as pyridine etc. An attempt to replace the terminal coordinated aqua ligands from ionic crystals is in progress in our laboratory. Catalytic study of POM clusters are another subject of interest. In chapter 5, we have described the chemistry of Mn(III) Schiff base complexes that are co-existed with POM anions. Catalysis aspect of this system is worth trying, because Mn(III) systems are known be to good catalysts. Systematic study on the preparation and enantioselective asymmetric epoxidation of simple olefins by chiral Schiff base complexes associated with POM cluster is under progress. The relevant effort has already been undertaken in our laboratory and the results will be published in near future.

List of Publications

1. V. Shivaiah, **T. Arumuganathan** and Samar K. Das*, Chirality of a Strandberg type heteropolyanion, $[S_2Mo_5O_{23}]^{4-}$, *Inorg. Chem. Commun*., **2004**, *7*, 367 369.

2. **T. Arumuganathan**, A. Srinivasa Rao, T. Vijay Kumar and Samar K. Das*, Two different Zinc(II)-aqua complexes held up by a metal-oxide based support: Synthesis, crystal structure and catalytic activity of $[HMTAH]_2[\{Zn(H_2O)_5\}\{Zn(H_2O)_4\}\{Mo_7O_{24}\}]\cdot 2H_2O$ (HMTAH = protonated hexamethylenetetramine) *J. Chem. Sci*., **2008**, *120*, 95 103.

3. **T. Arumuganathan**, A. Srinivasa Rao and Samar K. Das*, Non-covalent O···O interactions among isopolyanions using a cis-$\{MoO_2\}$ moiety by the assistance of N H···O hydrogen bonds, *J. Chem. Sci*., **2008**, *120***,** *3*, 297 304.

4. **T. Arumuganathan** and Samar K. Das*, Discrete Polyoxovanadate cluster into an Organic Free Metal Oxide Based Material: Syntheses, Crystal Structures and Magnetic Properties of a New Series of Lanthanide Linked-POV Compounds $[\{Ln(H_2O)_6\}_2As_8V_{14}O_{42}(SO_3)]\cdot 8H_2O$ (Ln = La^{3+}, Sm^{3+} and Ce^{3+}) *Inorg. Chem.* manuscript under revision

5. **T. Arumuganathan**, A. Srinivasa Rao and Samar K. Das*, Polyoxometalate Supported Transition Metal Complexes: Synthesis, Supramolecular Structures and Catalysis. (communicated)

6. **T. Arumuganathan** and Samar K. Das*, Reversible Crystal to Crystal Transformation Through Exclusion and Inclusion of Water: Breathing of Crystals. (communicated)

Posters and Presentations

1. **T. Arumuganathan** and S. K. Das*, Synthesis and Characterization of 2D Layered Structures of Polyoxovanadate Clusters: Poster presented at "Modern Trends in Inorganic Chemistry (MTIC)" held at Mumbai, India on December **2003**.

2. **T. Arumuganathan** and S. K. Das*, Anion Encapsulation by V/As Clusters Through Cluster Degradation and Contraction: Poster presented at annual in house symposium which was held in School of Chemistry, University of Hyderabad, India, March **2006**.

3. **T. Arumuganathan** and S. K. Das*, Functionalization of POM clusters, Synthesis, Spectroscopic, and Single Crystal Studies: Poster presented in MATCON-2007, international conference which was held in Cochin, India, March **2007**.

4. **T. Arumuganathan**, A. Srinivasa Rao and S. K. Das*, Functionalization of POM Clusters, Synthesis and Catalytic Application: Poster presented at annual in house symposium which was held in School of Chemistry, University of Hyderabad, India, March **2007**.
5. **T. Arumuganathan** and S. K. Das*, Reversible Water Exclusion and Inclusion in a Crystal To Crystal Transformation Through the Shrinkage and Expansion of the Unit Cell Volume. Oral and poster presentation in "Modern Trends in Inorganic Chemistry MTIC **2007**, December)" which was held in Indian Institute of Technology, Madras, India.

6. **T. Arumuganathan** and S. K. Das*, Metal oxide Based Clusters: Synthesis, Crystal Structures, Catalysis and Crystal to Crystal Transformation. Oral and Poster presentation in “Chemfest-2008” and awarded as the best presentation, which was held in March-**2008**, School of Chemistry, University of Hyderabad, India.